UNCOMMONLY STUDIED POST-TRANSLATIONAL MODIFICATIONS AS POTENTIAL REGULATORS OF TAU FUNCTION AND PATHOBIOLOGY

By

Mohammed Alhadidy

A DISSERTATION

Submitted to
Michigan State University
in partial fulfillment of the requirements
for the degree of

Neuroscience – Doctor of Philosophy

2024

ABSTRACT

Tau protein is associated with many neurodegenerative disorders known as tauopathies, such as Alzheimer's disease (AD), progressive supranuclear palsy (PSP), and Picks' disease (PiD). Depending on the alternative splicing of the microtubule-associated protein tau (MAPT) gene in the central nervous system, tau protein may carry either three or four microtubule-binding repeats (3R vs 4R) along with either two, one, or no N-terminal acidic repeats (2N, 1N, 0N) giving rise to 6 primary tau isoforms. Under disease conditions, tau protein aggregates into intracellular inclusions that feature distinct profiles of tau isoforms (e.g. 4R/3R in AD, 4R in PSP, and 3R in PiD). Aggregates of tau were traditionally thought of as the main driver of neurodegeneration in tauopathies. Increasingly, evidence points to earlier, soluble conformations of abnormally modified monomers and multimeric tau as toxic forms of tau. The biological processes driving tau from physiological species to pathological conformations remain incompletely understood; however, the functional consequences of tau mutations, protein-protein interactions, and post-translational modifications (PTMs) are likely contributors.

Phosphorylation and acetylation have been the most commonly and extensively studied PTMs of tau. Nonetheless, tau is subject to other PTMs that have not gained as much attention, such as carbamylation, prolyl-isomerization, polyamination, O-linked-N-acetyl β-d-N-glucosaminylation (O-GlcNAcylation), and SUMOylation among others. Moreover, our understanding of the role played by PTMs in regulating the adoption of soluble toxic conformations by tau is in its early days. Therefore, it is of paramount importance to fill those gaps by shedding more light on the understudied PTMs of tau and investigate their role in regulating the formation of pathological tau conformations.

In this dissertation, I set out to investigate three of the understudied PTMs of tau: polyamination, O-GlcNAcylation, and SUMOylation. First, I produced a set of recombinant tau proteins individually modified with the three PTMs using different purification approaches. The modified sites on recombinant tau isoforms were identified using mass spectrometry. Then, I assessed the impact of the three PTMs on the interactions of tau with microtubules (MTs) in terms of MT binding and tubulin polymerization. In addition, the unmodified and modified tau proteins were subjected to a set of in vitro biophysical and biochemical assays to determine the contribution of the three PTMs to tau's transition into the known pathological conformations, including formation of filamentous aggregates, oligomerization, exposure of the phosphatase-activating domain, misfolding, and in-cell seeding capability. Several effects of polyamination, O-GlcNAcylation, and SUMOylation on the interaction of tau with microtubules and the adoption of pathological conformations by tau were identified. Integrating the findings from this work with the current literature can provide insights on the potential role played by PTMs in disease.

I show that this framework to study PTMs using recombinant proteins is useful in investigating the regulation of tau pathobiology even by understudied PTMs. Furthermore, integrating the findings from this work with the current literature can provide insights on the potential role played by PTMs in disease. Taken together, this approach facilitates the advancement of our understanding of the relationships between PTMs and tau conformations in health and disease.

Foremost, I would like to dedicate this work to my late mother,
Azza Alghazy,
for her unconditional love, support, and always believing in me,
even when others did not.

I also dedicate this work to my family,
Ahlam Soliman and Malek Alhadidy,
for being everything to me during this journey.

ACKNOWLEDGEMENTS

First, I would like to thank my advisor, Dr. Nicholas Kanaan, for giving me the freedom to carve out my dissertation project under his guidance and providing whatever resources were needed to complete this work. Also, he encouraged me to develop a critical mindset to read literature and create my own view of research results relevant to my field. Finally, I appreciate his understanding during some hard times I went through during my Ph.D. training.

I also thank my current and previous dissertation committee members: Dr. Caryl Sortwell, Dr. Scott Counts, Dr. Benjamin Combs, and Dr. Irving Vega. They helped me refine my research approach and provided time to have discussions whenever needed. I would like to extend a special thanks to Dr. Caryl Sortwell for continuously supporting my personal and professional development during graduate school as a dissertation committee member and directing the trainee's individual development committee.

Special thanks go to the current and previous members of the Kanaan lab for never hesitating to provide their support: Tessa Grabinski, Rebecca Mueller, Ahmed Atwa, Dr. Matthew Benskey, Dr. Kelly Dubois, Marco Perez, Chelsey Yob, Dr. Hanna Trzeciakiewicz, Spencer Panoushek, and Mary Gifford. I owe Rebecca Mueller a special thanks for sharing her expertise in many techniques used to complete this work. I also would like to thank all members of the Translational Neuroscience department for being the most efficient team I have ever worked with: Dr. Jack Lipton, Michelle Gartland, Thuy Tran, and Betsy Matazel.

For their assistance with mass spectrometry, I would like to thank members of the Vega lab: Dr. Jared Lamp and Andrew Umstead. Also, I wanted to thank Paul Stemmer

from Wayne State University for his dedication to work out some challenges posed by mass spectrometry.

Finally, I would like to thank the Neuroscience program members (previous and current) for their continuous support during my time at MSU: Dr. A.J. Robison, Dr. James Galligan, Dr. Greg Swain, Shari Stockmeyer, Eleri Thomas, and Julie Delgado.

PREFACE

At the time of writing this dissertation, major sections of Chapter 1 have already been published as a minireview in Biochemical Society Transactions (PMID: 38348781). Chapters 2 and 3 are currently in preparation for publication and will be ready for submission soon. Chapter 4 is also being prepared for publications and expected to be submitted soon.

TABLE OF CONTENTS

LIST OF FIGURES

LIST OF ABBREVIATIONS

AAV	Adeno-associated virus
Ab	Amyloid-β
ACN	Acetonitrile
AD	Alzheimer's disease
AmBic	Ammonium bicarbonate
ANOVA	Analysis of variance
ANS	8-anilino-1-naphthalene sulfonic acid
AOS	Apraxia of speech
APP	Amyloid precursor protein
ARA	Arachidonic acid
BEMAD	β-elimination followed by Michael addition
CaMKII	Ca2+/calmodulin-dependent protein kinase II
CBD	Corticobasal degeneration
CBP	CREB-binding protein
CBS	Corticobasal syndrome
Cdk5	Cyclin-dependent kinase 5
CDS	Coding sequence
CK1	Casein kinase 1
CNS	Central nervous system
Cryo-EM	Cryogenic electron microscopy
CTE	Chronic traumatic encephalopathy
CV	Column volume

DI	Diagnostic ion
DIW	Deionized water
DMS	Differential mobility spectrometry
DTT	Dithiothreitol
DUB	Deubiquitinase
EL	Elution
ELISA	Enzyme-linked immunosorbent assay
EOAD	Early onset Alzheimer's disease
ETD	Electron transport dissociation
FA	Formic acid
FL	Flow-through
FLEXITau	Full-Length expressed stable isotope-labeled tau
FPLC	Fast protein liquid chromatography
FRET	Förster resonance energy transfer
FTDP-17	Frontotemporal dementia and parkinsonism linked to chromosome-17
FTLD	Frontotemporal lobar degeneration
G-PTM-D	Global post-translational modification discovery
GSK3b	Glycogen synthase kinase 3b
GWAS	Genome-wide association study
HCD	High-energy collision dissociation
HDAC6	Histone deacetylase 6
HMW	High molecular weight
IM-MS	Ion mobility mass spectrometry

K	Lysine
LB	Luria broth
LLS	Laser light scattering
LOAD	Late onset Alzheimer’s disease
M. Wt.	Molecular weight
m/z	Mass-to-charge ratio
MAPT	Microtubule-associated protein tau gene
MARK	Microtubule affinity-regulating kinase
MDBP	Methyl 2,5-dibromopentanoate
MS	Mass spectrometry
MTBR	Microtubule-binding repeat
MWCO	Molecular weight cutoff
N1	First N-terminal acidic insert
N2	Second N-terminal acidic insert
NFDM	Non-fat dry milk
NFT	Neuronal neurofibrillary tangle
NMR	Nuclear magnetic resonance
O-GlcNAc	O-linked-N-acetyl β-d-N-glucosamine
O-GlcNAcylation	O-linked-N-acetyl β-d-N-glucosaminylation
OGA	O-GlcNAcase enzyme
OGT	O-GlcNAc transferase enzyme
P1	First proline-rich domain
P2	Second proline-rich domain

PAD	Phosphatase-activating domain
PAGF	Pure akinesia with gait filature
PCR	Polymerase chain reaction
PGRN	Progranulin gene
PHF	Paired helical filament
PiD	Picks disease
PIMAX	Protein interaction module-assisted function X
PKA	Cyclic AMP-dependent protein kinase A
PNFA	Progressive nonfluent aphasia
PP1	Protein phosphatase 1
PRD	Proline-rich domain
PSEN1	Presenilin 1
PSEN2	Presenilin 2
PSM	Peptide spectral match
PSP	Progressive supranuclear palsy
PSP-P	Progressive supranuclear palsy with parkinsonism
PTMs	Post-translational modifications
Q	Glutamine
R’	Fifth microtubule-binding repeat
R1	First microtubule-binding repeat
R2	Second microtubule-binding repeat
R3	Third microtubule-binding repeat
R4	Fourth microtubule-binding repeat

RS	Richardson syndrome
S/T	Serine/threonine
SAE1	SUMO-activating enzyme subunit 1
SAE2	SUMO-activating enzyme subunit 2
SETD7	SET domain containing 7
SF	Straight filament
SNP	Single nucleotide polymorphism
SPD	Spermidine
SRM	Selected reaction monitoring
SSAT	Spermidine/spermine-N1-acetyltransferase enzyme
SUMO	Small ubiquitin-like modifier
Sup	Supernatant
TB	Terrific broth
TBS	Tris-buffered saline
TBS-T	Tris-buffered saline with 0.1% tween 20
TDP-43	TAR DNA-binding protein 43
TEM	Transmission electron microscopy
TEV	Tobacco etch virus
TG	Transglutaminase enzyme
ThS	Thioflavin S
ThT	Thioflavin T
TMB	3,3′,5,5′-Tetramethylbenzidine
TNT	Tau N-terminal antibody

TOC1	Tau oligomeric complex 1 antibody
TOMA1	Tau oligomer monoclonal antibody 1
TRAF6	Tumor necrosis factor receptor-associated factor 6
UA	Uranyl acetate
Ubc9	Ubiquitin-conjugating enzyme 9
UPS	Ubiquitin proteasome system
W	Wash

CHAPTER 1: DISSERTATION INTRODUCTION

Abstract

Tau protein is associated with many neurodegenerative disorders known as tauopathies, the most common of which is Alzheimer's disease (AD). Intracellular inclusions of tau are traditionally thought of as the main driver of neurodegeneration in tauopathies. Recent evidence points to soluble conformations of abnormally modified monomers and multimeric tau as likely toxic forms of tau, as opposed to filamentous aggregates. Factors driving tau from a physiological state to pathological conformations is a growing area of interest for researchers in the field. Certain avenues are currently under investigation including the functional consequences of pathological tau changes such as tau mutations, protein-protein interactions, and post-translational modifications (PTMs).

PTMs regulate several aspects of tau biology such as its normal physiological functions, proteasomal and autophagic clearance, solubility, and aggregation. Also, PTMs contribute to the transition of tau from normal to pathological conformations, such as oligomerization and misfolding. Phosphorylation and acetylation are the most extensively studied PTMs of tau; yet tau is subject to a much larger pool of PTMs that remain without enough examination such as carbamylation, prolyl-isomerization, polyamination, O-linked-N-acetyl β-d-N-glucosaminylation (O-GlcNAcylation), and SUMOylation among others. Moreover, our understating of how PTMs of tau specifically regulate its transition into pathological conformations needs further development. Filling this knowledge gap requires further investigation of the understudied territory of tau PTMs to gain a comprehensive picture of tau regulation.

The focus of this dissertation is to understand the role played by three of the understudied PTMs of tau (i.e. polyamination, O-GlcNAcylation, and SUMOylation) in regulating its transition into pathological conformations. Chapter 1 begins with a summary of our current knowledge of basic tau protein biology, tauopathies, pathological tau conformations, and PTMs. Then I provide an overview of the current methods to create recombinant tau proteins carrying specific PTMs and validate modification status. Then, I describe a set of biochemical and biophysical assays that assess the contribution of a given PTM to the different pathological tau conformations, including aggregation, oligomerization, exposure of the phosphatase-activating domain, misfolding, and seeding. By integrating these approaches, this work advances our understanding of the relationships between PTMs and pathological tau conformations.

Biology of Tau Protein

Tau protein is encoded by the microtubule-associated protein tau (*MAPT*) gene located on chromosome 17q21 (Caillet-Boudin et al., 2015; Goedert et al., 1988). The *MAPT* gene gives rise to six primary tau isoforms in the central nervous system (CNS) through alternative splicing (Figure 1.1A) (Wang & Mandelkow, 2016). Alternative splicing of exon 10 determines whether tau protein contains either three or four of the microtubule binding repeats (MTBRs), called 3R and 4R isoforms, respectively (Wang & Mandelkow, 2016). Furthermore, alternative splicing of exons 2 and 3 that encode for the N-terminal acidic repeats determines whether the 3R and 4R tau isoforms carry 2N, 1N, or 0N inserts (Wang & Mandelkow, 2016). Tau also has a unique isoform containing the additional exon 4a increasing its molecular weight from 45-65kDa to about 110kDa (Fischer & Baas, 2020). This larger tau isoform is called Big tau, and it is expressed mainly in the peripheral nervous system and select regions of the CNS such as the cerebellum and spinal cord (Fischer, 2023). Within the CNS, tau is expressed in neurons and mature oligodendrocytes (Mueller et al., 2021). On the contrary, its expression is lower in astrocytes with little to no expression in microglia (Kanaan, 2024). Furthermore, tau is distributed throughout most compartments of neuronal cells including dendrites, soma, axons, and nuclei (Kanaan & Grabinski, 2021).

In 1975, the tau protein was discovered and classified as a microtubule-associated protein that regulates microtubule dynamics (Cleveland et al., 1977; Weingarten et al., 1975; Witman et al., 1976). Over the years, accumulating evidence suggests a more diverse functional repertoire for tau that extends to several cellular compartments and pathways (Mueller et al., 2021; Tseng & Cohen, 2024). In addition to regulating

microtubule dynamics, tau may regulate axonal transport, axonal maturation, neuronal activity, and neurogenesis. Inside the nucleus, tau may also help maintain the integrity of genomic DNA (Wang & Mandelkow, 2016). In the axonal compartment of neurons, tau regulates axonal transport and cargo release through a signaling pathway that includes glycogen synthase kinase 3β (GSK3β) and protein phosphatase 1 (PP1) (Mueller et al., 2021). This process is regulated by the phosphatase-activating domain (PAD) located in the extreme N-terminus of tau (Kanaan et al., 2011). Furthermore, tau regulates myelination in mature oligodendrocytes by recruiting Fyn kinase after initial contacts between oligodendrocytes and axons are established (Muller et al., 2013; Witman et al., 1976). As is the case with the other intrinsically disordered proteins, pinpointing specific molecular functions can be complex and this remains an active area of investigation in the field (Holehouse & Kragelund, 2024).

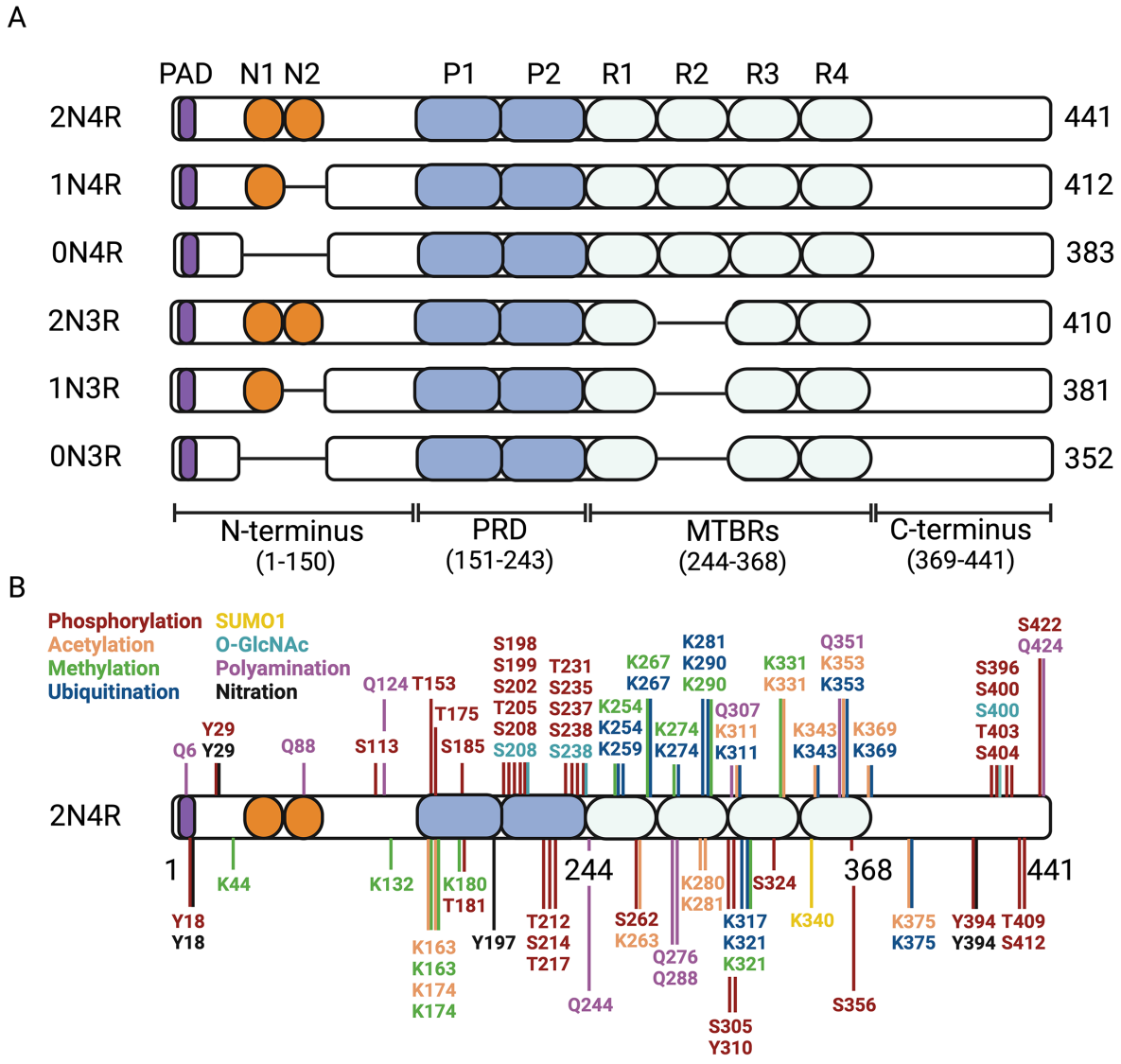

Figure 1.1. Domains and post-translational modifications (PTMs) of tau.
A, tau proteins contain multiple domains, including the acidic N-terminus (aa 1-150) containing the phosphatase-activating domain (PAD, aa 2-18) and the alternatively spliced N-terminal inserts (N1, aa 45-73 and N2, aa 74-102); the highly flexible proline-rich domain (PRD, aa 151-243) comprised of two subdomains (P1, 151-198; P2, 199-243); the microtubule-binding region (aa 244-368) that harbors four or three microtubule-binding repeats (MTBRs); and the C-terminal domain (aa 369-441). Alternative splicing of exons 2, 3, and 10 in the MAPT gene results in six different isoforms. Inclusion or exclusion of exon 10 yields three isoforms of four MTBR containing isoforms (4R) or three isoforms of three MTBR containing isoforms (3R), respectively. Each 3R and 4R isoform protein has either the N1 and N2 (2N), only the N1 (1N) or neither the N1 nor N2 (0N) N-

Figure 1.1 (cont'd)
terminal inserts. The amino acid length of each isoform is indicated to the right of the protein and the amino acids comprising each domain is indicated in parentheses below the domain name. B, several approaches (e.g. mass spectrometry and antibody-based assays) have been used to identify many tau PTMs in tauopathies, including Alzheimer's disease, corticobasal degeneration, progressive supranuclear palsy, and Pick's disease. This panel summarizes many of the known phosphorylation, acetylation, methylation, ubiquitination, SUMOylation, polyamination, glycosylation, and nitration sites in tau that were identified using human tissues (longest tau isoform, 2N4R, used as a reference). Several PTM sites involving lysine, serine or threonine residues overlap or have high proximity, which may lead to competition and/or complex interplay between different PTMs at specific sites. Figure created with BioRender.com.

Overview of Tauopathies

Tauopathies are a heterogenous group of neurodegenerative disorders that present clinically with a broad spectrum of cognitive, behavioral, and motor symptoms, and are associated with degeneration in brain regions related to the clinical impairments (Josephs, 2017; Kneynsberg et al., 2017). These disorders are characterized neuropathologically by the abnormal aggregation of filamentous tau into several forms of pathognomonic neuronal and/or glial inclusions (Goedert et al., 1988; LeDoux, 2014). Alzheimer's disease (AD) is characterized by neurofibrillary tangles (NFTs), neuropil threads and neuritic plaques, while tufted astrocytes and oligodendrocyte coiled bodies are common in progressive supranuclear palsy (PSP), astrocytic plaques and ballooned neurons are found in corticobasal degeneration (CBD), neuronal Pick bodies are characteristic of Pick's disease (PiD), and neurofibrillary tangles and astrocytic fibrillary deposits are found in chronic traumatic encephalopathy (CTE) (Arendt et al., 2016; Gotz et al., 2019; McKee et al., 2018).

At the protein level within the inclusions, some tauopathies feature primarily 4R tau isoforms (e.g. CBD and PSP), 3R tau isoforms (e.g. PiD), or both 3R and 4R tau proteins

(e.g. AD and CTE) (Wang & Mandelkow, 2016; Zhang et al., 2022). In addition to their diversity at the neuropathological and protein level, diversity at the structural level of the filamentous forms of tau is well established (King et al., 2001; Ksiezak-Reding et al., 1996; Ksiezak-Reding & Wall, 2005; Ksiezak-Reding et al., 1998). Traditional electron microscopy and biochemistry techniques highlighted differences in paired helical filaments from different tauopathies, including different core residues, diameters, and twist periodicities (Arima, 2006; Crowther, 1991; Crowther & Goedert, 2000; Ksiezak-Reding et al., 1994; Taniguchi-Watanabe et al., 2016; von Bergen et al., 2006; Wischik et al., 1985; Wischik et al., 1988; Wisniewski et al., 1984; Zhukareva et al., 2002). Building on these earlier studies, cryogenic electron microscopy (cryo-EM) was used to resolve structural differences among insoluble tau aggregates in several tauopathies with atomic resolution (Falcon et al., 2018; Fitzpatrick et al., 2017; Shi et al., 2021; Zhang et al., 2020). Collectively, cryo-EM studies indicate that tau assumes conformations within the filament cores unique to each of the tauopathies and this specificity may be helpful in post-mortem disease classification (Scheres et al., 2020; Shi et al., 2021).

Primary Tauopathies

Tau pathology represent the primary neuropathological feature in primary tauopathies; therefore, it is thought that tau is at least one of the primary drivers of diseases processes in this group of neurodegenerative disorders (Kovacs, 2016). The differences at the neuropathological, protein, and structural levels in tauopathies are also accompanied by differences in the clinical presentation that seems to be related to the brain region(s) affected (Olfati et al., 2022).

Corticobasal Degeneration

In the late 1960s, CBD was reported in literature as a separate entity for the first time (Rebeiz et al., 1967, 1968). Difficulty in using limbs with slowness and clumsiness was the main clinical symptom that all patients presented with (Rebeiz et al., 1968). CBD has an onset of 40-70 years of age, and patients present with a constellation of symptoms commonly referred to as corticobasal syndrome (CBS): asymmetrical rigidity and apraxia along with dystonia and alien limb syndrome (Armstrong et al., 2013; Litvan et al., 2000). Inclusions of tau in CBD are comprised of 4R tau isoforms, and they are located mainly within the frontal and parietal cortices along with the substantia nigra (Dickson et al., 2011; Kovacs, 2015). The hindbrain also is affected in CBD, but the pathology is typically denser in the forebrain when compared to PSP (Dickson et al., 2002). The defining neuropathological feature of CBD is the unique astrocytic plaques (Feany & Dickson, 1995). Furthermore, CBD brains contain ballooned neurons and globose NFTs, but these inclusions are shared with other tauopathies such as PSP (globose NFTs), AD, and PiD (ballooned neurons) (Dickson et al., 2011; Fujino et al., 2004).

Progressive Supranuclear Palsy

PSP has an onset of 60-70 years of age, and patients usually present with axial rigidity, unstable posture, falls, dysarthria, and dysphagia along with a progressive vertical gaze palsy (hence the name palsy) (Steele et al., 1964; Wen et al., 2023). The main brain regions affected in PSP patients include basal ganglia, subthalamic nucleus, and substantia nigra (Dickson et al., 2011). In 1964, the first cases of PSP were reported by Steele, Richardson, and Olszewski (Steele et al., 1964); thus, the typical clinical presentation of PSP described above was later named Richardson syndrome (RS)

(Williams et al., 2005). Another variant of PSP resembles parkinsonism, called PSP-parkinsonism (PSP-P), and its clinical symptoms include tremors that respond initially to treatment with levodopa (Williams et al., 2005). In fact, PSP may present with a wide range of clinical symptoms including progressive nonfluent aphasia or apraxia of speech (PNFA or AOS) (Josephs et al., 2005), CBS (Josephs et al., 2006; Tsuboi et al., 2005), or pure akinesia with gait filature (PAGF) (Ahmed et al., 2008; Williams et al., 2007). This heterogeneity in clinical presentation comes from different distributions of tau pathology inside the brain (Dickson et al., 2011). For example, tau pathology more predominant in brainstem is associated with PAGF; cortical predominant tau pathology is associated with CBS and AOS (Dickson et al., 2011).

Like CBD, PSP is a 4R tauopathy that feature both neuronal and glial tau pathology in the brain (Dickson et al., 2011). The unique neuropathological feature in PSP is the glial lesions called tufted astrocytes (Hauw et al., 1990; Yamada et al., 1992). Moreover, neuronal and oligodendrocytic lesions are abundant in PSP in the forms of globose NFTs and coiled bodies, respectively (Yamada et al., 1992). Even though globose NFTs and coiled bodies are also found in CBD, they are typically more abundant and characteristic of PSP (Dickson et al., 2011).

Pick's disease

Since 1892, Arnold Pick reported clinical cases presenting with personality changes, cognitive dysfunction, and focal cortical symptoms such as apraxia and aphasia (Karenberg, 2001). That disease entity later became known as PiD that has an onset of < 65 years of age (Dickson et al., 2011). Depending on the cortical areas involved, patients may present with personality changes (frontal and temporal cortices)

(Constantinidis et al., 1974), apraxia (frontal and parietal cortices) (Lang et al., 1994), and progressive aphasia (per-Sylvian atrophy including the left anterior temporal cortex with interconnected hippocampal neurons) (Dickson et al., 2011; Graff-Radford et al., 1990).

Unlike CBD and PSP, PiD is a 3R tauopathy that features both neuronal and glial tau pathology (Dickson et al., 2011). The characteristic neuropathological feature of PiD is the unique Pick bodies (round intraneuronal tau inclusions) present in cortical and hippocampal brain regions (de Silva et al., 2006; Dickson et al., 2011; Rewcastle & Ball, 1968). Another neuropathological feature observed in PiD is ramified astrocytes as well as ballooned neurons (referred to as Pick cells in PiD); yet ballooned neurons may be shared with other tauopathies as described above (e.g. CBD) (Dickson et al., 2011). Unlike CBD and PSP, pigmentation of substantia nigra typically remains intact in PiD (Williams, 2006).

Frontotemporal Dementia and Parkinsonism Linked to Chromosome-17

Frontotemporal Dementia and Parkinsonism Linked to Chromosome-17 (FTDP-17) are autosomal dominant neurodegenerative disorders characterized by mutations in genes located on chromosome 17 – the *MAPT* and progranulin (PGRN) genes (Boeve & Hutton, 2008). Therefore, FTDP-17 is further classified into FTDP-17-*MAPT* and FTDP17-*PGRN*. Nonetheless, mutations in the *MAPT* gene rather than *PGRN* gene account for most FTDP-17 cases (Goedert & Spillantini, 2000). The first evidence that *MAPT* mutations are linked to FTDP-17 cases came in the late 1990s; the reported *MAPT* mutations included G272V, V337M, P301L, and R406W (Hutton et al., 1998; Poorkaj et al., 1998). Since then, many other *MAPT* mutations were detected in FTDP-17 families; these mutations are in either coding regions or the intronic region after exon 10 (Spillantini

et al., 2000). FTDP-17 has an onset between 30-50 years of age, and afflicted individuals usually present with at least two out of three cardinal features: behavioral and personality disturbances (e.g. social inhibition, aggressive outburst, compulsive behavior), cognitive deficits, and motor dysfunction (sometimes referred to as parkinsonism-plus syndrome) (Wszolek et al., 2006). Furthermore, tau pathology exhibits a variable profile in terms of location (i.e. neuronal vs glial), tau isoforms (i.e. 4R, 3R, or 4R/3R), and inclusion type (e.g. neurofibrillary tangles) which may mimic either AD, CBD, PSP, or PiD (Goedert & Spillantini, 2000; Williams, 2006).

Familial cases of FTDP-17 provided evidence that mutations in the *MAPT* gene are sufficient to cause neurodegenerative dementias (Goedert & Spillantini, 2000). Missense mutations in exons 9, 12, and 13 (e.g. G272, V337M, and R406W) affect all six tau isoforms (Goedert & Spillantini, 2000). On the other hand, missense and deletion mutations in exon 10 (e.g. ΔK280, P301L, and P301S) affect only 4R tau isoforms (Goedert & Spillantini, 2000). Given that most of the mutations are located within the MTBR region, it is not surprising that these mutant forms of tau impair tau-induced microtubule assembly and binding (Bugiani et al., 1999; Hasegawa et al., 1998; Hong et al., 1998; Rizzu et al., 1999). In addition, some of these mutations are directly linked to tau-induced pathogenic mechanisms in disease (Alhadidy & Kanaan, 2024). For example, the P301L mutation increases tau oligomerization, promotes tau liquid-liquid phase separation, and enhances PAD exposure leading to hyperactivation of the PP1-GSK3β pathway and impairment of axonal transport (Combs et al., 2021; Kanaan et al., 2020; Maeda et al., 2018).

Intronic mutations mostly located in the 5' splice site of exon 10 represent the second type of *MAPT* mutations in FTDP-17 (Spillantini et al., 2000). Several studies determined a stem loop structure at the 5' splice site of exon 10 whose stability is disrupted by intronic mutations (D'Souza et al., 1999; Donahue et al., 2006; Grover et al., 1999; Hong et al., 1998; Hutton et al., 1998). Thus, some intronic mutations increase the inclusion of exon 10 and increase expression of 4R tau isoforms (Gallo et al., 2007; Niblock & Gallo, 2012; Varani et al., 1999). Indeed, evidence suggests that 4R tau is more pathogenic relative to 3R tau (Adams et al., 2010; Schoch et al., 2016).

Secondary Tauopathies

Secondary tauopathies include one or more co-pathologies along with tau inclusions in affected brain regions, and tau is a primary driver of disease processes in these disorders (Arendt et al., 2016). Furthermore, the associated co-pathologies also contribute to the pathophysiology of secondary tauopathies (Kovacs, 2016).

Alzheimer's Disease

AD is named after the neuroanatomist, Alois Alzheimer, who reported the first clinical case in patient named Auguste Deter at the Meeting of South-West German Psychiatrists in 1906 (Hippius & Neundorfer, 2003). Auguste D. was in her 50s and presented with memory impairment, hallucination, and aggressive behavior (Allsop, 2000). She was given the diagnosis of a rare form of presenile dementia, and she died with severe dementia five years later (Pantel, 2017; Yang et al., 2016). An autopsy of Auguste D.'s brain revealed the histological hallmarks of senile plaques and neurofibrillary tangles (Hippius & Neundorfer, 2003). Interestingly, another physician called Oscar Fischer published a paper describing neuritic plaques in the same year Alois Alzheimer

published his work (Goedert, 2009). Four years later Fischer published another paper in which he remarkably described eight stages of plaques that correlate with disease stage (Goedert, 2009). AD was described as Alzheimer's disease and the presbyophrenia of O. Fischer between 1949 and 1955, but it was later shortened to AD probably for the sake of convenience (Goedert, 2009).

The foundation laid by the seminal work from Drs. Alzheimer and Fischer ultimately led to the current neuropathological definition of AD including extracellular amyloid-β (Aβ) plaques and intracellular tau tangles (Glenner & Wong, 1984; Grundke-Iqbal, Iqbal, Quinlan, et al., 1986; Kosik et al., 1986; Masters et al., 1985; Terry et al., 1964). The required presence of amyloid plaques in addition to tau tangles to confirm diagnosis makes AD a secondary tauopathy (Irwin, 2016; Langerscheidt et al., 2024). AD represents the most common cause of dementia and the sixth-leading cause of death in USA ("2023 Alzheimer's disease facts and figures," 2023).

There are two main forms of AD: familial AD that represents only 5% of cases and sporadic AD accounting for the other 95% (Andrade-Guerrero et al., 2023). Familial or early onset AD (EOAD) represents an autosomal dominant form of the disease with onset < 65 years of age (Andrade-Guerrero et al., 2023). Several genetic mutations are linked to EOAD, most of which involves the amyloid precursor protein (APP), presenilin 1 (PEN1), and presenilin 2 (PSEN2) (Andrade-Guerrero et al., 2023). On the other hand, sporadic or late onset AD (LOAD) has onset > 65 years of age, and aging represents its primary risk factor (Zhao & Huai, 2023). Apoε4 reduces the age of onset of LOAD, and this allele is present in about 40-65% of cases (Meyer et al., 1998; Pires & Rego, 2023). In addition to the Apoε4 allele, genome-wide association studies (GWAS) linked LOAD to

dozens of susceptibility genes, many of which are related to Aβ homeostasis (Hampel et al., 2021).

In AD, Aβ plaques appear first in the neocortex (temporal and frontal lobes), spread into allocortex (e.g. hippocampus and other limbic areas), and eventually reach the brainstem (Grothe et al., 2017; Thal et al., 2002). Tau tangles, on the other hand, follow a distinctly different pattern that starts in the entorhinal region and spreads into limbic brain regions until it reaches the neocortex. This spatiotemporal pattern of progressive tau inclusion deposition is the basis of Braak staging for AD (Braak et al., 2006; Braak & Braak, 1991; van der Kant et al., 2020).

According to Braak staging, tau pathology starts in the transentorhinal region with little/no involvement of the entorhinal cortex proper (stage I). Pathology then progresses through the entorhinal cortex proper and into CA1 and CA2 (stage II). Stage III includes the tau pathology intensifying in the entorhinal cortex proper and beginning to spread into the temporal lobe gyri. At stage IV of disease, the pathology becomes increasingly intense in the transentorhinal and entorhinal regions. Furthermore, the cortical pathology spreads further through the temporal cortex and extends widely in most areas of the neocortex except for the occipital cortex. Thereafter, pathology continues to spread further into the neocortical regions and the first signs of tau pathology reaching the occipital cortex are detectable in stage V. At stage VI, most of the neocortical areas show severe pathology with the occipital cortex shows more involvement into the striate areas (Braak et al., 2006; Braak & Braak, 1991).

Even though the consensus is that tau pathology starts later than amyloid pathology, it is tau that strongly correlates with neuronal loss and cognitive decline

(Chetelat et al., 2010; Josephs et al., 2008; La Joie et al., 2020; Malpetti et al., 2022; Nelson et al., 2012; Whitwell et al., 2008). Patients usually present with memory impairment caused by dysfunction of the perforant pathway and neuronal loss in the entorhinal cortex (Gomez-Isla et al., 1996; Hyman et al., 1984; Hyman et al., 1986; Solodkin & Van Hoesen, 1996).

The amyloid cascade hypothesis is one of the leading frameworks to explain AD pathology for the past 20+ years (Barage & Sonawane, 2015; Karran et al., 2011; Naslund et al., 2000; Ricciarelli & Fedele, 2017). The hypothesis states that alterations in the production and/or clearance of Aβ leads to its accumulation. This initial event of Aβ accumulation drives a cascade of pathophysiological changes that eventually leads to tau pathology and the other neuropathological sequelae that characterize AD (Selkoe, 2000). Decades of research suggest that the amyloid cascade hypothesis cannot explain all pathophysiological aspects of AD (Herrup, 2015; Kepp et al., 2023; Selkoe & Hardy, 2016; Uddin et al., 2020). Nonetheless, recent clinical trials demonstrated that antibodies targeting the Aβ pathology provide, at least, a small benefit in some patients when administered early in the disease (Budd Haeberlein et al., 2022; van Dyck et al., 2023).

Chronic Traumatic Encephalopathy

As early as 1928, it became appreciated that fighters may suffer from the “punch-drunk” syndrome whose symptoms are currently described as traumatic encephalopathy syndrome (MARTLAND, 1928; McKee et al., 2023). About half a decade later, Coresellis et al. published a case series of 15 boxers whose brains showed degeneration in the cortex and substantia nigra (Corsellis et al., 1973). Neurofibrillary tau tangles develop in the brains of boxers after repeated head injuries, and they are concentrated in the

perivascular space (Geddes et al., 1999). CTE is not restricted to boxers but can extend to other high impact sports such as soccer and football as well as military-related percussive head injuries (Geddes et al., 1999; McKee et al., 2015; Omalu et al., 2006; Omalu et al., 2005).

CTE is caused by mild and repeated head injuries accompanied by transfer of acceleration and deceleration forces to the brain, with disease appearing at midlife (Chen, 2018; Omalu, 2014). According to the most recent McKee criteria, the presence of a single CTE lesion is sufficient for diagnosis (McKee et al., 2023). A CTE lesion is defined as phosphorylated tau aggregates in neurons at the depth of cortical sulci and around small blood vessels. Neuronal pathology may or may not be accompanied by glial tau pathology (McKee et al., 2023).

Unlike AD, tau pathology in CTE does not start in the entorhinal cortex or medial temporal lobe; instead, NFTs begin in the neocortex, especially the frontal lobe around small vessels in cerebral sulci (McKee et al., 2015; Omalu et al., 2006; Omalu et al., 2005). At stage I CTE, the perivascular tau pathology may be accompanied by mild ventricular enlargement (McKee et al., 2013). Tau pathology then progresses to form “hot spots” at the depth of cerebral sulci accompanied by a limited spread to the adjacent layers of superficial cortex (stage II). At stage III, neurofibrillary tau tangles spread throughout the frontal, temporal, parietal, and insular cortices along with other brain regions such as the amygdala, hippocampus, and entorhinal cortex. Tau pathology becomes widespread in most cortical and medial temporal lobe regions later at stage IV (McKee et al., 2013).

As a secondary tauopathy, CTE is also accompanied by other pathologies such as TAR DNA-binding protein 43 (TDP-43) and Aβ plaques (McKee et al., 2013). In fact, TDP-43 inclusions are reported in about 85% of CTE cases. Moreover, autopsy of the first two football cases of CTE as well as other patients showed a variable profile of Aβ plaques in the brain, with some cases having extensive Aβ plaques and others having none (McKee et al., 2015; Omalu et al., 2006). Different studies reported that 40-50% of CTE cases present also with Aβ plaques (McKee et al., 2013; Stein et al., 2015). Interestingly, Aβ pathology in CTE patients is strongly associated with the Apoε4 allele (Stein et al., 2015).

CTE Patients may present with a range of symptoms including cognitive impairment, mood disorders, parkinsonian symptoms, depressive disorder, aggressive behavior, and progressive dementia (Omalu et al., 2006; Omalu et al., 2005; Stern et al., 2013). Of note, the clinical symptoms are correlated with the stages of tau pathology spreading in CTE: stage I CTE is associated with headaches and lack of attention; stage II CTE is associated with memory impairment and depression; stage III associated with cognitive dysfunctions; stage IV is associated with dementia and aggression (McKee et al., 2013).

Pathological Tau Conformations in Tauopathies

In the 1980's, the discovery that tau is the primary constituent of neurofibrillary tangles provided substantial evidence for its importance in AD and other tauopathies (Arima et al., 1992; Bancher et al., 1987; Feany & Dickson, 1995; Mori et al., 1994; Wood et al., 1986). Under physiological conditions, tau lacks a stable three-dimensional structure (Uversky et al., 2008) and assumes an ensemble of conformations *in vitro,* such as the paperclip conformation (Jeganathan et al., 2008; Jeganathan et al., 2006). In

disease conditions, tau undergoes modifications and conformational changes likely involved in instigating a cascade of self-assembly forming filamentous (on-filament pathway) or non-filamentous (off-filament pathway) aggregates (Chen et al., 2020; Kjaergaard et al., 2018; Shammas et al., 2015). Our understanding of the mechanisms mediating tau toxicity and aggregation in neurodegenerative disorders has undergone substantial progress over the years (Samudra et al., 2023; Silva & Haggarty, 2020).

The toxicity of tau protein in neurodegenerative disorders was traditionally linked to tau filamentous aggregates such as NFTs (Cowan & Mudher, 2013). This is based on myriad studies showing aggregated tau pathology correlates strongly with cognitive decline in patients (Arriagada et al., 1992; Gomez-Isla et al., 1997; Grober et al., 1999). Moreover, studies in mice demonstrated that behavioral deficits are linked to the overexpression of pro-aggregation versus anti-aggregation tau mutants (Eckermann et al., 2007). However, later estimates suggest that tangle-bearing neurons are likely to survive for decades in the human brain (Morsch et al., 1999). Indeed, tangle-like inclusions are not necessary nor sufficient for neuronal dysfunction in mice (Cowan & Mudher, 2013). For example, neuronal dysfunction could be reversed by turning off expression of a mutant form of human tau despite the continued presence of tangle-like pathology in the rTg4510 transgenic mouse model (Santacruz et al., 2005). Moreover, tangle-bearing neurons in the rTg4510 mouse model remain functionally intact as indicated by two-photon calcium imaging (Kuchibhotla et al., 2014). Together, these findings highlight that tangles are not as detrimental as initially thought and suggest other pathological species of tau (i.e. pre-tangle forms) may be more critical to tau-mediated toxicity.

Earlier conformations of tau antecedent to fibrillar aggregation have drawn increasing attention. The formation of tau oligomers is considered an early event in the progressive accumulation of pathological tau in AD (Lasagna-Reeves et al., 2012; Maeda et al., 2006; Patterson et al., 2011). Oligomers are sufficient to cause synaptic and mitochondrial dysfunction in neurons of wild-type mice (Lasagna-Reeves et al., 2011). Remarkably, oligomeric tau impairs long-term potentiation in tau knockout mice (Puzzo et al., 2020). Moreover, treating primary mouse neurons with oligomeric tau induces electrophysiological dysfunction, such as inhibition of long-term potentiation (Fa et al., 2016; Hill et al., 2019). In agreement, neutralizing oligomeric tau with immunotherapy rescues tauopathy-induced memory deficits in both hTau and tau P301L mice (Castillo-Carranza, Gerson, et al., 2014; Castillo-Carranza, Sengupta, et al., 2014).

Tau undergoes additional conformational changes early during the progressive accumulation of pathology in human disease also associated with mechanisms of toxicity. For example, excessive exposure of the biologically active motif in the extreme N-terminus of tau (PAD) activates a PP1-GSK3β regulated pathway that disrupts axonal transport (Combs et al., 2021; Kanaan et al., 2011; LaPointe et al., 2009; Mueller et al., 2021). Another conformational change of tau believed to represent a misfolding event that precedes aggregation involves its N-terminus coming near the MTBR–an event that happens very early in AD (Carmel et al., 1996; Luna-Munoz et al., 2007). In addition, recent work by the Diamond lab and other shows that monomeric tau can exist in conformations capable of seeding aggregation in cell lines and animal models (Mirbaha et al., 2018; Mirbaha et al., 2022).

In fact, accumulating evidence suggests that the levels of pathological tau conformations in tauopathies correlate strongly with neuronal and synaptic losses in brain regions (Scheff & Price, 2006). For instance, entorhinal cortex (especially layer II) along with the perforant pathway, hippocampal formation, and nucleus basalis of Meynert (mainly in the posterior portion) are the first brain regions to experience neuronal and synaptic losses in early/mild AD (Gomez-Isla et al., 1996; Grothe et al., 2012; Heinonen et al., 1995; Kordower et al., 2001; Leal & Yassa, 2013; Mufson et al., 2000; Mufson et al., 2002; Price et al., 2001; Scheff et al., 2007; Scheff et al., 2006; Stoub et al., 2014; Stoub et al., 2006; Tagliavini & Pilleri, 1983; Tiernan, Ginsberg, et al., 2018; Vana et al., 2011). Such events of neurodegeneration in AD coincide with well-known markers of incipient tau pathology (i.e. pre-tangle markers such as phosphorylation at S422 and the AT8 epitope) (Braak et al., 2006; Guillozet-Bongaarts et al., 2006; Ikegami et al., 1996; Kimura et al., 1996; Luna-Munoz et al., 2007; Mercken et al., 1992; Morishima-Kawashima, Hasegawa, Takio, Suzuki, Yoshida, Titani, et al., 1995) as well as pathological tau conformations in the affected brain regions, including oligomerization, PAD exposure, misfolding, and seeding activity (Brady & Mufson, 1991; Christensen et al., 2019; Combs et al., 2016; Cox et al., 2016; Furman et al., 2017; Garcia-Sierra et al., 2000; Hyman, Kromer, et al., 1988; Kaufman et al., 2018; Lace et al., 2009; Mahady et al., 2023; Mesulam et al., 2004; Stopschinski et al., 2021; Tiernan et al., 2016; Tiernan, Mufson, et al., 2018; Vana et al., 2011). Furthermore, oligomerization, PAD exposure, misfolding, and adoption of seeding-competent conformation occur early in tauopathies other than AD, including 4R/3R (e.g. CTE), 4R (e.g. CBD), and 3R tauopathies (e.g. PiD), among others (Amorim et al., 2023; Castillo-Carranza, Gerson, et al., 2014; Combs et

al., 2016; Cox et al., 2016; Ferrer et al., 2014; Kanaan et al., 2016; Montalbano et al., 2023; Mufson et al., 2016). Taken together, these findings implicate common mechanisms of tau conformational changes and toxicity beginning early in tauopathies.

Factors driving conformational changes of tau that culminate in its toxicity and aggregation remain largely elusive. A well-studied factor that alters tau conformations and is linked to dementia symptoms is tau mutations causing inherited FTDP-17 (Goedert & Spillantini, 2000). Some of these mutations may alter splicing increasing the expression of 4R tau isoforms (e.g. P301L) (Hutton et al., 1998), alter microtubule binding, and/or enhance tau aggregation (Chen et al., 2023; Ghetti et al., 2000; Huang & Stultz, 2008; Murrell et al., 1999; Neumann et al., 2001; von Bergen et al., 2001). Another emerging factor that elicits conformational changes of tau is protein-protein interactions. Examples include heat shock protein 90, histone deacetylase 6 (HDAC6), bassoon, and EFhd2 among many others (Balmik et al., 2020; Martinez et al., 2022; Soliman et al., 2021; Tortosa et al., 2009; Vega, 2016; Vega et al., 2008; Vega et al., 2019; Weickert et al., 2020). Finally, PTMs are also potential mediators of conformational changes linked to tau pathology (Alquezar et al., 2020).

Post-translational Modifications of Tau

Tau is subject to a broad range of PTMs, including phosphorylation, acetylation, methylation, ubiquitination, nitration, SUMOylation, polyamination, glycosylation, and carbamylation, prolyl-isomerization among others (Figure 1.1B) (Alquezar et al., 2020; Guo et al., 2017).A significant body of literature demonstrates that PTMs have roles in regulating tau localization, degradation, and aggregation, but the precise impact of

specific and combinatorial PTMs on the tau's physiology and pathophysiology requires continued investigation (Ye et al., 2022).

Phosphorylation

Tau contains 85 potential phosphorylation sites that include serine, threonine, and tyrosine, the majority of which are located within the proline-rich domain (PRD) and C-terminus of tau (Park et al., 2018). Phosphorylation represents a physiological phenomenon for fetal tau, tightly regulated during development of the embryo (Mawal-Dewan et al., 1994; Yu et al., 2009). Phosphorylation of tau is regulated by a multitude of protein kinases and phosphatases, including GSK3β, cyclin-dependent kinase 5 (cdk5), cdk2, Ca2+/calmodulin-dependent protein kinase II (CaMKII), 5' adenosine monophosphate-activated protein kinase (AMPK), casein kinase 1 (CK1), microtubule affinity-regulating kinases (MARKs), cyclic AMP-dependent protein kinase A (PKA), PKB, PKC, tyrosine kinases (e.g. Fyn and Abl), PP1, PP2A, and PP5 (Noble et al., 2013; Park et al., 2018). PP2A seems to account for about 70% of tau dephosphorylation taking place in the human brains (Gong et al., 1993).

In AD patients, abnormal phosphorylation is one of the earliest changes in tau PTMs reported for paired helical filaments (PHFs) as well as cytosolic tau (Grundke-Iqbal, Iqbal, Tung, et al., 1986; Kopke et al., 1993). Many of the phosphorylation sites on disease-related PHF tau also are present in the normal adult brain, but certain phosphorylation sites are unique to PHF tau (Hoffmann et al., 1997; Matsuo et al., 1994). Some of tau phosphorylation sites characteristic of AD and other tauopathies, and they can be detected by commercially available antibodies, such as pT181 (AT270), pS202/T205/S208 (AT8), pT212/S214 (AT100), pT181 (AT270), p231 (AT180), and

pS396/S404 (PHF1) (Goedert et al., 1994; Goedert et al., 1995; Mercken et al., 1992; Otvos et al., 1994; Zheng-Fischhofer et al., 1998).

Tau phosphorylation can impact several aspects of tau biology including aggregation, microtubule binding, and tau clearance among many others (Noble et al., 2013; Park et al., 2018). Early studies on tau phosphorylation suggested that phosphorylation is an event that precedes and subsequently promotes assembly of tau into PHF aggregates (Alonso et al., 2001; Bancher et al., 1989; Perez et al., 2000). Follow-up studies demonstrated that phosphorylation of tau at specific epitopes correlates with the severity and stage of AD (Augustinack et al., 2002; Luna-Munoz et al., 2007). These findings supported the notion that phosphorylation of tau drives its aggregation into PHFs (Yang et al., 2023). However, as more evidence accumulated, this view on tau phosphorylation was challenged. For example, phosphorylation at S305, S262, and S214 inhibits rather than enhances tau aggregation (Schneider et al., 1999; Strang et al., 2019). Furthermore, mice overexpression GSK3β do not demonstrate an increase in the aggregated insoluble tau (despite increased tau phosphorylation) compared to non-GSK3β overexpressing mice (Spittaels et al., 2000). Collectively, these studies helped clarify that the relationship between tau phosphorylation and aggregation is more complex than originally thought (Noble et al., 2013).

Site-specific phosphorylation of tau can influence its ability to regulate microtubule dynamics (Yang et al., 2023). For example, phosphorylation of tau at S262 and Y310 reduces its binding to microtubules (Ait-Bouziad et al., 2020; Biernat et al., 1993; Drewes et al., 1995). Moreover, tau phosphorylation is a critical mediator of tau clearance through the ubiquitin proteasome system (UPS) (Dickey et al., 2007). It was proposed that

phosphorylation at certain sites (e.g. pS202/T205 and pS396/S404) primes tau for ubiquitination by the ubiquitin ligase CHIP promoting tau clearance through the UPS (Dickey, Dunmore, et al., 2006; Dickey, Yue, et al., 2006). Therefore, clearance of tau through the UPS becomes interrupted in disease conditions leading to accumulation of abnormally phosphorylated tau (Alquezar et al., 2020).

As our knowledge of pathological tau conformations grew, it became clear that phosphorylation of tau at specific sites represents a pathogenic event in tauopathies (Alhadidy & Kanaan, 2024). For example, phosphorylation of tau at T175 increases PAD exposure potentially dysregulating axonal transport (Hintermayer et al., 2020). In addition, tau pseudophosphorylated at S199/S202/T205 demonstrates higher PAD exposure and enhanced oligomerization along with impairment of axonal transport (Christensen et al., 2023; Kanaan et al., 2020).

Acetylation

Acetylation is the second most studied PTM of tau. There are 44 lysine residues in its sequence that could serve as acetylation sites, but tau acetylation seems concentrated within the PRD and MTBR (Park et al., 2018). In the late 2000s to early 2010s, sites of tau acetylation were first reported by the Gan, Lee and Trojanowski groups (Cohen et al., 2011; Min et al., 2010). Three tau acetylation sites reported in the two studies were common, these were K164, K281, and K369.

Tau acetylation is regulated by a balance between histone acetyltransferases and histone deacetylases (Alquezar et al., 2020). The activity of p300 and CREB-binding protein (CBP), known histone acetyltransferases, is reduced in AD (Schueller et al., 2020). Furthermore, the expression of histone deacetylases is dysregulated in AD; while

the levels of HDAC6 are elevated, the levels of sirtuin 1 are reduced (Ding et al., 2008; Julien et al., 2009). Indeed, enhancing the activity of p300 and CBP rescued memory deficits in THY-Tau22 mice (Chatterjee et al., 2018).

The effect of acetylation on tau biology was investigated in several *in vitro* and *in vivo* studies. For example, *in vitro* acetylation of K18 tau fragment (spanning the 4 MTRBs of tau) inhibits the tau-induced microtubule polymerization (Cohen et al., 2011). In cell lines, enhancing tau acetylation (by silencing the tau deacetylase sirtuin 1) inhibits the ubiquitination and clearance of tau (Min et al., 2010). Furthermore, the acetylation mimic at K280Q and K281Q reduces tau's ability to induce microtubule assembly compared to unmodified tau (Trzeciakiewicz et al., 2017).

In agreement with the *in vitro* studies, acetylation mimic at K174Q alone or in combination with K281Q demonstrated a slower turnover of tau or enhancement in the tauopathy-related memory impairment in mice, respectively (Min et al., 2015; Tracy et al., 2016). Furthermore, expression of the acetylation mimic at K280Q of tau in drosophila increased the observed tauopathy phenotype (Gorsky et al., 2016). On the other hand, expression of acetylation mimic K280Q in mice expressing mutant P301S tau reduced tau phosphorylation, decreased neuroinflammation, and restored synaptic function (Ajit et al., 2019). In addition, expression of multiple acetylation mimics at K164Q, K280Q, K281Q, and K369Q blunted tau phosphorylation and the associated tauopathy phenotype in drosophila (Gorsky et al., 2017). The above *in vivo* results are challenging to reconcile, but they may reflect differences in disease models, acetylation sites, and outcome measures. Even though acetylation of tau at K174 and/or K280 was observed in AD and

other tauopathies, its salience in health and disease remains undetermined (Irwin et al., 2013; Irwin et al., 2012; Min et al., 2015).

Cook et al. reported a unique site of tau acetylation within MTBR region at the KXGS motifs (Cook, Carlomagno, et al., 2014). At these locations, enhancing acetylation at K decreases phosphorylation on the neighboring serine residues decreasing tau fibrillization and inhibiting microtubule polymerization (Carlomagno et al., 2017; Cook, Carlomagno, et al., 2014). Of note, hypoacetylation at the KXGS motif was reported in AD and rTg4510 mice (Cook, Carlomagno, et al., 2014). Building upon those interesting observations, the Giasson group assessed the behavior of tau acetylation mimics at all 4 KXGS motifs of tau (K259Q, K290Q, K321Q, and K353Q) (Xia, Bell, et al., 2021). In agreement with previous studies, the acetylation mimic at all 4 KXGS motifs showed reduced tau fibrillization and microtubule-binding. Nonetheless, further studies are warranted to determine the impact acetylation may have on the adoption of pathological conformations by tau.

Ubiquitination

Ubiquitination is a PTM that involves the covalent attachment of 9 kDa protein (ubiquitin) to one or more lysine residues of the modified protein (Ciechanover, 2015). The ubiquitination machinery includes an enzymatic cascade comprised of three enzymes: ubiquitin-activating enzymes (E1), ubiquitin-conjugating enzymes (E2), and ubiquitin ligases (E3) (Hershko et al., 1983). Protein modification by ubiquitination is reversed using the enzymes called deubiquitinases (DUBs), allowing for the recycling of ubiquitin in the cell. Ubiquitinated proteins are eventually targeted to the proteasome for their clearance through the UPS (Hough et al., 1986; Waxman et al., 1987).

The discovery of tau ubiquitination is not surprising given that ubiquitin was detectable in senile plaques and NFTs in AD since the 1980s (Mori et al., 1987; Morishima-Kawashima et al., 1993; Perry et al., 1987). Tau ubiquitination takes place at K254, K311, and K353, and polyubiquitination of tau can happen through K6, K11, K48 and K63 of ubiquitin (Cripps et al., 2006; Tan et al., 2008). Furthermore, a subset of tau oligomers is labelled with K63-linked ubiquitin at 11 sites and is elevated in AD (Puangmalai et al., 2022). K48-linked ubiquitination directs tau towards UPS, while K63-linked ubiquitination directs tau towards autophagic clearance (Alquezar et al., 2020; Cripps et al., 2006; Tan et al., 2008). Three E3 ubiquitin ligases are currently identified for tau: CHIP, tumor necrosis factor receptor-associated factor 6 (TRAF6), and axotrophin/MARCH7 (Park et al., 2018). On the other hand, only one DUB, Otub1, is identified for tau (Wang et al., 2017).

Under normal condition, tau is directed to proteasomal degradation in ubiquitin-dependent and -independent fashion (Cardozo & Michaud, 2002; David et al., 2002; Grune et al., 2010; Zhang et al., 2005). In AD, ubiquitinated tau is accumulated, in part, because of reduced proteasomal activity reported in disease conditions (Keller et al., 2000; Lopez Salon et al., 2000). Of note, PHF and oligomeric species of tau induce proteasomal dysfunction, potentially creating a feedforward cycle of tau accumulation (Keck et al., 2003; Myeku et al., 2016). It is not clear how ubiquitination of tau contributes to the pathophysiology of tauopathies, but evidence suggests that ubiquitination is an early-to-intermediate event while tau tangles are maturing (Bancher et al., 1991; Garcia-Sierra et al., 2012; Iwatsubo et al., 1992).

Several aspects of normal tau biology are changed upon ubiquitinating tau. For example, monoubiquitinating full-length tau with axotrophin (E3 ubiquitin ligase) decreases its ability to bind microtubules (Flach et al., 2014). Furthermore, modifying tau at K353 using K48- or K63-linked diubiquitin decreased the formation of filamentous aggregates and inhibited microtubule assembly (Munari et al., 2020). When tau is phosphorylated by GSK3β and then subjected to ubiquitination with CHIP for more than two days, tau transitioned into β-sheet containing aggregates without using an aggregation inducer (Kim et al., 2021). Apart from one study that showed increased oligomeric tau upon deubiquitination in primary neurons, the effect of ubiquitination on the development of pathological tau conformations is unknown (Wang et al., 2017).

Methylation

Methylation is a lysine-directed PTM, that was first reported on PHF tau extracted from AD cases in 2012 (Thomas et al., 2012). Thomas et al. reported monomethylation of tau on seven sites detected by mass spectrometry (MS): K44, K163, K174, K180, K254, K267, and K290. Tau methylation is not a unique phenomenon to AD tau. In fact, soluble tau is modified by mono- and dimethylation in normal human brains at residues that partially overlap with those reported in AD (K44, K267, and K290) (Funk et al., 2014; Huseby et al., 2019). Most reported sites of methylation lie within or flanking the MTBR region of tau (Ye et al., 2022).

Direct comparison of tau methylation sites between cognitively normal and AD patients showed that they share methylation at K44, K267, and K290 (Huseby et al., 2019). Nonetheless, methylation of tau is enriched in the soluble protein fraction and seems to increase with more advanced stages of AD (Bichmann et al., 2021). Enzymes

responsible for regulating tau methylation are not completely defined but SET domain containing 7 (SETD7) was recently reported as a protein lysine methyl transferase for tau (Bichmann et al., 2021).

Methylation regulates several aspects of tau biology. Increasing methylation levels of recombinant tau decreases tau aggregation and seems to favor the formation of globular rather than filamentous aggregates (Funk et al., 2014). Furthermore, induction of microtubule assembly by tau is reduced with tau methylation in a methylation-dependent fashion. Studies in stem cells showed that methylation of tau regulates its subcellular localization (Bichmann et al., 2021). For example, tau methylated at K130 and K132 localizes preferentially in the nuclear compartment. Despite that accumulating knowledge, exactly how methylation regulates the adoption of pathological tau conformations by tauopathies is not clear.

Advances in Detecting Tau PTMs in Tauopathies

Given the accumulating evidence that PTMs are strong regulators of several aspect of tau biology, increasing efforts are put forth to characterize the PTMs of tau through MS (Arakhamia et al., 2020; Kametani et al., 2020; Kyalu Ngoie Zola et al., 2023; Mukherjee et al., 2023; Wesseling et al., 2020). Perhaps not surprisingly, different tauopathies demonstrate different tau PTM profiles in sarkosyl-soluble and -insoluble fractions, and now efforts are being made to better understand the interplay between tau PTMs and structural differences in tau aggregates. For example, the structural diversity of tau aggregates between AD and CBD can be explained by difference in the PTM profile of tau (Arakhamia et al., 2020). As mentioned earlier, cryo-EM clearly corroborated that there is heterogeneity in tau aggregates extracted from different tauopathies (Falcon et

al., 2018; Fitzpatrick et al., 2017; Shi et al., 2021; Zhang et al., 2020). Taken together, the current advances in our understanding of tau conformations and characterization of PTMs are highly suggestive of PTMs mediating the diversity of tau conformers in tauopathies.

An Approach to Study PTMs of Tau

As detailed earlier, several lines of evidence demonstrate that tau PTMs can change tau biology, leading to alterations in the levels of pathogenic conformations that are associated with neurotoxicity (Christensen et al., 2023; Cook, Stankowski, et al., 2014; Hintermayer et al., 2020). Subsequently, a better understanding of how PTMs affect tau aggregation, conformation and function is of high interest in the field. In fact, studying recombinant tau proteins modified with one or more PTMs is a central approach to gain insights on the regulation of tau biology by specific PTMs (Alhadidy & Kanaan, 2024). Herein, we describe a set of *in vitro* assays that can be collectively used to determine the contribution of PTMs in the transition of tau into known pathological conformations using recombinant protein (Alhadidy & Kanaan, 2024).

Methods to Produce Recombinant Tau Protein with PTMs

The ability to produce modified forms of highly purified proteins facilitates the ability to examine the impacts of PTMs on tau conformations. We describe several methods through which tau can be modified with PTMs *in vitro* (Figure 1.2A):

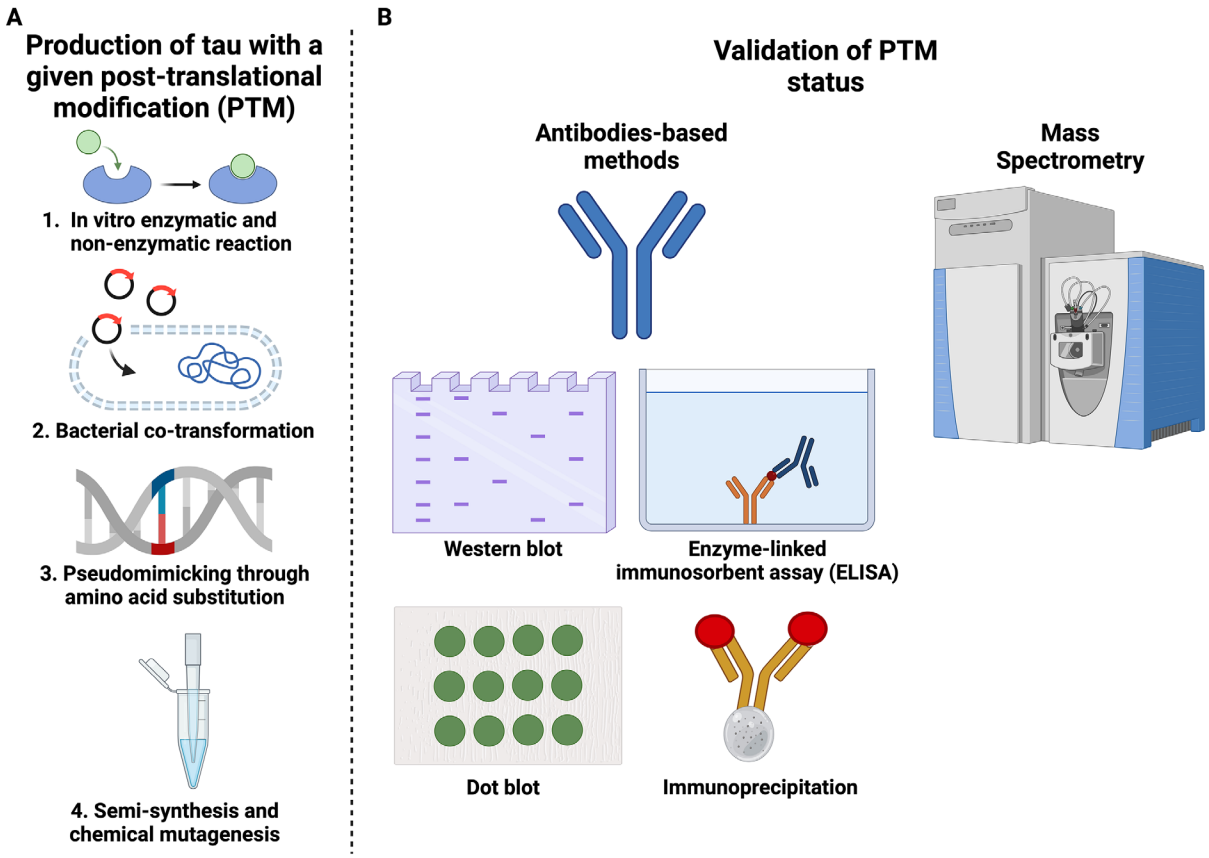

Figure 1.2. Generation of tau modified with a specific post-translational modification (PTM) *in vitro*.
A, four different methods are used to produce tau modified with specific PTMs. First, recombinant tau protein is incubated with a specific enzyme (e.g. kinase) in the presence of adequate substrate (e.g. phosphate) to introduce a given PTM (e.g. phosphorylation or acetylation). Non-enzymatic reactions involve directly incubating recombinant tau protein with a substrate (e.g. glucose) to introduce the PTM of interest (e.g. glycation). Second, bacteria are co-transformed with a plasmid that encodes tau and other plasmids that carry the machinery required for a specific PTM (e.g. O-GlcNAc transferase enzyme to introduce O-GlcNAcylation). Third, recombinant tau protein is produced with amino acid substitutions that mimic a given PTM (e.g. serine/threonine are substituted with either glutamate or aspartate to mimic phosphorylation). Fourth, semi-synthesis of tau fragments containing site-specific PTMs of interest is followed by ligating the modified fragments together. Alternatively, tau is synthesized with cysteine mutations followed by chemical modifications to introduce the PTM of interest. B, approaches to validate the PTM of interest on tau proteins. Antibody-based methods require the presence of site-specific antibodies to verify the modification status of tau protein. Mass spectrometry can verify PTMs through targeted methods (e.g. selected reaction monitoring) with or without enrichment of modified peptides. The FLEXITau (Full-Length Expressed stable Isotope-labeled Tau) method is used where isotope-labelled tau is introduced to the sample as a standard to quantify the extent of modification. Figure created with BioRender.com.

In Vitro Modification with Enzymatic and Non-enzymatic Reactions

The use of enzymatic modifications is the cornerstone of studying tau PTMs *in vitro*, especially for phosphorylation and acetylation. Purified recombinant tau protein is incubated with an enzyme (kinase or acetyltransferase) in the presence of an adequate substrate (phosphate or acetyl-CoA). This approach provided opportunities to map specific tau sites that are modified by individual kinases and acetyltransferases (Cohen et al., 2011; Lund et al., 2001; Martin et al., 2013; Min et al., 2015; Min et al., 2010; Reynolds et al., 2000; Sengupta et al., 1998; Trzeciakiewicz et al., 2017; Wang et al., 2002). Moreover, the enzymatic approach informed studies elucidating how phosphorylation and acetylation affects tau's regulation of microtubule dynamics (Cohen et al., 2011; Wang et al., 2000). Enzymatic modification was also used to study how PTMs alter the conformation of tau and impact its potential to aggregate *in vitro* (Acosta et al., 2022; Cantrelle et al., 2021; Chakraborty et al., 2023; Kamah et al., 2014; Kim et al., 2021; Meng et al., 2022; Rankin et al., 2007; Yuzwa et al., 2014).

Incubation of recombinant tau with a substrate can directly induce PTMs in the absence of enzymes (Cohen et al., 2013; Liu et al., 2016; Nacharaju et al., 1997). An example is glycation of tau induced by incubating tau with glucose. Subsequently, tau becomes heavily glycated (>10 sites) within the microtubule-binding region (Nacharaju et al., 1997). Glycation differentially regulates aggregation propensity of tau isoforms using heparin as an inducer *in vitro* (Liu et al., 2016).

These methods provided a substantial base of knowledge about the effect of PTMs on tau; however, they are limited by the inability to introduce PTMs in a site-specific manner. Moreover, the isolated nature of *in vitro* reactions (i.e. containing only purified

tau and enzymes) and using substrates at concentrations higher than those observed in cells raises the possibility of modifying sites that are not modified *in situ*.

Co-transformation of Bacterial Cells

Co-transforming bacterial cells with a tau plasmid and other plasmids that carry the machinery to produce specific PTMs is another established method to study tau PTMs. The co-transformation approach was successfully used to produce O-linked-N-acetyl β-d-N-glucosamine (O-GlcNAc) modified tau protein, leading to the identification of S400 as a potential site of O-linked-N-acetyl β-d-N-glucosaminylation (O-GlcNAcylation) (Yuzwa et al., 2011). O-GlcNAc modification of tau impedes the rate and extent of its aggregation in the presence of heparin. Moreover, O-GlcNAc modification did not induce detectable global conformation changes in tau as assessed using nuclear magnetic resonance (NMR) (Yuzwa et al., 2014).

A challenge with independently co-transforming bacterial cells with tau and modification machinery is the potential misfolding and trapping of tau into inclusion bodies preventing its modification (Sui, Xu, et al., 2015). To circumvent this problem, a novel approach called the protein interaction module-assisted function X (PIMAX) system was created. The PIMAX system expresses a protein of interest and the enzyme as fusion proteins with Fos and Jun, respectively, in bacteria. The Fos and Jun interaction brings tau near kinases, such as GSK-3β and CDK-5. Phosphorylation of tau by this approach enhances the aggregation of tau in the presence of heparin as measured by thioflavin T (Sui, Xu, et al., 2015). In addition, tau phosphorylated by the PIMAX approach can aggregate without an inducer and is toxic to SH-SY5Y cells (Liu et al., 2020).

These approaches should prove useful for studying tau PTMs catalyzed by other enzymes as well. For example, understudied PTMs of tau, such as SUMOylation, may be effectively studied through this approach (Weber et al., 2014). Another advantage of this method is that it induces PTMs inside a biological system, such as bacterial cells. However, this method is still limited by not allowing site-specific PTMs.

Mimicking PTMs with Alternative Amino Acids

Modification mimicking approaches involve the substitution of specific amino acids with alternative amino acids that recapitulate the effects of a specific PTM. In the case of phosphorylation, serine and threonine residues are mutated to glutamate or aspartate to mimic the additional negative charge from phosphorylation or to alanine to prevent phosphorylation (Cao et al., 2018; Christensen et al., 2023; Eidenmuller et al., 2000; Eidenmuller et al., 2001; Guillozet-Bongaarts et al., 2006; Leger et al., 1997; Morris et al., 2020). In the case of acetylation, lysine residues are changed to glutamine to mimic the neutralization of charge induced by acetylation or to arginine to mimic a nonacetylated lysine (Cook, Carlomagno, et al., 2014). A recent report utilized mimicked methylation of tau by substituting lysine with phenylalanine to increase the hydrophobicity at a given methylation site (Xia et al., 2023). This method offers the advantage of allowing the introduction of one or more site-specific PTMs, but it is limited by the artificial nature of the modifications.

Site-specific PTMs using mimetic approaches enriched our understanding of the roles PTMs play in regulating tau biology in health and disease. Pseudophosphorylation at either T175 or the S199/S202/T205 alters tau conformation leading to increased exposure of tau's PAD (Christensen et al., 2023; Hintermayer et al., 2020; Jeganathan et

al., 2008), which is a conformational change linked to tau-induced axonal transport impairment (Kanaan et al., 2012). Moreover, pseudophosphorylation at S202 and T205 enhances the aggregation of tau in the presence of arachidonic acid (Eidenmuller et al., 2001), and modification of S199 or T205 alone is sufficient to impair axonal transport (Morris et al., 2020). In addition, pseudophosphorylation at S199/S202/T205 impedes the cleavage of tau by caspase 3 at D421 (Cao et al., 2018). Similarly, pseudophosphorylation of tau at S422 inhibits caspase-3-mediated cleavage at D421 (Guillozet-Bongaarts et al., 2006) and is linked to causing transport impairment (Tiernan et al., 2016). Another example is pseudoacetylation of tau within the KXGS motifs, which reduces its ability to form filaments as assessed by thioflavin S (Carlomagno et al., 2017). Conversely, pseudoacetylation at either K274 or K280/K281 of tau increases its propensity to aggregate (Rane et al., 2019; Trzeciakiewicz et al., 2017).

PTM mimetics, such as pseudophosphorylation, can faithfully recapitulate the effects of their physiological counterparts. For example, pseudophosphorylation at regulatory phosphorylation sites often reproduce the effects of bona fide phosphorylation with GSK3β and cyclin-dependent kinase 5 (Combs et al., 2011; Eidenmuller et al., 2001; Fath et al., 2002; Fischer et al., 2009; Haase et al., 2004; Liu et al., 2002; Lund et al., 2001; Rankin et al., 2007; Sun & Gamblin, 2009). Despite the advantages of targeting specific residues, PTM mimetics have important caveats. It must be acknowledged that they are not the physiological PTM and may produce artifactual changes warranting validation studies with the physiological modifications (Limorenko & Lashuel, 2022; Prokopovich et al., 2017). Moreover, not all PTMs of tau have amino acid substitution that mimic their effects (e.g. O-GlcNAcylation). Finally, this approach requires the investigator

to choose specific amino acids to modify, leaving other sites potentially modified *in situ* unchanged.

Semi-synthesis and Chemical Mutagenesis

The semi-synthesis method is a more recent approach that allows the introduction of site-specific PTMs on tau (Haj-Yahya & Lashuel, 2018). The full-length tau protein is synthesized in a series of fragments that can be chemically modified with the PTM of interest. Then, the modified fragments are brought together by fragment ligation reactions. The semi-synthesis strategy was first used to introduce acetylation at K280. Interestingly, tau acetylated at K280 aggregated with the same rate as the acetylation mimetic K280Q in the presence of heparin (Haj-Yahya & Lashuel, 2018). However, electron microscopy showed that acetylated K280 tau produced oligomeric and short fibrillar aggregates while the K280Q mimetic produced short filaments with no oligomers observed (Haj-Yahya & Lashuel, 2018). This result, along with the others observed with pseudophosphorylation, emphasizes the importance of expanding the approaches for introducing site-specific PTMs to fully understand their impact on tau behavior.

Semi-synthesis was also used to study the effects of tau phosphorylation at specific residues. For example, phosphorylation of tau at S356 inhibited tau aggregation with heparin *in vitro* and reduced seeding in tau biosensor cells that measures seeding activity (Haj-Yahya et al., 2020). Not only was this method used to introduce phosphorylation, but also to introduce uncommonly studied PTMs of tau such as carboxymethyl lysine (Ellmer et al., 2019) and ubiquitination (Munari et al., 2020). Diubiquitination of tau at K353 inhibits aggregation, whereas carboxymethyl lysine modification left aggregation unaltered.

A newer strategy to introduce site-specific PTMs in tau is known as chemical mutagenesis (Lindstedt et al., 2021). This method uses cysteine mutants of tau as the means to introduce site-specific PTMs in a two-step reaction. The first reaction involves the formation of dehydroalanine using bis-alkylation elimination strategy with methyl 2,5-dibromopentanoate (MDBP) followed by a second reaction where the PTM of interest is introduced in a site-specific manner through thia-Michael addition. Phosphorylation of tau is introduced through sodium thiophosphate and dimethylation through captamine. However, this process requires substituting the two native cysteine of tau (C291 and C322) with serine to circumvent inadvertently modifying these sites. Even though modifying both cysteines to serine did not appear to change the microtubule-polymerizing activity of tau (McKibben & Rhoades, 2019), it is not clear whether this modification may alter other aspects of tau pathobiology (e.g. protein-protein interactions, aggregation and conformational changes).

Semi-synthesis and chemical mutagenesis allow for the introduction of site-specific PTMs, circumventing one of the main obstacles faced in other methods. Moreover, they represent a bona fide PTM (semi-synthesis) or versions of PTMs that more closely resemble the *in-situ* modifications (chemical mutagenesis) when compared to mimetic mutants. However, it is not yet clear whether these approaches will be possible for PTMs.

Validation of PTM Status

After producing tau carrying a specific PTM, the modification status must be verified using methods such as those described below (Figure 1.2B):

Antibody-based Approaches

This approach utilizes antibodies specific for a given PTM to determine the modification status of a target protein. Over the years, a plethora of antibodies that detect PTMs were generated, with a heavy focus on phosphorylated tau. Some of these antibodies are tau-specific and/or site-specific, such as AT8, pS422, PHF1, Tau AcK280, and Tau S400 O-GlcNAc, among many others. Antibodies can verify the modification status of tau in multiple biochemical assays such as western blot (Cohen et al., 2011; Hamdane et al., 2003; Yuzwa et al., 2014), enzyme-linked immunosorbent assays (ELISAs), dot blots (Brici et al., 2018), and immunoprecipitation (Takamura et al., 2022). However, it is difficult to determine the stoichiometry of a given modification site using antibody-dependent approaches and the efficacy of confirming PTMs with antibodies is inherently linked to the validation and degree of specificity of the antibody. A good example of the later concern was demonstrated in a report that tested more than 30 commercially available antibodies for tau (Ercan et al., 2017). Some antibodies are specific, while others can be easily affected with modifications at neighboring sites. Validation and assessing the degree of specificity paved the way to then use the validated tau antibodies to identify PTM profiles of tau in different stages of AD (Ercan-Herbst et al., 2019).

Mass Spectrometry

MS is a technique used to identify and quantify specific PTMs on tau. This approach was used to study tau PTMs in cognitively unimpaired and tauopathy patients (Morishima-Kawashima, Hasegawa, Takio, Suzuki, Yoshida, Watanabe, et al., 1995). In addition, tryptic digestion and mass spectrometry was used to determine phosphorylation

(Lund et al., 2001), acetylation (Cohen et al., 2011), methylation (Funk et al., 2014), and glycation sites on tau *in vitro* (Liu et al., 2016). Moreover, tryptic digestion was used to determine the double glycine remnants of ubiquitination on lysine sites of tau (Yan et al., 2022). Indeed, the double glycine remnants on tau were used to identify ubiquitination sites at K254, K311, and K353 within the MTBR of tau purified from AD brains (Cripps et al., 2006).

The detection of other PTMs is more challenging using tryptic digestions of proteins, such as SUMOylation and O-GlcNAcylation (Ma & Hart, 2017; Osula et al., 2012). For SUMOylation, two methods were developed to shorten the SUMO isopeptide tail on lysine residues. This was achieved using either microwave-assisted aspartic digestion (Osula et al., 2012) or a specialized enzyme called WaLP (Lumpkin et al., 2017). Alternatively, this is achieved by using a combination of Lys-C and Asp-N enzymes (Hendriks et al., 2018). O-GlcNAcylation is difficult to identify using MS as well (Ma & Hart, 2017). High-energy collision dissociation (HCD) can cleave the O-GlcNAc moiety off proteins, eliminating the possibility of detecting site-specific localization on a specific serine and/or threonine residue. Yet, the cleavage of O-GlcNAc moiety produces diagnostic ions that are useful to verify the modification status of tau. Alternative approaches include using electron transport dissociation (ETD), which is a gentler fragmentation method that preserves O-GlcNAc moieties. A third approach is to replace O-GlcNAc moieties through beta-elimination followed by Michael addition (BEMAD) with dithiothreitol (DTT) (Ma & Hart, 2017).The BEMAD method produces a more stable modification with DTT that is detectable with HCD and provides site-specific information about the location of O-GlcNAc. However, this method requires the dephosphorylation of

proteins before the DTT reactions because phosphorylated residues may give false positive results (Ma & Hart, 2017).

In the past 5 years, more advanced MS-based strategies were developed to allow quantitative evaluation of PTMs on tau. A prominent example is the Full-Length Expressed stable Isotope-labeled Tau (FLEXITau) strategy in which isotope-labelled tau is added to the sample followed by tryptic digestion and running the sample on the mass spectrometer using selected reaction monitoring (SRM) (Mair et al., 2016).The stoichiometry of PTMs is determined by measuring the reduction of unmodified tau peptides in the biological sample, that contain the light isotope, relative to the isotope-labelled tau (change in heavy to light chain ratios). This method was used successfully to characterize phosphorylation sites on tau expressed in Sf9 cells (Drepper et al., 2020). Moreover, FLEXITau was later used to determine PTMs on tau extracted from AD with quantitative results showing that PTMs accumulate on tau to varying degrees as disease progresses (Wesseling et al., 2020). Finally, mass spectrometry is used to measure tau turnover and quantify site-specific tau PTMs (e.g. phosphorylation at T111, T205, S208, T217 and T231) to develop robust biomarker assays for AD in biofluids (e.g. cerebrospinal fluid and plasma) (Azevedo et al., 2022; Barthelemy et al., 2022; Sato et al., 2018).

Assays to Assess Pathogenic Tau Conformations

Once modified forms of tau are generated and validated, a series of assays are available to determine the impact on pathogenic conformations (Figure 1.3):

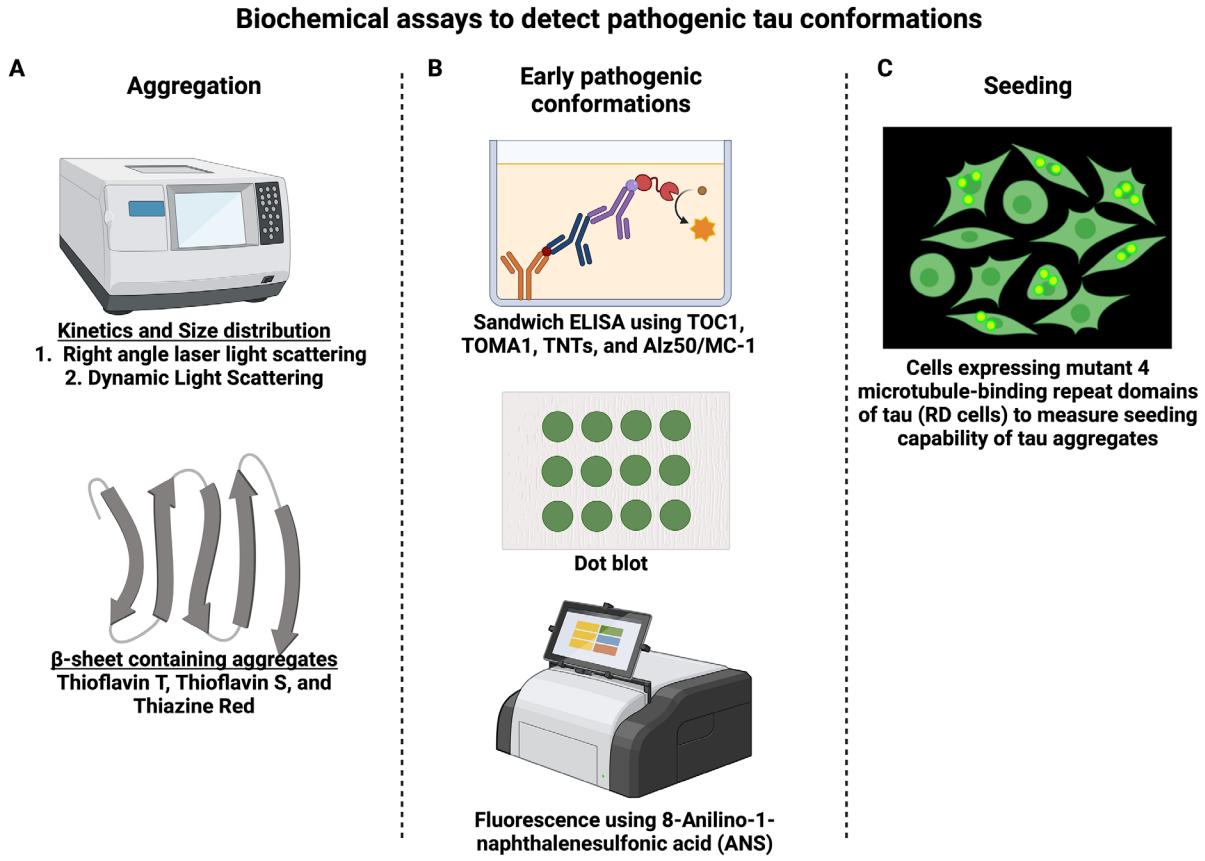

Figure 1.3. Biochemical methods to assess the impact of post-translational modifications on pathogenic tau conformations.
A, tau aggregation is induced *in vitro* and monitored by light scattering assays. Right angle laser light scattering allows the determination of aggregation kinetics such as extent of aggregation (i.e., maximum scatter), nucleation rate (i.e., lag time), and elongation rate. Dynamic light scattering helps determine the size distribution of tau populations forming in an aggregation reaction. Alternatively, β-sheet binding dyes, such as thioflavin T, thioflavin S, and thiazine red, can monitor the transition of tau into β-sheet containing structures (i.e., fibrils). B, conformational changes that precede aggregation, including exposure of the phosphatase-activating domain and oligomerization, can be monitored with conformation-dependent antibodies (e.g. TNTs, TOC1, TOMA1, Tau22, and Alz50/MC-1) in non-denaturing immunoassays such as ELISAs or dot blots. Oligomerization of tau involves hydrophobic clustering that is monitored by 8-Anilino-1-naphthalenesulfonic acid (ANS) assays. C, RD cells (cells expressing mutant 4 microtubule-binding repeat domains of tau) can be utilized to determine seeding capability.

Assessing Tau Aggregation

The process of tau aggregation involves transitioning into β-sheet-containing structures as assessed by spectroscopic techniques (von Bergen et al., 2005). This conformational transition is predominantly mediated by the two hexapeptide motifs located in tau's MTBR2 and MTBR3 (Chen et al., 2019; Rojas Quijano et al., 2006; von Bergen et al., 2005). *In vitro* tau aggregation is instigated by several inducers, among which heparin and arachidonic acid are the most used (Sui, Liu, et al., 2015). Several reagents allow for the fluorometric quantification of β-sheet-containing aggregates of tau, and other amyloid proteins, including thioflavin T, thioflavin S, and thiazine red (Chang et al., 2009; Santa-Maria et al., 2006; Xue et al., 2017). These fluorometric methods are useful to quantify the β-sheet forming aggregates of tau *in vitro* and are sometimes used to evaluate aggregation kinetics. However, it is worth noting that both thioflavin S and thiazine red also stimulate tau aggregation by lowering the energy barrier to fibrillization (Chang et al., 2009).

Another way to study the kinetics of tau aggregation is through right angle laser light scattering (LLS) (Necula & Kuret, 2004). Right angle LLS allows for the assessment of the nucleation rate, rate of elongation, and extent of aggregation. This approach was used to evaluate the aggregation kinetics of several forms of tau, including full-length, mutant, isoforms, and truncated forms of tau (Combs & Gamblin, 2012; Combs et al., 2011; Cox et al., 2016; Gamblin, King, Dawson, et al., 2000). Furthermore, this technique was used to assess the impact of PTMs, such as phosphorylation, on aggregation kinetics (Chang et al., 2011; Tiernan et al., 2016).

Dynamic LLS allows for the determination of size distribution of a given population of protein aggregates (Eichmann et al., 2016). To date, tau has not been extensively studied using dynamic LLS experiments. A few studies assessed the extent of oligomerization of tau mutants in the presence of heparin and size of tau condensates during liquid-liquid phase separation (Hochmair et al., 2023; Trzeciakiewicz et al., 2020).

Assessing Early Pathogenic Conformations

Several antibodies were developed against the early pathogenic tau conformations mentioned above. For oligomeric tau, three antibodies are used extensively in literature: tau oligomeric complex 1 (TOC1) (Patterson et al., 2011), tau oligomer monoclonal antibody 1 (TOMA1) (Castillo-Carranza, Sengupta, et al., 2014), and T22 (Lasagna-Reeves et al., 2012). Other oligomeric or aggregated conformation tau antibodies also exist and will undoubtedly prove useful in studying tau conformation (Gibbons et al., 2020; McMillan et al., 2023). In addition, a set of antibodies called tau N-terminal antibodies (TNTs) are also available that detect conformation-dependent PAD exposure in tau (Combs et al., 2016; Kanaan et al., 2011). Moreover, the conformational change that precedes tau aggregation where the N-terminus of tau is closely associated with the MTBR is detected with the Alz50 and MC1 antibodies (Carmel et al., 1996; Hyman, Van Hoesen, et al., 1988; Jicha et al., 1997). These antibodies are useful in detecting pathological conformations and multimers in human and animal model tissues, cell culture models and *in vitro* recombinant protein experiments across many studies in the literature.

The use of conformation-dependent antibodies requires maintenance of the proteins native state in non-denaturing assays, such as sandwich ELISAs or dot blots (Castillo-Carranza, Sengupta, et al., 2014; Combs et al., 2016; Ercan-Herbst et al., 2019;

Koss et al., 2016; Patterson et al., 2011). Using such assays, the impact of PTMs on pathogenic tau conformations is measurable. For example, pseudophosphorylation of tau at S199/S202/T205 and T175 increase exposure of the PAD (Christensen et al., 2023; Hintermayer et al., 2020). Conversely, pseudophosphorylation of tau at S422 did not modify the extent of tau oligomerization or PAD exposure (Tiernan et al., 2016). Phosphorylation of tau at S199/S202/T205 increases its reactivity with Alz50 and MC1 antibodies in dot blot assays as well (Shahpasand et al., 2012).

Fluorometric measurements using 8-anilino-1-naphthalene sulfonic acid (ANS) were used to measure the hydrophobic clustering that takes place during tau oligomerization (Zhu et al., 2011). Interestingly, tau oligomers show higher hydrophobicity when compared with filamentous tau, offering a way to distinguish between the two tau species (Lo Cascio et al., 2020). A subset of tau oligomers is SDS, heat and reducing condition stable and are visualizable using SDS-PAGE followed by western blot (Patterson et al., 2011). This may prove useful in studying this subtype of tau oligomers in the presence of a given PTM. For example, phosphorylation at S422 increases these highly stable dimers of tau upon aggregation in the presence of arachidonic acid (Tiernan et al., 2016).

Assessing Conformations Associated with Seeding Activity

Transfer of tau pathology from the entorhinal cortex to other synaptically connected brain regions is proposed as a mechanism by which pathology spreads in AD (de Calignon et al., 2012; DeVos et al., 2018; Liu et al., 2012). The Diamond laboratory developed a sensitive assay using tau biosensor cells that measures seeding activity of tau (Holmes et al., 2014). This and similar assays are relatively widely used to assess

seeding activity of tau extracts from both human and animal brains, yielding valuable insights about the prion-like nature of tau, conformers of tau capable of seeding, and tau's interactome (Kaufman et al., 2016; Martinez et al., 2022; Sanders et al., 2014). This work highlighted that tau monomers exist as a dynamic ensemble of conformational states that show varying degrees seeding competence depending upon the accessibility of the regions that mediate aggregation in microtubule-binding region (i.e., VQIINK/VQIVYK) (Hou et al., 2021; Mirbaha et al., 2018; Sharma et al., 2018). Tau biosensor cells were also used with aggregates prepared from recombinant tau, where the impact of PTMs on seeding behavior was investigated. For example, tau phosphorylated by recombinant extracellular signal-regulated kinase 2 or with a whole rat brain extract can seed aggregation in the absence of tau fibrils (Despres et al., 2019).

Other Approaches to Further Our Understanding of Tau PTMs

We provided an overview of the *in vitro* approaches currently available to study pathogenic tau conformations and the impact of PTMs on tau. However, our knowledge of all possible pathogenic tau conformations is far from complete (Kang et al., 2020). Biochemical approaches are well-complemented by structural tau studies that utilize biophysics to determine changes in tau conformations (Acosta et al., 2022; Elbaum-Garfinkle & Rhoades, 2012; Zabik et al., 2017). For example, structural changes leading to changes in tau conformations are measurable using additional biophysical methods such as NMR, intramolecular Förster resonance energy transfer (FRET), differential mobility spectrometry (DMS), and ion mobility mass spectrometry (IM-MS) [reviewed in (Zabik et al., 2017)]. Moreover, molecular dynamic simulations are useful in detecting conformational ensembles of tau monomers, potentially paving the way to studying tau

multimerization (He et al., 2023). Finally, recent advances in cryo-EM imaging led to unprecedented atomic-level resolution of the fibrillar structures tau forms in human disease and *in vitro* (Falcon et al., 2018; Fitzpatrick et al., 2017; Lovestam et al., 2022; Scheres et al., 2020; Shi et al., 2021; Zhang et al., 2019; Zhang et al., 2020). As structural, molecular simulations, advanced imaging, and biochemical approaches converge and continue to advance, the landscape of tau conformations will be deciphered providing clues to the pathobiology of tau in disease.

Dissertation Objectives

Identifying PTMs that impact tau pathology is crucial to understand disease pathogenesis, as well as develop disease-modifying therapies, diagnostics, and biomarkers for tauopathies. Most efforts in the field aim at addressing the role played by phosphorylation and acetylation in regulating tau behavior under health and disease conditions (Alhadidy & Kanaan, 2024). Nonetheless, other uncommon PTMs of tau were identified, may have a role in regulating tau biology, and have not received as much attention as phosphorylation and acetylation (Alquezar et al., 2020).

The overall goal of this work is to determine the impact some of the understudied PTMs of tau have on the development of pathological tau species: polyamination, O-GlcNAcylation, and SUMOylation. To this end, we utilized the approach described above to produce and purify recombinant tau proteins individually modified with each PTM. Then, the unmodified and modified recombinant tau proteins were tested in the biochemical and biophysical assays for the development of pathological tau conformations: aggregation, oligomerization, PAD exposure, misfolding, and seeding.

Moreover, the effects the PTMs on basic tau biology such as microtubule binding and polymerizations were determined.

Specific aim 1: Determine the impact of polyamination with SPD on the development of pathological tau conformations.

Polyamination is mediated by the action of transglutaminase enzyme that cross-links tau protein through its glutamine and lysine residues. This mechanism was posited as a contributing factor to tau aggregation in tauopathies and mouse models (Halverson et al., 2005; Murthy et al., 1998; Singer et al., 2002; Zemaitaitis et al., 2000). However, another potential outcome of the polyamination reaction involves the incorporation of cellular polyamines [such as putrescine and spermidine (SPD)] onto glutamine residues of tau protein (Miller & Johnson, 1995). Interestingly, the levels of polyamines are elevated in AD brains (Inoue et al., 2013; Morrison & Kish, 1995). Some studies investigated tau aggregation in the presence of polyamines in the cellular milieu (Sandusky-Beltran et al., 2019; Sandusky-Beltran et al., 2021). Nonetheless, precisely how the direct incorporation of SPD onto glutamine residues of tau changes its pathobiology was unknown. This question is addressed in the first aim of my dissertation as described below:

This aim is addressed in Chapter 2 using recombinant tau proteins modified with SPD through *in vitro* polyamination reactions. First, I tested the significance of SPD polyamination on tau's ability to bind and induce polymerization of microtubules. Multimerization of recombinant tau proteins was induced with arachidonic acid, and aggregation kinetics monitored using LLS. Formation of filamentous tau aggregates in the unaggregated and aggregated tau samples were investigated using thioflavin S, electron

microscopy, and seeding assays. Eventually the extent of tau oligomerization, PAD exposure, misfolding, and multimerization were determined using western blot and sandwich ELISA. Based on the literature, I hypothesized that polyamination facilitates tau aggregation, oligomerization, PAD exposure, misfolding, and seeding.

Specific aim 2: Determine the impact of O-GlcNAcylation on the development of pathological tau conformations.

Tau is subject to O-GlcNAcylation by the action O-GlcNAc transferase (OGT) enzyme, and interestingly the levels of O-GlcNAcylated tau are reduced in AD brains (Arnold et al., 1996; Liu et al., 2009; Yang & Qian, 2017). O-GlcNAcylation reduces the rate and extent of heparin-induced tau aggregation, competes with phosphorylation of serine/threonine residues, and decreases neuronal loss and tau aggregation in animal models (Gatta et al., 2016; Hastings et al., 2017; Liu et al., 2004; Liu et al., 2009; Smet-Nocca et al., 2011; Wang et al., 2020; Yuzwa et al., 2014; Yuzwa et al., 2012). However, it is not clear whether those effects are accompanied by a reduction in the formation of pathological tau conformations such as oligomerization, PAD exposure, misfolding, and seeding. This question was addressed in the second aim of my dissertation as described below:

This aim is addressed in Chapter 3 using recombinant tau proteins modified O-GlcNAc by co-transforming bacterial cells with tau and OGT. First, I tested the significance of O-GlcNAcylation on tau's ability to bind and induce polymerization of microtubules. Multimerization of recombinant tau proteins was induced with arachidonic acid, and aggregation kinetics monitored using LLS. Formation of filamentous tau aggregates in the unaggregated and aggregated tau samples were investigated using

thioflavin S, electron microscopy, and seeding assay. The extent of tau oligomerization, PAD exposure, misfolding, and multimerization were determined western blot and sandwich ELISA. As suggested by the previous studies, I hypothesized that O-GlcNAcylation inhibits tau oligomerization, PAD exposure, misfolding, and seeding.

Specific aim 3: Determine the impact of SUMOylation on the development of pathological tau conformations.

SUMOylation involves the covalent incorporation of a small ubiquitin-like modifier (SUMO) protein isoform (SUMO1, SUMO2, and SUMO3) onto lysine residues of modified proteins (Mahajan et al., 1997; Matunis et al., 1996). Recently, tau SUMOylation was reported in AD and PSP cases, with SUMO1 but not SUMO2/3 consistently colocalizing with phosphorylated tau aggregates (Luo et al., 2014; Takamura et al., 2022). There is an interplay among tau SUMOylation, phosphorylation, and ubiquitination; SUMOylation and phosphorylation seem to have a positive correlation, while SUMOylation and ubiquitination show a negative correlation in cells (Dorval & Fraser, 2006; Luo et al., 2014). Furthermore, the reduced ubiquitination of tau that follows its SUMOylation eventually culminates into enhanced aggregation (Luo et al., 2014). These findings agree with the findings of tau SUMOylation in tauopathies where SUMO1 colocalizes with phosphorylated tau aggregates (Dorval & Fraser, 2006; Luo et al., 2014). However, directly testing whether SUMOylation of tau enhances its aggregation and development of the other pathological tau conformations such as oligomerization, PAD exposure, misfolding, and seeding was not done previously. This gap in our knowledge is addressed in the third aim of my dissertation as described below:

This aim is addressed in Chapter 4 using recombinant tau proteins modified either SUMO1 or SUMO2 by co-transforming bacterial cells with tau, SUMOylation machinery along with the respective SUMO isoform. First, I tested the significance of SUMOylation on tau's ability to bind and induce polymerization of microtubules. Then, multimerization of recombinant tau proteins was induced with arachidonic acid. Formation of filamentous tau aggregates in the unaggregated and aggregated tau samples was investigated using electron microscopy and seeding assay. The extent of tau oligomerization, PAD exposure, misfolding, and multimerization were determined using sandwich ELISAs. Given the association of SUMO with tau aggregates in tauopathies, I hypothesized that SUMOylation enhances tau aggregation, oligomerization, PAD exposure, misfolding, and seeding.

Dissertation Significance

A deeper understanding of PTMs' influence on the development of tau pathology is a cornerstone to advancing the field. Indeed, there are many unanswered questions about the PTM code governing tau behavior; herein, I will focus on addressing the impact of polyamination, O-GlcNAcylation, and SUMOylation on the development of aggregates and pathological conformations of tau. This work will represent a significant step towards identifying how uncommon PTMs regulate tau behavior. An expanded view on tau PTMs is instrumental in guiding future efforts to develop therapies, diagnostics, and biomarkers for tauopathies.

CHAPTER 2: POLYAMINATION WITH SPERMIDINE ENHANCES PATHOLOGICAL TAU CONFORMATIONS WHILE REDUCING FILAMENTOUS AGGREGATE FORMATION *IN VITRO*

Abstract

Tau is subject to a broad range of post-translational modifications (PTMs) that regulate its biological activity in health and disease, including microtubule dynamics, aggregation, adoption of pathological conformations, and seeding. The most studied PTMs of tau are phosphorylation and acetylation; however, the salience of other less commonly studies PTMs of tau remains largely elusive. Tissue transglutaminase (TG) is an enzyme whose activity is elevated in Alzheimer's disease (AD). TG action on tau may lead to two potential outcomes: intramolecular and intermolecular cross-linking along with the incorporation of the cationic polyamines [e.g. spermidine (SPD)] onto glutamine resides (Q) of tau. Several studies posited that TG-catalyzed intermolecular cross-linking of tau induces the formation of insoluble tau aggregates. On the contrary, the effects of SPD polyamination on tau biology remain unexamined even though SPD levels are significantly elevated in AD. In this work, we describe a method to produce recombinant SPD-modified tau where SPD modifications take place on multiple Q residues mainly within the N-terminus. SPD modification does not significantly alter tau's binding to microtubules, but SPD-modified tau accelerates microtubule polymerization. We hypothesize that the regulation of tau N-terminus by SPD polyamination enhances microtubule polymerization. Further biochemical and biophysical testing showed that SPD polyamination of tau markedly reduces tau aggregation into filamentous aggregates. In addition, the reduction in filamentous structures is accompanied by lower β-sheet content and seeding capability of tau aggregates. Furthermore, SPD modification promotes the adoption of pathological conformations (e.g. oligomerization and misfolding) by tau with or without aggregation. Therefore, further testing is warranted to determine

when the increase in pathological tau conformations by SPD polyamination will results in cellular dysfunction. Taken together with previous in vivo studies on polyamine stress response, these data suggest that SPD polyamination of tau favors the formation of off-pathway multimers that adopt pathological conformations rather than on-pathway filamentous aggregates.

Introduction

Alzheimer's disease (AD), in addition to other tauopathies, is characterized by the accumulation of abnormal forms of tau protein in intracellular inclusions (e.g. neurofibrillary tangles) that are closely associated with the progression of cognitive symptoms (Arriagada et al., 1992; Brier et al., 2016; Gomez-Isla et al., 1997; Gotz et al., 2019; Guillozet et al., 2003; Jack et al., 2010; Malpetti et al., 2022; Tanner & Rabinovici, 2021; Wilcock & Esiri, 1982). Tau protein is produced as six main isoforms within the human brain (Park et al., 2016). Some tau isoforms harbor four (4R) or three (3R) of the microtubule-binding repeats (MTBRs) and either two, one, or no N-terminal acidic inserts (2N, 1N, and 0N) (Alhadidy & Kanaan, 2024). Depending on the type of tauopathy, aggregates of tau may comprise 3R tau isoforms [e.g. Pick's disease (PiD)], 4R isoforms [e.g. progressive supranuclear palsy (PSP) and corticobasal degeneration (CBD)], or 4R/3R isoforms [e.g. AD and chronic traumatic encephalopathy (CTE)] (Wang & Mandelkow, 2016; Zhang et al., 2022).

In addition to abnormal tau aggregation, several aberrations in cellular functions take place and lead to neurodegeneration in tauopathies (Silva & Haggarty, 2020). Examples of such aberrations include synaptic dysfunction, dysregulated axonal transport, failure of protein degradation and clearance, mitochondrial dysfunction, and neuroinflammation among others (Chen et al., 2018; Colnaghi et al., 2019; Henley et al., 2014; Mao et al., 2022; Matsuzaki et al., 2015; Schorova & Martin, 2016; Silva & Haggarty, 2020; van Niekerk et al., 2007; Wang et al., 2021). The exact mechanisms through which tau contributes to cellular dysfunctions in tauopathies is an active area of investigation. Indeed, tau undergoes conformational alterations linked to cellular

dysfunctions, toxicity, and neurodegeneration under disease conditions (Alhadidy & Kanaan, 2024).

Oligomerization is a conformational change of tau that emerges early in tauopathies and contributes to several cellular dysfunctions such as disruption of intracellular transport, impairment of protein degradation, synaptic dysfunction, and dysregulated cellular bioenergetics (Cox et al., 2016; Kanaan et al., 2016; Lasagna-Reeves et al., 2012; Maeda et al., 2007; Maeda et al., 2006; Niewiadomska et al., 2021; Patterson et al., 2011). In addition, tau adopts a conformation that involves excessive exposure of the phosphatase-activating domain (PAD) at the extreme N-terminus (Combs et al., 2016; Combs & Kanaan, 2017; Kanaan et al., 2011). Subsequently, hyperactivation of signaling pathway involving protein phosphatase 1 (PP1) and glycogen synthase kinase 3 β (GSK3β) leads to disrupted axonal transport (Kanaan et al., 2011; Morris & Brady, 2022; Mueller et al., 2021). The field also identified conformational changes of tau that mediate its aggregation and propagation along functionally connected brain circuitry (de Calignon et al., 2012; DeVos et al., 2018; Liu et al., 2012).

In a soluble state, tau is described as an “unfolded” protein that transiently assumes a global hairpin folds under native conditions (Jeganathan et al., 2006). The global hairpin conformation, also known as the paperclip conformation, is formed by the folding of tau’s C-terminus near the microtubule-binding region, and the N-terminus of tau folding over the C-terminus (Abraha et al., 2000; Jeganathan et al., 2006). Early during pathological tau aggregation, tau assumes a conformation different from the paperclip where the N-terminus of tau directly folds over the microtubule-binding region. This third conformational change is thought to represent a critical checkpoint along the path of tau

aggregation, and it is detected by the Alz50 and MC1 antibodies (Carmel et al., 1996; Jicha et al., 1997; Ksiezak-Reding et al., 1988).

Tau pathology propagates from one brain region to another through functionally connected brain regions (Goedert et al., 2017; Zhang et al., 2022). This process entails several steps where tau first transfers from a cell to another followed by seeding of tau pathology in the recipient cell (Clavaguera et al., 2009; de Calignon et al., 2012; Fu et al., 2016; Liu et al., 2012). More recently, the Diamond group proposed that tau assumes conformational ensembles that have different ability to seed aggregation (Mirbaha et al., 2018; Mirbaha et al., 2022; Sharma et al., 2018). The seeding-competent conformation is regulated by the aggregation prone motifs of tau spanning amino acids 275-VQIINK-280 and 306-VQIVYK-311 (Chen et al., 2019; Falcon et al., 2015). To date, the reported pathological conformations of tau are common in tauopathies suggesting similar events of conformational changes and toxicity under disease conditions (Alhadidy & Kanaan, 2024; Combs et al., 2016; Garcia-Sierra et al., 2003; Lasagna-Reeves et al., 2012; Mroczko et al., 2019; Niewiadomska et al., 2021; Patterson et al., 2011; Weaver et al., 2000).

Our understanding of the factors driving the adoption of pathological conformations by tau concurrently underwent tremendous progress (Alhadidy & Kanaan, 2024). Tau mutations linked to familial frontotemporal dementia regulate the adoption of pathological conformations by tau (Goedert & Spillantini, 2000). For instance, the P301L mutations enhances oligomerization and induces PAD exposure leading to disruption of axonal transport through the PP1- GSK3β pathway (Combs et al., 2021; Kanaan et al., 2020). Furthermore, the S320F mutation induces a seeding-competent conformation of tau

(Chen et al., 2023). Another factor that regulates the formation of pathological tau conformations is tau-protein interactions (Pires & Drummond, 2021). Proteins such as heat shock protein 90 and Bassoon enhance tau oligomerization and seeding capability, respectively (Martinez et al., 2022; Tortosa et al., 2009; Weickert et al., 2020). Furthermore, evidence suggests that post-translational modifications (PTMs) of tau are also potential modulators of pathological tau conformations in health and disease (Alhadidy & Kanaan, 2024).

PTMs take place on all domains of tau protein, and they alter several aspects of tau biology as demonstrated in cell lines, animal models, and human tauopathies (Alhadidy & Kanaan, 2024; Alquezar et al., 2020; Cook, Stankowski, et al., 2014; Park et al., 2018). In fact, PTMs of tau regulate its microtubule dynamics, clearance through the proteasomal and autophagic pathways, and aggregation propensity (Cook, Carlomagno, et al., 2014; Gorsky et al., 2017; Luo et al., 2014; Man et al., 2023; Park et al., 2018; Puangmalai et al., 2022). In addition, disease-relevant PTMs have the capacity to alter the adoption of pathological conformations by tau (Christensen et al., 2023; Man et al., 2023; Park et al., 2018; Strang et al., 2019; Xia et al., 2020). For example, phosphorylation within the AT8 epitope region of tau increases oligomerization, PAD exposure, and misfolding (Christensen et al., 2023; Jeganathan et al., 2006; Kanaan et al., 2020). In addition, acetylation of tau may enhance its seeding competency and transmissibility from cell to another (Tseng et al., 2021). Phosphorylation and acetylation are the most thoroughly investigated PTMs of tau, and several therapeutic strategies that modulate these two PTMs are currently under investigation in clinical trials (Alhadidy & Kanaan, 2024; Congdon & Sigurdsson, 2018). However, the effects of less common

PTMs such as SUMOylation, glycosylation, and polyamination are not well known (Alquezar et al., 2020; Gong et al., 2016; Ivanov et al., 2020; Luo et al., 2014). This limitation creates important gaps in our understanding of tau biology and pathogenesis of tauopathies.

Tissue transglutaminase (TG) is an enzyme expressed in the central nervous system and plays a potential role in the development of AD and other tauopathies (De Vivo et al., 2009). Several studies demonstrated that tau is subject to the catalytic action of TG (Dudek & Johnson, 1993; Halverson et al., 2005; Miller & Johnson, 1995; Murthy et al., 1998; Zemaitaitis et al., 2000). TG-catalyzed reactions may lead to one of two outcomes: crosslinking between glutamine (Q) and lysine (K) residues and/or incorporation of polyamines [e.g. putrescine, spermidine (SPD), and spermine] onto Q residues (Dudek & Johnson, 1993; Miller & Johnson, 1995; Murthy et al., 1998). Interestingly, the activity and expression levels of TG are elevated in the prefrontal cortex of AD patients compared to controls (G. V. Johnson et al., 1997). Furthermore, the TG-catalyzed crosslinks are detectable in tau purified from the brains of AD patients and P301L mice (Halverson et al., 2005; Wilhelmus et al., 2009). *In vitro* studies determined that cross-linking of tau involves Q6, Q88, Q124, Q244, Q276, Q288, Q351, and Q424 (Murthy et al., 1998). Depending on whether cross-linking of tau is intramolecular or intermolecular, tau may or may not form misfolded filamentous structures (Dudek & Johnson, 1993; Konno et al., 2005). Despite the extensive work on the impact of TG-catalyzed crosslinking on tau, the other potential outcome of polyamine incorporation onto Q residues of tau is a nascent area of investigation.

Polyamines are polycationic amines universally present in all types of living cells (Bae et al., 2018). The major polyamines in eukaryotic cells are spermine, SPD, and putrescine; they are essential for normal cellular functioning and survival (Igarashi & Kashiwagi, 2019; Park & Igarashi, 2013). In AD, two reports indicated that SPD levels are significantly elevated in the brain (Inoue et al., 2013; Morrison & Kish, 1995). Moreover, work conducted by the Lee group utilizing several mouse models of tauopathy is strongly suggestive of a polyamine stress response that enhances the progression of tau pathology (Hunt et al., 2015; Sandusky-Beltran et al., 2019; Sandusky-Beltran et al., 2021). Nonetheless, the impact of SPD incorporation onto Q residues of tau on its physiological functions, aggregation, and conformational changes linked to toxicity and neurodegeneration in tauopathies remains completely unknown.

Herein, we describe a method to produce recombinant SPD-modified 2N4R (SPD hT40) and 2N3R (SPD hT39) tau isoforms using an *in vitro* polyamination reactions catalyzed by TG. A set of biochemical and biophysical assays were employed to determine the impact SPD polyamination has on tau's ability to bind or polymerize microtubules, adopt pathogenic conformations, and aggregate *in vitro*. SPD polyamination of tau enhanced the polymerization of microtubules *in vitro*. In addition, SPD-modified hT40 enhanced pathological tau conformations and decreased filamentous tau structures upon aggregation. SPD modification of hT39 favored relatively large globular aggregates and increased the formation of pathological tau conformations. We hypothesize that SPD polyamination of tau may contribute to the pathogenesis of tauopathies by increasing the formation of microtubule labile ends and enhancing the formation of pathological tau conformations at the expense of filamentous aggregates.

Materials and Methods

Preparation of recombinant unmodified and SPD-modified tau proteins

Recombinant tau protein was prepared from a 4L bacterial culture as described previously (Combs et al., 2017), with the exception that BL21 bacteria (NEB, #C2527H) were used. At the end of the purification procedure, the concentration of recombinant tau protein was determined using the BCA method (Thermo, # A53225) before starting the polyamination reaction with SPD. Polyamination reactions were performed *in vitro* using a method like that reported by Song and coworkers (Song et al., 2013). Briefly, SPD at 8 mM (Sigma, # S2626-1G) and TG enzyme (Sigma, # TS398) at 0.2 μM were added to tau in reaction buffer (50mM Tris HCl, pH 8, 10 mM calcium chloride and 5 mM DTT) followed by a 1-hour incubation at 37 °C. Unmodified tau proteins were subjected to the same reaction conditions, but TG was excluded. Then, the TG enzyme was inactivated by heating at 70 °C for 2 min. The TG-catalyzed reaction produces SPD-modified monomeric proteins as well as intra- and inter-protein crosslinked proteins. Thus, the SPD-modified tau was further purified by passing the polyamination reaction through 100 kDa MWCO Amicon filter (0.5 ml; Millipore, # UFC510096) to remove inter-protein crosslinked tau (i.e. high molecular weight species) from the sample (Figure AI.1). Unmodified tau proteins were subjected to the same process of passing through a 100 kDa MWCO concentrators. The flow-through (FL) was collected for further purification. Each concentrator membrane was washed with 6 rounds of 400 μl of buffer A (500 mM NaCl, 10 mM Tris, and 5 mM Imidazole pH 8). All the FL samples were pooled and subsequently desalted through HiPrep 26/10 desalting column (Cytiva, #17508701) to fully buffer exchange the samples into Buffer A using fast protein liquid chromatography

(FPLC). A desalting column was equilibrated with 5 column volumes (CVs) of buffer A, then protein samples were run over the column in 5 CVs of buffer A at a flow rate of 5 ml/min and fractions containing tau were collected. Finally, heavy metal affinity chromatography was used to purify the tau proteins (6x His tagged) from other proteins in the polyamination reaction (e.g. TG) using a 5ml HiTrap Talon crude column (Cytiva, #28953767). The HiTrap Talon column was equilibrated in 5 CVs of buffer A, the proteins were run over the column, the column was washed with 5 CVs of buffer A, and then tau proteins were eluted in 10 CVs of buffer B (81 ml of buffer A supplemented with 19 ml of 500 mM imidazole buffer pH 8 along with 40 µl of 500 mM PMSF stock) at flow rate of 3 ml/min in 5 ml fractions. The elution fractions containing the highly purified monomeric tau bands were concentrated to a concentration between 2-4 mg/ml and was supplemented with 1 mM DTT. The final unmodified and SPD-modified tau proteins were aliquoted and frozen at -80 °C. The final concentration of recombinant tau proteins was determined using the SDS-Lowry method as described previously in (Combs et al., 2017).

Western blot validation of recombinant tau proteins

To confirm the polyamination status of recombinant tau proteins, 0.5 µg was loaded on 4-20% TGX gels (Biorad, # 5671095) and run at 250 V for 32 min, followed by transfer onto nitrocellulose membrane using the Biorad wet transfer system at 40 mAmp for 50 min. The membrane was then blocked with 2% non-fat dry milk (NFDM) in 1X tris buffer saline (TBS) for 1 hour at room temperature followed by incubation in primary antibodies overnight at 4 °C. Primary antibodies used were Tau5 (Nicholas M. Kanaan at Michigan State University, RRID: AB_2721194) (Carmel et al., 1996; LoPresti et al., 1995; Porzig et al., 2007) at 1:100,000 in 2% NFDM and anti-spermine (Abcam, # ab26975,

RRID: AB_470871, cross reacts 100% with SPD) at 1:2,000 in 2% NFDM. The following day, the blot was washed 3 times (5 min each) with 1X TBS supplemented with 0.1% Tween 20 (TBS-T 0.1%). Then, secondary antibodies in 2% NFDM were added for 1 hour at room temperature. Secondary antibodies used were goat anti-mouse IgG1 680 (LI-COR Biosciences, # 926-68050, RRID: AB_2783642) at 1:20,000 and goat anti-rabbit IgG 800 (LI-COR Biosciences, # 926-32211, RRID: AB_621843) at 1:20,000. The blot was then washed 3 times (5 min each) with TBS-T 0.1%. LI-COR Odyssey classic imager and Image Studio Lite Ver 5.2 were used to visualize the blots.

Recombinant tau protein preparation for tandem Mass spectrometry

Unmodified and SPD-modified tau proteins were digested using a combination of trypsin (Promega, #V5280) and rLysC (Promega, #V167A). First, each recombinant tau protein sample (3 µg) was subjected to 5 rounds of buffer exchange with 25 mM ammonium bicarbonate (AmBic) pH 8 using 0.5 ml Amicon filter with 3K MWCO (15,000 RCF for 10 min; Millipore, # UFC500396). Then, recombinant tau proteins were recovered from the filter by centrifugation at 15,000 RCF for 2 min and vacuum dried using Vacufuge. The dried pellets of recombinant tau proteins were reconstituted in 50ul of digestion buffer (12.5 mM AmBic pH 8 + acetonitrile (ACN) 50%) and incubated at 37 °C for 90 min with rLysC (150 ng of enzyme per 3 µg of recombinant protein). Then, trypsin was added (300 ng of enzyme per 3 µg of recombinant protein) and incubated at 37 °C for 16-18 hours. The following day, digested protein samples were subjected to vacuum drying and stored at -20 °C until running on mass spectrometry (MS).

Tandem MS of recombinant tau proteins

We used Thermo Scientific Ultimate 3000 RSLCnano System coupled with nanoscale liquid chromatography for analysis. Desalting of digested peptides was conducted in-line using a 3 μm diameter bead, C18 Acclaim PepMap trap column (75 μm × 20 mm) with 2% ACN, 0.1% formic acid (FA) for 5 min at a flow rate of 2 μl/min at 40 °C. The trap column was then brought in line with a 2 μm diameter bead, C18 EASY-Spray column (75 μm × 250 mm) for analytical separation over 128 min with a flow rate of 350 nl/min at 40 °C. The mobile phase included two buffers: 0.1% FA (Buffer A) and 0.1% FA in ACN (Buffer B), and a gradient was used for separation as follows: 12.5 min desalting, 95 min 4–40% B, 2 min 40–65% B, 3 min 65–95% B, 11 min 95% B, 1 min 95–4% B, 3 min 4% B. We injected 1 μg of each sample for analysis. Top 20 data-dependent mass spectrometric analysis was performed with a Q Exactive HF-X Hybrid Quadrupole-Orbitrap Mass Spectrometer. MS1 resolution was 60K at 200 m/z with a maximum injection time of 45 ms, AGC target of 3e6, and scan range of 300–1500 m/z. MS2 resolution was 30K at 200 m/z, with a maximum injection time of 54 ms, AGC target of 1e5, and isolation range of 1.3 m/z. High-energy collision dissociation (HCD) normalized collision energy was 28. Only ions with charge states from +2 to +6 were selected for fragmentation, and dynamic exclusion was set to 30 s. The electrospray voltage was 1.9 kV at a 2.0 mm tip to inlet distance. The ion capillary temperature was 280 °C and the RF level was 55.0. All other parameters were set as default.

MS data analysis to determine SPD modification sites

RAW data files were analyzed with the MetaMorpheus software version 1.0.1 developed by the Smith laboratory (Miller et al., 2023). For hT40 proteins, the following

FASTA files used were downloaded from Uniprot (November 2021) and used for analysis: Escherichia coli (strain K12) (UP000000625), trypsin (Q29463), Lys-C (Q02SZ7), and full-length tau sequence (2N4R isoform, P10636-8). The same FASTA files were used to analyze the hT39 proteins using with 2N3R tau isoform sequence (P10636-5) instead of the 2N4R sequence. Mass shift corresponding to the non-acetylated SPD were used to search for modifications: +128.1313485 for SPD (Schopfer et al., 2024; Yu et al., 2015). In addition, fragmentation pattern of SPD was determined by running SPD alone on MS. Mass-to-charge-ratios (m/z) corresponding to diagnostic ions (DIs) were identified: 54.048, 57.059, 71.075, 111.109, 128.132. The search parameters for SPD modification included both mass shift and the identified diagnostic ions of SPD.

The analysis sequence included mass calibration, global post-translational modification discovery (G-PTM-D) (Li et al., 2017), and a classic search. Mass calibration was conducted using the following criteria: protease = trypsin; maximum missed cleavages = 2; minimum peptide length = 7; maximum peptide length = unspecified; initiator methionine behavior = Variable; variable modifications = Oxidation on M; max mods per peptide = 2; max modification isoforms = 1024; precursor mass tolerance = ±15.0000 ppm; product mass tolerance = ±25.0000 ppm. The criteria utilized for G-PTM-D were protease = trypsin; maximum missed cleavages = 2; minimum peptide length = 7; maximum peptide length = unspecified; initiator methionine behavior = Variable; max modification isoforms = 1024; variable modifications = Oxidation on M; G-PTM-D modifications count = 3; precursor mass tolerance(s) = ±5.0000 ppm around 0 ,128.131348525 Da; product mass tolerance = ±20.0000 ppm. Finally, a classic search was conducted using the following criteria: protease = trypsin; search for truncated

proteins and proteolysis products = False; maximum missed cleavages = 2; minimum peptide length = 7; maximum peptide length = unspecified; initiator methionine behavior = Variable; variable modifications = Oxidation on M; max mods per peptide = 2; max modification isoforms = 1024; precursor mass tolerance = ±5.0000 ppm; product mass tolerance = ±20.0000 ppm; report peptide spectral match (PSM) ambiguity = True. SPD polyamination site of tau detected at a false discovery rate of 1% are reported. MetaDraw version 1.0.5 was utilized to review the PSMs of modified and unmodified tau peptides (samples of these peptides are included in Figure AI.2 and AI.3).

Tubulin polymerization assay

Tubulin polymerization in the presence of recombinant tau proteins was assessed using the Tubulin Polymerization Assay Kit (Cytoskeleton, #BK011P). Kit reagents were reconstituted and stored as indicated in the manual. The assay began by incubating the 96-well plate provided with the kit at 37 °C for 10 min (Synergy H1 Hybrid Multi-Mode Reader and Gen5 software v3.11, BioTek). Recombinant tau proteins were prepared as 10 µM stocks in general tubulin buffer (80 mM PIPES pH 6.9, 2 mM $MgCl_2$, and 0.5 mM EGTA) and left at room temperature. Then, tubulin master mix was prepared and kept on ice using the recipe for enhancer detection: 355 µl of Buffer 1, 4.4 µl of 100 mM GTP, and 85 µl of tubulin 10 mg/ml. Once the 10-min incubation of the 96-well plate was over, recombinant tau proteins (10 µM stocks) were added (5 µl/well) to the plate and warmed up to 37 °C for exactly 1 min. Then, the tubulin master mix was added (50 µl/well) yielding a final tau concentration of 1 µM. Fluorescence signal was measured for 1 hour to monitor tubulin polymerization using the kinetic mode at excitation and emission wavelengths of 360 nm and 450 nm, respectively. Each tau protein sample was loaded in duplicate

(technical replicates) and the experiment was performed 4 independent times (biological replicates). Background levels of blank (general tubulin buffer only) were subtracted from the fluorescence readings before further analyzing the data. Nonlinear regression using "specific binding with Hill slope" was used to fit the tubulin polymerization data in GraphPad Prism v10.2.1 and calculate the steady state equilibrium (V_{max}) along with the time to half maximal polymerization (K_d).

Microtubule-binding assay

Assays were performed using Microtubule Binding Protein Spin-Down Assay Biochem Kit (Cytoskeleton, # BK029). Kit reagents were reconstituted as indicated in the manual. Tubulin aliquots (20 µl) were thawed, supplemented with cushion buffer (2 µl; 80 mM PIPES pH 7.0, 1 mM $MgCl_2$, 1 mM EGTA, and 60% sucrose), and incubated at 35 °C for exactly 40 min. Then, general tubulin buffer (200 µl; 80 mM PIPES pH 7.0, 1 mM $MgCl_2$, and 1 mM EGTA) supplemented with paclitaxel at 20 µM was added to the polymerized tubulin. Microtubule-binding reactions were set up at room temperature including tubulin (20 µl, 2 µM tubulin dimer), recombinant tau proteins (0.5 µM), and general tubulin buffer to a final volume of 50 µl. After 30 min of incubation at room temperature, binding reactions were then loaded on 100 µl of sucrose cushion buffer in 0.2 ml polycarbonate tubes (Thermo Scientific, # 45233) followed by centrifugation at 100,000 RCF for 40 min. For all centrifugation steps, S100-AT3 Fixed Angle Rotor (Thermo Scientific, # 45585) and Sorvall™ MTX 150 Micro-Ultracentrifuge (Thermo Scientific, # 46960) were employed. Then, 30 µl of the supernatant was carefully removed to avoid disturbing the microtubule pellet. Laemmli buffer was added to the supernatant immediately (6µl of 6X Laemmli buffer). The rest of the supernatant was discarded,

followed by washing the microtubule pellet with general tubulin buffer (100 µl) supplemented with 20 µM paclitaxel. The microtubule pellet was subjected to centrifugation at 100,000 RCF for an additional 20 min. The previous washing step was repeated one more time, followed by careful removal of the supernatant. The final pellet was resuspended in 60 µl of 1X Laemmli buffer. The assay was conducted 4 independent times.

For each biological replicate, the supernatant and pellet (15 µl each) fractions were subjected to SDS-PAGE. Unmodified and SPD-modified tau samples were loaded on two separate 4-20% Novex tris-glycine gels (Invitrogen, # WXP42020BOX) that was run at 225 V for 45 min. After SDS-PAGE, the two gels were cut between the 250 and 37 kDa marker bands and added to the same transfer cassette to transfer onto a nitrocellulose membrane. This step allows for the quantification of all tau bands on the same blot to minimize the variability in blotting procedure across samples. The rest of the blotting procedure was performed as described earlier. Primary antibodies used were the Tau5 antibody at 1:100,000 and the tubulin 5H1 antibody at 1:5,000 (Nicholas M. Kanaan at Michigan State University, RRID: AB_2832941) (Wang et al., 1993). Secondary antibodies used were goat anti-mouse IgG1 680 and goat anti-mouse IgM 800 (LI-COR Biosciences, # 926-32280, RRID: AB_2814919) at 1:20,000 each. LI-COR Odyssey classic imager and Image Studio Lite Ver 5.2 were used to visualize fluorescent signals of the antibody probes. Tau bands were quantified in all supernatant and pellet fractions followed by calculating the percentage of tau in pellet relative to total tau using the following equation:

$$\% \text{ Tau in Pellet} = \text{Tau in Pellet} / (\text{Tau in Pellet} + \text{Tau in Sup}) \times 100$$

In vitro recombinant tau aggregation reaction

Aggregation of different tau proteins was induced by arachidonic acid (ARA; Cayman Chemical, # 90010) in 200 µl reactions as described previously (Gamblin, King, Kuret, et al., 2000; Tiernan et al., 2016). Briefly, 2 µM of tau (M. Wt. = 43426 for hT39; M. Wt. = 46673 for hT40) was induced to aggregate *in vitro* by incubation in tau aggregation buffer (10 mM sodium HEPES, 0.1 mM EDTA, 200 mM NaCl, 5 mM DTT, pH 7.6) with (aggregated) or without (unaggregated; ethanol vehicle was used) 75 µM ARA. ARA stocks were prepared in 100% ethanol at 2 mM immediately prior to use and kept on ice. Finally, ARA was added as the final component in the reaction sample and then the samples were gently mixed by minimally shaking the tube/cuvette. Aggregation reactions were incubated at room temperature for 6 hours.

Right angle laser light scattering

The right-angle laser light scattering (LLS) assay measures tau aggregation kinetics over time (Gamblin, King, Dawson, et al., 2000; Tiernan et al., 2016). LLS was measured using class IIb laser with wavelength of 475 nm and maximum power of 20 mW (B & W INC., model # BWI-475-20-E) and digital camera (Thor Labs, model # DCC1240M). Images were acquired using uc480 Viewer version 4.2 with the pixel clock set at 11 MHz. Images were acquired for hT40 samples at a frame rate of 2 fps and exposure of 250 ms, while a frame rate of 1 fps and exposure time to 300 ms was used for hT39 samples. Polymerization reactions of tau were transferred into glass cuvettes with path length of 5 mm (Starna Cells, #3-G-5), and laser light scattering was measured at time zero prior to addition of ARA to obtain baseline measurements. After addition of ARA and gently mixing the samples, images were serially acquired at 1, 2, 3, 4, 5, 10, 15,

20, 25, 30, 35, 40, 45, 50, 55, 60, 75, 90, 105, 120, 150, 180, 240, 300, and 360 min. Each experiment was conducted 4 independent times. Image analysis was performed with Adobe Photoshop CS6 (Adobe Systems INC.) using the marquee tool. The region of interest used for densitometry measurements was set to 150 pixels X 15 pixels and adjusted to the center of the glass cuvette within the band of scattered light. Pixel intensity was recorded using the histogram feature. Scattered light intensity (intensity) measurements during the 6 hours were fitted using nonlinear Gompertz function (Cox et al., 2016; Necula & Kuret, 2004; Sun & Gamblin, 2009; Winsor, 1932):

$$Y=a*\exp(-\exp(-((x-t_i)/b)))$$

The Gompertz equation describes polymerization kinetics using the following three parameters (Necula & Kuret, 2004; Winsor, 1932): a is the maximum light scattering at equilibrium; $b = 1/k_{app}$, where k_{app} is the proportional growth rate of the filament population in units of $time^{-1}$. Lag times, defined as time before detectable polymerization occurs, were calculated as $t_i - b$.

Thioflavin S fluorescence

At the end of the tau aggregation reaction with ARA (described above), β-sheet containing aggregates were quantified using a thioflavin S (ThS) assay as described (Cox et al., 2016; Tiernan et al., 2016). Immediately before starting the assay, a 0.0175% ThS solution was prepared in water, filtered through a 0.22 μM membrane, and protected from light. Then, 150 μl of each tau sample was mixed with 6 μl of ThS solution and incubated for 5 min at room temperature. The samples (150 μl/well) were then loaded onto a black walled 96-well plate (Costar, # 3915) and immediately read using the Promega Glomax multi-detection system at 490 nm excitation and 510-570 nm emission wavelengths.

Control buffers for unaggregated and aggregated reactions were also loaded and read to obtain background measurements, then their absorbance values were subtracted from the tau sample values.

Sample preparation for imaging with transmission electron microscopy

Transmission electron microscopy (TEM) allows for the visualization of and measurement of tau aggregates (Tiernan et al., 2016). To this end, uranyl acetate (UA; Electron Microscopy Sciences, # 22400) solution was freshly prepared by dissolving 20 mg of UA in 1 ml of deionized water (DIW) (2% UA solution) at room temperature. After UA completely dissolves into DIW, the solution was sterile filtered using 0.22 μM membrane (Fisher Scientific, # 13-1001-06). To prepare the grids, each unaggregated and aggregated tau sample (10 μl) was first fixed with 2% glutaraldehyde (Electron Microscopy Sciences, # 16100) at room temperature for 10 min. Then, each sample (5 μl) was absorbed onto formvar-coated copper grids (Electron Microscopy Sciences, #FCF300-CU) for 1 minute, followed by one rapid rinse in DI water and another rapid rinse in UA solution. Finally, the grids were incubated with UA solution for 1 min at room temperature, then the solution was wicked away, and grids were left to dry for at least 1.5 hours before imaging. Grids were prepared from 4 independent experimental replicates of unaggregated and aggregated tau and imaged using JEOL JEM-1400 Plus electron microscope at 80 kV. Electron micrographs were captured and saved through AMT XR81 digital camera and AMT software version 602.6.

Quantitative TEM Measurements

For each grid, three images were captured at 5000X magnification for quantitative TEM. Electron micrographs were then processed using ImageJ v1.54 using a method like

that described by Tiernan and coworkers (Tiernan et al., 2016). First, the scale bar was adjusted at 373 pixels/800 nm. Then, images were smoothed 3 times to allow for the automatic thresholding to capture the visible tau aggregates. Finally, particle count and size (nm^2) along with the total area occupied by tau aggregates (% Area) were collected by the "Analyze Particles" command. For the "Analyze Particles" command, size was set at 0-infinity and circularity was set at 0-1. The data were prepared for analysis and graphing using GraphPad Prism v10.2.1. Frequency distribution plots using 700 nm^2-wide and 50 nm^2-wide bins for hT40 and hT39, respectively, were created. The sum of particles in 3 images/replicate was calculated and counted as 1 independent replicate, with a total of 4 independent replicates. The following populations of hT40 were plotted according to criteria like those reported by Tiernan et al. (Tiernan et al., 2016): < 700 nm^2 for globular aggregates only; 700-2100 nm^2 for globular aggregates > 700 nm^2 along with short filaments; 2100-5000 nm^2 for short filaments only; > 5000 nm^2 for long filaments only. Aggregates of hT39 were globular in nature and split into sizes smaller and larger than 450 nm^2.

Western blot for unaggregated and aggregated reactions

Unaggregated and aggregated tau samples were prepared for SDS-PAGE by diluting to 0.5 µM in 6X Laemmli sample buffer. Samples were boiled at 95 °C for 5 min, followed by vortexing and quick spin down. Samples (500 ng/lane) were loaded on 20-well 4-20% Novex tris-glycine gel (as described above). Proteins were transferred to nitrocellulose membrane using the Biorad wet transfer system (as described above). The blot was blocked with 2% NFDM for 1 hour at room temperature, followed by incubation in Tau5 antibody at a dilution of 1:100,000 in 2% NFDM overnight at 4 °C. The following

day, the membrane was washed 3 times with TBST, 5 min each. The goat anti-mouse IgG1 680 secondary antibody was used at a dilution of 1:20,000 in 2% NFDM, and membranes were incubated in secondary at room temperature for 1 hour. Membranes were washed with TBST 3 times, 5 min each, before imaging the blot using LI-COR Odyssey classic imager and Image Studio Lite Ver 5.2. Tau bands corresponding to monomeric tau (monomer band) and higher molecular weight multimers (HMW band) were quantified in the unaggregated and aggregated tau samples.

Sandwich enzyme-linked immunosorbent assay (sELISA)

To detect pathological tau conformations using conformation-dependent antibodies (i.e. TOC1, TOMA1, TNT2, and Alz50), tau samples must be kept under native conditions (Castillo-Carranza, Sengupta, et al., 2014; Combs et al., 2016; Combs et al., 2017; Jicha et al., 1997; Ward et al., 2013). Therefore, sandwich ELISA assays were used to measure pathological tau conformations in 4 independent replicates. All steps were performed at room temperature. The following capture antibodies were used in sandwich ELISA assays: [TOC1 (Kanaan Lab, RRID: AB_2832939), TOMA1 (Millipore, #MABN819), TNT2 (Kanaan Lab, RRID: AB_2736931), and Alz50 (P. Davies Albert Einstein College of Medicine, New York, USA, RRID: AB_2313937) along with Tau13 (Kanaan Lab, RRID: AB_2721193) to measure total tau] (Carmel et al., 1996; Castillo-Carranza, Sengupta, et al., 2014; Combs et al., 2016; Combs & Kanaan, 2017; Garcia-Sierra et al., 2003; Hyman, Van Hoesen, et al., 1988; Jicha et al., 1997; Patterson et al., 2011; Ward et al., 2013). Capture antibodies were diluted in borate saline buffer (100 mM borate acid, 25 mM sodium borate, 75 mM NaCl, and 0.25 mM thimerosal) at 2 ng/µl. Then, sandwich ELISA plates (96-well plates, Corning, #3590) were coated with the

capture antibodies (50 µl/well) for 1 hour. Wells were then washed 2 times with ELISA wash buffer [200 µl/well; 100 mM borate acid, 25 mM sodium borate, 75 mM NaCl, 0.25 mM thimerosal, 0.4% (w/v) bovine serum albumin, and 0.05% (v/v) Tween-20], followed by blocking with 5% NFDM in ELISA wash buffer (200 µl/well) for 1 hour. Two washes with ELISA wash buffer were performed, followed by the addition of unaggregated and aggregated tau samples for 1.5 hours. Tau samples were prepared from unaggregated and aggregated hT40 reactions in TBS buffer at the following concentrations (50µl /well): 2.5 nM for Tau13; 5 nM for TNT2; 20 nM for TOC1 and Alz50; 150 nM for TOMA1. Tau samples were prepared from unaggregated and aggregated hT39 reactions in TBS buffer at the following concentrations (50 µl/well): 2.5 nM for Tau13; 40 nM for Alz50; 100 nM for TNT2; 150 nM for TOC1 and TOMA1. Then, wells were washed 4 times with ELISA wash buffer (200 µl/well). The detection antibody R1 (Kanaan Lab, RRID: AB_2832929) (Berry et al., 2004) was diluted at 1:10,000 in 5% NFDM and added to the wells (50 µl/well) for 1.5 hours. Then, sandwich ELISA wells were washed 4 times with ELISA wash buffer. Secondary antibody used was Goat Anti-Rabbit IgG Antibody (H+L), Peroxidase (Vector Laboratories, #PI-1000-1, RRID: AB_2916034) at 1:5,000 in 5% NFDM for 1 hour (50 µl/well). After 4 final washes with ELISA wash buffer, the peroxidase reaction was developed using 3,3′,5,5′-Tetramethylbenzidine (TMB; 50 µl/well; Sigma, # T0440). The peroxidase reaction was stopped with 4% sulphuric acid, followed by reading the absorbance at 450 nm using SpectraMax Plus 384 microplate reader (Molecular Devices). The absorbance values were further processed using GraphPad Prism v10.2.1. Using the following equation [$\%A = 100 - (100 * 10^{-A})$, where A is absorbance] to calculate

percentage light absorbed (% Light Abs). The % Light Abs is a linear scale as opposed to raw absorbance values (an inverse log scale).

Seeding assay in tau biosensor cells

The Diamond group produced HEK293 cells that stably express the 4R repeat domain of tau with the P301S mutation fused to CFP or YFP (Tau RD P301S Biosensor Cells; purchased from ATCC, #CRL-3275, RRID: CVCL_DA04) (Holmes et al., 2014). Cells were grown in DMEM (Gibco) supplemented with 10% FBS, 1% Penicillin-Streptomycin (Gibco), and 1x GlutaMAX (Gibco), and maintained at 37 °C and 5% CO_2. A cell aliquot was thawed and passaged at least once before use in experiments. Cells were plated at 12,000 cells/well in Poly-D-Lysine coated 96-well plates (100 µl media/well; Corning, #354461). After 24 hours, Lipofectamine 2000 (Invitrogen, # 11668027) was used to deliver the following treatment samples: unaggregated hT40, aggregated hT40 aggregates, unaggregated SPD-modified hT40, and aggregated SPD-modified hT40 (at a final concentration of 150 nM). In two separate tubes, Lipofectamine reagent or protein sample was diluted in OptiMEM (Gibco, # 31985062) and incubated at room temperature for 20 min. The first tube contained 1 µl Lipofectamine 2000 in addition to 9 µl OptiMEM, and the other tube contained 7.5 µl unaggregated or aggregated tau + 2.5 µl OptiMEM. Next, the Lipofectamine was mixed with the tau protein (20 µl) and incubated for an additional 20 min at room temperature. The Lipofectamine/protein mixture was then added to the cells (20 µl). Two days following treatment, cells were fixed with pre-warmed 4% paraformaldehyde (Electron Microscopy Sciences, # 15714-S) in 1X cytoskeleton buffer (10 mM MES, 138 mM KCl, 3 mM $MgCl_2$, and 4 mM EGTA, pH 6.1) for 20 min at

room temperature. Then, cells were washed 3 times with 1X TBS for 5 min each. The nuclear stain DAPI (1:10,000) was included in the first wash.

Cells were imaged using a Lionheart FX Automated Microscope (BioTek) using a 10x objective. Nine images per well were captured with GFP and DAPI filter cubes using the same acquisition settings. Images were processed and analyzed using Gen5 software v3.11 (BioTek). Seeded aggregates and nuclei were detected in the GFP and DAPI channels, respectively, using separate sets of size and pixel-intensity thresholds. For each well, the total number of aggregates was normalized to the total number of cells to obtain the number of seeds per cell (seeds/cell = number of GFP+ objects/number of DAPI+ objects).

Statistics

Statistical analysis was performed using GraphPad Prism v10.2.1. Unpaired, two-tailed unpaired t-test was employed to analyze the following results: V_{max} and K_d of tubulin polymerization assay; Lag time, k_{app}, and max LLS; % Area from quantitative TEM for hT40. Mann Whitney test was used (violation of normality) for % Area from quantitative EM for hT39. Two-way analysis of variance (ANOVA) followed by the post-hoc Holm-Sidak with all possible comparisons were used to analyze the following results: % Tau in pellet of microtubule-binding assay; ThS signal; Monomer and HMW bands for stable multimers; % Light Abs of sandwich ELISA assays; seeds/cell of seeding assay in RD cells. Differences in outcomes were deemed statistically significant at $p \leq 0.05$.

Results

In vitro polyamination produces SPD-modified tau on several Q residues throughout the different tau domains

Western blotting with anti-tau and anti-SPD antibodies confirmed the TG+SPD treated hT40 and hT39 proteins were polyaminated with SPD (Figure 2.1A and B). The control unmodified hT40 and hT39 did not show SPD signal, while all tau proteins were labeled with Tau5 (Figure 2.1A and B).

Next, MS was employed to provide additional insight into the specific Q residues modified by SPD in hT40 and hT39 proteins. MS results confirm that both SPD hT40 and SPD hT39 were polyaminated with SPD at several residues. Both proteins share similar modified Q residues throughout the tau protein, including residues Q6, Q26, Q49, Q88, Q124, and Q424 (Figure 2.1C). SPD modifications on Q33 and Q307 were only detected in SPD hT40 but not SPD hT39 (Figure 2.1C). Sample mass spectra of modified and unmodified versions of the tau peptide spanning amino acids 407-438 from the hT40 and hT39 protein preparations are demonstrated in Figure AI.2 and AI.3. It is noteworthy that the control unmodified hT40 and hT39 proteins did not show MS-based evidence of SPD modifications.

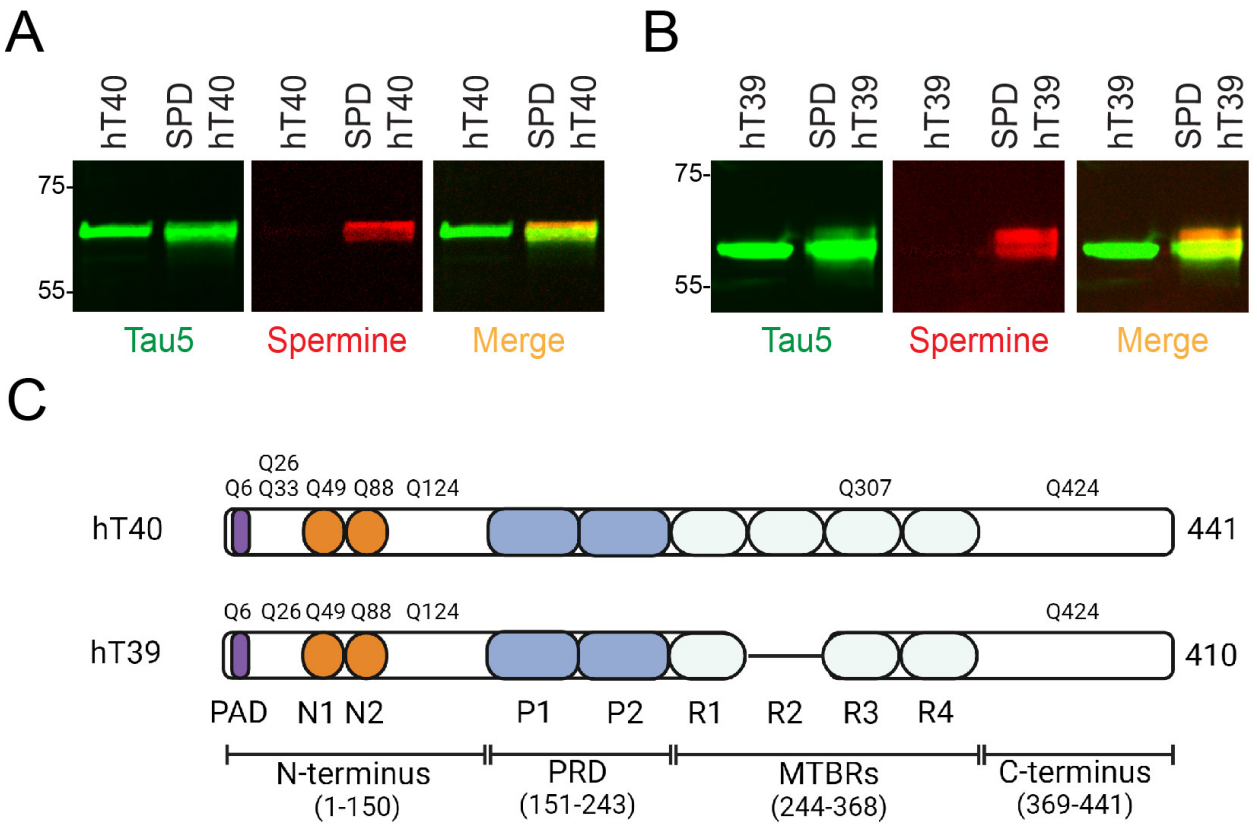

Figure 2.1. Identification of Q residues on tau modified with SPD.
A, western blot of SPD hT40 probed with the Tau5 (green) and Spermine antibodies (red). B, western blot of SPD hT39 probed with the Tau5 and Spermine antibodies. C, glutamine residues modified with SPD on tau as detected by mass spectrometry. Residues are numbered according to the sequence of full-length tau (hT40, 441 aa). Q6 is located with the phosphatase-activating domain–a domain of tau whose abnormal exposure is linked to dysregulation of axonal transport. Q49 and Q88 are located within the N1 and N2 acidic inserts, respectively. Q307 was detected within the MTBR of SPD hT40, but not SPD hT39. Q424 is located within the C-terminus of both SPD hT40 and hT39. Abbreviations: SPD, spermidine; Q, glutamine; hT40, 2N4R tau isoform; hT39, 2N3R tau isoform; PRD, proline rich domain; MTBRs, microtubule-binding repeats. Panel B created with BioRender.com.

SPD-modified tau accelerates microtubule polymerization in vitro

Tubulin polymerization assays were used to determine how SPD modification affects the ability of tau to modulate microtubule polymerization kinetics *in vitro* (Figure 2.2A and B). SPD-modified hT40 significantly decreased the time to half maximal

polymerization (Figure 2.2C; K_d, t = 3.115, p < 0.05), but did not affect the steady state equilibrium (Figure 2.2C; V_{max}, t = 1.675, p > 0.05) when compared to unmodified hT40. SPD-modified hT39 significantly decreased the time to half maximal polymerization (Figure 2.2D; K_d, t = 6.977, p < 0.05) and increased the steady state equilibrium (Figure 2.2D; V_{max}, t = 5.614, p < 0.05;) when compared to unmodified hT39.

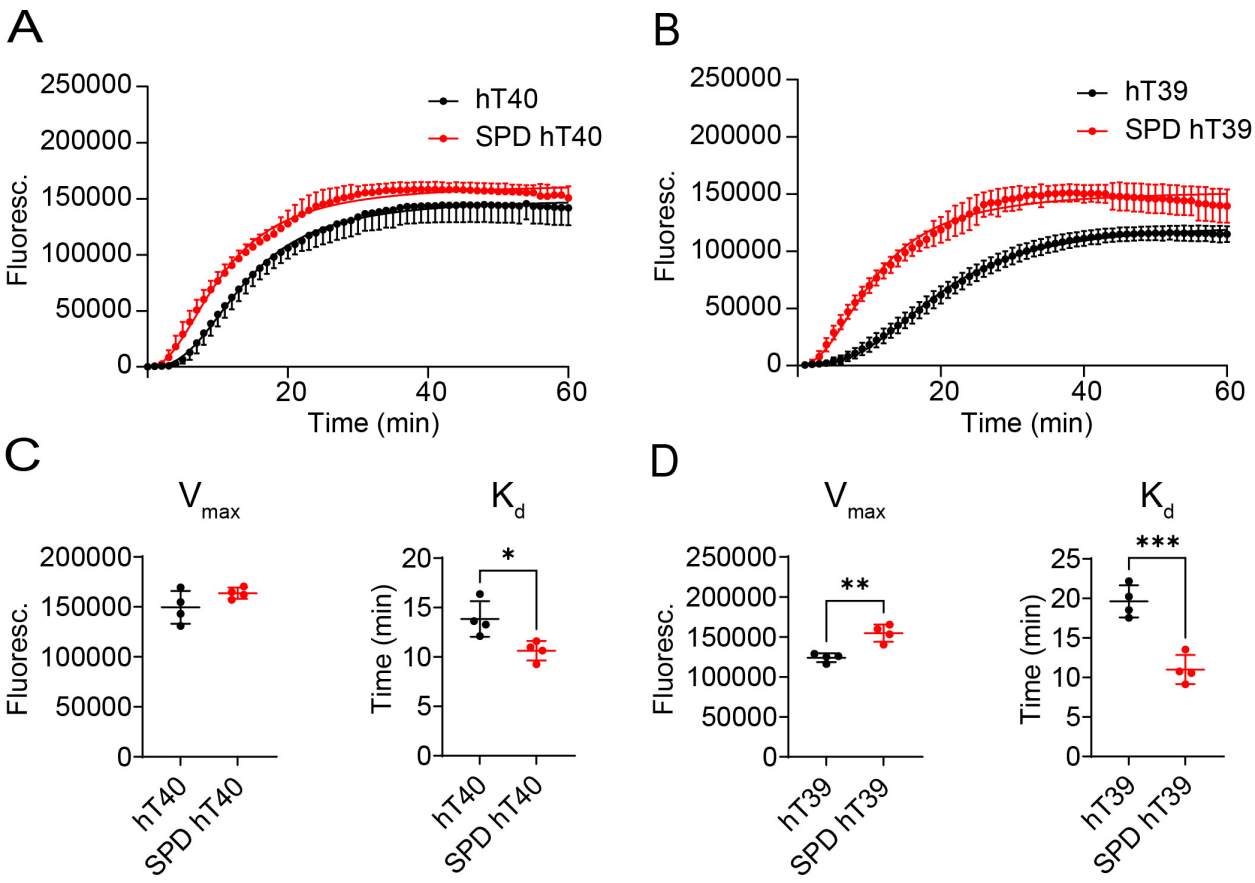

Figure 2.2. Polyamination of tau with SPD accelerates tubulin polymerization *in vitro*.
A, curve fit of fluorescence signal corresponding to microtubule polymerization in the presence of hT40 proteins over 60 min. B, curve fit of fluorescence signal corresponding to microtubule polymerization in the presence of hT39 proteins tau over 60 min. C, V_{max} of microtubule polymerization for unmodified hT40 and SPD hT40 proteins (left panel). K_d of microtubule polymerization for unmodified hT40 and SPD hT40 (right panel). D, V_{max} of microtubule polymerization for unmodified hT39 and SPD hT39 proteins (left panel). K_d of microtubule polymerization for unmodified hT39 and SPD hT39 (right panel).

Figure 2.2 (cont'd)
Abbreviations: SPD, spermidine; hT40, 2N4R tau isoform; hT39, 2N3R tau isoform; V_{max}, steady state equilibrium; K_d, time to half maximal polymerization. Data represented as mean +/- SD. * p≤0.05; ** p≤0.01; *** p≤0.001; **** p≤0.0001.

SPD modification of tau alters its ability to bind microtubules in vitro

Microtubule-binding assays were used to determine how SPD modification affects tau's ability to bind pre-formed microtubules. Experiments were conducted using either the hT40 or hT39 tau isoforms independently (Figure 2.3A and C). Two-way ANOVA revealed a significant main effect for tau in the microtubule fraction [$F_{(1,12)} = 2300$, $p < 0.05$]. Regardless of SPD modification status, post-hoc testing indicated a statistically significant increase in % tau in pellet for hT40 proteins (Figure 2.3B; $t = 32.44$, $p < 0.05$ for hT40; $t = 35.37$, $p < 0.05$ for SPD hT40).

Two-way ANOVA detected a statistically significant interaction between the PTM status of hT39 proteins and the microtubule fraction [$F_{(1,12)} = 7.304$, $p < 0.05$]. Regardless of SPD modification status, there was a significant increase in % Tau in pellet for hT39 proteins (Figure 2.3D; $t = 100.1$, $p < 0.05$ for hT39; $t = 103.9$, $p < 0.05$ for SPD hT39). Furthermore, the % of SPD-modified hT39 in the microtubule fraction was mildly (4.5%) but significantly higher than that of unmodified hT39 (Figure 2.3D; $t = 4.609$, $p < 0.05$).

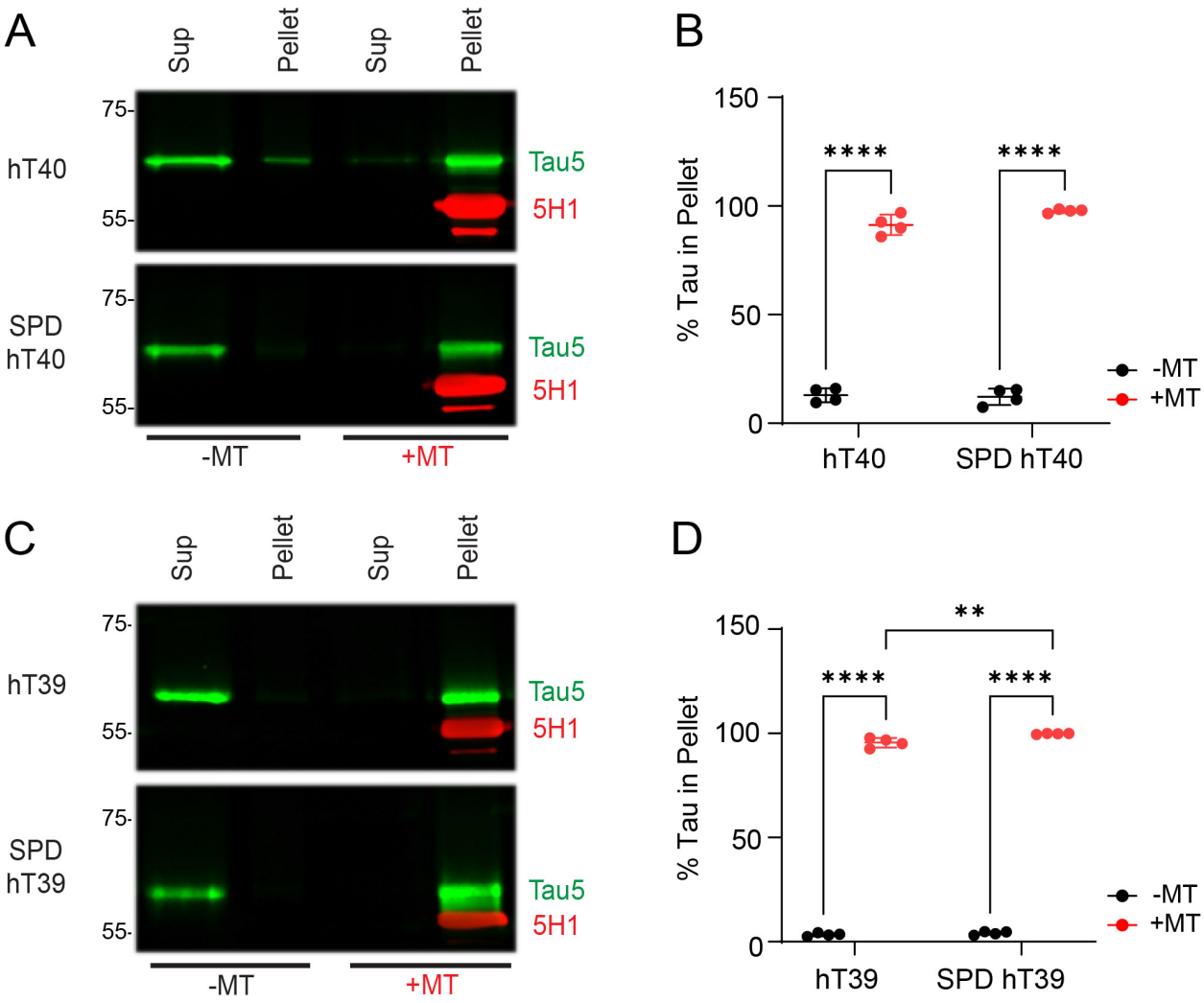

Figure 2.3. Polyamination of tau with SPD alters binding of tau to microtubules *in vitro*.

A, representative western blot of microtubule-binding assay for unmodified and SPD-modified hT40 proteins using Tau5 and 5H1 (tubulin) antibodies. B, quantification of the fraction of tau detected in the pellet of polymerized microtubules for unmodified and SPD-modified hT40. C, western blot of microtubule-binding assay for unmodified and SPD-modified hT39 proteins using Tau5 and 5H1 (tubulin) antibodies. D, quantification of the fraction of tau detected in the pellet of polymerized microtubules for unmodified and SPD-modified hT39. Abbreviations: SPD, spermidine; hT40, 2N4R tau isoform; hT39, 2N3R tau isoform; MT, microtubules; Sup, supernatant. Data represented as mean ± SD. * $p \leq 0.05$; ** $p \leq 0.01$; *** $p \leq 0.001$; **** $p \leq 0.0001$.

SPD modification of tau alters its aggregation kinetics in vitro

Right-angle LLS assays were used to determine the impact of SPD modification on the kinetics of tau aggregation *in vitro* (Figure 2.4A and B). We observed 18% reduction the maximum light scattering with SPD-modified hT40 compared to the unmodified hT40 (Figure 2.4G; $t = 6.796$, $p < 0.05$). Moreover, SPD modification slowed down the aggregation rate of hT40 by 45% (Figure 2.4D; $t = 9.276$, $p < 0.05$), with no difference in lag time (Figure 2.4C; $t = 1.152$, $p > 0.05$). On the other hand, SPD modification did not significantly change in the aggregation kinetics of hT39 protein (Figure 2.4E, F, and I; $t = 1.152$, $p > 0.05$ for lag time; $t = 0.1427$, $p > 0.05$ for k_{app}; $t = 1.814$, $p > 0.05$ for max).

SPD modification of tau reduces its β-sheet containing aggregates in vitro

ThS assays were performed at the end of aggregation reactions to determine the extent of β-sheet containing aggregate formation *in vitro*. Two-way ANOVA detected a statistically significant interaction between the PTM and aggregation of hT40 [$F_{(1, 12)} = 480.7$, $p < 0.05$] and hT39 [$F_{(1,12)} = 41.56$, $p < 0.05$] proteins. Upon aggregating hT40 and hT39 proteins, there was a significant increase in the ThS signal compared to their respective unaggregated samples regardless of the SPD modification [Figure 2.4H and J; $t = 87.64$, $p < 0.05$ for unmodified hT40; $t = 56.63$, $p < 0.05$ for SPD hT40; $t = 29.37$, $p < 0.05$ for unmodified hT39; $t = 20.25$, $p < 0.05$ for SPD hT39]. Of note, the SPD-modified aggregates of tau had significantly less ThS signal compared to the unmodified aggregated tau proteins (Figure 2.4H and J; $t = 31.85$ for hT40, $p < 0.05$; $t = 9.433$ for hT39, $p < 0.05$).

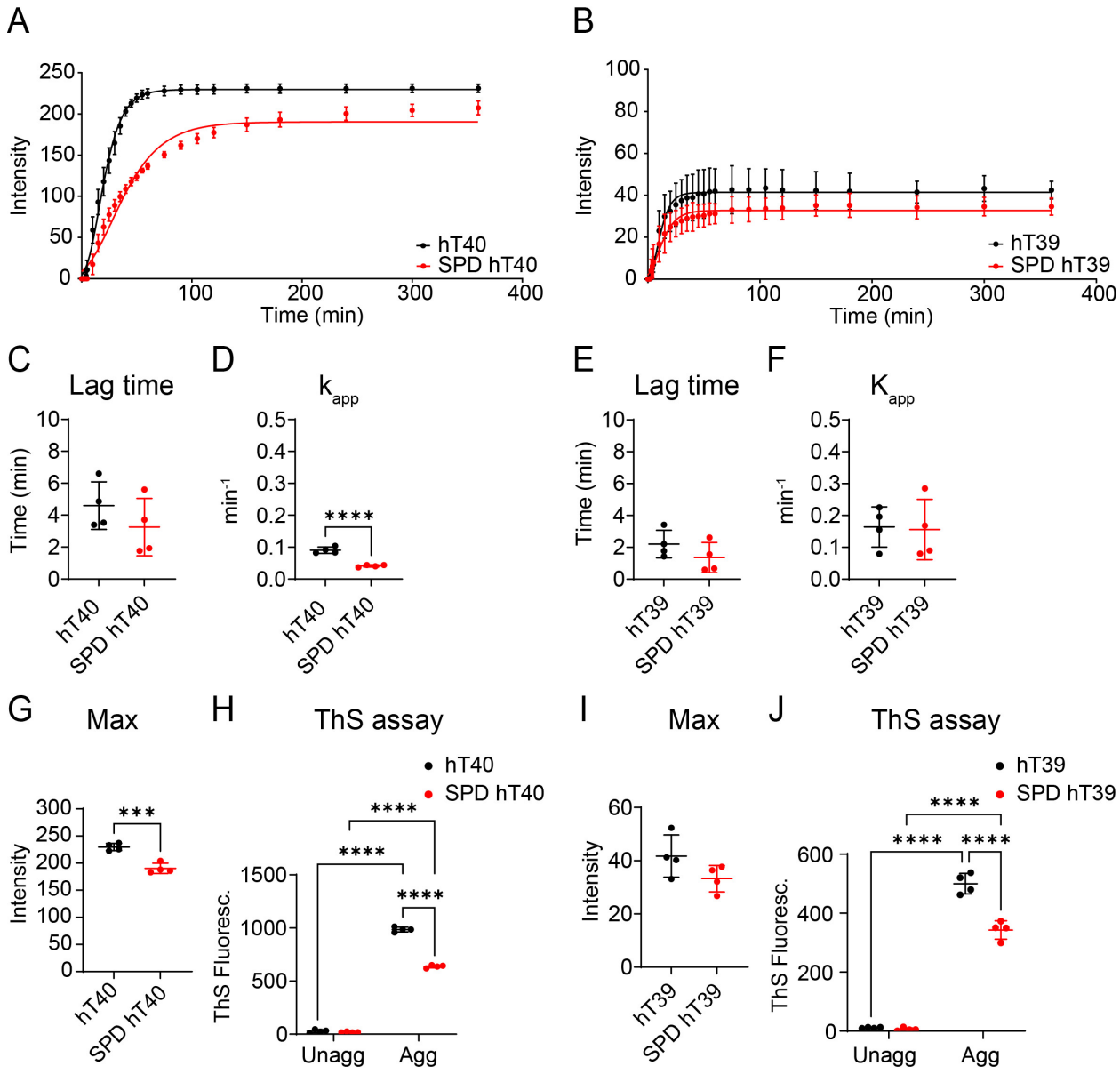

Figure 2.4. SPD modification decreases the rate and extent of tau multimerization, while reducing β-sheet containing aggregates *in vitro*.

A, LLS intensity of unmodified and SPD-modified hT40 proteins. B, LLS intensity of unmodified and SPD-modified hT39 proteins. C, lag time to aggregation for unmodified and SPD-modified hT40 proteins. D, k_{app} for unmodified and SPD-modified hT40 proteins. E, lag time to aggregation for unmodified and SPD-modified hT39 proteins. F, k_{app} for unmodified and SPD-modified hT39 proteins. G, max polymerization for unmodified and SPD-modified hT40 proteins. H, ThS fluorescence signal after 6 hours of tau aggregation for unmodified and SPD-modified hT40 proteins. I, max polymerization for unmodified and SPD-modified hT39 proteins. J, ThS fluorescence signal after 6 hours of tau aggregation for unmodified and SPD-modified hT39 proteins. Abbreviations: SPD, spermidine; hT40,

Figure 2.4 (cont'd)
2N4R tau isoform; hT39, 2N3R tau isoform; unagg, unaggregated; agg, aggregated; LLS, laser light scattering; ThS, thioflavin S; kapp, rate of tau multimerization; max, maximum light scattering. Data represented as mean ± SD. * p≤0.05; ** p≤0.01; *** p≤0.001; **** p≤0.0001.

SPD modification alters the formation of tau aggregates in vitro

Unaggregated and aggregated tau samples were visualized on TEM to assess morphology and quantify aggregate sizes. There was a 74% reduction in the total mass of aggregates with SPD-modified hT40 compared to unmodified hT40 (Figure 2.5A and D; $t = 9.163$, $p < 0.05$). Furthermore, the number of globular (< 700 nm^2), short filamentous (2100-5000 nm^2), and long filamentous (> 5000 nm^2) aggregates was reduced with SPD modification of hT40 (Figure 2.5C, upper and lower panels).

No difference was observed in the aggregated mass between unmodified and SPD-modified hT39 samples (Figure 2.5B and F; Mann Whitney $U = 6$, $p > 0.05$). The size distribution of aggregates showed that SPD-modified hT39 proteins form less globular aggregates < 450 nm^2 along with a higher number of globular aggregates > 450 nm^2 (Figure 2.5E, upper and lower panels).

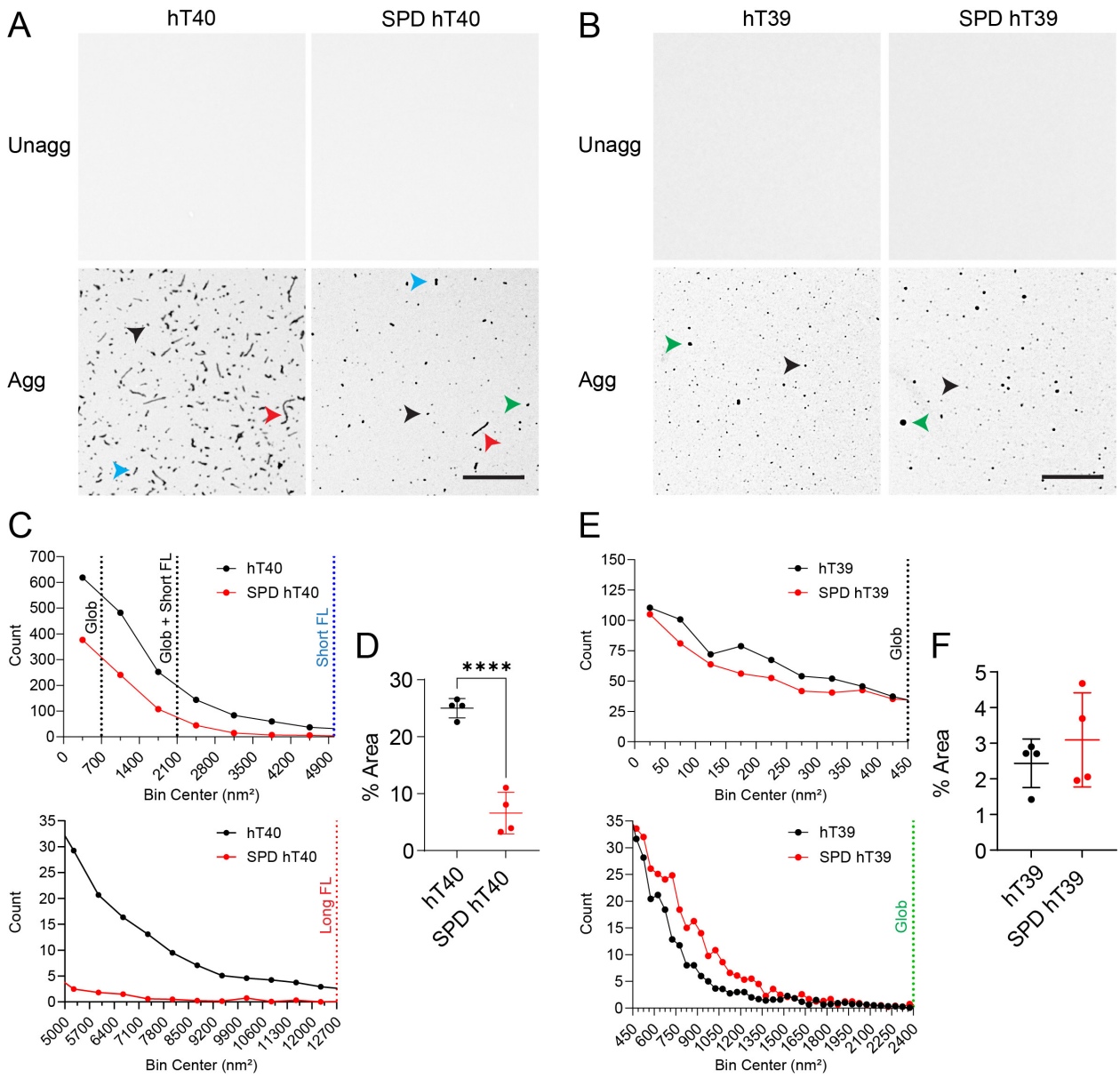

Figure 2.5. SPD modification alters the sizes of tau aggregates *in vitro*.
A, electron micrographs of unaggregated and aggregated hT40 proteins. Scale bar: 800nm. Globular aggregates < 700 nm^2 highlighted with black arrowheads; short (2100-5000 nm^2) and long (> 5000 nm^2) filaments highlighted with blue and red arrowheads, respectively. B, electron micrographs of unaggregated and aggregated hT39 proteins. Scale bar: 800nm. Globular aggregates < 450 nm^2 highlighted with black arrowheads; globular aggregates > 450 nm^2 highlighted with green arrowhead. C, size distribution of aggregates formed by unmodified and SPD-modified hT40 proteins. D, total mass of aggregates observed with unmodified and SPD-modified hT40 expressed as percentage of field area. E, size distribution of aggregates formed by unmodified and SPD-modified hT39 proteins. F, total mass of aggregates observed with unmodified and SPD-modified

Figure 2.5 (cont'd)
hT39 expressed as percentage of field area. Abbreviations: SPD, spermidine; hT40, 2N4R tau isoform; hT39, 2N3R tau isoform; unagg, unaggregated; agg, aggregated; % Area, % of aggregates per field. Data represented as mean ± SD. * $p \leq 0.05$; ** $p \leq 0.01$; *** $p \leq 0.001$; **** $p \leq 0.0001$.

SPD modification increases the stable multimers in unaggregated and aggregated tau in vitro

Tau aggregation leads to the formation of heat, SDS and reducing condition stable multimers. Here, SDS-PAGE and western blotting were employed to assess the extent to which SPD modification of tau affects the formation of these stable multimers (Figure 2.6A and D). A significant increase in the stable multimers upon aggregating hT40 proteins was observed at high molecular weight (i.e. the stable multimers) in unmodified and SPD-modified samples [Figure 2.6C; two-way ANOVA, Aggregation factor: $F_{(1, 12)} = 72.79$, $p < 0.05$; $t = 5.401$, $p < 0.05$ for unmodified hT40; $t = 6.665$, $p < 0.05$ for SPD hT40]. Moreover, stable multimers were 40% higher in SPD-modified hT40 compared to unmodified hT40 (Figure 2.6C; two-way ANOVA, PTM factor: $F_{(1, 12)} = 49.70$, $p < 0.05$; $t = 5.617$, $p < 0.05$). Of note, stable multimers were 50% higher in the unaggregated SPD-modified hT40 relative to the unaggregated unmodified hT40 (Figure 2.6C; $t = 4.353$, $p < 0.05$). Even though we detected a significant main effect of PTM on the monomeric tau signal [$F_{(1, 12)} = 5.158$, $p < 0.05$], post-hoc testing did not reveal any statistically significant differences in between the unmodified and SPD-modified hT40 proteins.

Stable multimers were significantly elevated upon aggregating SPD-modified but not unmodified hT39 proteins [Figure 2.6F; two-way ANOVA, Aggregation factor: $F_{(1, 12)} = 11.89$, $p < 0.05$; $t = 1.492$, $p > 0.05$ for unmodified hT39; $t = 3.385$, $p < 0.05$ for SPD hT39]. Furthermore, SPD-modified hT39 had higher levels of stable multimers in both the

unaggregated and aggregated samples when compared to unmodified hT39 [Figure 2.6F; two-way ANOVA, PTM factor: $F_{(1,\ 12)}$ = 41.55, p < 0.05; t = 3.611, p < 0.05 for unaggregated samples; t = 5.505, p < 0.05 for aggregated samples]. No significant differences were observed in the monomeric tau signal in the unaggregated and aggregated of the hT39 samples regardless of SPD modification status (Figure 2.6E).

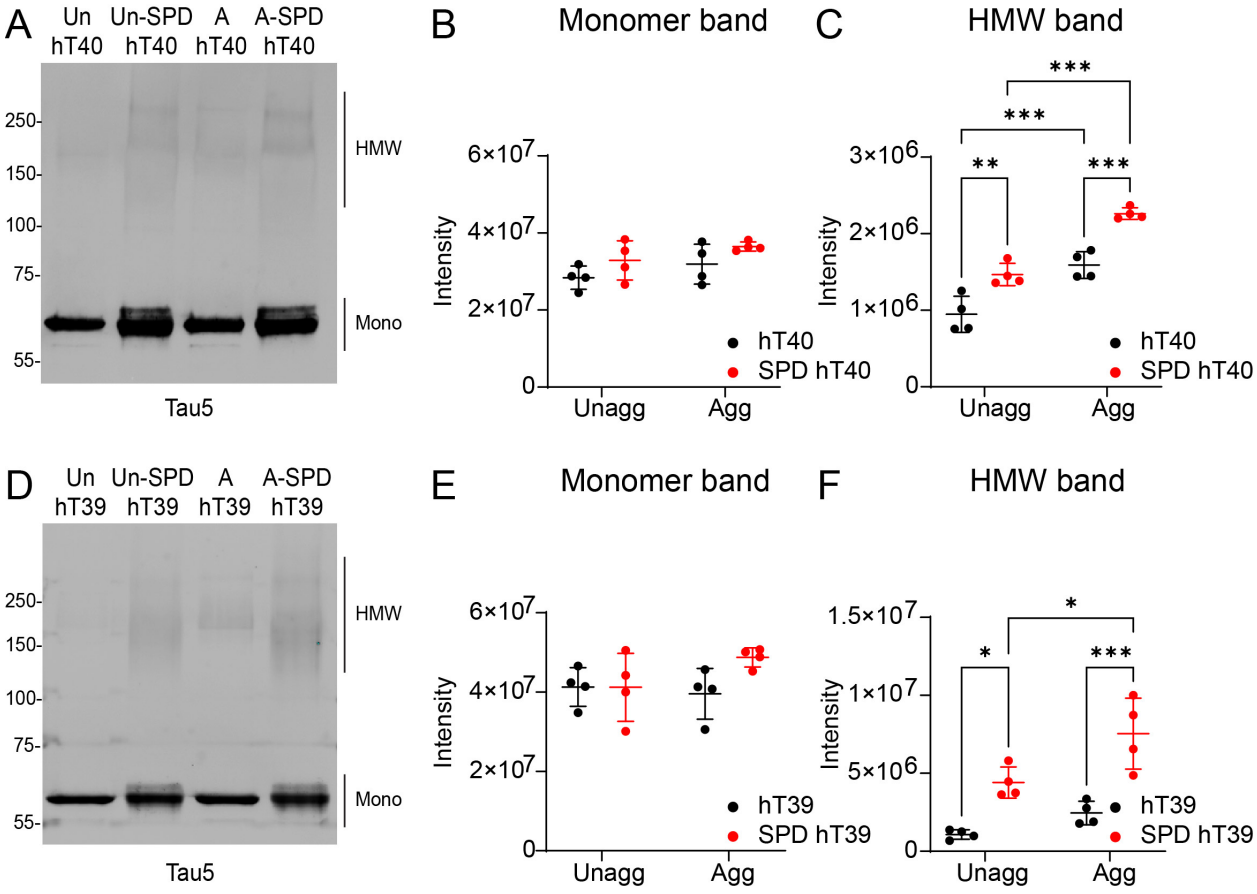

Figure 2.6. SPD modification increases stable multimers in unaggregated and aggregated tau samples.
A, western blot of unaggregated and aggregated hT40 samples probed with Tau5 antibody. B, quantification of monomeric tau bands in hT40 samples. C, quantification of the high molecular weight (HMW) stable multimer tau bands in hT40 samples. D, western blot of unaggregated and aggregated hT39 samples probed with Tau5 antibody. E, quantification of monomeric tau bands in hT39 samples. F, quantification of HMW tau bands in hT39 samples. Abbreviations: SPD, spermidine; hT40, 2N4R tau isoform; hT39, 2N3R tau isoform; un/unagg, unaggregated; agg, a/aggregated; HMW, high molecular weight. Data represented as mean ± SD. * p≤0.05; ** p≤0.01; *** p≤0.001; **** p≤0.0001.

SPD modification of tau enhances the formation of its pathological conformations in vitro

Several antibodies are available to detect oligomeric tau species, which are linked to toxicity and neurodegeneration (Alhadidy & Kanaan, 2024; Castillo-Carranza, Gerson, et al., 2014; Patterson et al., 2011; Ward et al., 2013). Oligomeric tau was quantified in unaggregated and aggregated tau samples using sandwich ELISAs with two different oligomeric tau antibodies (i.e. TOC1 and TOMA1). Both sandwich ELISA assays showed an increase in TOC1-positive [Figure 2.7A, left panel; two-way ANOVA, Interaction: $F_{(1, 12)} = 8.959$, $p < 0.05$; $t = 16.75$, $p < 0.05$ for unmodified hT40; $t = 12.51$, $p < 0.05$ for SPD hT40] and TOMA1-positive [Figure 2.7B, left panel; two-way ANOVA, Interaction: $F_{(1, 12)} = 9.751$, $p < 0.05$; $t = 15.23$, $p < 0.05$ for unmodified hT40; $t = 10.82$, $p < 0.05$ for SPD hT40] oligomeric tau in the aggregated samples of unmodified and SPD-modified hT40 relative to their respective unaggregated proteins. Of note, the unaggregated SPD-modified hT40 samples had significantly higher levels of both oligomeric tau species relative to unmodified hT40 (Figure 2.7A, left panel for TOC1; $t = 19.48$, $p < 0.05$ for TOC1; Figure 2.7B, left panel for TOMA1; $t = 19.60$, $p < 0.05$ for TOMA1). Moreover, the aggregated samples of SPD-modified hT40 contained higher fractions of oligomeric tau relative to the aggregated unmodified hT40 (Figure 2.7A, left panel for TOC1; $t = 15.24$, $p < 0.05$ for TOC1; Figure 2.7B, left panel for TOMA1; $t = 15.19$, $p < 0.05$ for TOMA1).

The patterns observed with hT40 proteins were the same with hT39 proteins (Figure 2.7A and B, right panels). Both sandwich ELISA assays showed an increase in TOC1-positive [Figure 2.7A, right panel; two-way ANOVA, Aggregation factor: $F_{(1, 12)} = 104.2$, $p < 0.05$; $t = 6.99$, $p < 0.05$ for unmodified hT39; $t = 7.444$, $p < 0.05$ for SPD hT39] and TOMA1-positive [Figure 2.7B, right panel; two-way ANOVA, Interaction: $F_{(1, 12)} =$

16.57, $p < 0.05$; $t = 2.668$, $p < 0.05$ for unmodified hT39; $t = 8.426$, $p < 0.05$ for SPD hT39] oligomeric tau in the aggregated samples of unmodified and SPD-modified hT39 relative to their respective unaggregated proteins. Of note, the unaggregated SPD-modified hT39 samples had significantly higher levels of both oligomeric tau species relative to unmodified hT40 [Figure 2.7A, right panel for TOC1; two-way ANOVA, PTM factor: $F_{(1, 12)} = 221.9$, $p < 0.05$ for TOC1; $t = 10.31$, $p < 0.05$ for TOC1; Figure 2.7B, right panel for TOMA1; $t = 3.25$, $p < 0.05$ for TOMA1]. Moreover, the aggregated samples of SPD-modified hT39 contained higher fractions of oligomeric tau relative to the aggregated unmodified hT40 (Figure 2.7A, right panel for TOC1; $t = 10.76$, $p < 0.05$ for TOC1; Figure 2.7B, right panel for TOMA1; $t = 9.007$, $p < 0.05$ for TOMA1).

Tau adopts pathogenic conformations associated with modifications of monomeric tau and following multimerization that are also linked to toxicity (Alhadidy & Kanaan, 2024; Christensen et al., 2023; Hintermayer et al., 2020; Kanaan et al., 2011). Those conformations include exposure of the PAD of tau that spans amino acids 2-18 and whose abnormal exposure is linked to dysfunction of axonal transport (Combs et al., 2021; Kanaan et al., 2011; LaPointe et al., 2009). The extent to which SPD modification can influence the adoption of a PAD-exposed conformations was assessed using sandwich ELISAs with the TNT2 antibody. Aggregated samples showed significantly higher TNT2 signal compared to their unaggregated counterparts [Figure 2.7C, left panel; two-way ANOVA, Interaction: $F_{(1, 12)} = 93.47$, $p < 0.05$] in the unmodified hT40 samples ($t = 25.01$, $p < 0.05$) and the SPD-modified hT40 samples ($t = 11.34$, $p < 0.05$). Moreover, TNT2 signal was significantly higher in unaggregated SPD-modified hT40 relative to unmodified hT40 (Figure 2.7C, left panel; $t = 11.61$, $p < 0.05$), suggesting this modification may

expose PAD without aggregation. There was not a significant difference in TNT2 signal between aggregated unmodified and aggregated SPD-modified hT40 ($t = 2.059$, $p > 0.05$).

We also assessed the impact of SPD modification on PAD exposure of the hT39 isoform. Aggregated samples showed significantly higher TNT2 signal compared to their unaggregated counterparts [Figure 2.7C, right panel; two-way ANOVA, Aggregation factor: $F_{(1, 12)} = 316.7$, $p < 0.05$] in the unmodified hT39 samples ($t = 12.70$, $p < 0.05$) and the SPD-modified hT39 samples ($t = 12.47$, $p < 0.05$). Moreover, TNT2 signal was significantly higher in unaggregated SPD-modified hT39 relative to unmodified hT39 [Figure 2.7C, right panel; two-way ANOVA, PTM factor: $F_{(1, 12)} = 609.2$, $p < 0.05$; $t = 17.57$, $p < 0.05$], suggesting this modification may expose PAD without aggregation. There was also a significant difference in TNT2 signal between aggregated unmodified and aggregated SPD-modified hT39 ($t = 17.34$, $p < 0.05$).

Another misfolded conformation involves the N-terminus of tau coming into close proximity to the microtubule-binding region of tau, and it represents an aggregation prone folding event that occurs early in disease (Carmel et al., 1996; Hyman, Van Hoesen, et al., 1988; Jicha et al., 1997). The extent to which SPD modification can influence the adoption of a the Alz50 conformation was assessed using sandwich ELISAs. Alz50-positive tau was significantly higher in the aggregated samples relative to their respective unaggregated proteins [Figure 2.7D, left panel; two-way ANOVA, Interaction: $F_{(1, 12)} = 313.1$, $p < 0.05$] in both the unmodified tau samples ($t = 50.08$, $p < 0.05$) and SPD-modified hT40 samples ($t = 25.05$, $p < 0.05$). Moreover, the Alz50-positive conformation was more abundant in unaggregated SPD-modified hT40 relative to unmodified hT40

(Figure 2.7D, left panel; t = 34.33, p<0.05). Unlike TNT2 signal, aggregated SPD-modified hT40 showed higher Alz50-positive tau relative to unmodified hT40 aggregates (t = 9.310, p < 0.05).

We also assessed the degree of tau misfolding in unaggregated and aggregated hT39 samples. Aggregated samples showed significantly higher Alz50 signal compared to their unaggregated counterparts [Figure 2.7D, right panel; two-way ANOVA, Interaction: $F_{(1, 12)} = 48.87$, p < 0.05] in the unmodified hT39 samples (t = 21.11, p < 0.05) and the SPD-modified hT39 samples (t = 11.23, p < 0.05). Moreover, Alz50 signal was significantly higher in unaggregated SPD-modified hT39 relative to unmodified hT39 (Figure 2.7D, right panel; t = 27.91, p < 0.05), suggesting this modification may induce tau misfolding without aggregation. There was also a significant increase in Alz50 signal in the aggregated SPD-modified hT39 relative to the aggregated unmodified hT39 (t = 18.02, p < 0.05).

For all unaggregated and aggregated hT40 and hT39 proteins, total tau levels were measured using Tau13 as capture antibody (Figure AI.4). No significant differences were observed in total tau levels within the hT40 samples. Even though we detected a significant main effect of PTM on total tau signal for hT39 samples [two-way ANOVA, $F_{(1, 12)} = 6.355$, p < 0.05], post-hoc testing did not reveal any statistically significant differences between unmodified and SPD-modified hT39 samples in unaggregated and aggregated states.

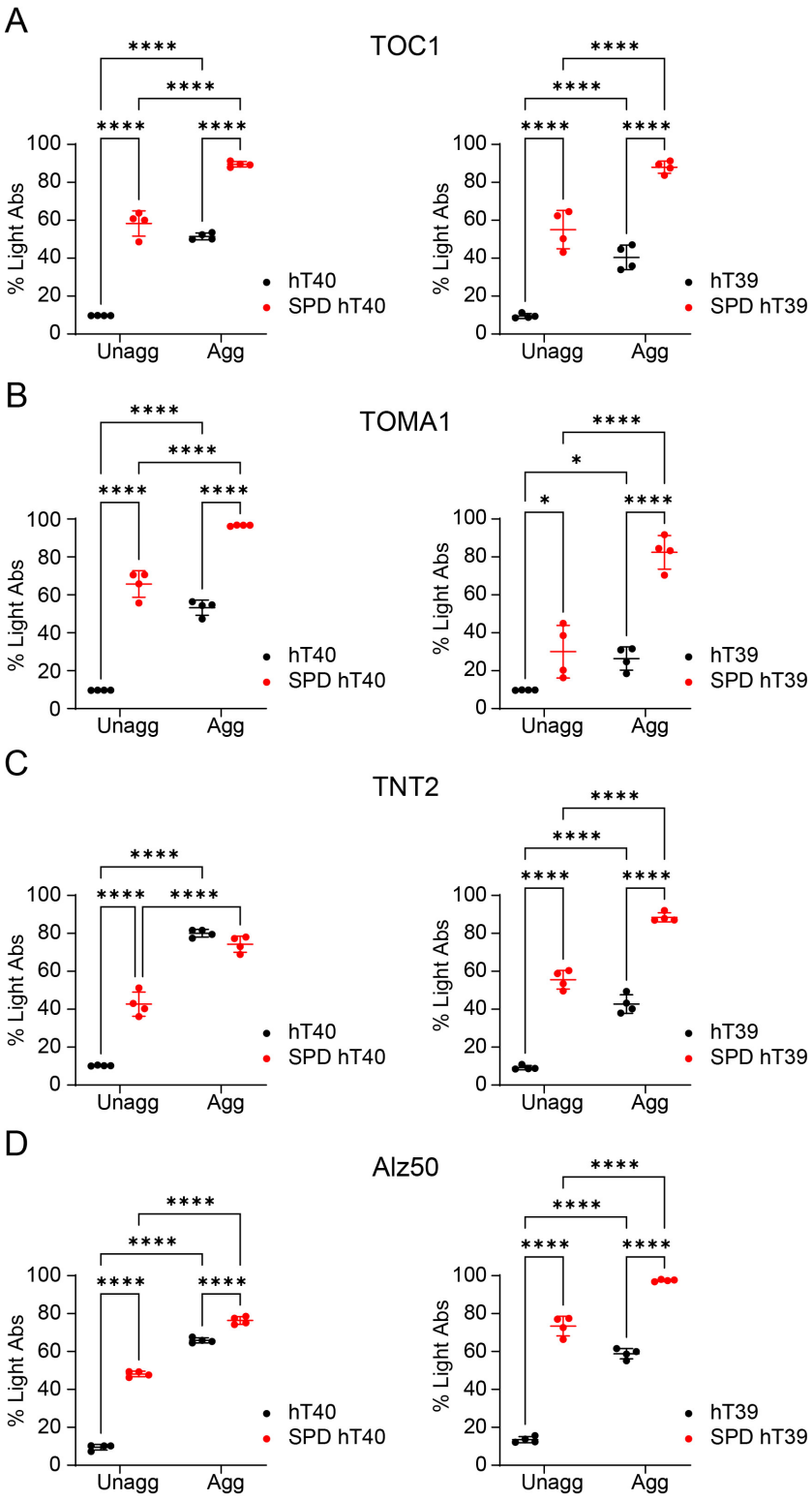

Figure 2.7. SPD modification of tau increases its pathological conformations independent of aggregation *in vitro*.

Figure 2.7 (cont'd)
A, sandwich ELISAs measuring TOC1-positive oligomeric tau in unaggregated and aggregated hT40 (left panel) and hT39 (right panel) proteins. The TOC1 antibody was used for capture and R1 antibody for detection. B, sandwich ELISAs measuring TOMA1-positive oligomeric tau in unaggregated and aggregated hT40 (left panel) and hT39 (right panel) proteins. The TOMA1 antibody was used for capture and R1 antibody for detection. C, sandwich ELISAs measuring PAD exposure in unaggregated and aggregated hT40 (left panel) and hT39 (right panel) proteins. The TNT2 antibody was used for capture and R1 antibody for detection. D, sandwich ELISAs measuring Alz50-positive misfolded tau conformation in unaggregated and aggregated hT40 (left panel) and hT39 (right panel) proteins. The Alz50 antibody was used for capture and R1 antibody for detection. Abbreviations; SPD, spermidine; hT40, 2N4R tau isoform; hT39, 2N3R tau isoform; unagg, unaggregated; agg, aggregated; TOC1, tau oligomeric complex 1 antibody; TOMA1, oligomer-specific monoclonal antibody; TNT2, tau N-terminal 2 antibody to measure PAD exposure; Alz50, misfolded tau conformation antibody. Data represented as mean ± SD. * $p \leq 0.05$; ** $p \leq 0.01$; *** $p \leq 0.001$; **** $p \leq 0.0001$.

SPD modification reduces tau seeding in tau biosensor HEK cells

Tau RD P301S biosensor HEK cells were used to determine whether SPD modification alters tau seeding competency. The seeding efficiencies of unaggregated and aggregated samples of unmodified and SPD-modified hT40 were tested (Figure 2.8A). The aggregated samples of unmodified hT40 induced seeding of tau aggregation relative to its unaggregated samples [Figure 2.8B; two-way ANOVA, Interaction: $F_{(1, 12)} = 29.48$, $p < 0.05$; $t = 8.891$, $p < 0.05$]. In contrast, aggregates of SPD-modified hT40 failed to seed aggregation in tau biosensor cells relative to its unaggregated samples (Figure 2.8B; $t = 1.212$, $p > 0.05$). Moreover, tau seeding was significantly lower (73%) in SPD-modified hT40 aggregates relative to the aggregated hT40 samples ($t = 7.369$, $p < 0.05$).

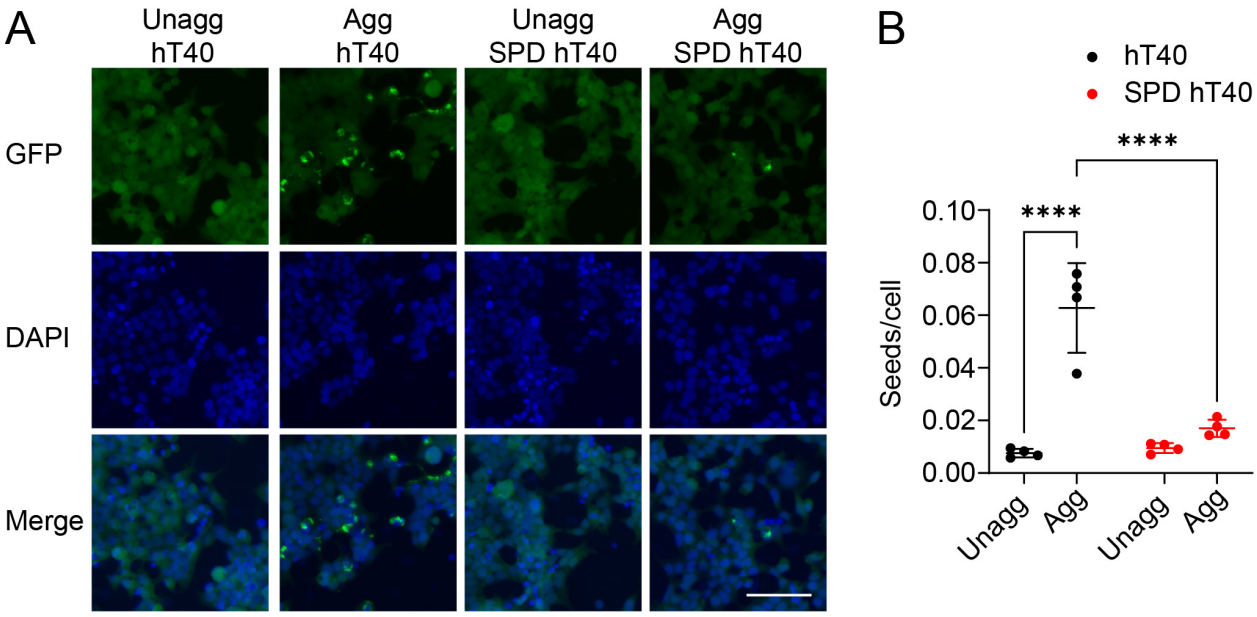

Figure 2.8. SPD modification of tau reduces its seeding competency in tau biosensor cells.
A, images of tau seeds in cells treated with unaggregated and aggregated hT40 proteins (green) along with DAPI staining (blue) as a surrogate for cell count. Scale bar: 200µm. B, quantification of number of seeds per cell in cultures treated with unaggregated and aggregated hT40 proteins. Abbreviations, SPD, spermidine; hT40, 2N4R tau isoform; hT39, 2N3R tau isoform; unagg, unaggregated; agg, aggregated; GFP, green fluorescent protein channel (green); DAPI, 4',6-diamidino-2-phenylindole channel (blue). Data represented as mean ± SD. * p≤0.05; ** p≤0.01; *** p≤0.001; **** p≤0.0001.

Discussion

Tau undergoes a plethora of PTMs in normal and disease conditions, the most studied of which are phosphorylation and acetylation (Alhadidy & Kanaan, 2024). PTMs regulate several aspects of tau protein biology including protein-protein interactions, aggregation, conformational changes, microtubule binding, degradation, and clearance (Alhadidy & Kanaan, 2024; Alquezar et al., 2020). However, the effects of some PTMs, such as TG-mediated polyamination, remains largely elusive (Dudek & Johnson, 1993; Halverson et al., 2005; Miller & Johnson, 1995; Murthy et al., 1998; Zemaitaitis et al., 2000). Several of the early studies focused mainly on the cross-linking of tau by TG with

minimal interest in polyamine incorporation onto Q residues of tau (Miller & Johnson, 1995). Of note, metabolic profiling of polyamine levels indicated increased SPD levels in AD brains (Inoue et al., 2013; Morrison & Kish, 1995). Furthermore, studies in animal models of tauopathy reported a polyamine stress response that contributes to the progression of tau pathology (Sandusky-Beltran et al., 2021) (Hunt et al., 2015; Sandusky-Beltran et al., 2019). Thus, it is critical to determine the salience of incorporating SPD onto Q residues of tau (Inoue et al., 2013; Morrison & Kish, 1995).

In this work, we sought to produce SPD-modified tau and test the effects of SPD polyamination on several aspects of tau biology, including microtubule binding and polymerization, pathological tau conformations, aggregation, and seeding capability *in vitro*. We found that the incubating recombinant tau with TG and SPD resulted in SPD polyamination on several Q residues mainly within the N-terminus of tau. Most modifications occurred in both hT40 and hT39 tau proteins (Q6, Q26, Q49, Q88, Q124, and Q424), while a few were detected only in hT40 protein (Q33 and Q307). Interestingly, two of these sites (Q307 and Q424) were previously shown to participate as amine acceptors in TG-mediated cross-linking of hT40 and hT39 tau isoforms (Murthy et al., 1998). In addition, Q6, Q88 and Q124 were reported to act as amine acceptors in TG-mediated cross-linking of hT40 (Murthy et al., 1998).

Given the well-known association of tau with microtubules and its role in regulating microtubule dynamics (Alonso et al., 1994; Amniai et al., 2009; Black et al., 1996; Breuzard et al., 2013; Cleveland et al., 1977; Weingarten et al., 1975), we examined how SPD modification of tau alters microtubule binding and polymerization kinetics. Our results show that SPD modification does not significantly affect binding of either the hT40

or hT39 tau isoforms to preformed microtubules, but SPD-modified tau increases the microtubule polymerization rate. Moreover, SPD-modified hT39 increases the extent of microtubule polymerization. Considering that polyamines are positively charged (Bae et al., 2018) and microtubules are negatively charged (Minoura & Muto, 2006), it is reasonable to surmise that electrostatic forces between tau and tubulin may enhance polymerization of microtubules.

The Rhoades group showed that tubulin polymerization depends on tubulin's interactions with the proline-rich domain (PRD) and the MTBR region (McKibben & Rhoades, 2019). Furthermore, the interactions of tubulin with the two domains are negatively regulated by the N-terminal domain of tau. Therefore, it is likely that the incorporation of SPD on the N-terminus of tau releases the inhibitory effects exerted by the N-terminal domain on tubulin's interactions with PRD and MTBR regions. These results may have implications for SPD-modified tau enhancing microtubule polymerization at the labile ends as was recently described (Qiang et al., 2018) or potentially increasing the production of labile MT (Baas & Qiang, 2019). It seems that polyamination of tau may have implications in the physiological and potentially disease-associated roles of tau related to microtubule binding and regulation, which deserves further investigation.

PTMs as potential regulators of tau biology are intimately linked to processes associated with tau in human disease, including the adoption of pathological conformations in monomeric or multimeric tau species (Alhadidy & Kanaan, 2024). Sustained conformation-dependent PAD exposure is a pathological event that occurs early in AD and is linked to dysregulation of axonal transport (Kanaan et al., 2011).

Activation of a signaling pathway involving PP1 and GSK3β mediates the PAD exposure-induced dysregulation of axonal transport (Combs et al., 2021; LaPointe et al., 2009). In this work, we demonstrated that SPD modification of tau promotes a conformational change leading to increased PAD exposure in aggregated as well as unaggregated tau. Together, these findings suggest SPD modification can enhance PAD exposure and may be associated with axonal transport impairment with or without tau aggregation. The effects of SPD polyamination on PAD exposure are reminiscent of other specific PTMs and mutant forms of tau such as phosphorylation at sites within the AT8 epitope and the P301L mutation, respectively (Christensen et al., 2023; Combs et al., 2021; Hintermayer et al., 2020; Kanaan et al., 2011; Morris et al., 2020).

Oligomerization of tau occurs in early Braak stages before the development of cognitive symptoms in AD patients (Lasagna-Reeves et al., 2012; Maeda et al., 2006). A considerable body of work has demonstrated that oligomeric tau species can mediate dysfunction and degeneration, and there is a developing consensus that tau filaments are not as toxic as traditionally thought (Cowan & Mudher, 2013). Indeed, tau oligomers are linked to several disease mechanisms including axonal transport impairment (Vossel et al., 2015), mitochondrial and synaptic dysfunction (Lasagna-Reeves et al., 2011), reduced protein synthesis (Jiang et al., 2021), inhibited long-term potentiation (Hill et al., 2019), and memory impairment (Fa et al., 2016). In fact, the tauopathy phenotype is reversed with immunotherapies that target oligomeric tau species in rodent models of tauopathy (Bittar et al., 2022; Castillo-Carranza, Gerson, et al., 2014). SPD modification of tau increases the oligomeric tau species formed when aggregation is induced. Furthermore, it also enhances oligomer formation in unaggregated tau samples

suggesting that this PTM may further exacerbate the toxic mechanisms associated with tau oligomers.

Tau also assumes a misfolded conformation in disease conditions where the N-terminus folds onto the microtubule-binding region, and it is thought to precede the formation of filamentous tau aggregates (Carmel et al., 1996). This misfolded conformation is detected with the Alz50 antibody that was originally developed against paired helical filaments isolated from AD brain tissue (Wolozin et al., 1986). Our results showed that SPD modification of tau increases the Alz50 conformation in unaggregated and aggregated samples. This finding agrees with previous work demonstrating that the importance of other PTMs, such as phosphorylation at the S202 and T205, for adoption of the Alz50 conformation by tau (Steinhilb et al., 2007).

SPD modification decreases the extent of tau filamentous aggregation, as indicated by reduced β-sheet structure formation (ThS) and LLS signal. Confirming this effect, TEM demonstrated that SPD polyamination of tau markedly reduces the formation of filamentous tau aggregates. In parallel, the levels of oligomeric, PAD-exposed, and Alz50-positive tau conformations with SPD-modified tau were higher than those observed with unmodified tau even without inducing aggregation. This pattern of tau polymerization with SPD polyamination highlights the idea that pathological tau conformations are not necessarily linked to the formation of filamentous aggregates. It is also suggestive that tau polymerization can follow on- or off-filament pathways (Kjaergaard et al., 2018). Taken together, these findings suggest that SPD polyamination favors an off-filament pathway of tau polymerization.

Previous work by the Diamond group and others demonstrates that tau seeding represents an early change during the development of tau pathology (Holmes et al., 2014; Manca et al., 2023; Woerman et al., 2016) and that seeding capability of tau is linked to conformational changes that can either enhance or impede seeding (Dinkel et al., 2011; Falcon et al., 2015). Recent studies suggest that PTMs, such as phosphorylation and acetylation, are one factor that alters tau's ability to seed aggregation (Despres et al., 2019; Tseng et al., 2021). In this work, we observed a reduced capability of SPD hT40 to seed aggregation in tau biosensor cells. This result suggests that the conformations of tau species formed by SPD modification, including the globular aggregates, are not capable of seeding tau aggregation.

In the context of AD, TG activity and SPD levels are significantly elevated suggesting polyamination pathways are dysregulated in disease (Inoue et al., 2013; G. V. Johnson et al., 1997; Morrison & Kish, 1995). In fact, modulating polyamine metabolism has a significant impact on tauopathy phenotypes in mouse models of tauopathy. In an adeno-associated virus (AAV) C-terminal truncated tau mouse model, the Lee group showed that knocking out the spermidine/spermine-N1-acetyltransferase enzyme (SSAT) decreases putrescine and SPD levels, reduces loss of neurons in the hippocampus and cortex (NeuN+ neurons), but does not change tau aggregate levels (Sandusky-Beltran et al., 2019). On the other hand, AAV-mediated overexpression of arginase 1 (a polyamine metabolism enzyme) in the rTg4510 mouse model reduces tau tangle-like pathology in the hippocampi (i.e. Gallyas silver positive inclusions) and in formic-acid insoluble tau, but there was no change in overt neuron loss (Hunt et al., 2015). These studies suggest that polyamine pathways are involved in tau-mediated toxicity

likely due to non-filamentous forms of pathogenic tau, which complements our findings that SPD modification of tau favors the formation of pathogenic tau conformations at the expense of forming filamentous tau aggregates. It is noteworthy that the level of tau polyamination was not directly examined in the above *in vivo* studies, which warrants further investigation to determine the role tau polyamination and its relationship to pathogenic tau species in animal models of tauopathy.

To date, most *in vivo* studies have focused on the potential outcomes of cross-linking tau by TG and the modulation of polyamine metabolism pathways in the context of tau aggregation and pathology (Dudek & Johnson, 1993; Halverson et al., 2005; Konno et al., 2005; Murthy et al., 1998; Wang et al., 2008), but no studies have assessed the impacts of direct polyamination of tau. Here, we show that SPD polyamination alters tau function in relationship to microtubule polymerization and the formation of pathological tau conformations. Our work suggests that SPD polyamination may direct tau towards off-filament pathway of polymerization, where pathological tau conformations are increased at the expense of filamentous aggregates (Kjaergaard et al., 2018). Further efforts are required to directly test the salience of tau polyamination in human disease and models of tauopathy.

CHAPTER 3: O-GLCNAC MODIFICATION DIFFERENTIALLY REGULATES MICROTUBULE-BINDING AND PATHOLOGICAL CONFORMATIONS OF TAU ISOFORMS *IN VITRO*

Abstract

Alzheimer's disease (AD) is a neurodegenerative disease characterized by the accumulation of neurofibrillary tangles in the brain. Local reduction of glucose metabolism in the brain is thought to contribute to the pathophysiology of AD through the downregulation of the hexosamine biosynthetic pathway. In agreement, post-translational modification (PTM) of serine/threonine (S/T) residues of tau with O-linked β-d-N-acetylglucosamine (O-GlcNAc; referred to as O-GlcNAcylation) is downregulated in the AD brain while its phosphorylation and aggregation are increased. Moreover, O-GlcNAcase (OGA) inhibitor treatment reduces phosphorylated and aggregation of tau in mouse models of tauopathy. Importantly, several lines of evidence suggest that filamentous tau aggregates may not be the most toxic species of tau in disease. Indeed, some pre-filamentous conformational changes of tau protein are intimately linked to toxicity and neurodegeneration in tauopathies, such as oligomerization, misfolding, and excessive exposure of the phosphatase-activating domain (PAD) located in the extreme N-terminus of tau. However, the direct impact of tau O-GlcNAcylation on the development of pathological tau conformations is unknown. It is becoming increasingly appreciated that PTMs may differentially regulate the pathobiology of tau in an isoform-dependent manner. Consequently, it is paramount to investigate the impact of O-GlcNAcylation on the 4R and 3R tau isoforms. In this work, we assessed the impact of O-GlcNAcylation on the development of pathological tau conformations for the longest 4R and 3R tau isoforms (hT40 and hT39 respectively) using recombinant proteins. Mass spectrometry indicated that tau is modified by O-GlcNAc on multiple S/T mainly concentrated within the proline-rich domain and C-terminus, including the previously reported S400 along with novel

residues. O-GlcNAcylation of hT40 did not impact microtubule polymerization, but increased binding to preformed microtubules. O-GlcNAcylation reduces β-sheet containing aggregates and seeding capability of hT40. Despite O-GlcNAcylation interfering with the formation of seeding competent filamentous tau, it does not alter the formation of pathogenic non-filamentous tau conformations (i.e. oligomerization, misfolding, and PAD exposure). Like the case with hT40, O-GlcNAcylation reduces β-sheet containing aggregates without altering microtubule polymerization of hT39. Contrary to the case with hT40, O-GlcNAcylation decreases binding of hT39 to preformed microtubules. Furthermore, O-GlcNAcylation of hT39 enhances formation of pathogenic non-filamentous tau conformations (i.e. oligomerization, misfolding, and PAD exposure). Taken together, our data suggest that O-GlcNAcylation regulates the microtubule-binding and formation of pathological tau conformations differently between 4R and 3R tau isoforms. These findings may have implications on the future testing of OGA inhibitors as therapeutics in different tauopathies.

Introduction

Alzheimer's disease (AD) is a secondary tauopathy that is neuropathologically characterized by the accumulation of intracellular neurofibrillary tangles (NFTs) of tau (Gotz et al., 2019). Traditionally, the amyloid cascade hypothesis has been the central paradigm explaining the pathogenesis of AD, where amyloid-β (Aβ) pathology is thought to be the main culprit and primary driver of the disease (Barage & Sonawane, 2015; Karran et al., 2011; Naslund et al., 2000; Ricciarelli & Fedele, 2017). Nonetheless, therapies targeting the amyloid pathology in AD have shown limited success in clinical trials (Budd Haeberlein et al., 2022; van Dyck et al., 2023). Furthermore, primary tauopathies [e.g. corticobasal degeneration (CBD), progressive supranuclear palsy (PSP), and Pick's disease (PiD)] standout as examples where tau pathology develops independently of Aβ co-pathology (Gotz et al., 2019). Therefore, there is growing interest in studying potential factors, other than Aβ, that regulate the pathobiology of tau in health and disease (Goedert et al., 2024; Vejandla et al., 2024).

Our understanding of the processes driving the transition of tau from its soluble forms into pathological species has witnessed remarkable progress (Alhadidy & Kanaan, 2024). Growing evidence points to common mechanisms of conformational changes of tau that occur early during the development of tauopathies (Alhadidy & Kanaan, 2024; Combs et al., 2016; Garcia-Sierra et al., 2003; Lasagna-Reeves et al., 2012; Mroczko et al., 2019; Niewiadomska et al., 2021; Patterson et al., 2011; Weaver et al., 2000). Some of these tau conformations contribute to its neurodegenerative effects more intensely than filamentous tau aggregates. A conformational change of tau that happens early during the deposition of pathological tau in disease is oligomerization (Cox et al., 2016; Kanaan

et al., 2016; Lasagna-Reeves et al., 2012; Patterson et al., 2011). Tau oligomers are linked to neurodegeneration and several manifestations of cellular dysfunction, such as disruption of intracellular transport, impairment of protein degradation, synaptic dysfunction, and dysregulating cellular bioenergetics (Niewiadomska et al., 2021). In fact, immunotherapy targeting tau oligomers is sufficient to rescue neurodegeneration without decreasing tangle-like pathology in mouse models of tauopathy (Castillo-Carranza, Sengupta, et al., 2014; Santacruz et al., 2005; Sydow et al., 2011; Van der Jeugd et al., 2012).

Another pathological conformation is exposure of the phosphatase-activating domain (PAD) in the extreme N-terminus of tau (Gotz et al., 2019). PAD spans amino acids 2-18 and becomes abnormally exposed in AD (21734277; 28413156; 26671985). Some post-translational modifications (PTMs) (e.g. pT175 and pS199/pS202/pT205) and mutations (e.g. P301L) of tau induce excessive PAD exposure, thereby activating a signaling pathway regulated by protein phosphatase 1 (PP1) and glycogen synthase kinase 3 β (GSK3β) (Christensen et al., 2023; Combs et al., 2021; Hintermayer et al., 2020; Kanaan et al., 2011). The disrupted regulation of the PP1-GSK3β eventually culminates into aberrant phosphorylation of motor proteins (e.g. the kinesin-1 motor complex) leading to premature cargo release and dysregulation of intracellular transport (Morris & Brady, 2022; Mueller et al., 2021).

Tau propagation through structurally and functionally connected neurons represents a potential mechanism through which tau pathology progresses in the brain (Ahmed et al., 2014; Braak & Braak, 1991; Franzmeier et al., 2020; Mezias et al., 2017; Schoonhoven et al., 2023). This process entails tau transferring from one cell to another,

and then within the recipient cell the transferred “seed” templates the pathological conformation in the endogenous tau to form pathology (Clavaguera et al., 2009; de Calignon et al., 2012; Fu et al., 2016; Liu et al., 2012). Relatively recently, the Diamond group proposed that tau assumes conformational ensembles with different ability to seed aggregation (Mirbaha et al., 2018; Mirbaha et al., 2022; Sharma et al., 2018). The seeding-competent conformation is dependent upon the aggregation prone motifs of tau spanning amino acids 275-VQIINK-280 and 306-VQIVYK-311 (Chen et al., 2019; Falcon et al., 2015). Factors driving the transition of tau into seeding-competent conformations is an active area of investigation, but there is evidence than tau mutations (e.g. S320F) and PTMs (e.g. acetylation and phosphorylation) may regulate the transition process (Chen et al., 2023; Despres et al., 2019; Tseng et al., 2021).

In early disease stages, tau also undergoes misfolding where its N-terminus folds over the microtubule-binding repeats (MTBR) region (Carmel et al., 1996; Ferrer et al., 2014). This conformational change represents a critical checkpoint along the path of tau aggregation, and it is detected by the Alz50 and MC1 antibodies developed by Peter Davies (Carmel et al., 1996; Jicha et al., 1997; Ksiezak-Reding et al., 1988). Oligomerization, PAD exposure, misfolding, and adoption of seeding-competent conformation happen early in tauopathies, including 4R/3R (e.g. AD), 4R (e.g. CBD), and 3R tauopathies (e.g. PiD), among others (Castillo-Carranza, Gerson, et al., 2014; Combs et al., 2016; Cox et al., 2016; Ferrer et al., 2014; Montalbano et al., 2023). These findings implicate common mechanisms of tau conformational changes and toxicity beginning early in tauopathies.

Many factors regulate the adoption of pathological conformations by tau including mutations (e.g. P301L), protein-protein interactions (e.g. heat shock protein 90 and histone deacetylase 6), and PTMs (Alhadidy & Kanaan, 2024). In fact, certain PTMs of tau are common among tauopathies and sufficient to induce pathological conformations (Ferrer et al., 2014). For example, phosphorylation at sites within the AT8 epitope induces oligomerization, PAD exposure, and misfolding of tau (Christensen et al., 2023; Jeganathan et al., 2008; Kanaan et al., 2020). Early studies on the PTMs of tau focus mainly on their impact on the formation of filamentous tau aggregates (Park et al., 2018). Therefore, it is crucial to continue studying new and previously reported PTMs of tau through the lens of how they impact pathological conformations (Alhadidy & Kanaan, 2024).

Tau is subject to modification with O-linked β-d-N-acetylglucosamine (O-GlcNAc), commonly referred to as O-GlcNAcylation (Arnold et al., 1996; Yang & Qian, 2017). O-GlcNAcylation is a PTM that involves the incorporation of GlcNAc onto serine/threonine (S/T) residues of proteins (Yang & Qian, 2017). GlcNAc moiety is produced and activated to uridine diphosphate-N-acetylglucosamine through the hexosamine biosynthetic pathway (Paneque et al., 2023). Subsequently, cellular proteins become subject to O-GlcNAcylation through the action of O-GlcNAc transferase (OGT) enzyme (Aquino-Gil et al., 2017). O-GlcNAcylation can be reversed through the action of O-GlcNAcase (OGA) enzyme, allowing for recycling of GlcNAc through the GlcNAc salvage pathway (Yang & Qian, 2017).

AD patients show regional hypometabolism in the brain that predicts future decline in cognitive and memory functions (Costantini et al., 2008; de Leon et al., 2001; De Santi

et al., 2001; Ibanez et al., 1998; Raut et al., 2023). In agreement, O-GlcNAcylation of tau and other proteins in the brain is lower in AD compared to nondemented individuals (Liu et al., 2004; Liu et al., 2009). These findings instigated an interest in the role played by O-GlcNAcylation in regulating tau pathobiology (Gong et al., 2016). O-GlcNAcylation of tau affects its aggregation and phosphorylation (Yuzwa et al., 2014; Yuzwa et al., 2012; Zhu et al., 2014). In the presence of heparin, O-GlcNAcylation at S400 reduces the rate and extent of tau aggregation (Yuzwa et al., 2014; Yuzwa et al., 2012). Also, tau modification with O-GlcNAc is inversely related to its phosphorylation in recombinant tau proteins, cell lines, rat brain slices, mouse brains, and AD tissue (Gatta et al., 2016; Liu et al., 2004; Liu et al., 2009; Smet-Nocca et al., 2011). Indeed, administration of OGA inhibitors, such as Thiamet G and MK-8719, in wild-type rats (Yuzwa et al., 2008), rTg4510 mice (Graham et al., 2014; Hastings et al., 2017; Wang et al., 2020), and JNPL3 mice (Yuzwa et al., 2012) enhanced tau O-GlcNAcylation while reducing its phosphorylation. Treating animal models with Thiamet G also reduced neuronal loss, prevented brain atrophy, and inhibited tau aggregation (Hastings et al., 2017; Wang et al., 2020; Yuzwa et al., 2012). However, precisely how O-GlcNAcylation of tau regulates the formation of early pathological tau conformations that precede filamentous aggregate formation remains unknown (Alhadidy & Kanaan, 2024; Mroczko et al., 2019; Niewiadomska et al., 2021).

Herein, we produced recombinant O-GlcNAc modified 2N4R (hT40) and 2N3R (hT39) tau isoforms in bacterial cells by co-transformation. A set of biochemical and biophysical assays were employed to determine the impact of O-GlcNAcylation on tau's interaction with microtubules, as well as tau aggregation and adoption of pathological

conformations. Our results suggest that tau O-GlcNAcylation does not interfere with MT polymerization but may differentially regulate MT binding in an isoform dependent fashion. In addition, the findings suggest that O-GlcNAcylation differentially affects the formation of pathological tau conformations in a tau isoform dependent manner. Thus, further elucidating the temporal profile and role of O-GlcNAcylation in the context of AD and other tauopathies is crucial.

Materials and Methods

Cloning of OGT enzyme

The coding sequence (CDS) of human OGT was amplified by polymerase chain reaction (PCR) from the OGT ORF vector (abm, #32487011) using the Platinum PCR Supermix High Fildelity (Invitrogen, #12532016). Forward and reverse primers were designed to amplify OGT CDS while also introducing NdeI and XhoI restriction sites to the forward and reverse primers, respectively.

Forward primer: CATATGATGGCGTCTTCCGTGGG (NdeI site underlined)
Reverse primer: CTCGAGTTATGCTGACTCAGTGACTTCAA (XhoI site underlined)

The PCR product was subjected to A tailing using native Taq polymerase (Invitrogen, #18038-042) followed by ligation into the pCR2.1-TOPO backbone using the TOPO TA cloning (Invitrogen, #450640). The sequence of OGT CDS was confirmed using Sanger sequencing. OGT CDS was then digested with NdeI (Thermo, #FD0583) and XhoI (Thermo, #FD0694), ran on 1% agarose gel (Biorad, #1613101), and the OGT CDS band was extracted using GeneJET Gel Extraction Kit (Thermo, #K0691). In parallel, the pHis-hTG2 plasmid (Addgene, #100719) was digested with the same enzymes, ran on agarose gel, and the vector band extracted. The vector and OGT CDS DNA were

ligated using the T4 enzyme (Thermo, #EL0011). The ligation product was used to transform TOP10 Chemically Competent cells (Thermo, #C404010) before plating the competent cells in agar plates (Fischer Bioreagents, #BP1423-500) supplemented with Kanamycin at 50mg/ml (Sigma, #K1876). Colonies were picked up from the agar plate, followed by shaking (250 RPM) in Luria Broth (Fischer Bioreagents, #BP1426-2) at 37° C overnight. On the following day, the DNA plasmid was extracted from bacterial cultures using QIAprep Spin Miniprep Kit (Qiagen, #27104). The OGT CDS was verified with diagnostic digestion and sanger sequencing.

Preparation of recombinant unmodified and O-GlcNAc-modified tau proteins

Recombinant tau proteins were prepared by co-transforming BL21 bacteria (NEB, #C2527H) with two plasmids: a plasmid expressing tau under the T7 promoter as described previously (28882311) and the pHis-OGT plasmid. The purification procedure for O-GlcNAc-modified tau proteins was performed using 2 L terrific broth (TB) cultures grown in the presence of ampicillin (50 µg/ml) and kanamycin (25 µg/ml) as selection markers. Moreover, TB was supplemented with GlcNAc (2 mM; Sigma, #U4375) and PUGNAC (10 µM; Sigma, #A7229) to enrich GlcNAc and inhibit the activity of O-GlcNAcase enzyme, respectively. Unmodified tau proteins were grown in the same way with the exception that kanamycin, GlcNAc, and PUGNAC were excluded from TB. Bacterial pellets were lysed using 0.5 M NaCl, 10 mM Tris, and 5 mM Imidazole, pH 8 in the presence of protease inhibitors and PUGNAC (10 µM) at weight: volume ratio of 1:5. PUGNAC was not included in lysing the bacterial pellets for unmodified tau proteins. The bacterial lysate was subjected to centrifugation at 107,377 RCF for 45 min at 4 °C using

a Type 70 Ti rotor (Beckman Coulter, #337922). Supernatant was collected, then the residual bacterial pellet was further lysed in RIPA buffer (10 ml; CST, #9806) supplemented with the same inhibitors by sonicating for 4 times, 30 seconds each. Another centrifugation step was performed to collect the supernatant extracted with the RIPA buffer, followed by pooling the two supernatants (lysis buffer and RIPA buffer) together for further purification. The rest of the purification procedure was performed as described previously (Combs et al., 2017). Briefly, three stages of fast protein liquid chromatography were performed: heavy metal affinity chromatography using a 5 ml HiTrap Talon crude column (Cytiva, #28953767); size exclusion chromatography using HiPrep 16/60 Sephacryl S-500 HR (Cytiva, #28935606); anion exchange chromatography using 5 ml HiTrap Q HP (Cytiva, #17115401). The elution fractions containing the highly purified monomeric tau bands were concentrated to a concentration between 2-4 mg/ml and was supplemented with 1 mM DTT. The final unmodified and O-GlcNAc-modified tau proteins were aliquoted and frozen at -80 °C. The final concentration of recombinant tau proteins was determined using the SDS-Lowry method as described previously (Combs et al., 2017).

Western blot validation of recombinant tau proteins

To confirm the O-GlcNAcylation status of recombinant tau proteins, proteins were loaded on 4-20% Novex tris-glycine gels (Invitrogen, #WXP42020BOX) and run at 225 V for 45 minutes, followed by transfer on nitrocellulose membrane using the Biorad wet transfer system at 40 mAmp for 50 minutes. The membrane was then blocked with 2% non-fat dry milk (NFDM) in 1X tris buffer saline (TBS) for 1 hour at room temperature followed by incubation in primary antibodies overnight at 4 °C. Primary antibodies used

were Tau5 (Nicholas M. Kanaan at Michigan State University, RRID: AB_2721194) (LoPresti et al., 1995; Porzig et al., 2007) at 1:100,000 in 2% NFDM and Anti-Tau (GlcNAc Ser400) (Anaspec, #AS-55945,) at 1:100 in 2% NFDM. The following day, the blot was washed 3 times (5 minutes each) with 1X TBS supplemented with 0.1% Tween 20 (TBS-T 0.1%). Then, secondary antibodies in 2% NFDM were added for 1 hour at room temperature. Secondary antibodies used were peroxidase-conjugated goat anti-mouse IgG1 (Thermo Fisher Scientific, #PA1-74421, RRID: AB_10988195) at 1:5000 and peroxidase-conjugated goat anti-rabbit IgG (Vector Laboratories, #PI-1000-1, RRID: AB_2916034) at 1:2500. The blots were washed 3 times (5 minutes each) with TBS-T 0.1%, followed by the peroxidase development reaction using the Clarity Max™ Western ECL Substrate kit (Biorad, #1705062S). ChemiDoc MP Imaging System and Image Lab 6.0.1 were used to visualize the chemiluminescence signal verifying the O-GlcNAc tau modification status.

Recombinant tau protein preparation for tandem mass spectrometry

Unmodified and O-GlcNAc-modified tau proteins were digested using a combination of Asp-N (Promega, #V V1621) and rLysC (Promega, #V167A). First, each recombinant tau protein sample (10 µg) was subjected to 5 rounds of buffer exchange with 25 mM ammonium bicarbonate (AmBic) pH 8 using 0.5 ml Amicon filter with 3K MWCO (15,000 RCF for 10 minutes; Millipore, #UFC500396). Then, recombinant tau proteins were recovered from the filter by centrifugation at 15,000 RCF for 2 minutes and vacuum dried using Vacufuge. The dried pellets of recombinant tau proteins were reconstituted in 50 µl of digestion buffer (12.5 mM AmBic pH 8 + acetonitrile (ACN) 50%) and incubated at 37 °C for 16-18 hours with Asp-N (150 ng of enzyme). The following

day, digested protein samples were subjected to vacuum drying and stored at 4 °C until the second digestion was initiated. Lys-C (500 ng of enzyme) was added and incubated at 37 °C for 16-18 hours. The following day, digested protein samples were subjected to vacuum drying and stored at -20 °C until running on mass spectrometer.

Tandem mass spectrometry of recombinant tau proteins

We utilized an approach like that described by Yang et al. (Yang et al., 2021). The Vanquish Neo nanoHPLC system interfaced to a Thermo Scientific Orbitrap Eclipse mass spectrometer (Thermo Fisher Scientific) was used for analysis. For each sample, 1 µg was injected and desalted with an AccalaimTM PepMapTM C18 Nano trap column (3 µm, 100 Å, 75 µm × 2 cm) in 100% Buffer A (0.1% formic acid in HPLC water) at 3 µl/min for 5 min. Samples were separated in a linear gradient of 5–35% Buffer B (80% ACN and 0.1% formic acid) over 105 min and washing at 90% Buffer B for 12 min using an Easy Spray PepMapTM RSLC C18 nano column (2 µm, 100 Å, 75 µm × 250 mm). Before the following injection, the column was equilibrated at 1.0 % Buffer B for 5 min. Mass spectra were collected using data dependent mass spectrometry (MS) analysis with a duty cycle of 2 sec. To collect precursor masses, orbitrap [resolution (R) of 120,000 at 200 m/z] with internal calibration was used. For precursors carrying charges between 2 and 8 and with intensities over 5×10^4 at R = 30,000, stepped HCD spectra at HCD energies of 15, 25, and 35% were acquired with dynamic exclusion of 15 sec. The most 20 abundant fragments are monitored for oxonium ions with m/z of 138.0545, 204.0867, 366.1396, 126.005, 144.0655, 168.0654, 186.076, 274.0921, and 292.1027 Da. If at least one oxonium ion was detected at 15 ppm mass accuracy, the corresponding precursor ion was used to collect an EThcD spectrum in the orbitrap at R of 30,000. For charges of 2

and 3, ETD target was 5.0×10^5; for charges of 4 to 8, ETD target was 2.0×10^5. Supplemental collision energy at 15% was also included. Reaction time of ETD was variable according to the precursor charge state. For a charge of 2, ETD reaction time was 125 ms; for a charge of 3, ETD reaction time was 100 ms; for a charge of 4, ETD reaction time was 75ms; for charges ≥5, ETD reaction time was 50 ms.

MS data analysis to determine O-GlcNAc modification sites

RAW data files were analyzed with the MetaMorpheus software version 1.0.1 developed by the Smith laboratory (Miller et al., 2023). For hT40 proteins, the following FASTA files used were downloaded from Uniprot (November 2021) and used for analysis: Escherichia coli (strain K12) (UP000000625), Asp-N (Q9R4J4), Lys-C (Q02SZ7), and full-length tau (2N4R isoform, P10636-8). The same FASTA files were used to analyze the hT39 proteins except for full-length tau (2N4R isoform, P10636-8) that was replaced with 2N3R tau isoform (P10636-5). A mass shift of +203.079 Da ($C_8H_{13}NO_5$) was used to search for O-GlcNAc modifications (Ma & Hart, 2017). In addition, the following mass-to-charge-ratios (m/z) corresponding to diagnostic ions (DIs) were investigated: +126.055 Da ($C_6H_7NO_2$), +138.055 Da ($C_7H_7NO_2$), +144.066 Da ($C_6H_9NO_3$), +168.066 Da ($C_8H_9NO_3$), +186.076 Da ($C_8H_{11}NO_4$), and +204.087 Da ($C_8H_{13}NO_5$) (28150883).

The analysis sequence included mass calibration, global post-translational modification discovery (G-PTM-D) (Li et al., 2017), and a classic search. Mass calibration was conducted using the following criteria: protease = Asp-N/Lys-C; maximum missed cleavages = 2; minimum peptide length = 7; maximum peptide length = unspecified; initiator methionine behavior = Variable; variable modifications = Oxidation on M; max mods per peptide = 2; max modification isoforms = 1024; precursor mass tolerance =

±15.0000 PPM; product mass tolerance = ±25.0000 PPM. The criteria utilized for G-PTM-D were protease = Asp-N/Lys-C; maximum missed cleavages = 2; minimum peptide length = 7; maximum peptide length = unspecified; initiator methionine behavior = Variable; max modification isoforms = 1024; variable modifications = Oxidation on M; G-PTM-D modifications count = 3; precursor mass tolerance(s) = ±5.0000 PPM around 0, 203.079372521 Da; product mass tolerance = ±20.0000 PPM. Finally, a classic search was conducted using the following criteria: protease = Asp-N/Lys-C; search for truncated proteins and proteolysis products = False; maximum missed cleavages = 2; minimum peptide length = 7; maximum peptide length = unspecified; initiator methionine behavior = Variable; variable modifications = Oxidation on M; precursor mass tolerance = ±5.0000 PPM; product mass tolerance = ±20.0000 PPM; report PSM ambiguity = True. Sites of O-GlcNAc modification on tau detected at a false discovery rate of 1% are reported. MetaDraw version 1.0.5 was utilized to review the PSMs of modified and unmodified tau peptides (samples of these peptides are included in Figures AII.1 and AII.2).

Tubulin polymerization assay

Tubulin polymerization in the presence of recombinant tau proteins was assessed using the Tubulin Polymerization Assay Kit (Cytoskeleton, #BK011P). Kit reagents were reconstituted and stored as indicated in the manual. The assay began by incubating the 96-well plate provided with the kit at 37 °C for 10 minutes (Synergy H1 Hybrid Multi-Mode Reader and Gen5 software v3.11, BioTek). Meanwhile, recombinant tau proteins were prepared as 10 µM stocks in general tubulin buffer (80 mM PIPES pH 6.9, 2 mM $MgCl_2$, and 0.5 mM EGTA) and left at room temperature. Then, a tubulin master mix was prepared and kept on ice using the recipe for enhancer detection (kit manual): 355 µl of

Buffer 1, 4.4 µl of 100 mM GTP, and 85 µl of tubulin 10 mg/ml. Once the 10-minute incubation of the 96-well plate was over, recombinant tau (10 µM stocks) were loaded (5 µl) onto the plate and warmed up to 37 °C for exactly 1 minute. Then, the tubulin master mix was loaded (50 µl) on each tau protein sample yielding a final tau concentration of 1 µM. Fluorescence signal was measured for 1 hour to monitor tubulin polymerization using the kinetic mode at excitation and emission wavelengths of 360 nm and 450 nm, respectively. Each tau protein sample was loaded in duplicate (technical replicates) with a sample size of 4 (independent biological replicates). Background levels of blank (general tubulin buffer only) were subtracted from the fluorescence readings before further analyzing the data. Nonlinear regression using “specific binding with Hill slope” was used to fit the tubulin polymerization data in GraphPad Prism v10.2.1 and calculate the steady state equilibrium (V_{max}) along with the time needed to reach half maximal polymerization (K_d).

Microtubule-binding assay

Assays were performed in using Microtubule Binding Protein Spin-Down Assay Biochem Kit (Cytoskeleton, #BK029). Kit reagents were reconstituted as indicated in the manual. Tubulin aliquots (20 µl) were thawed, supplemented with cushion buffer (2 µl; 80 mM PIPES pH 7.0, 1 mM $MgCl_2$, 1 mM EGTA, and 60% sucrose), and incubated at 35 °C for exactly 40 minutes. Then, general tubulin buffer (200 µl; 80 mM PIPES pH 7.0, 1 mM $MgCl_2$, and 1 mM EGTA) supplemented with paclitaxel at 20 µM was added to the polymerized tubulin. Microtubule-binding reactions were set up at room temperature including tubulin (10 µl), recombinant tau proteins (1 µM), and general tubulin buffer to a final volume of 50 µl. After 30 minutes of incubation at room temperature, binding

reactions were loaded on 100 µl of sucrose cushion buffer in 0.2 ml polycarbonate tubes (Thermo Scientific, #45233) followed by centrifugation at 100,000 RCF for 40 minutes. For all centrifugation steps, S100-AT3 Fixed Angle Rotor (Thermo Scientific, #45585) and Sorvall™ MTX 150 Micro-Ultracentrifuge (Thermo Scientific, #46960) were employed. Then, 30 µl of the supernatant were carefully removed (Sup) to avoid disturbing the microtubule pellet. Laemmli buffer was added to the supernatant immediately (6 µl of 6X Laemmli buffer). The rest of the supernatant was discarded, followed by washing the microtubule pellet with general tubulin buffer (100 µl) supplemented with 20 µM paclitaxel. The microtubule pellet was subjected to centrifugation at 100,000 RCF for an additional 20 minutes. The previous washing step was repeated one more time, followed by careful removal of the supernatant. The final pellet was resuspended in 60 µl of 1X Laemmli buffer. The assay was conducted 4 independent times.

For each biological replicate, Sup and Pellet (15 µl each) were subjected to SDS-PAGE. Unmodified and O-GlcNAc-modified tau samples were loaded on two separate 4-20% Novex tris-glycine gels (Invitrogen, #WXP42020) that was run at 225 V for 40-45 minutes. After SDS-PAGE, the two gels were cut between the 250 and 37 kDa marker bands. Two gels were added to the same transfer sandwich and transferred onto one nitrocellulose membrane. This step allows for the quantification of tau bands from two experimental replicates on the same blot to minimize the variability in blotting procedure across samples. The rest of the blotting procedure was performed as described earlier. Primary antibodies used were the Tau5 antibody at 1:100,000 (same as above) and the tubulin 5H1 antibody at 1:10,000 (Nicholas M. Kanaan at Michigan State University, RRID: AB_2832941) (Wang et al., 1993). Secondary antibodies used were goat anti-

mouse IgG1 680 (LI-COR Biosciences, #926-68050, RRID: AB_2783642) and goat anti-mouse IgM 800 (LI-COR Biosciences, #926-32280, RRID: AB_2814919) at 1:20,000 each. LI-COR Odyssey classic imager and Image Studio Lite Ver 5.2 were used to visualize fluorescent signals of the antibody probes. Tau bands were quantified in all Sup and Pellet fractions followed by calculating the percentage of tau in Pellet relative to total tau using the following equation:

$$\% \text{ Tau in Pellet} = \text{Tau in Pellet}/(\text{Tau in Pellet} + \text{Tau in Sup}) \times 100$$

In vitro recombinant tau aggregation reaction

Aggregation of tau proteins was induced by arachidonic acid (ARA; Cayman Chemical, #90010) in 200 µl reactions as described previously (Gamblin, King, Kuret, et al., 2000; Tiernan et al., 2016). Briefly, 2 µM of tau (M. Wt. = 43426 for hT39; M. Wt. = 46673 for hT40) was induced to aggregate *in vitro* by incubation in tau aggregation buffer (10 mM sodium HEPES, 0.1 mM EDTA, 200 mM NaCl, 5 mM DTT, pH 7.6) with (aggregated) or without (unaggregated; ethanol vehicle was used) 75 µM ARA. ARA stocks were prepared in 100% ethanol at 2 mM immediately prior to use. Finally, ARA was added as the final component in the reaction sample and then the samples were gently mixed by minimally shaking the tube/cuvette. Aggregation reactions were incubated at room temperature for 6 hours.

Right angle laser light scattering

As tau polymerizes into aggregates, the intensity of scattered light increases as a function of time and is used to measure tau aggregation kinetics (Gamblin, King, Dawson, et al., 2000; Tiernan et al., 2016). Laser light scattering (LLS) was measured using class IIb laser with wavelength of 475 nm and maximum power of 20 mW (B & W INC., model

#BWI-475-20-E) and digital camera (Thor Labs, model #DCC1240M). Images were acquired using uc480 Viewer version 4.2 with the pixel clock set at 11 MHz. Images were acquired for hT40 samples at a frame rate of 2 fps and exposure of 150 ms, while a frame rate of 1 fps and exposure time to 300 ms was used for hT39 samples. Polymerization reactions of tau were transferred into glass cuvettes with path length of 5 mm (Starna Cells, #3-G-5), and laser light scattering was measured at time zero, prior to addition of ARA to obtain baseline measurements. After addition of ARA and gently mixing the samples, images were serially acquired at 1, 2, 3, 4, 5, 10, 15, 20, 25, 30, 35, 40, 45, 50, 55, 60, 75, 90, 105, 120, 150, 180, 240, 300, 360 minutes. Each experiment was conducted 4 independent times. Image analysis was performed with Adobe Photoshop CS6 (Adobe Systems INC.) using the marquee tool. The region of interest used for densitometry measurements was set to 150 pixels X 15 pixels and adjusted to the center of the glass cuvette within the band of scattered light. Pixel intensity was recorded using the histogram feature. Scattered light intensity (Is) measurements during the 6 hours were fitted using nonlinear Finke-Watzky function (Morris et al., 2008) according to the following equation:

$$[B]_t = [A]_0 - ((k_1/k_2+[A]_0)/(1+(k_1/k_2[A]_0 \exp(k_1+k_2[A]_0)t))$$

To compare aggregation kinetics of different proteins, the following parameters were calculated: k_1 represents the rate constant of nucleation; k_2 represents the rate constant of elongation; $[A]_0$ represents maximum scattering.

Thioflavin S fluorescence

At the end of the tau aggregation reaction with ARA (described above), β-sheet containing aggregates were quantified using a thioflavin S assay as described (Tiernan

et al., 2016). Immediately before starting the assay, a 0.0175% thioflavin S (ThS) solution was prepared in water, filtered through a 0.22 μM membrane, and protected from light. Then, 150 μl of each tau sample was mixed with 6 μl of ThS solution and incubated for 5 minutes at room temperature. The samples (150 μl/well) were then loaded onto a black 96-well plate (Costar, #3915) and immediately read using the Promega Glomax multi-detection system at 490 nm excitation and 510-570 nm emission wavelengths. Control buffers for unaggregated and aggregated reactions were loaded and read to obtain background measurements, then their absorbance values were subtracted from the other values before analysis.

Sample preparation for imaging with transmission electron microscopy

Transmission electron microscopy (TEM) was used to visualize and measure aggregate density and size (Tiernan et al., 2016). To this end, uranyl acetate (UA; Electron Microscopy Sciences, #22400) solution was freshly prepared by dissolving 20 mg of UA in 1 ml of deionized water (DIW) (2% UA solution) at room temperature. After UA completely dissolves into DIW, the solution was sterile filtered using 0.22 μM membrane (Fisher Scientific, #13-1001-06). To prepare the grids, each unaggregated and aggregated tau sample (10 μl each) was fixed with 2% glutaraldehyde (Electron Microscopy Sciences, #16100) at room temperature for 10 minutes. Then, each sample (5μl) was absorbed onto formvar-coated copper grids (Electron Microscopy Sciences, #FCF300-CU) for 1 minute, followed by one rapid rinse in DI water and another rapid rinse in UA solution. Finally, the grids were incubated with UA solution for 1 minute at room temperature, then the solution was wicked away, and grids were left to dry for at least 1.5 hours before imaging. Grids were prepared from 4 independent replicates of

unaggregated and aggregated tau grids and imaged using JEOL JEM-1400 Plus electron microscope at 80 kV. Electron micrographs were captured and saved through AMT XR81 digital camera and AMT software version 602.6.

Quantitative TEM

For each grid, three images were captured at 5000 X magnification for quantitative TEM. Electron micrographs were then processed using ImageJ v1.54 using a method like that described by Tiernan et al. (Tiernan et al., 2016). First, the image scale was adjusted according to the scale bar attached to the TEM images. Then, images were smoothened 3 times to allow for the automatic thresholding to capture the visible tau aggregates. Finally, the percentage area of aggregated mass (% Area) was collected by the "Analyze Particles" command. For the "Analyze Particles" command, size was set at 0-infinity and circularity was set at 0-1.

Output of "Analyze Particles" command was further processed using GraphPad Prism v10.2.1 to obtain frequency distribution using 700 nm^2-wide and 50 nm^2-wide bins for hT40 and hT39, respectively. The sum of particles in 3 images/replicate was calculated and counted as 1 independent replicate, with a total of 4 independent replicates. The following populations of hT40 were plotted according to criteria like those reported by Tiernan et al. (Tiernan et al., 2016): < 700 nm^2 for globular aggregates only; 700-2100 nm^2 for globular aggregates > 700 nm^2 along with short filaments; 2100-5000 nm^2 for short filaments only; > 5000 nm^2 for long filaments only. Aggregates of hT39 were globular in nature and split into sizes smaller and larger than 1200 nm^2.

Western blot for unaggregated and aggregated reactions

Unaggregated and aggregated tau samples were prepared for SDS-PAGE by diluting to 0.5 μM in 6X Laemmli sample buffer. Samples were boiled at 95 °C for 5 minutes in a heat block, followed by vortex and quick spin down. Samples (500 ng/lane) were loaded on 20-well 4-20% Novex tris-glycine gel (Invitrogen, #WXP42020). Proteins were transferred to nitrocellulose membrane using the Bio-Rad wet transfer system. The blot was blocked with 2% NFDM for 1 hour at room temperature, followed by incubation in Tau5 antibody (as above) at a dilution of 1:100,000 in 2% NFDM overnight at 4 °C. The following day, the membrane was washed 3 times with TBST, 5 minutes each. The goat anti-mouse IgG1 680 (as above) secondary antibody was used at a dilution of 1:20,000 in 2% NFDM, and membranes were incubated in secondary at room temperature for 1 hour. Membranes were washed with TBST 3 times, 5 minutes each, before imaging the blot using LI-COR Odyssey classic imager and Image Studio Lite Ver 5.2. Tau bands corresponding to monomeric tau (monomer band) and higher molecular weight multimers (HMW band) were quantified in the unaggregated and aggregated tau samples.

Sandwich enzyme-linked immunosorbent assay (sELISA)

To detect pathological tau conformations using conformation-dependent antibodies (i.e. TOC1, TOMA1, TNT2, and Alz50), tau samples must be kept under native conditions (Castillo-Carranza, Sengupta, et al., 2014; Combs et al., 2016; Combs et al., 2017; Jicha et al., 1997; Ward et al., 2013). Therefore, sandwich ELISA assays were employed to measure pathological tau conformations. All steps were performed at room temperature. The following capture antibodies were used in sandwich ELISA assays: TOC1 (Nicholas M. Kanaan at Michigan State University, RRID: AB_2832939) to

measure TOC1-positive oligomeric tau, TOMA1 (Millipore, #MABN819) to measure TOMA1-positive oligomeric tau, TNT2 (Nicholas M. Kanaan at Michigan State University, RRID: AB_2736931) to measure PAD exposed tau, Alz50 (P. Davies Albert Einstein College of Medicine, New York, USA, RRID: AB_2313937) to measure misfolded tau, and Tau13 (Nicholas M. Kanaan at Michigan State University, RRID: AB_2721193) to measure total tau (Carmel et al., 1996; Castillo-Carranza, Sengupta, et al., 2014; Combs et al., 2016; Combs & Kanaan, 2017; Garcia-Sierra et al., 2003; Hyman, Van Hoesen, et al., 1988; Jicha et al., 1997; Patterson et al., 2011; Ward et al., 2013). Capture antibodies were diluted to 2 ng/µl in borate saline buffer (100 mM borate acid, 25 mM sodium borate, 75 mM NaCl, and 0.25 mM thimerosal). Then, sandwich ELISA plates (96-well plates, Corning, #3590) were coated with the capture antibodies (50 µl/well) for 1 hour. Wells were washed 2 times with ELISA wash buffer (200 µl/well; 100 mM borate acid, 25 mM sodium borate, 75 mM NaCl, 0.25 mM thimerosal, 0.4% (w/v) bovine serum albumin, and 0.05% (v/v) Tween-20), followed by blocking with 5% NFDM in ELISA wash buffer (200 µl/well) for 1 hour. Two washes with ELISA wash buffer were performed, followed by the addition of unaggregated and aggregated tau samples for 1.5 hours. Tau samples were prepared from unaggregated and aggregated hT40 reactions in TBS buffer at the following concentrations (50 µl /well): 2.5 nM for Tau13; 5 nM for TNT2; 20 nM for TOC1 and Alz50; 150 nM for TOMA1. Tau samples were prepared from unaggregated and aggregated hT39 reactions in TBS buffer at the following concentrations (50 µl/well): 2.5 nM for Tau13; 20 nM for Alz50; 50 nM for TNT2; 150 nM for TOC1 and TOMA1. Then, wells were washed 4 times with ELISA wash buffer (200 µl/well). The detection antibody R1 (Nicholas M. Kanaan at Michigan State University, RRID: AB_2832929) (Berry et al.,

2004) was diluted at 1:10,000 in 5% NFDM and added to the wells (50 µl/well) for 1.5 hours. Then, sandwich ELISA wells were washed 4 times with ELISA wash buffer. The secondary antibody used was Goat Anti-Rabbit IgG Antibody (H+L), Peroxidase (Vector Laboratories, #PI-1000-1, RRID: AB_2916034) at 1:5,000 in 5% NFDM for 1 hour (50µl/well). After 4 final washes with ELISA wash buffer, the peroxidase reaction was developed using 3,3′,5,5′-Tetramethylbenzidine (TMB; 50 µl/well; Sigma, #T0440). The peroxidase reaction was stopped with 4% sulphuric acid, followed by reading the absorbance at 450nm using SpectraMax Plus 384 microplate reader (Molecular Devices). Each assay was run using 4 independent experimental samples.

The absorbance values were further processed using GraphPad Prism v10.2.1 according to the following equation to calculate the percentage light absorbed (% Light Abs, %A):

$$\%A = 100 - (100 * 10^{-A})$$

Seeding assay in tau biosensor cells

HEK293 cells stably expressing the repeat domain of tau with the P301S mutation fused to CFP or YFP (Tau RD P301S Biosensor Cells; ATCC, #CRL-3275, RRID: CVCL_DA04) (Holmes et al., 2014) were grown in DMEM (Gibco) supplemented with 10% FBS, 1% Penicillin-Streptomycin (Gibco), and 1x GlutaMAX (Gibco), and maintained at 37 °C and 5% CO2. A cell aliquot was thawed and passaged at least once before use in experiments. Cells were plated at 12,000 cells/well in Poly-D-Lysine coated 96-well plates (100µl media/well; Corning, #354461). After 24 hours, Lipofectamine 2000 (Invitrogen, #11668027) was used to deliver the following treatment samples into cells: unaggregated hT40, aggregated hT40 aggregates, unaggregated O-GlcNAc modified

hT40, and aggregated O-GlcNAc modified hT40 (at a final concentration of 150 nM). In two separate tubes, Lipofectamine reagent or protein sample was diluted in OptiMEM (Gibco, #31985062) and incubated at room temperature for 20 minutes. The first tube contained 1 μl Lipofectamine 2000 in addition to 9 μl OptiMEM, and the other tube contained 7.5 μl unaggregated or aggregated tau + 2.5 μl OptiMEM. Next, the Lipofectamine was mixed with the tau protein (20 μl total) and incubated for an additional 20 minutes at room temperature. The Lipofectamine/protein mixture was then added to the cells (20 μl). Two days following treatment, cells were fixed with pre-warmed 4% paraformaldehyde (Electron Microscopy Sciences, #15714-S) in 1X cytoskeleton buffer (10 mM MES, 138 mM KCl, 3 mM $MgCl_2$, and 4 mM EGTA, pH 6.1) for 20 min at room temperature. Then, cells were washed 3 times with 1X TBS, 5 minutes each. The nuclear stain DAPI (1:10,000) was included in the first wash.

Cells were imaged using a Lionheart FX Automated Microscope (BioTek) using a 10x objective. Nine images per well were captured with GFP and DAPI filter cubes using the same acquisition settings. Images were processed and analyzed using Gen5 software v3.11 (BioTek). Seeded aggregates and nuclei were detected in the GFP and DAPI channels, respectively, using separate sets of size and pixel-intensity thresholds. For each well, the total number of aggregates was normalized to the total number of cells to obtain the number of seeds per cell (seeds/cell = number of GFP+ objects/number of DAPI+ objects).

Statistics

Statistical analysis was performed using GraphPad Prism v10.2.1. Unpaired, two-tailed t-test was employed to analyze the following results: V_{max} and K_d of tubulin

polymerization assay; Max and k_1 of LLS for hT40; Max of LLS for hT39; % Area of quantitative TEM. Mann-Witney U was used for violations of normality and/or equal variances: k_2 of LLS data for hT40; k_1 and k_2 of LLS data for hT39. Two-way analysis of variance (ANOVA) followed by the post-hoc Holm-Sidak with all possible comparisons were used to analyze the following results: % Tau in pellet of microtubule-binding assay; ThS fluorescence; Monomer and HMW bands for stable multimers; % light absorbed of sandwich ELISA assays; seeds/cell of seeding assay in RD cells. Differences in outcomes were deemed statistically significant at $p \leq 0.05$.

Results

Co-transformation of bacterial cells with tau and OGT introduces O-GlcNAc modifications on serine and threonine residues of tau

Recombinant hT40 and hT39 proteins modified with O-GlcNAc were produced using the co-transformation and purification approaches described in the methods section. To confirm the modification status of the final protein preparations, western blotting for O-GlcNAc Ser400 tau and total tau was employed. Unmodified hT40 and hT39 did not have signal with the Anti-Tau O-GlcNAc Ser400 antibody, while the modified hT40 and hT39 were labeled by the Anti-Tau O-GlcNAc Ser400 antibody (Figure 3.1 A, top panel). Both unmodified and modified tau proteins showed similar reactivity to the Tau5 antibody, a pan-tau antibody (Figure 3.1A, lower panel).

Availability of O-GlcNAc modified tau antibodies are limited to the Ser400 modification site antibody. To more robustly identify which S/T residues are modified throughout the hT40 and hT39 proteins, MS analysis was employed. MS demonstrated that hT40 and hT39 share several of the same O-GlcNAc modified S/T residues, including

T175, T181, S400, S413/T414/S416, S422, T427, and S433 (Figure 3.1B). In addition, O-GlcNAc modifications on S184/S185 and S195/S198/S199 were detected only in O-GlcNAc-modified hT40, while modifications on T386 and S396 were detected only in O-GlcNAc-modified hT39 (Figure 3.1B, lower panel). The O-GlcNAc modifications were detected by mass shifts and diagnostics ion in O-GlcNAc-modified hT40 and hT39 samples. The diagnostics ions observed with O-GlcNAc-modified tau proteins and mass spectra of the peptide spanning amino acids 402-429 from the O-GlcNAc-modified hT40 and hT39 protein preparations are demonstrated in Figures AII.1 and AII.2.

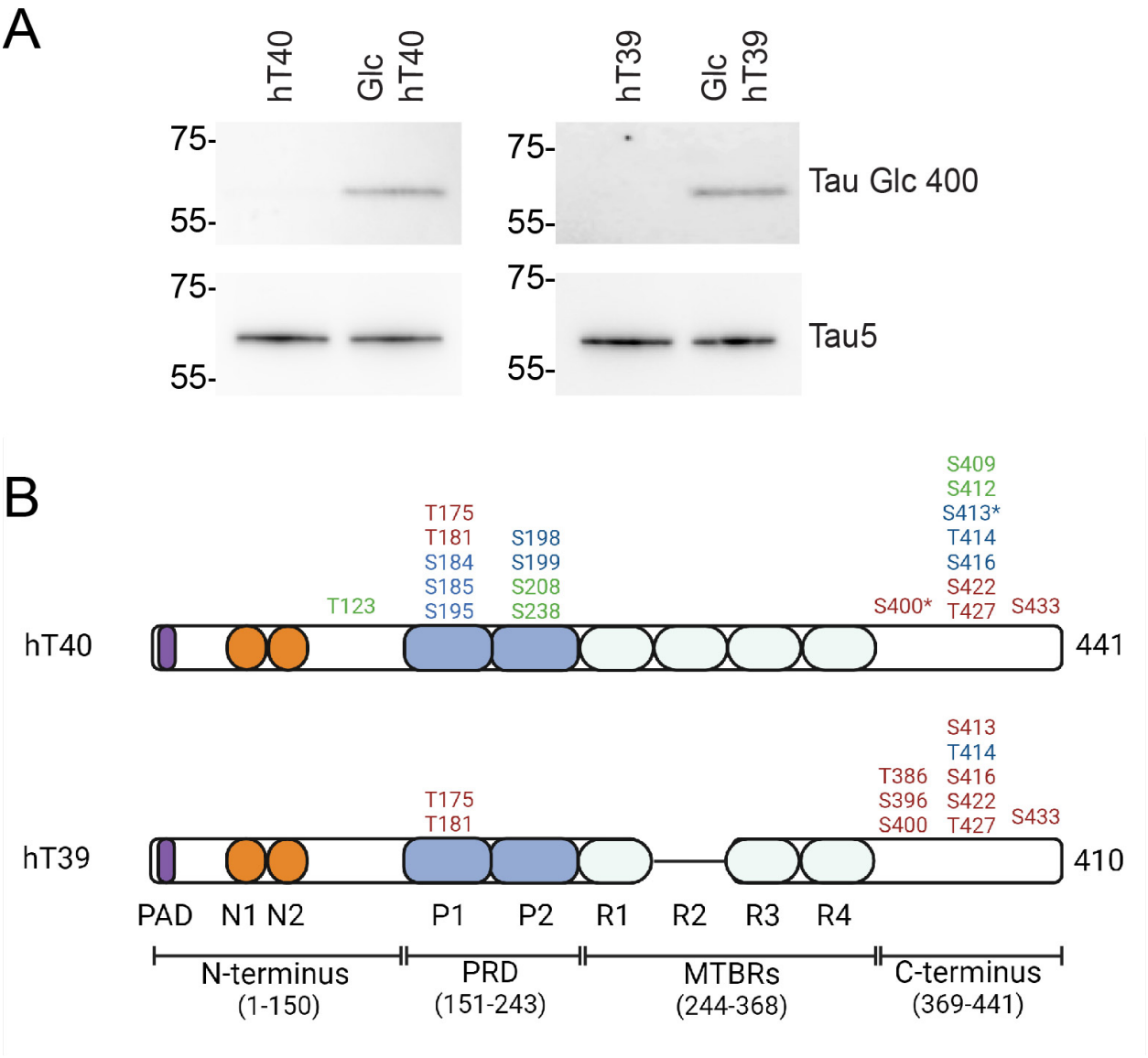

Figure 3.1. Identification of S/T residues on tau modified with O-GlcNAc.
A, western blot of hT40 (left blots) and hT39 (right blots) proteins probed with the Tau5 (total tau) and Anti-Tau O-GlcNAc-Ser400 antibodies. B, S/T residues modified with O-GlcNAc on tau as detected by mass spectrometry. Residues are numbered according to the sequence of full-length tau (hT40, 2N4R, 441 amino acids). Residues highlighted in red are confirmed modification sites in our study. For some O-GlcNAc sites, site-specific information could not be determined (in blue). Residues highlighted in green represent O-GlcNAc modification sites reported in previous studies but not in our study. Asterisk (*) represents modification sites common between our study and previous studies. O-GlcNAc sites are concentrated within the PRD and C-terminus. Abbreviations: O-GlcNAc, O-linked-N-acetyl β-d-N-glucosamine; Glc, O-GlcNAcylated; S/T, serine/threonine; hT40, 2N4R tau isoform; hT39, 2N3R tau isoform; PRD, proline rich domain; MTBRs, microtubule-binding repeats. Panel B created with BioRender.com.

O-GlcNAc-modified tau does not alter microtubule polymerization in vitro

Tubulin polymerization assays were used to determine how O-GlcNAc modification affects tau ability to modulate the microtubule polymerization kinetics *in vitro* (Figure 3.2A and B). O-GlcNAc-modified hT40 did not change the steady state polymerization (Figure 3.2C, left panel; V_{max}, t = 1.745, p > 0.05) nor the time to half maximal polymerization (Figure 3.2C, right panel; K_d, t = 1.978, p > 0.05) of microtubules when compared to unmodified hT40. Similarly, O-GlcNAc-modified hT39 did not alter the steady state polymerization (Figure 3.2D, left panel; V_{max}, t = 0.1206, p > 0.05) nor the time to half maximal polymerization (Figure 3.2D, right panel; K_d, t = 1.583, p > 0.05) of microtubules time to half maximal polymerization relative to unmodified hT39.

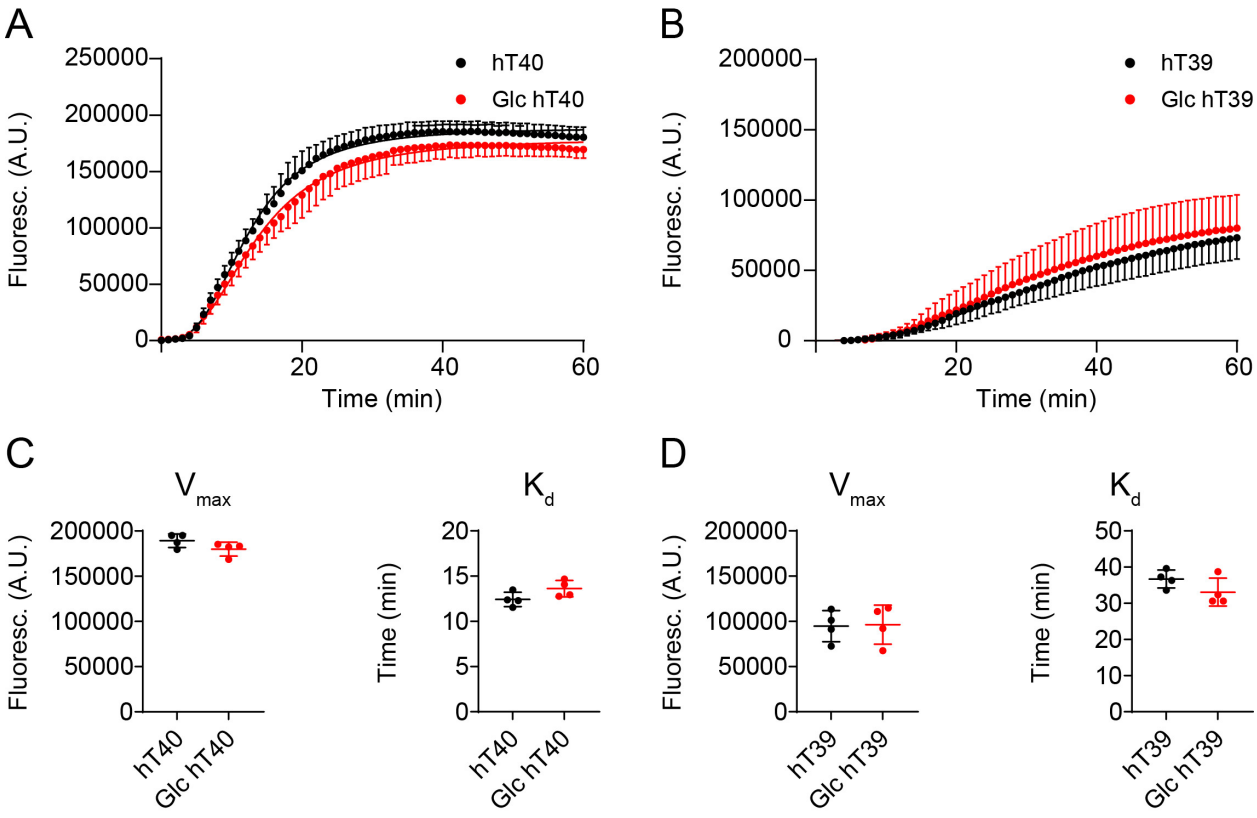

Figure 3.2. O-GlcNAc modification of tau does not alter tubulin polymerization *in vitro*.

Figure 3.2 (cont'd)
A, curve fit of fluorescence signal corresponding to microtubule polymerization in the presence of either unmodified hT40 (black) or O-GlcNAc modified hT40 (red) over 60 minutes. B, curve fit of fluorescence signal corresponding to microtubule polymerization in the presence of either unmodified hT39 (black) or O-GlcNAc modified hT39 (red) over 60 minutes. C, Vmax of microtubule polymerization for unmodified hT40 and Glc hT40 proteins (left panel). Kd of microtubule polymerization for unmodified hT40 and Glc hT40 (right panel). D, Vmax of microtubule polymerization for unmodified hT39 and Glc hT39 proteins (left panel). Kd of microtubule polymerization for unmodified hT39 and Glc hT39 (right panel). Abbreviations: O-GlcNAc, O-linked-N-acetyl β-d-N-glucosamine; Glc, O-GlcNAcylated; hT40, 2N4R tau isoform; hT39, 2N3R tau isoform; Vmax, steady state equilibrium; Kd, time to half maximal polymerization. Data represented as mean +/- SD.

O-GlcNAc modification differentially affects binding of tau to microtubules in vitro

Microtubule-binding assays were used to determine how O-GlcNAc modification affects tau's ability to bind pre-formed microtubules. Experiments were conducted using either the hT40 or hT39 tau isoforms independently (Figure 3.3A and C). Two-way ANOVA analysis revealed a statistically significant interaction between the PTM status of proteins and the presence of microtubules [$F_{(1,12)} = 14.59$, $p < 0.05$]. Post-hoc analysis showed a statistically significant shift of unmodified and O-GlcNAc-modified hT40 into the pellet fraction upon adding them to pre-formed microtubules ($t = 19.10$, $p < 0.05$ for hT40; $t = 24.50$, $p < 0.05$ for Glc hT40). Moreover, there was a significant 30% increase of O-GlcNAc-modified hT40 in the pelleted microtubule fraction relative to unmodified hT40 (Figure 3.3B; $t = 5.953$, $p < 0.05$).

For the hT39 isoform, two-way ANOVA showed a statistically significant interaction between the PTM status of proteins and the presence of microtubules [$F_{(1, 12)} = 21.85$, $p < 0.05$]. Furthermore, post-hoc analysis demonstrated a statistically significant shift of unmodified and O-GlcNAc-modified hT39 into the pellet fraction upon adding them to pre-formed microtubules ($t = 14.77$, $p < 0.05$ for hT39; $t = 8.164$, $p < 0.05$ for Glc hT39).

Contrary to the case with hT40, O-GlcNAc-modified hT39 in the pelleted microtubule fraction was significantly lower than unmodified hT39 by 45% (Figure 3.3D; $t = 6.731$, $p < 0.05$).

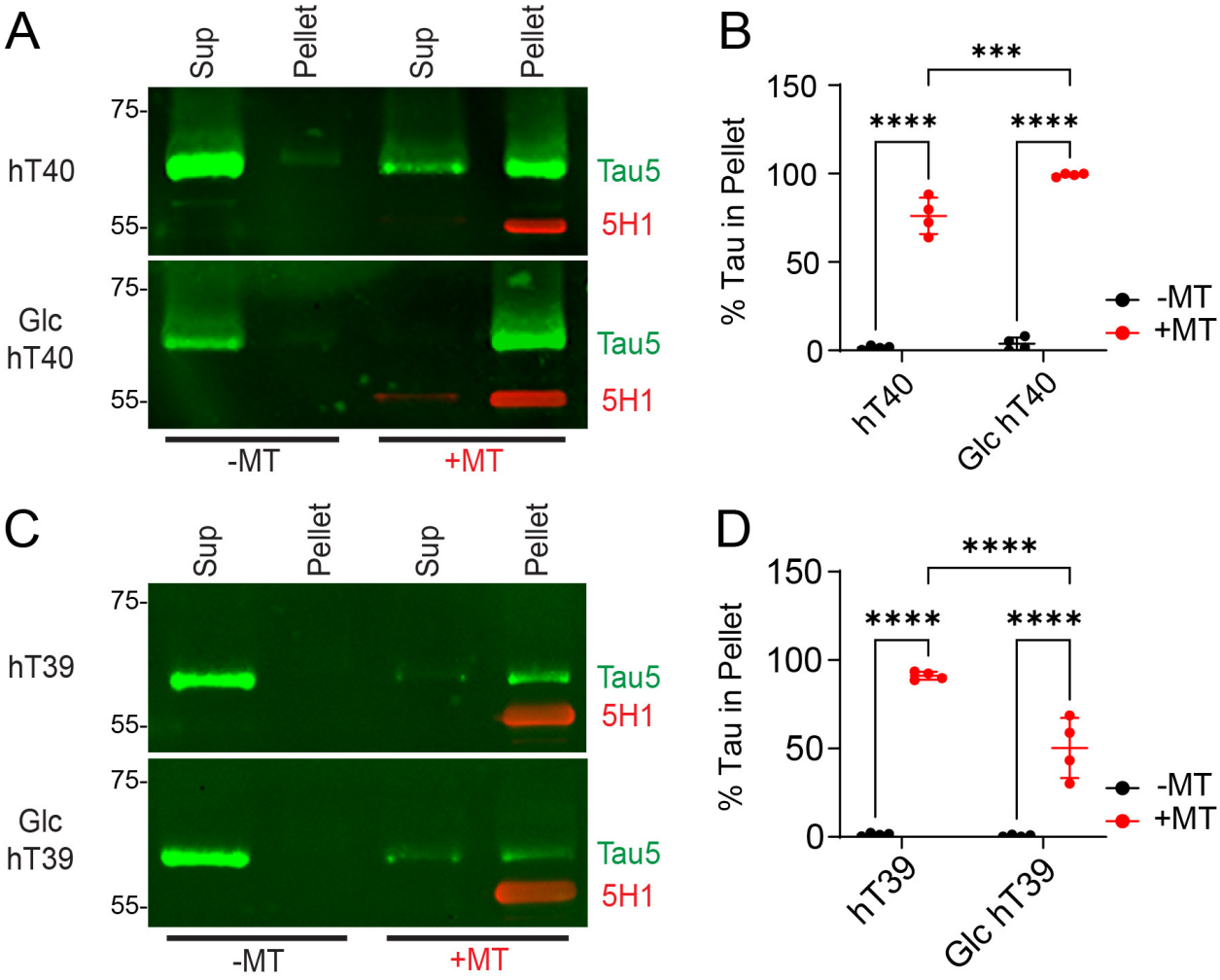

Figure 3.3. O-GlcNAc modification differentially alters binding of tau to microtubules *in vitro*.
A, western blot of microtubule-binding assay for unmodified and O-GlcNAc modified hT40 proteins using Tau5 and 5H1 (tubulin) antibodies. B, quantification of the fraction of tau detected in the pellet of polymerized microtubules for unmodified and O-GlcNAc modified hT40. C, western blot of microtubule-binding assay for unmodified and O-GlcNAc modified hT39 proteins using Tau5 and 5H1 (tubulin) antibodies. D, quantification of the fraction of tau detected in the pellet of polymerized microtubules for unmodified and O-GlcNAc modified hT39. Abbreviations: O-GlcNAc, O-linked-N-acetyl β-d-N-glucosamine; Glc, O-GlcNAcylated; hT40, 2N4R tau isoform; hT39, 2N3R tau isoform; MT,

Figure 3.3 (cont'd)
microtubules; Sup, supernatant. Data represented as mean ± SD. * $p \leq 0.05$; ** $p \leq 0.01$; *** $p \leq 0.001$; **** $p \leq 0.0001$.

O-GlcNAc modification of tau alters its aggregation kinetics in vitro

Right-angle LLS assays were used to determine the impact of O-GlcNAc modification on the kinetics of tau aggregation *in vitro* (Figure 3.4A and B). We observed 32% reduction the maximum light scattering with O-GlcNAc-modified hT40 compared to the unmodified hT40 (Figure 3.4G; $t = 4.042$, $p < 0.05$). However, O-GlcNAc modification did not affect the rate constants of nucleation (Figure 3.4C; $t = 2.212$, $p > 0.05$) or elongation (Figure 3.4D; Mann Whitney $U = 4$, $p > 0.05$) of hT40 protein. Similarly, O-GlcNAc modification decreased the maximum light scattering of hT39 proteins by 27% (Figure 3.4I; $t = 2.523$, $p < 0.05$) and the rate constant of nucleation by 65% (Figure 3.4E; Mann Whitney $U = 0$, $p < 0.05$). However, O-GlcNAc modification did not affect the rate of elongation (Figure F; Mann Whitney $U = 7$, $p > 0.05$).

O-GlcNAc modification of tau reduces its β-sheet containing aggregates in vitro

ThS assays were performed at the end of aggregation reactions to determine the extent of β-sheet containing aggregate formation *in vitro*. Two-way ANOVA revealed a statistically significant interaction between the PTM and aggregation status of proteins [$F_{(1, 12)} = 15.62$, $p < 0.05$ for hT40 proteins; $F_{(1, 12)} = 5.548$, $p < 0.05$ for hT39 proteins]. Upon aggregating hT40 and hT39 proteins, there was a significant increase in the ThS signal compared to their respective unaggregated samples regardless of the O-GlcNAc modification (Figure 3.4H and J; $t = 22.19$, $p < 0.05$ for unmodified hT40; $t = 16.6$, $p < 0.05$ for GlcNAc hT40; $t = 9.383$, $p < 0.05$ for unmodified hT39; $t = 6.052$, $p < 0.05$ for GlcNAc hT39). Moreover, the O-GlcNAc-modified aggregates of hT40 and hT39 showed

lower ThS fluorescence compared to their respective unmodified tau aggregates (Figure 3.4H and J; 24% reduction, $t = 5.448$, $p < 0.05$ for hT40 proteins; 32% reduction, $t = 3.394$, $p < 0.05$ for hT39 proteins).

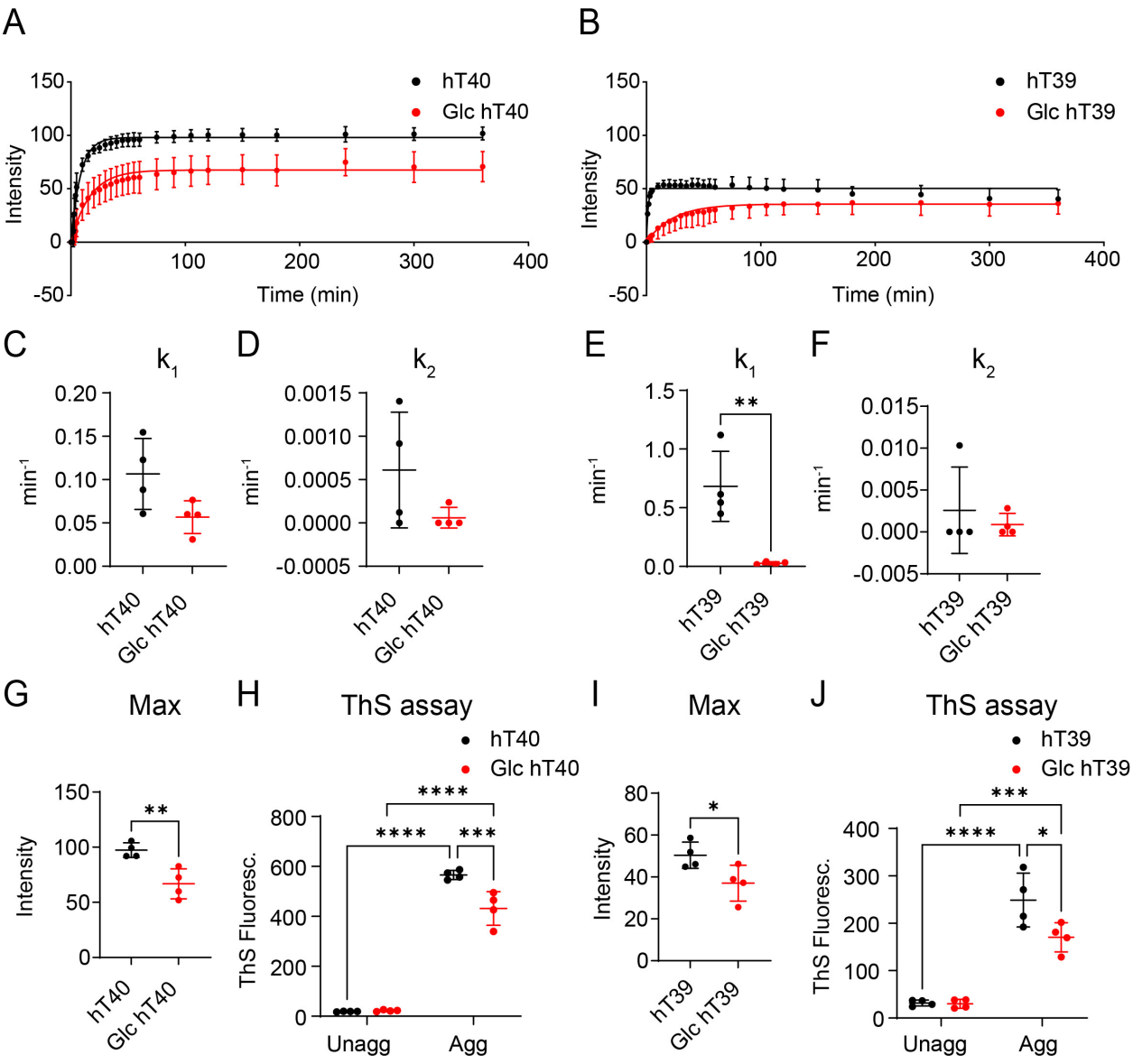

Figure 3.4. O-GlcNAc modification of tau decreases the extent of tau multimerization and β-sheet containing aggregates *in vitro*.
A, LLS of unmodified hT40 and O-GlcNAc-modified hT40. B, LLS of unmodified hT39 and O-GlcNAc modified hT39. C, k_1 for aggregation of unmodified hT40 and O-GlcNAc modified hT40 proteins. D, k_2 for aggregation of unmodified hT40 and O-GlcNAc modified hT40. E, k_1 for aggregation of unmodified hT39 and O-GlcNAc modified hT39 proteins. F, k_2 for aggregation of unmodified hT39 and O-GlcNAc modified hT39. G, max

Figure 3.4 (cont'd)
polymerization for unmodified hT40 and O-GlcNAc modified hT40. H, ThS fluorescence after 6 hours of tau aggregation for unmodified hT40 and O-GlcNAc modified hT40. I, max polymerization for unmodified hT39 and O-GlcNAc modified hT39. J, ThS fluorescence after 6 hours of tau aggregation for unmodified hT39 and O-GlcNAc modified hT39. Abbreviations: O-GlcNAc, O-linked-N-acetyl β-d-N-glucosamine; Glc, O-GlcNAcylated; hT40, 2N4R tau isoform; hT39, 2N3R tau isoform; unagg, unaggregated; agg, aggregated; LLS, laser light scattering; ThS, thioflavin S; k_1, rate constant of nucleation; k_2, rate constant of elongation; max, maximum light scattering. Data represented as mean +/- SD. * $p \leq 0.05$; ** $p \leq 0.01$; *** $p \leq 0.001$; **** $p \leq 0.0001$.

O-GlcNAc modification differentially alters the size of tau aggregates in vitro

Upon investigating the unaggregated and aggregated hT40 samples using TEM (Figure 3.5A), there was no significant change in the aggregated mass of O-GlcNAc modified hT40 compared to unmodified hT40 (Figure 3.5D; $t = 0.3362$, $p > 0.05$). Of note, the number of globular aggregates < 700 nm^2 was increased upon O-GlcNAcylation of hT40 (Figure 3.5C, upper panel). On the other hand, the number of long filamentous aggregates (> 5000 nm^2) decreased with O-GlcNAc-modified hT40 compared to unmodified hT40 (Figure 3.5C, lower panel).

There was no statistically significant difference in the aggregated mass between unmodified and O-GlcNAc modified hT39 (Figure 3.5F; $t = 1.875$, $p > 0.05$). The size distribution of globular aggregates formed by O-GlcNAc-modified hT39 showed a decrease in the number of globular aggregates < 1200 nm^2 (Figure 3.5E, upper panel). Conversely, the number of globular aggregates > 1200 nm^2 was higher with O-GlcNAc-modified hT39 relative to unmodified hT39 (Figure 3.5E, lower panel).

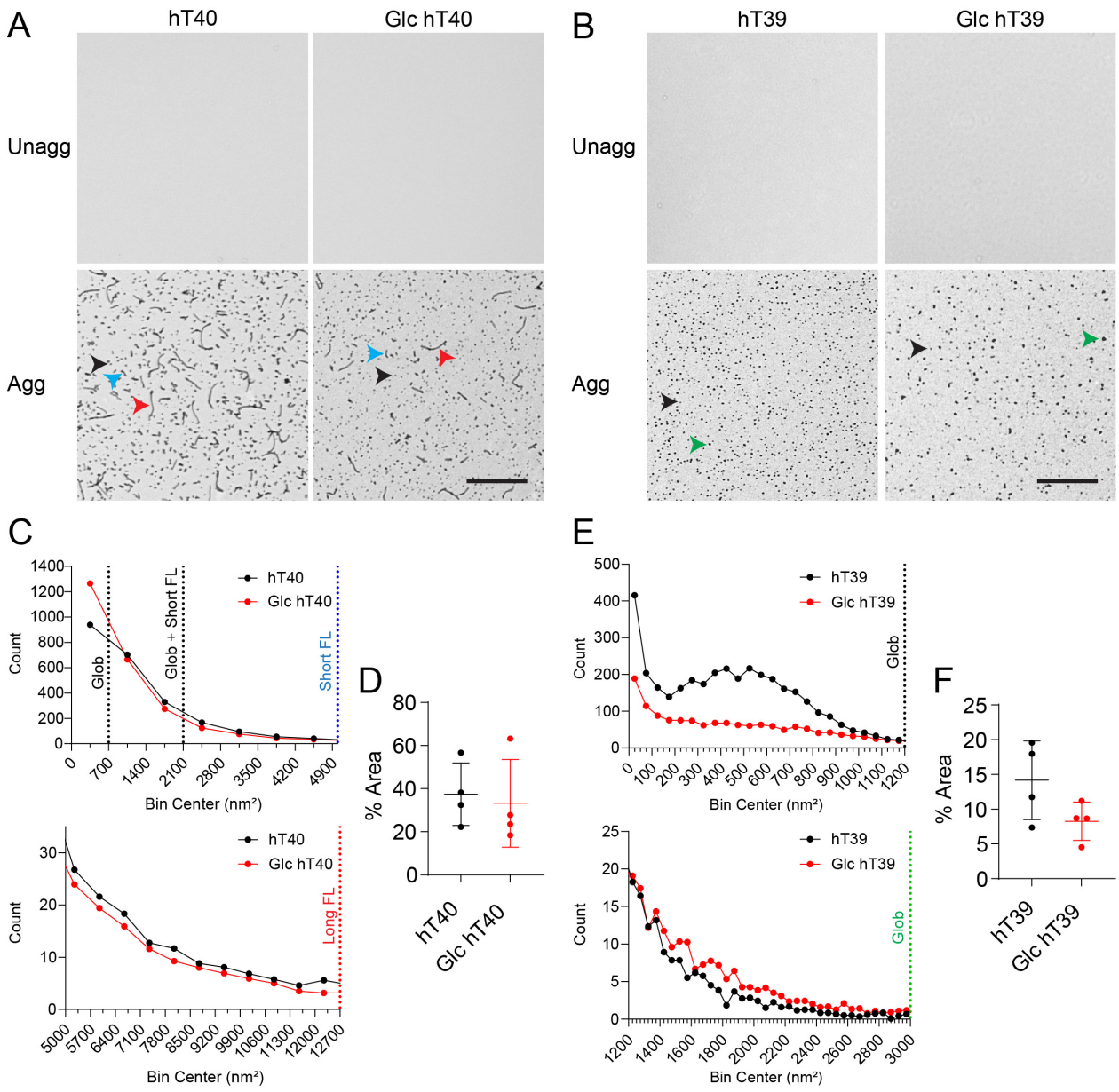

Figure 3.5. O-GlcNAc modification alters the size distribution of tau aggregates *in vitro*.

A, electron micrographs of unaggregated and aggregated hT40 proteins. Scale bar: 800nm. Globular aggregates < 700 nm^2 highlighted with black arrowheads; short (2100-5000 nm^2) and long (> 5000 nm^2) filaments highlighted with blue and red arrowheads, respectively. B, electron micrographs of unaggregated and aggregated hT39 proteins. Scale bar: 800nm. Globular aggregates < 1200 nm^2 highlighted with black arrowheads; globular aggregates > 1200 nm^2 highlighted with green arrowhead. C, size distribution of aggregates formed by unmodified and Glc hT40 proteins. D, total mass of aggregates observed with unmodified and Glc hT40 expressed as percentage of field area. E, size distribution of aggregates formed by unmodified and Glc hT39 proteins. F, total mass of

Figure 3.5 (cont'd)
aggregates observed with unmodified and Glc hT39 expressed as percentage of field area. Abbreviations: O-GlcNAc, O-linked-N-acetyl β-d-N-glucosamine; Glc, O-GlcNAcylated; hT40, 2N4R tau isoform; hT39, 2N3R tau isoform; unagg, unaggregated; agg, aggregated; % Area, % of aggregates per field. Data represented as mean ± SD. * $p \leq 0.05$; ** $p \leq 0.01$; *** $p \leq 0.001$; **** $p \leq 0.0001$.

O-GlcNAc modification differentially alters the formation of stable tau multimers in vitro

Tau aggregation leads to the formation of heat, SDS and reducing condition stable multimers. Here, SDS-PAGE and western blotting were employed to assess the extent to which O-GlcNAc modification of tau affects the formation of these stable multimers (Figure 3.6A and B). Two-way ANOVA showed a significant main effect of aggregation on the levels of stable multimers for hT40 proteins [Figure 3.6C; $F_{(1,12)} = 83.99$, $p < 0.05$]. A significant increase in the stable multimers upon aggregating hT40 proteins regardless of the O-GlcNAc modification was observed (3-fold increase, $t = 6.431$, $p < 0.05$ for unmodified hT40; 3.8-fold increase, $t = 6.530$, $p < 0.05$ for GlcNAc hT40). Furthermore, two-way ANOVA revealed a significant main effect of aggregation on the levels of monomeric tau [Figure 3.6B; $F_{(1,12)} = 14.98$, $p < 0.05$]. The intensity of monomeric tau band was reduced by 23% in aggregated O-GlcNAc-modified hT40 when compared to unaggregated O-GlcNAc-modified hT40 ($t = 3.657$, $p < 0.05$). No difference was observed in the monomeric tau signal upon aggregating the unmodified hT40 ($t = 1.816$, $p > 0.05$).

We also assessed the extent to which O-GlcNAc modification affect the monomeric and stable multimers bands in hT39 proteins. Two-way ANOVA demonstrated a significant main effect of aggregation on the levels of monomeric tau in hT39 proteins [Figure 3.6E; $F_{(1,12)} = 30.81$, $p < 0.05$]. There was a statistically significant reduction in monomeric tau signal upon aggregation regardless of the O-GlcNAc modification status

(36% decrease, $t = 5.536$, $p < 0.05$ for unmodified hT39; 27.5% decrease, $t = 3.314$, $p < 0.05$ for GlcNAc hT39). Furthermore, two-way ANOVA indicated a significant main effect of both aggregation and PTM status on the stable tau multimers [Figure 3.6F; $F_{(1,12)} = 11.67$, $p < 0.05$ for aggregation; $F_{(1, 12)} = 25.32$, $p < 0.05$ for PTM]. Despite the increase in stable multimers upon aggregating O-GlcNAc modified hT39 ($t = 3.107$, $p < 0.05$), post-hoc analysis confirmed that stable multimers were lower with O-GlcNAc-modified hT39 proteins in the unaggregated and aggregated samples (72% decrease, $t = 4.250$, $p < 0.05$ for unaggregated samples; 37% decrease, $t = 5.505$, $p < 0.05$ for aggregated samples).

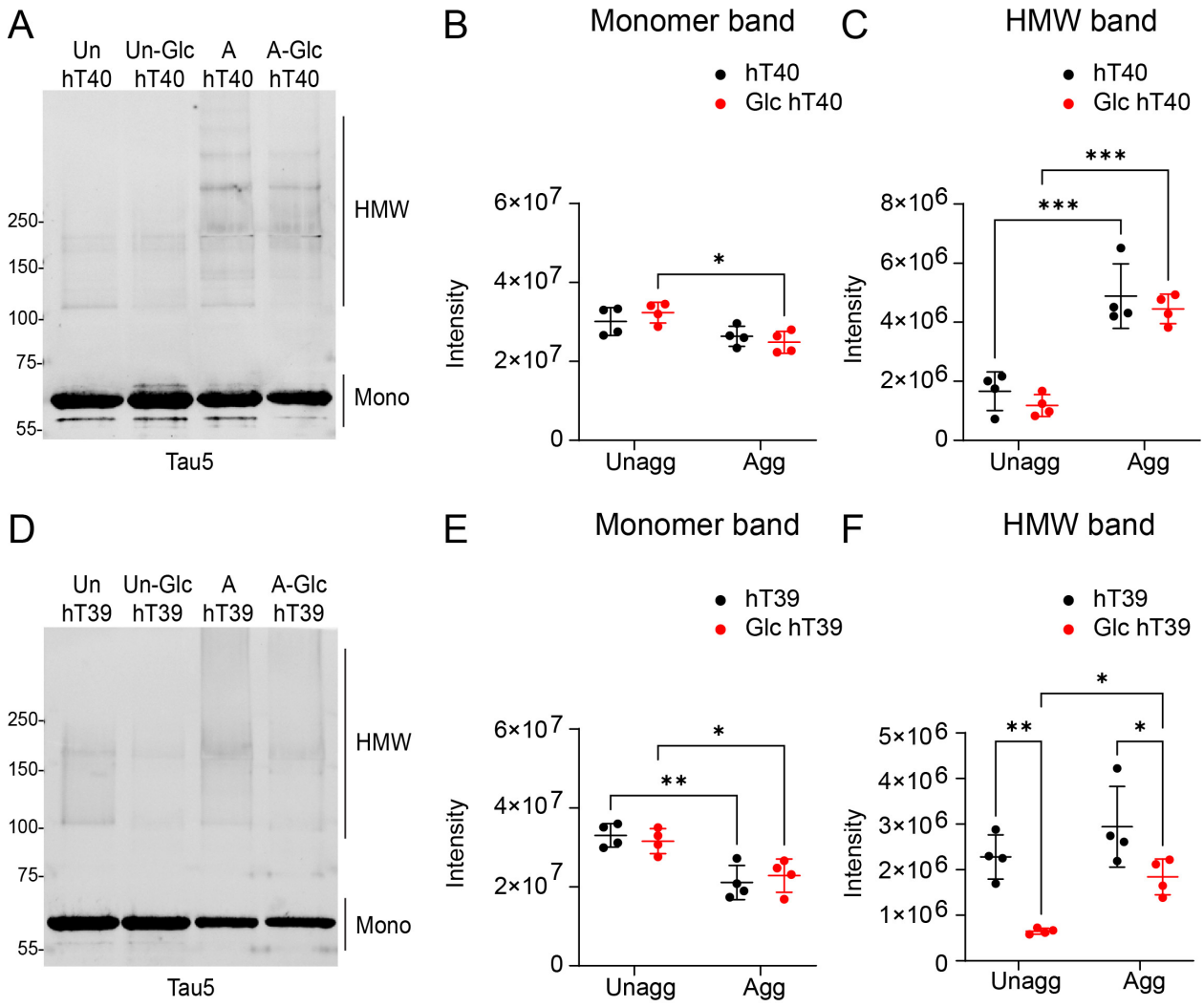

Figure 3.6. O-GlcNAc modification differentially alters the formation of stable tau multimers.

A, western blot of unaggregated and aggregated hT40 samples probed with Tau5 antibody. B, quantification of monomeric tau bands in hT40 samples. C, quantification of HMW tau bands in hT40 samples. D, western blot of unaggregated and aggregated hT39 samples probed with Tau5 antibody. E, quantification of monomeric tau bands in hT39 samples. F, quantification of HMW tau bands in hT39 samples. Abbreviations: O-GlcNAc, O-linked-N-acetyl β-d-N-glucosamine; Glc, O-GlcNAcylated; hT40, 2N4R tau isoform; hT39, 2N3R tau isoform; unagg, unaggregated; agg, aggregated; Mono, monomer band; HMW, high molecular weight band. Data represented as mean ± SD. * $p \leq 0.05$; ** $p \leq 0.01$; *** $p \leq 0.001$; **** $p \leq 0.0001$.

O-GlcNAc modification differentially alters the formation of pathological tau conformations in vitro

Several antibodies are available to detect oligomeric tau species, which are linked to toxicity and neurodegeneration (Alhadidy & Kanaan, 2024; Castillo-Carranza, Gerson, et al., 2014; Patterson et al., 2011; Ward et al., 2013). Oligomeric tau species were quantified in unaggregated and aggregated tau samples using sandwich ELISAs with two different oligomeric tau antibodies (i.e. TOC1 and TOMA1). Two-way ANOVA demonstrated a significant interaction between the PTM and aggregation factors on the levels of TOC1-positive oligomeric tau in hT40 samples [$F_{(1, 12)} = 13.65$, $p < 0.05$]. Post-hoc analysis showed an increase in TOC1-positive oligomeric tau in the aggregated samples of unmodified and O-GlcNAc modified hT40 relative to their respective unaggregated tau proteins (Figure 3.7A, left panel for TOC1; $t = 40.09$, $p < 0.05$ for unmodified hT40; $t = 34.86$, $p < 0.05$ for GlcNAc hT40). In addition, aggregated O-GlcNAc modified hT40 showed a small (8%) yet significant reduction in TOC1 signal relative to the aggregated unmodified hT40 samples ($t = 3.916$, $p < 0.05$). Conducting TOC1 sandwich ELISA assays with the hT39 protein samples [two-way ANOVA; Interaction: $F_{(1, 12)} = 62.15$, $p < 0.05$] revealed increased TOC1-positive oligomeric tau in the aggregated samples of unmodified and O-GlcNAc modified hT39 proteins relative to their respective unaggregated samples (Figure 3.7A, right panel; $t = 19.66$, $p < 0.05$ for unmodified hT39; $t = 30.81$, $p < 0.05$ for GlcNAc hT39). In contrast to hT40, aggregated O-GlcNAc modified hT39 samples had 45% higher TOC1-positive oligomeric tau relative to the aggregated samples of unmodified hT39 ($t = 11.02$, $p < 0.05$).

Then, we assessed the levels of TOMA1-positive oligomeric tau species in the unmodified and O-GlcNAc-modified tau samples. Aggregation of unmodified and O-GlcNAc modified hT40 elicited an increase in the TOMA1 signal when compared to the unaggregated samples (Figure 3.7B, left panel; Aggregation factor: $F_{(1, 12)} = 62.43$, $p < 0.05$; $t = 6.484$, $p < 0.05$ for unmodified hT40; $t = 4.691$, $p < 0.05$ for GlcNAc hT40). The same finding was also observed upon the aggregation of unmodified and O-GlcNAc modified hT39 proteins, where the TOMA1 signal was increased compared to the unaggregated hT39 tau samples (Figure 3.7B, right panel; Aggregation factor: $F_{(1, 12)} = 67.75$, $p < 0.05$; $t = 19.66$, $p < 0.05$ for unmodified hT39; $t = 30.81$, $p < 0.05$ for GlcNAc hT39). Unlike the TOC1 results, no differences were observed between unmodified and O-GlcNAc modified hT40 and hT39 proteins in unaggregated and aggregated samples.

Tau is known to adopt pathological conformations associated with modifications of monomeric tau and following multimerization (Alhadidy & Kanaan, 2024; Christensen et al., 2023; Hintermayer et al., 2020; Kanaan et al., 2011). Those conformations include exposure of the PAD of tau that spans amino acids 2-18 and whose abnormal exposure has been linked to dysfunction of axonal transport (Combs et al., 2021; Kanaan et al., 2011; LaPointe et al., 2009). Another misfolded conformation involves the N-terminus of tau coming into close proximity to the microtubule-binding region of tau that is thought to happen early in disease and precede tau aggregation (Carmel et al., 1996; Hyman, Van Hoesen, et al., 1988; Jicha et al., 1997).

The extent to which O-GlcNAc modification can influence the adoption of pathological conformations was assessed using sandwich ELISA with TNT2 for PAD exposure and Alz50 for the misfolding. Regardless of O-GlcNAc modification, aggregated

hT40 samples showed higher TNT2 signal compared to the unaggregated samples (Figure 3.7C, left panel; Aggregation factor: $F_{(1, 12)} = 10007$, $p < 0.05$; $t = 70.19$, $p < 0.05$ for unmodified hT40; $t = 71.28$, $p < 0.05$ for GlcNAc hT40). On the other hand, two-way ANOVA demonstrated a significant interaction between the PTM and aggregation factors on the levels of TNT2 signal in hT39 samples [$F_{(1, 12)} = 48.81$, $p < 0.05$]. The TNT2 signal was higher in the aggregated hT39 relative to the unaggregated samples regardless of their modification status (Figure 3.7C, right panel; $t = 13.48$, $p < 0.05$ for unmodified hT39; $t = 23.36$, $p < 0.05$ for GlcNAc hT39). No differences in TNT2 signal were detected among the unaggregated samples of unmodified and O-GlcNAc modified hT39 proteins ($t = 0.06469$, $p > 0.05$). However, the TNT2 signal in the aggregated O-GlcNAc modified hT39 samples was 60% higher than the aggregated samples of unmodified hT39 ($t = 9.945$, $p < 0.05$).

Two-way ANOVA demonstrated a significant interaction between the PTM and aggregation factors on the levels of Alz50 signal in both hT40 [$F_{(1, 12)} = 6.067$, $p < 0.05$] and hT39 [$F_{(1, 12)} = 6.067$, $p < 0.05$] samples. Alz50-positive misfolded tau was higher in the aggregated hT40 samples relative to the unaggregated samples regardless of the O-GlcNAc modification (Figure 3.7D, left panel; $t = 68.42$, $p < 0.05$ for unmodified hT40; $t = 64.93$, $p < 0.05$ for GlcNAc hT40). Of note, Alz50-positive misfolded conformation was significantly increased by 40% in the unaggregated O-GlcNAc modified hT40 relative to unmodified hT40 ($t = 2.832$, $p < 0.05$). However, no difference was observed in the Alz50 signal between the aggregated samples of unmodified and O-GlcNAc modified hT40 proteins ($t = 0.6514$, $p > 0.05$).

Regardless of the O-GlcNAcylation status of proteins, aggregated hT39 samples showed higher Alz50 signal compared to the unaggregated samples (Figure 3.7D, right panel; $t = 13.33$, $p < 0.05$ for unmodified hT39; $t = 24.95$, $p < 0.05$ for GlcNAc hT39). On the other hand, aggregated O-GlcNAc modified hT39 showed higher Alz50-positive tau relative to unmodified hT39 aggregates ($t = 11.19$, $p < 0.05$).

For all unaggregated and aggregated hT40 and hT39 proteins, total tau levels were measured using Tau13 as capture antibody (Figure AII.3). No differences were observed in total tau levels across the hT40 or the hT39 samples.

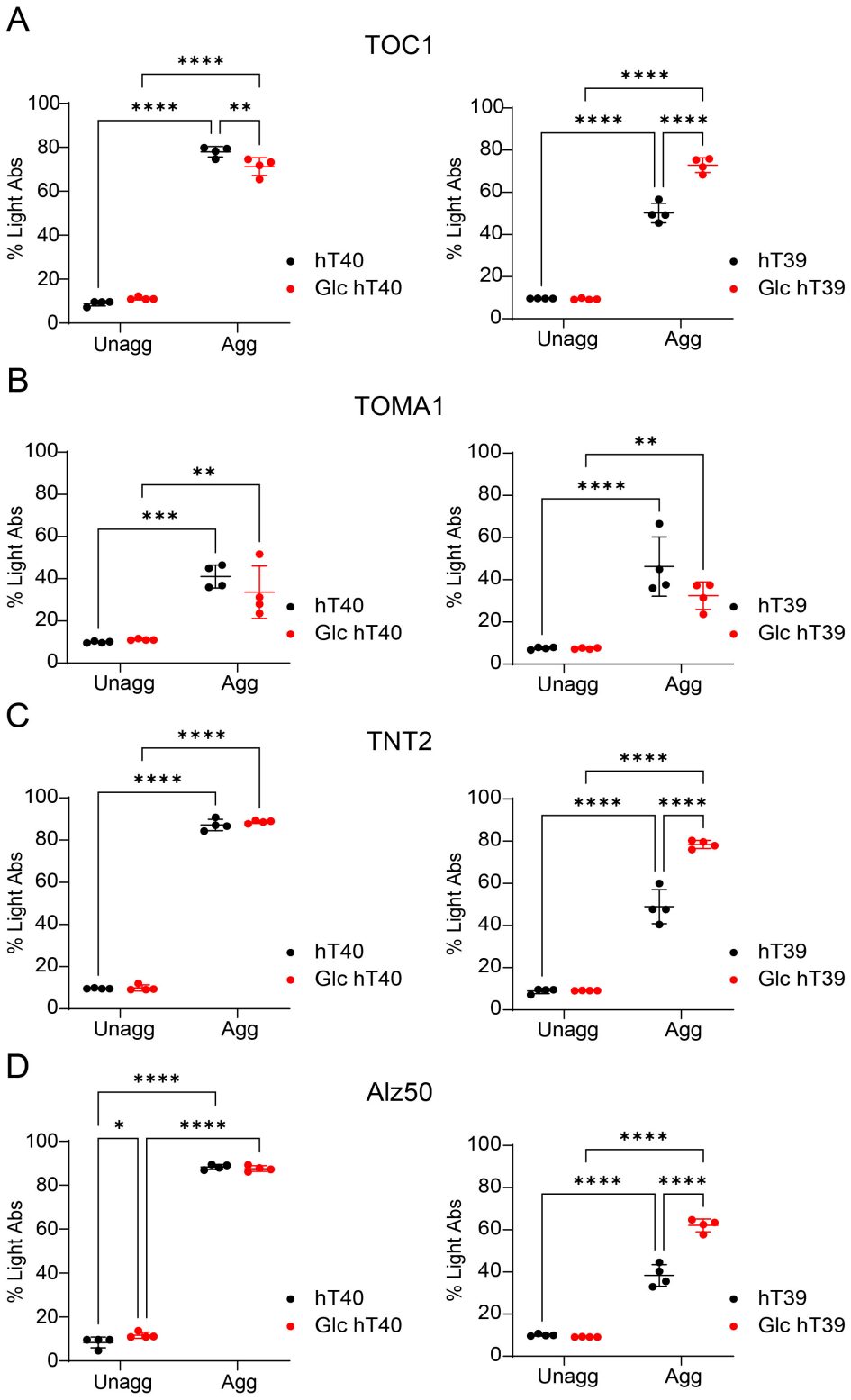

Figure 3.7. O-GlcNAc modification of tau alters the formation of pathological conformations upon aggregation *in vitro*.

Figure 3.7 (cont'd)
A, sandwich ELISA assay measuring oligomeric tau in unaggregated and aggregated hT40 (left panel) and hT39 (right panel) proteins using TOC1 antibody for capture and R1 antibody for detection. B, sandwich ELISA assay measuring oligomeric tau in unaggregated and aggregated hT40 (left panel) and hT39 (right panel) proteins using TOMA1 antibody for capture and R1 antibody for detection. C, sandwich ELISA assay measuring PAD exposure in unaggregated and aggregated hT40 (left panel) and hT39 (right panel) proteins using TNT2 antibody for capture and R1 antibody for detection. D, sandwich ELISA assay measuring misfolded tau conformation in unaggregated and aggregated hT40 (left panel) and hT39 (right panel) proteins using Alz50 antibody for capture and R1 antibody for detection. Abbreviations; O-GlcNAc, O-linked-N-acetyl β-d-N-glucosamine; Glc, O-GlcNAcylated; hT40, 2N4R tau isoform; hT39, 2N3R tau isoform; unagg, unaggregated; agg, aggregated; TOC1, tau oligomeric complex 1 antibody; TOMA1, oligomer-specific monoclonal antibody; TNT2, tau N-terminal 2 antibody to measure PAD exposure; Alz50, misfolded tau conformation antibody; R1, tau rabbit polyclonal antibody. Data represented as mean ± SD. * $p \leq 0.05$; ** $p \leq 0.01$; *** $p \leq 0.001$; **** $p \leq 0.0001$.

O-GlcNAc modification of tau reduces its seeding capability in tau biosensor cells

Tau RD P301S biosensor cells were used to determine whether O-GlcNAc modification alters hT40 seeding competency. In unaggregated samples, no seeding was observed with unmodified or O-GlcNAc-modified hT40 treated cells (Figure 3.8A and B). Regardless of the O-GlcNAc modification [two-way ANOVA; Interaction: $F_{(1, 12)} = 28.78$, $p < 0.05$], the aggregated hT40 samples significantly induced seeding in the cells relative to the unaggregated samples ($t = 11.13$, $p < 0.05$ for unmodified hT40; $t = 3.542$, $p < 0.05$ for GlcNAc hT40). However, significantly less seeding (65% lower) was observed in the cells treated with O-GlcNAc modified hT40 aggregates compared to the aggregates of unmodified hT40 ($t = 7.546$, $p < 0.05$).

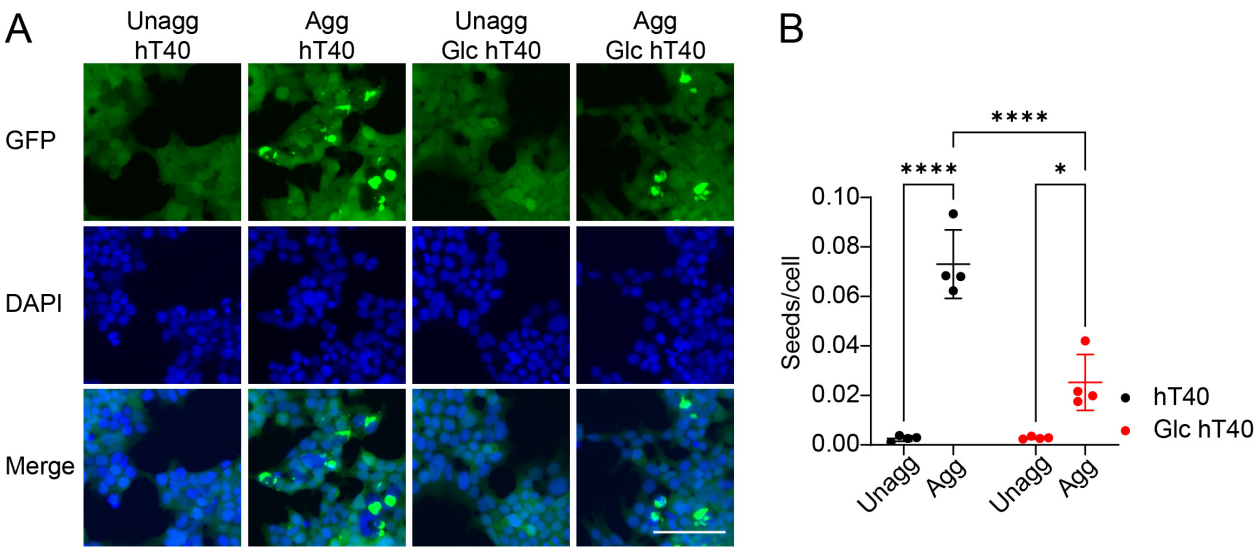

Figure 3.8. O-GlcNAc modification of tau reduces its seeding competency in tau biosensor cells.
A, images of tau seeds in cells treated with unaggregated and aggregated hT40 proteins (green) along with DAPI staining (blue) as a surrogate for cell count. Scale bar: 200 µm. B, quantification of number of seeds per cell in cells treated with unaggregated and aggregated hT40 proteins. Abbreviations: O-GlcNAc, O-linked-N-acetyl β-d-N-glucosamine; Glc, O-GlcNAcylated, 2N4R tau isoform; unagg, unaggregated; agg, aggregated; GFP, green fluorescent protein channel (green); DAPI, 4',6-diamidino-2-phenylindole channel (blue). * $p \leq 0.05$; ** $p \leq 0.01$; *** $p \leq 0.001$; **** $p \leq 0.0001$.

Discussion

PTMs regulate several aspects of tau protein biology including aggregation, conformational changes, microtubule binding, degradation, and clearance (Alhadidy & Kanaan, 2024; Alquezar et al., 2020). Tau is subject to modification with O-GlcNAc as reported in studies utilizing recombinant proteins, cell lines, animal models, and AD brains (Liu et al., 2004; Liu et al., 2009; Morris et al., 2015; Yuzwa et al., 2014; Yuzwa et al., 2008; Yuzwa et al., 2011). O-GlcNAcylation of the longest tau isoform (2N4R isoform, hT40) competes with phosphorylation and inhibits formation of filamentous tau aggregates (Smet-Nocca et al., 2011; Yuzwa et al., 2008; Yuzwa et al., 2012). The previously observed effects of O-GlcNAcylation on tau biology are partially attributed to

modifying S400 (Cantrelle et al., 2021; Yuzwa et al., 2014). In this work, we show that tau is modified by O-GlcNAcylation on S400 in addition to several novel sites (e.g. T175, T181, S422, S427, and S433) (Smet-Nocca et al., 2011; Yuzwa et al., 2011). Of note, O-GlcNAcylation sites are concentrated within the proline-rich domain (PRD) and C-terminal domain of tau (Alhadidy & Kanaan, 2024; El Mammeri et al., 2022).

As mentioned previously, we observed O-GlcNAc modification at sites not previously reported, such as T175, T181, S422, S427, and S433. Similarly, previous MS studies identified O-GlcNAc modification at sites that was not identifiable in our study such as S208, S238, and T231 (Smet-Nocca et al., 2011; Yuzwa et al., 2011). This difference in detectable modification sites is not surprising given the challenging nature of detecting O-GlcNAc sites using mass spectrometry (Ma & Hart, 2017). Furthermore, variations in recombinant protein preparation, bacterial strains used for co-transformation, digestion conditions, and MS detection protocols may explain differences in O-GlcNAc sites identified among different studies.

Several of the O-GlcNAc modification sites, including the novel sites identified in our study, are potentially important in the context of disease because they are phosphorylated in tauopathies. For example, phosphorylation at T175 and T181 in the PRD of tau increases significantly in multiple tauopathies, such as AD, PiD, and CBD (Barthelemy et al., 2019; Ferrer et al., 2014; Jack et al., 2018; Liu et al., 2009; Moszczynski et al., 2017; Suarez-Calvet et al., 2020; Wesseling et al., 2020; Xia, Prokop, et al., 2021). On the C-terminus of tau, phosphorylation at S422 and the PHF-1 epitope (S396/S404) is universally upregulated early in several tauopathies (Ferrer et al., 2014; Guillozet-Bongaarts et al., 2006; Guillozet-Bongaarts et al., 2007; Kimura et al., 1996;

Mondragon-Rodriguez et al., 2014; Otvos et al., 1994; Vana et al., 2011). It is intriguing that reduced O-GlcNAcylation of tau is co-incident with increased phosphorylation at S422 and PHF-1 (Liu et al., 2009). Therefore, the relationship between O-GlcNAcylation and phosphorylation of these sites warrants further investigation (Cantrelle et al., 2021; Yuzwa et al., 2008).

The functional implications of O-GlcNAc modification of tau are not well studied; however, PTMs of tau are known to impact its ability to modulate microtubule dynamics and binding (Alonso et al., 1994; Amniai et al., 2009; Black et al., 1996; Breuzard et al., 2013; Cleveland et al., 1977; Cohen et al., 2011; Haj-Yahya et al., 2020; Weingarten et al., 1975). Our results show that the rate and extent of microtubule polymerization did not change in the presence of O-GlcNAc-modified tau proteins. In agreement, the Vocadlo group published identical results where O-GlcNAcylation of hT40 did not alter microtubule polymerization (Yuzwa et al., 2014). On the other hand, tau's binding to microtubules was reduced with O-GlcNAcylation of hT39 and increased with O-GlcNAcylation of hT40. These findings suggest that O-GlcNAcylation differentially regulates the binding of tau isoforms to microtubules

The opposite effect on hT40 and hT39 is a novel finding, which may be explained by the additional hT39-specific modification of T386 and S396 in fifth microtubule-binding repeat of tau (R'). Indeed, a recent study by the Hong group utilized nuclear magnetic resonance (NMR) to elucidate the role of tau jaws in binding to microtubules (Gustke et al., 1994; Mukrasch et al., 2007; Preuss et al., 1997). NMR spectra indicated that the R' binds to Taxol-stabilized microtubules with an affinity higher than any other microtubule-binding repeats (El Mammeri et al., 2022). In addition, this interface between microtubules

and R' region is sequestered away from water, likely by the dynamic second proline-rich domain (P2) and the first microtubule-binding repeat (R1) (El Mammeri et al., 2022). The additional modifications at T386 and S396, along with S400, on R' of hT39 may disrupt the sequestration of the R' microtubule interface from water by modifying the net charge of R'. On the other hand, hT40 has less O-GlcNAc-modified sites at the R' region but relatively more abundant O-GlcNAcylation at S184/S185/S195 and S198/S199 of the P2 region. The heavier density of O-GlcNAcylation at the P2 region may enhance water sequestration of the R' microtubule interface mediated by the dynamicity of P2 and R1 regions. Taken together, these findings suggest that O-GlcNAcylation may regulate microtubule binding a tau isoform-dependent manner.

O-GlcNAcylation of tau decreases the extent of tau aggregation (LLS) with a reduction in β-sheet containing aggregates (ThS). In addition, TEM demonstrated that O-GlcNAc modification of hT40 disfavors the formation of long filamentous tau aggregates. Corroborating our results, Yuzwa et al. previously reported impeded aggregation and reduced the β-sheet content of O-GlcNAcylated full-length tau (Yuzwa et al., 2014). On the other hand, the size of globular hT39 increases with O-GlcNAcylation, suggesting this modification has an impact on tau multimerization. Additional evidence that O-GlcNAcylation differentially regulates the multimerization of tau isoforms was the direction of change in stable multimers formed upon aggregation (Patterson et al., 2011; Tiernan et al., 2016). O-GlcNAc-modified hT40 showed an increase in stable multimers upon aggregation comparable to that observed with unmodified hT40. Conversely, the stable multimers are reduced both in the unaggregated and aggregated conditions of O-GlcNAcylated hT39 when compared to unmodified hT39. The slightly increased size of

multimers formed by O-GlcNAcylated hT39 along with their reduced stability under SDS and heat suggests that their conformation is different from the multimers formed by the unmodified hT39.

PTMs are intimately linked to processes associated with tau pathobiology, including the adoption of pathological conformations linked to tauopathies (Alhadidy & Kanaan, 2024). PAD exposure is a pathological tau conformation that occurs early in AD and is linked to dysregulation of axonal transport (Kanaan et al., 2011). The resultant hyperactivation of PP1-GSK3β mediates the PAD exposure-induced dysregulation of axonal transport (Combs et al., 2021; LaPointe et al., 2009). In our experiments, we measured the extent of PAD exposure using the TNT2 antibody (Combs et al., 2016). We demonstrated that O-GlcNAc modification of hT39 enhances PAD exposure in aggregated conditions. Conversely, no change in the extent of PAD exposure was detected upon modifying hT40 with O-GlcNAc. One may predict that O-GlcNAc-modified hT39 elicits axonal transport abnormalities like those observed with other PTMs, such as phosphorylation at T175 (Hintermayer et al., 2020) and at S199/S202/T205 (Christensen et al., 2023).

In addition, oligomerization of tau is an event detected in early Braak stages (starting from stage I) before the development of cognitive symptoms in AD patients (Lasagna-Reeves et al., 2012; Maeda et al., 2006). Tau oligomers are linked to several disease mechanisms including mitochondrial and synaptic dysfunction (Lasagna-Reeves et al., 2011), reduced protein synthesis (Jiang et al., 2021), inhibited long-term potentiation (Hill et al., 2019), and memory impairment (Fa et al., 2016). The process of tau oligomerization can be modulated by PTMs such as phosphorylation at the S199,

S202 and T205 (Kanaan et al., 2020). In our experiments, we measured the abundance of oligomeric tau species using TOC1 (Patterson et al., 2011; Ward et al., 2013) and TOMA1 antibodies (Castillo-Carranza, Gerson, et al., 2014; Montalbano et al., 2023). O-GlcNAc modification of hT39 increases the oligomeric tau species in aggregated samples, suggesting that this PTM may further exacerbate the dysfunctions associated with hT39 oligomers. On the other hand, O-GlcNAcylation of hT40 does not alter TOMA1-positive tau while slightly reducing the TOC1-positive tau in aggregated hT40 samples. Thus, O-GlcNAcylation may again show isoform-dependent differences in the adoption of oligomeric tau species.

Relatively recently, the Diamond group and others demonstrated that tau seeding may play a role in propagating tau pathology between neurons in the brain and in cell models (Holmes et al., 2014; Manca et al., 2023; Woerman et al., 2016). The seeding capability of tau is linked to conformational changes that either enhance or impede seeding (Dinkel et al., 2011; Falcon et al., 2015) and depends on the two motifs regulating tau's propensity to form β-sheet containing aggregates in R2 (275-VQIINK-280) and R3 (306-VQIVYK-311) (Chen et al., 2019; Falcon et al., 2015; Rojas Quijano et al., 2006; von Bergen et al., 2005). Consistent with reduced β-sheet content in O-GlcNAc modified hT40 aggregates, we observed a reduced capability of O-GlcNAc modified hT40 to seed aggregation in tau biosensor HEK cells. This result suggests that the conformations of tau species formed by O-GlcNAc modification do not seed tau aggregation as potently as unmodified tau. These results suggest O-GlcNAc modification may be protective against the formation of seed competent tau species. Unfortunately, a cell line that effectively

assess hT39 seeding was not available for testing; thus, the impact of O-GlcNAc modification on 3R tau seeding remains unknown.

Early in disease, tau assumes a misfolded conformation in tauopathies that involves the N-terminus of tau folding over its microtubule-binding region and is thought to precede the formation of filamentous tau aggregates (Carmel et al., 1996). This misfolded conformation is detected with the Alz50 and MC1 antibodies originally developed against paired helical filaments isolated from AD (Jicha et al., 1997; Wolozin et al., 1986). Nonetheless, these misfolded tau conformations are detectable in tauopathies other than AD, such as CBD, PiD, and progressive supranuclear palsy (Ferrer et al., 2014). Our results showed that O-GlcNAc modification of hT39 increases the Alz50 conformation in aggregated hT39 samples. This finding suggests that O-GlcNAc modification may increase the propensity of hT39 to adopt aggregation-prone conformations. In fact, our TEM data suggests that O-GlcNAcylated hT39 tend to grow into globular aggregates that are slightly larger in size when compared to those formed by the unmodified hT39 protein. O-GlcNAcylation of hT40 did not alter the extent of Alz50 conformation formed, suggesting isoform-dependent differences exist with this conformation as well.

Collectively, our findings add to the growing body of literature showing that an enzymatic or non-enzymatic PTM may differentially regulate the 4R and 3R tau isoforms (Chakraborty et al., 2023; Combs et al., 2011; Liu et al., 2016; Voss & Gamblin, 2009). For example, enzyme-mediated acetylation inhibits the aggregation of 2N4R tau isoform but increases the aggregation of the 0N3R isoform (Chakraborty et al., 2023). In addition,

nonenzymatic glycation enhances aggregation of the 2N4R tau isoform but inhibits aggregation of the 1N3R isoform (Liu et al., 2016).

The effects O-GlcNAcylation has on the different tau isoforms highlights important considerations for testing OGA inhibitors in animal models and clinical trials. OGA inhibitors were tested for their utility in treating tauopathies using animal models that express only 4R human tau isoforms (Graham et al., 2014; Hastings et al., 2017; Permanne et al., 2022; Wang et al., 2020). Animal studies suggested that OGA inhibitors are beneficial in reducing tangle pathology; hence, they were advanced in the clinical trial pipeline for AD (Bartolome-Nebreda et al., 2021; Congdon et al., 2023; Lane-Donovan & Boxer, 2024). However, AD pathology is composed of both 4R and 3R proteins, and other tauopathies show differences in their tau isoform composition to include only 3R tau (e.g. PiD) (Gotz et al., 2019). It would be beneficial to test OGA inhibitors in mouse models that express 3R tau isoforms, such as mThy-1 3R Tau, as well as 4R tau isoforms (Rockenstein et al., 2015). Given the differential regulation of tau isoforms by O-GlcNAcylation, it is plausible that OGA inhibitors also differentially affect the tauopathy phenotype in mice expressing 4R versus 3R tau isoforms.

In summary, we report novel O-GlcNAc modification sites on the hT40 and hT39 isoforms of tau. O-GlcNAcylation affects several aspects of the pathobiology of tau in isoform-dependent manner. For hT40, O-GlcNAcylation increases microtubule-binding, decreases the filamentous and β-sheet containing aggregates, and inhibits tau seeding without altering the formation of pathological tau conformations (e.g. oligomerization and PAD exposure). For hT39, O-GlcNAcylation decreases microtubule-binding, decreases β-sheet containing aggregates, and markedly enhances the formation of pathological tau

conformations (e.g. oligomerization and PAD exposure). Further studies in animal models and results from clinical trials will provide further insights into the role played by O-GlcNAcylation in contributing to or mitigating tauopathies (Bartolome-Nebreda et al., 2021; Congdon et al., 2023; Lane-Donovan & Boxer, 2024).

CHAPTER 4: SUMOYLATION REDUCES KNOWN PATHOLOGICAL CONFORMATIONS AND FILAMENTOUS AGGREGATE FORMATION OF TAU *IN VITRO*

Abstract

Tauopathies are neurodegenerative diseases characterized by the accumulation of intracellular tau inclusions in the brain. Several studies suggest that the filamentous neuronal and glial inclusions of tau may not be the most toxic species of tau in disease. Indeed, multiple non-filamentous conformational changes of tau protein can contribute to toxicity and neurodegeneration in tauopathies, such as oligomerization, misfolding, and aberrant exposure of the phosphatase-activating domain located in the far N-terminus. Known factors that drive the adoption of pathological tau conformations include mutations, protein-protein interactions, and post-translational modifications (PTMs). The most studied PTMs of tau are phosphorylation and acetylation, but other less commonly studied PTMs of tau were reported; their role in regulating tau pathobiology has not received the same attention. SUMOylation is an under-studied PTM of tau that involves incorporating small ubiquitin-like modifier (SUMO) isoforms onto its lysine residues. SUMOylation colocalizes with tau aggregates in Alzheimer's disease (AD) and progressive supranuclear palsy. Furthermore, enhancing tau SUMOylation mutually increases its phosphorylation, reciprocally decreases its ubiquitination, and inhibits tau clearance. The impact SUMOylation has on the development of pathological tau conformations is not known. Furthermore, the longest tau isoform containing all four microtubule-binding repeats, the 2N4R isoform, is the primary subject of prior studies on tau SUMOylation. Other isoforms of tau carry only three microtubule-binding repeats, and they comprise tau aggregates in tauopathies such as AD, chronic traumatic encephalopathy and Pick's disease. Therefore, we set out to determine the impact of SUMOylation on development of pathological tau conformations formed by the longest

4R and 3R tau isoforms (hT40 and hT39, respectively) using recombinant proteins. Mass spectrometry indicated that tau is modified by SUMOylation on multiple lysine residues mainly concentrated within the microtubule-binding region. We also found that SUMO1 and SUMO2 modification of both tau isoforms significantly impedes microtubule polymerization and their ability to bind microtubules. SUMO1- and SUMO2-modified hT40 aggregation is reduced and shifts from being both globular and filamentous aggregates (with unmodified tau) to predominantly globular structures. Furthermore, several pathological conformations of hT40 are reduced upon SUMOylation (SUMO1 and SUMO2) except for a subset of oligomeric tau species that are increased specifically with SUMO2 modification. On the other hand, aggregates of SUMO1- and SUMO2-modified hT39 comprise mainly globular aggregates (like unmodified hT39) and pathological tau conformations are reduced with both SUMO isoforms. Finally, SUMO1 and SUMO2 hT40 aggregates do not promote seeding in tau biosensor cells. Taken together, our data suggests that SUMOylation of tau disrupts tau-mediated microtubule regulation, favors formation of globular tau aggregates over filamentous aggregates, and largely reduces adoption of pathological tau conformations. Our findings warrant further investigation of tau SUMOylation in human disease and *in vivo* models of tauopathies to assess its role in disease pathogenesis and potential therapeutic avenues.

Introduction

Tauopathies, such as Alzheimer's disease (AD), represent a heterogenous group of neurodegenerative disorders characterized by the intracellular accumulation of abnormal tau protein (Gotz et al., 2019). Intracellular tau inclusions are primarily within neurons in some tauopathies [e.g. AD and Pick's disease (PiD)], or within both neuronal and glial cells in others [e.g. chronic traumatic encephalopathy (CTE), corticobasal degeneration (CBD), and progressive supranuclear palsy (PSP)] (Cherry et al., 2021; Kneynsberg et al., 2017). Moreover, tau aggregates are comprised of isoforms containing three microtubule-binding repeats (3R) of tau (e.g. PiD), isoforms containing four microtubule-binding repeats (4R) of tau (e.g. CBD and PSP), or both the 3R and 4R tau isoforms (e.g. AD and CTE) (Cherry et al., 2021; Gotz et al., 2019; Kneynsberg et al., 2017). Despite their heterogeneity, tauopathies share some common pathological features, such as synaptic loss, axonal degeneration, and neuroinflammation (Caamano-Moreno & Gargini, 2023; Kneynsberg et al., 2017; Langworth-Green et al., 2023).

A growing body of literature suggests that common mechanisms of conformational changes and toxicity of tau, other than filamentous aggregates, are implicated early in disease development (Alhadidy & Kanaan, 2024; Combs et al., 2016; Garcia-Sierra et al., 2003; Lasagna-Reeves et al., 2012; Mroczko et al., 2019; Niewiadomska et al., 2021; Patterson et al., 2011; Weaver et al., 2000). A prominent example of such conformations that occur early during the deposition of pathological tau is oligomerization (Cox et al., 2016; Kanaan et al., 2016; Lasagna-Reeves et al., 2012; Patterson et al., 2011). Tau oligomers are linked to neurodegeneration and cellular dysfunction, such as disruption of intracellular transport, impairment of protein degradation, synaptic dysfunction, and

dysregulating cellular bioenergetics (Niewiadomska et al., 2021). Certain post-translational modifications (PTMs) and tau mutations may facilitate the oligomerization of tau (e.g. pS199/pS202/pT205 and P301L, respectively), potentially facilitating tau liquid-liquid phase separation without inducing filamentous tau aggregation (Boyko & Surewicz, 2022; Kanaan et al., 2020).

The second example of a conformational change linked to oligomerization is exposure of the phosphatase-activating domain (PAD) in the extreme N-terminus of tau (Kanaan et al., 2011). PAD spans amino acids 2-18 and becomes abnormally exposed in tauopathies (Combs & Kanaan, 2017; Cox et al., 2016; Kanaan et al., 2016; Kanaan et al., 2011). Like oligomerization, excessive PAD exposure is induced by some PTMs (e.g. pT175 and pS199/pS202/pT205) and mutations (e.g. P301L) of tau, thereby activating a signaling pathway involving protein phosphatase 1 (PP1) and glycogen synthase kinase 3 β (GSK3β) (Christensen et al., 2023; Combs et al., 2021; Hintermayer et al., 2020; Kanaan et al., 2011). Disrupted regulation of the PP1-GSK3β eventually culminates into aberrant phosphorylation of motor proteins (e.g. kinesin-1 motor complex) leading to premature cargo release and dysregulated axonal transport (Morris & Brady, 2022; Mueller et al., 2021).

Tau pathology propagates from one brain region to another in a way unique to each tauopathy (Zhang et al., 2022). This process entails tau first transferring from a cell to another followed by seeding of tau pathology in the recipient cell (Clavaguera et al., 2009; de Calignon et al., 2012; Fu et al., 2016; Liu et al., 2012). More recently, the Diamond group proposed that tau assumes two conformational ensembles in tauopathies that have different ability to seed aggregation (Mirbaha et al., 2018; Mirbaha et al., 2022;

Sharma et al., 2018). The seeding-competent conformation is dependent upon the aggregation prone motifs of tau spanning amino acids 275-VQIINK-280 and 306-VQIVYK-311 (Chen et al., 2019; Falcon et al., 2015). Factors driving the formation of seeding-competent conformation ensembles is an active area of investigation, but PTMs (e.g. acetylation) and mutations (e.g. S320F) of tau likely play an important role (Chen et al., 2023; Tseng et al., 2021).

In a soluble state, tau is described as an “unfolded” protein that transiently assumes a global hairpin folds under native conditions (Jeganathan et al., 2006). The global hairpin conformation, also known as the paperclip conformation, is formed by the folding of tau’s C-terminus near the microtubule-binding region, and the N-terminus of tau folding over the C-terminus (Abraha et al., 2000; Jeganathan et al., 2006). Early during pathological tau aggregation, tau assumes a conformation different from the paperclip where the N-terminus of tau directly folds over the microtubule-binding region. This third conformational change is thought to represent a critical checkpoint along the path of tau aggregation, and it is detected by the Alz50 and MC1 antibodies (Carmel et al., 1996; Jicha et al., 1997; Ksiezak-Reding et al., 1988). Taken together, accumulating evidence posits similar events of conformational changes and toxicity of tau regulated by tau PTMs and mutations among many other factors.

SUMOylation is a lysine directed PTM that involves covalently linking cellular proteins with small ubiquitin-like modifier (SUMO) protein (Mahajan et al., 1997; Matunis et al., 1996). Mammalian cells express at least three isoforms of SUMO protein: SUMO1, SUMO2, and SUMO3 (Acuna et al., 2023; Komiya et al., 2017). SUMO2 and 3 are highly homologous sharing more than 90% of protein sequence (usually grouped as SUMO2/3),

whereas SUMO1 shows only 50% structural homology to SUMO2/3 (Suk et al., 2023). Analogous to the ubiquitination machinery, SUMOylation machinery features an activating enzyme (E1), a conjugating enzyme (E2), and a ligase (E3) (Seeler & Dejean, 2003). Moreover, SUMOylation of proteins is a dynamic and reversible process that recycles SUMO and is regulated also by the activity of SUMO proteases (SUMO/sentrin-specific proteases, SENPs) (Kumar & Zhang, 2015). The E1 enzyme comprises a heterodimer composed of SUMO-activating enzyme subunits 1 and 2 (SAE1 and SAE2) that utilizes adenosine triphosphate (ATP) to activate SUMO chains (Celen & Sahin, 2020; Desterro et al., 1999; E. S. Johnson et al., 1997). Unlike ubiquitination, the E2 enzyme for SUMOylation (ubiquitin-conjugating enzyme 9, Ubc9) can perform the role of E3 ligase along with its main conjugating function (Celen & Sahin, 2020; Giraud et al., 1998; Johnson & Blobel, 1997).

Interestingly, the SUMOylation pathway regulates a multitude of cellular functions (Wilkinson et al., 2010) including the same processes adversely affected in tauopathies such as synaptic function (Colnaghi et al., 2019; Henley et al., 2014; Matsuzaki et al., 2015; Schorova & Martin, 2016), axonal transport (Chen et al., 2018; van Niekerk et al., 2007), and immune responses (Mao et al., 2022; Wang et al., 2021). Indeed, several studies points to a dysregulated SUMO pathway in neurodegenerative disorders including AD (Dorval & Fraser, 2007; Lee et al., 2013). GWAS studies in AD brains identified single nucleotide polymorphisms (SNPs) in a homolog of SAE2 along with the UBE2I gene encoding the E2 enzyme Ubc9 (Ahn et al., 2009; Corneveaux et al., 2010; Grupe et al., 2007). In addition, the SUMO protease SENP3 is downregulated in late onset AD relative to nondemented controls (Weeraratna et al., 2007). Taken together, these findings

instigated an interest in targeting SUMOylation pathways as a therapeutic approach for AD and other tauopathies (Mandel & Agarwal, 2022).

In addition to potentially regulating neuronal functions in tauopathies, SUMOylation also directly labels tau protein on its lysine residues (Dorval & Fraser, 2006). Supporting this notion is the finding that aggregates of phosphorylated tau (labelled with the AT8 phospho-tau antibody) colocalize with SUMO1 labelling in the cortical neurons of AD patients but not in control subjects (Luo et al., 2014). Similarly, phosphorylated (AT8) 4R tau aggregates colocalize with SUMO1 staining in both neuronal and glial cells of PSP patients but not in control subjects (Takamura et al., 2022). On the contrary, phosphorylated tau did not colocalize with SUMO2/3 staining in PSP (Takamura et al., 2022). Furthermore, a previous report shows that modification of proteins by SUMO1 is unaltered but by SUMO2/3 is lower in AD patients relative to controls (Lee et al., 2014). These findings suggest that tau is preferentially modified by SUMO1 compared to SUMO2/3 in tauopathies due to a global downregulation of protein modification by SUMO2/3. However, it could also be that tau is inherently more susceptible to modification with SUMO1 compared to SUMO2 as posited by *in vitro* studies (Dorval & Fraser, 2006).

Studies in cell lines showed an interplay between tau SUMOylation and other PTMs, especially ubiquitination and phosphorylation (Dorval & Fraser, 2006; Luo et al., 2014). Enhancing ubiquitination levels of tau by inhibiting proteasomal degradation (by MG132) reduced tau SUMOylation (Dorval & Fraser, 2006). On the other hand, increasing tau SUMOylation by overexpressing SUMO1 decreased tau ubiquitination, reduced tau degradation, increased tau phosphorylation at disease-relevant sites (i.e. pT205, pT231,

pS396, pS404), and increased tau aggregation (Dorval & Fraser, 2006; Luo et al., 2014). Similarly, increasing tau phosphorylation by okadaic acid (a phosphatase inhibitor) led to an increase in tau SUMOylation (Dorval & Fraser, 2006; Luo et al., 2014). Apart from the interplay between SUMOylation and other PTMs, our knowledge of the direct effects SUMOylation has on tau biology, such as microtubule dynamics, tau aggregation, and formation of pathological tau conformations, remains to be elucidated.

Herein, we describe a method to produce recombinant SUMO-modified 2N4R and 2N3R tau isoforms (unmodified, SUMO1-, and SUMO2-modified) in bacterial cells by co-transformation. Then, a set of biochemical and biophysical assays were employed to determine the impact SUMOylation has on microtubule polymerization/binding as well as tau aggregation and adoption of its pathological conformations. Our results suggest that SUMOylation markedly reduces tau's ability to stimulate microtubule polymerization and bind microtubules *in vitro*. In addition, SUMOylation of tau reduces multimerization into filamentous aggregates and adoption of pathological conformations. Therefore, evaluating the effects of tau SUMOylation *in vivo* is warranted to further characterize the effects of SUMOylation within the context of tauopathies.

Materials and Methods

Cloning of tobacco etch virus (TEV) protease cleavage site in pSUMO1 and pSUMO2

Plasmids containing the SUMOylation machinery (i.e. SAE1, SAE2, Ubc9) along with either SUMO1 (pSUMO1, Addgene, #52258) and SUMO2 (pSUMO2, Addgene, #52259) proteins were a gift from Primo Schär laboratory (Weber et al., 2014). SUMO1 and SUMO2 proteins are tagged on their N-termini with 6X histidine tag cleavable with thrombin. Tau is subject to proteolytic cleavage by thrombin (Arai et al., 2005); thus, we

replaced thrombin cleavage site (QDLVPR/M) with TEV protease cleavage site (ENLYFQ/M) in both plasmids (see below for details of recombinant tau purification). First, the fragment of DNA in pSUMO plasmids between MluI and SphI (contains thrombin cleavage site) was amplified by polymerase chain reaction (PCR) using the Platinum PCR Supermix High Fildelity (Invitrogen, #12532016):

Forward primer 1: ACGCGTTGCGCGAGAAGATT (MluI site underlined)
Reverse primer 1: GCATGCAAAAAACCCCTCAAGAC (SphI site underlined)

The PCR product was subjected to A tailing using native Taq polymerase (Invitrogen, #18038-042) followed by ligation into the pCR2.1-TOPO backbone using TOPO TA cloning (Invitrogen, #450640). The sequence of the amplified fragment was confirmed using Sanger sequencing with the M13F and M13R primers. Then, site-directed mutagenesis (Agilent, #210518) was conducted in two steps: mutation of QD to EN and mutation of VPR to YFQ. The first site-directed mutagenesis reaction (QD to EN) was conducted using the following primer set at an annealing temperature of 61 °C:

Forward primer 2: CACCATCATCACCACAGCGAGAACCTGGTTCCGCGTATGTCTG
Reverse primer 2: CAGACATACGCGGAACCAGGTTCTCGCTGTGGTGATGATGGTG

Successful mutagenesis was confirmed by sanger sequencing using M13F and M13R primers. Then, the second site-directed mutagenesis reaction (VPR to YFQ) was conducted using the following primer set at an annealing temperature of 66 °C:

Forward primer 3: CACCACAGCGAGAACCTGTACTTCCAGATGTCTGACCAGGAGGC
Reverse primer 3: GCCTCCTGGTCAGACATCTGGAAGTACAGGTTCTCGCTGTGGTG

Successful mutagenesis was confirmed by sanger sequencing M13F and M13R primers. pCR2.1-TOPO plasmid carrying the TEV protease cleavage site was digested

with MluI (Thermo, #FD0564) and SphI (also called PaeI, Thermo, #FD0604), ran on 1% agarose gel (Biorad, #1613101), and the TEV protease fragment was extracted using GeneJET Gel Extraction Kit (Thermo, #K0691). In parallel, the pSUMO1 and pSUMO2 plasmids were digested with the same enzymes, run on an agarose gel, and the linearized plasmid vector band extracted. Digested plasmid vector and TEV protease insert fragments were then ligated using the T4 enzyme (Thermo, #EL0011). The ligation product was used to transform XL10-gold Ultracompetent Cells (Agilent, #200315) before plating the competent cells onto agar plates (Fischer Bioreagents, #BP1423-500) supplemented with streptomycin at 50μg/ml (Sigma, #S9137). Colonies were picked from the agar plate, followed by shaking (250 RPM) in Luria Broth (LB; Fischer Bioreagents, #BP1426-2) at 37 °C overnight. On the following day, DNA plasmid was extracted from bacterial cultures using QIAprep Spin Miniprep Kit (Qiagen, #27104). Extracted plasmids were sent for sanger sequencing to ensure successful cloning.

Insertion of 6X his tag in tau C-Halo constructs

SUMOylated tau proteins were purified from bacterial cells co-transformed with C-Halo tagged tau along with N-His tagged SUMO1 or SUMO2 proteins (see below for details of recombinant tau purification). To produce and purify unmodified tau proteins, we modified the tau C-Halo constructs to also include a 6X His tag on the Halo tag (C-HaloHis). We employed overlap extension PCR to amplify the Halo tag region while introducing 6X His tag to the C-terminus of Halo tag (Heckman & Pease, 2007). The outer primers (primers a and d) were designed to carry restriction sites for KpnI (forward primer) and PsiI (reverse primer) to clone the modified HaloHis fragment back into tau C-Halo constructs:

Primer a: GTTTGGGTACCGAGCCAACCA (KpnI site underlined)

Primer b: GTG**ATGATGATGATGATG**ACCGGAAATCTCCAGAGTAGAC

(His tag bolded)

Primer c: **CATCATCATCATCAT**CACTAATAGAATTGGCATGCAAGCTGAT

(His tag bolded)

Primer d: CAGCTTATAATGGTTACAAATAAAGCAATAGCATCAC (PsiI site underlined)

The first round of PCR (PCR Supermix High Fildelity, Invitrogen, #12532016) involved setting up two reactions with the same template (Tau C-Halo) along with two different primer sets: primers a and b; primers c and d. Successful amplification of the AB and CD fragments was confirmed by running the PCR products on 1% agarose gel. Then, the AB and CD fragments were extracted from agarose gel using GeneJET Gel Extraction Kit (Thermo, #K0691). Concentrations of the two fragments were determined using NanoDrop 2000 spectrophotometer (Thermo, #ND-2000).

The second round of PCR utilized the AB and CD fragments (50ng each for a total of 100ng DNA in the reaction) along with primers a and d (the outer primers). To ensure successful amplification of the final AD fragment, product of the second round of PCR was run on 1% agarose gel, followed by gel extraction. The PCR product was subjected to A tailing using native Taq polymerase (Invitrogen, #18038-042) followed by ligation into the pCR2.1-TOPO backbone using TOPO TA cloning (Invitrogen, #450640). Sequence of the amplified fragment containing the inserted 6X His tag (C-HaloHis) was confirmed using Sanger sequencing with M13F and M13R primers.

At the final stage of cloning, the pCR2.1-TOPO plasmid containing the C-HaloHis fragment was digested with KpnI (Thermo, #FD0524) and PsiI (Thermo, #FD2064). In parallel, the tau C-Halo plasmids were digested with the same enzymes, ran on agarose

gel, and the plasmid vector band extracted. Digested vector and C-HaloHis fragment were then ligated using the T4 enzyme (Thermo, #EL0011). The ligation product was used to transform XL10-gold Ultracompetent Cells (Agilent, #200315) before plating the competent cells onto agar plates (Fischer Bioreagents, #BP1423-500) supplemented with Ampicillin at 100 μg/ml (Sigma, #A0166). Colonies were picked from the agar plate, followed by shaking (250 RPM) in Luria Broth (Fischer Bioreagents, #BP1426-2) at 37 °C overnight. On the following day, DNA plasmids were extracted from bacterial cultures using QIAprep Spin Miniprep Kit (Qiagen, #27104). Extracted plasmids were sent for sanger sequencing to ensure successful cloning.

Purification of recombinant unmodified, SUMO1-, and SUMO2-modified tau proteins

An illustration of the conceptual framework for the production and purification of SUMO-modified tau proteins is depicted in Figure AIII.1. Recombinant tau proteins were prepared by co-transforming BL21 bacteria (NEB, #C2527H) with two plasmids: a plasmid expressing C-Halo tagged tau under the T7 promoter and either the pSUMO1 or pSUMO2 plasmids. Purification procedure for SUMO-modified tau proteins was performed using 4L LB cultures grown in the presence of ampicillin (50 μg/ml) and streptomycin (25 μg/ml) as selection markers. Unmodified tau proteins were grown in the same way with the exception that streptomycin was excluded from LB. Moreover, bacterial cells were only transformed with tau plasmids to produce unmodified tau proteins (i.e. tau C-Halo constructs) in the presence of ampicillin at 100 μg/ml.

Bacterial pellets were lysed using Buffer A (0.5 M NaCl, 10 mM Tris, and 5 mM Imidazole, pH 8) in the presence of protease inhibitors [10 μg/mL pepstatin (Fisher Scientific, Pittsburgh, PA, BP267125), 10 μg/mL leupeptin (Sigma-Aldrich, St. Louis, MO,

L2884), 10 µg/mL bestatin (Sigma, 10874515001), 10 µg/mL aprotinin (Sigma, A6279), and 1 mM PMSF (Sigma-Aldrich, 78830)] (Combs et al., 2017). Bacterial lysates were subjected to centrifugation at 107,377 RCF for 45 min at 4°C using a Type 70 Ti rotor (Beckman Coulter, #337922). Cleared supernatant was then processed through heavy metal affinity chromatography using a 5ml HiTrap Talon crude column (Cytiva, #28953767) as described previously (Combs et al., 2017). The eluted fractions (containing only SUMOylated proteins, including tau) were concentrated to less than 15 ml (conc talon 1) using 30K MWCO membrane (Millipore, #UFC903024). Then, conc talon 1 was subsequently desalted through HiPrep 26/10 desalting column (Cytiva, #17508701) to fully buffer exchange the samples into HaloLink buffer [50 mM Tris.HCl, pH 8.5; 150 mM NaCl; 1 mM Dithiothreitol (DTT)] using fast protein liquid chromatography (FPLC). Desalting column was equilibrated with 5 column volumes (CVs) of HaloLink buffer, then protein samples were injected and eluted in 1 CV of HaloLink buffer at a flow rate of 5 ml/min (denoted as desalted sample 1 and pre HaloLink sample). Volume of desalted sample 1 ranged from 25-30 ml, then it was subjected to the HaloLink purification protocol.

HaloLink resin (Promega, #G1915) was resuspended by vortexing for 30 seconds, followed by transferring 20 ml of the resuspended resin to 50 ml conical tube. The resin was pelleted by centrifugation at 5,000 RCF for 5 minutes, followed by discarding the supernatant. The pellet was then resuspended in 30 ml of HaloLink buffer and rotated on a tube revolver for 5 minutes at room temperature. Resin was pelleted by centrifugation as described above (wash 1). Two more washes (total of 3 washes) were performed as described above, and the resin was kept in the final wash until the desalted sample 1 was

ready for further purification. HaloLink resin was pelleted after wash 3 by centrifugation followed by adding desalted sample 1 and rotating the tube using tube revolver at room temperature for 3 hours. Tau-bound HaloLink resin was pelleted by centrifugation at 5,000 RCF for 5 minutes, and the supernatant was collected (post HaloLink sample). Following the washing protocol used at the beginning of HaloLink procedure, the resin pellet was washed 4 times with HaloLink buffer supplemented with NP-40 (Sigma, #NP40S) at 0.1%. Supernatant from washes 1 and 4 was saved to determine the efficiency of the purification procedure. Finally, the resin was resuspended in 4 ml of HaloLink elution buffer (HaloLink buffer supplemented with 0.5 mM EDTA), to which a combination of two TEV protease enzymes was added: 900 units of TEV Protease (NEB, #P8112S) and 600 units of ProTEV Plus (Promega, #V6101). We used a combination of 2 TEV proteases because we empirically determined that NEB TEV protease cleaves better at ENLYFQM (to cleave his tag off the N-terminus of SUMO1 or SUMO2), while Promega ProTEV Plus cleaves better at ENLYFQS (to cleave Halo tag off the C-terminus of tau). Elution was conducted overnight at 4°C using a tube revolver. On the following day, the resin was pelleted by centrifugation at 10,000 RCF for 5 minutes. Supernatant from HaloLink elution was carefully collected, and the resin was resuspended again in 4 ml of HaloLink elution buffer to collect any residual tau. Resuspended resin was pelleted again as described above, and the two supernatants from the HaloLink elution were pooled and used for further purification.

HaloLink eluate was subsequently desalted through HiPrep 26/10 desalting column to fully buffer exchange the samples into Buffer A. Desalting column was equilibrated with 5 CVs of Buffer A, then HaloLink eluate was injected and eluted in 1 CV

of Buffer A at a flow rate of 5 ml/min (denoted as desalted sample 2). Volume of desalted sample 1 ranged from 20-25 ml, then it was subjected to heavy metal affinity chromatography to remove the two TEV protease enzymes (both enzymes are labelled with His tag on their N-termini).

Heavy metal affinity chromatography using a 5 ml HiTrap Talon crude column was conducted as described previously (Combs et al., 2017). Flow-through fractions containing purified tau were concentrated using 30K MWCO membrane to a concentration of 2-4 mg/ml and supplemented with 1 mM DTT. Purified tau proteins were aliquoted and frozen at -80 °C, and their final concentrations were determined using the SDS-Lowry method as described previously in (Combs et al., 2017). The following molecular weights were used to calculate the molarity of recombinant tau preparations: hT40, 47232 Da; SUMO1-modifed hT40, 58347 Da; SUMO2-modifed hT40, 57823 Da; hT39, 43985 Da; SUMO1-modifed hT39, 55100 Da; SUMO2-modifed hT39, 54576 Da.

Western blot validation of recombinant tau proteins

To confirm the SUMOylation status of recombinant tau proteins, proteins were loaded on 4-20% Novex tris-glycine gels (Invitrogen, #WXP42020BOX) and run at 225 V for 45 minutes, followed by transfer on nitrocellulose membrane using the Biorad wet transfer system at 40 mAmp for 50 minutes. The membrane was then blocked with 2% non-fat dry milk (NFDM) in 1X tris buffer saline (TBS) for 1 hour at room temperature followed by incubation in primary antibodies in 2% NFDM overnight at 4 °C. Primary antibodies used were Tau5 (Nicholas M. Kanaan at Michigan State University, RRID: AB_2721194) at 1:100,000 (Carmel et al., 1996; LoPresti et al., 1995; Porzig et al., 2007), SUMO1 Mouse Monoclonal IgG2b (Cytoskeleton, #ASM01, RRID: AB_2884966) at

1:2,000, and SUMO2 Mouse Monoclonal IgG2a (Cytoskeleton, #ASM23, RRID: AB_2884967) at 1:500. The following day, the blot was washed 3 times (5 minutes each) with 1X TBS supplemented with 0.1% Tween 20 (TBS-T 0.1%). Then, secondary antibodies were diluted at 1:20,000 in 2% NFDM and incubated with the membranes for 1 hour at room temperature. The secondary antibodies were goat anti-mouse IgG1 680 (LI-COR Biosciences, #926-68050, RRID: AB_2783642), goat anti-mouse IgG2a 800 (LI-COR Biosciences, #926-32351, RRID: AB_2782998), and goat anti-mouse IgG2b 800 (LI-COR Biosciences, #926-32352, RRID: AB_2782999). The blot was washed 3 times (5 minutes each) with TBS-T 0.1%, followed by imaging with LI-COR Odyssey classic imager. Image Studio Lite Ver 5.2 were used to visualize protein bands verifying the modification status of tau.

Recombinant tau protein preparation for tandem mass spectrometry

Unmodified, SUMO1-, and SUMO2-modified tau proteins were digested using a combination of Asp-N (Promega, #V1621) and rLysC (Promega, #V167A). First, each recombinant tau protein sample (3 µg) was subjected to 5 rounds of buffer exchange with 25 mM ammonium bicarbonate (AmBic) pH 8 using 0.5 ml Amicon filter with 3K MWCO (15,000 RCF for 10 minutes; Millipore, #UFC500396). Then, recombinant tau proteins were recovered from the filter by centrifugation at 15,000 RCF for 2 minutes and vacuum dried using a Vacufuge. The dried pellets of recombinant tau proteins were reconstituted in 50 µl of digestion buffer [12.5 mM AmBic pH 8 + acetonitrile (ACN) 50%] and incubated at 37 °C for 16-18 hours with Asp-N (150 ng of enzyme). The following day, digested protein samples were subjected to vacuum drying and stored at 4 °C until the second digestion was initiated. Lys-C (500 ng of enzyme) was added and incubated at 37 °C for

16-18 hours. The following day, digested protein samples were subjected to vacuum drying and stored at -20 °C until running on mass spectrometry (MS).

Tandem MS of recombinant tau proteins

Samples were analyzed using a Vanquish Neo nanoHPLC system interfaced to a Thermo Scientific Orbitrap Eclipse mass spectrometer (Thermo Fisher Scientific). One µg of each digested sample was injected and desalted an AccalaimTM PepMapTM C18 Nano trap column (3 µm, 100 Å, 75 µm × 2cm) at 3 µL/min with 100% Solvent A (0.1% formic acid in HPLC water) for 5 min. The trapped peptides were then separated with an Ion Opticks Aurora Ultimate TS C18 nano column (1.7 µm, 120 Å, 75 µm × 250 mm) using a linear gradient of 5.0–42.0% solvent B (80% ACN, 0.1% formic acid) over 60 min. Flow rate was 250 nl/min and temperature was 40 °C. A wash at 100% B for 7 min followed by system equilibration at 1.0 % B for 5 min was completed before each injection. Data dependent MS analysis was carried out with a duty cycle of 3 s. Precursor masses were detected in the orbitrap at resolution (R) = 120,000 (at m/z 200) with a lock mass of 445.1200. Data-dependent mass spectrometric analysis was performed. MS1 resolution was 120K at 200 m/z with a maximum injection time of 246 ms, AGC target of 4e5, and scan range of 350–1500 m/z. MS2 resolution was 30K at 200 m/z, with a maximum injection time of 54 ms, AGC target of 5e4, and isolation window of 0.7 m/z. HCD normalized collision energy was 30. Only ions with charge states from +2 to +7 were selected for fragmentation, and dynamic exclusion was set to 30 s. The electrospray voltage was 2.1 kV at a 2.0 mm tip to inlet distance. The ion capillary temperature was 275 °C and the RF level was 30.0. All other parameters were set as default.

MS data analysis to determine SUMO modification sites

RAW data files were analyzed with the MetaMorpheus software version 1.0.1 developed by the Smith laboratory (Miller et al., 2023). For hT40 proteins, the following FASTA files used were downloaded from Uniprot (November 2021) and used for analysis: Escherichia coli (strain K12) (UP000000625), Asp-N (Q9R4J4), Lys-C (Q02SZ7), and full-length tau (2N4R isoform, P10636-8). The same FASTA files were used to analyze the hT39 proteins except for full-length tau (2N4R isoform, P10636-8) that was replaced with 2N3R tau isoform (P10636-5). Mass shift of +1318.60 Da ($C_{57}H_{86}N_{14}O_{22}$) for SUMO1 and +960.43 Da ($C_{41}H_{60}N_{12}O_{15}$) for SUMO2 were used to search for SUMOylation sites (Osula et al., 2012). In addition, the following masses of diagnostic ions (b ions from the fragmentation of SUMO tail left after Asp-N digestion) were investigated:

For SUMO1 (isopeptide tail = DVIEVYQEQTGG): DV (214.096); DVI (327.180); DVIE (456.223); DVIEV (555.292); DVIEVY (718.355); DVIEVYQ (846.413); DVIEVYQE (975.456).

For SUMO2 (isopeptide tail = DVFQQQTGG): DV (214.096); DVF (361.165); DVFQ (489.223); DVFQQ (617.282); DVFQQQ (745.341); DVFQQQT (846.388).

Two diagnostic ions generated by isopeptide tails of SUMO1 and SUMO2 are close in mass (underlined). Therefore, three diagnostic ions were required to deem that a specific lysine residue is modified by either SUMO1 or SUMO2. The analysis sequence included mass calibration, global post-translational modification discovery (G-PTM-D) (Li et al., 2017), and a classic search. Mass calibration was conducted using the following criteria: protease = Asp-N/Lys-C; maximum missed cleavages = 2; minimum peptide length = 7; maximum peptide length = unspecified; initiator methionine behavior =

Variable; variable modifications = Oxidation on M; max mods per peptide = 2; max modification isoforms = 1024; precursor mass tolerance = ±15.0000 PPM; product mass tolerance = ±25.0000 PPM. The criteria utilized for G-PTM-D were protease = Asp-N/Lys-C; maximum missed cleavages = 2; minimum peptide length = 7; maximum peptide length = unspecified; initiator methionine behavior = Variable; max modification isoforms = 1024; variable modifications = Oxidation on M; G-PTM-D modifications count = 2; precursor mass tolerance(s) = ±5.0000 PPM around 0, 960.43, 1318.60 Da; product mass tolerance = ±20.0000 PPM. Finally, a classic search was conducted using the following criteria: protease = Asp-N/Lys-C; search for truncated proteins and proteolysis products = False; maximum missed cleavages = 2; minimum peptide length = 7; maximum peptide length = unspecified; initiator methionine behavior = Variable; variable modifications = Oxidation on M; precursor mass tolerance = ±5.0000 PPM; product mass tolerance = ±20.0000 PPM; report PSM ambiguity = True. Sites of SUMO modification on tau detected at a false discovery rate of 1% are reported. MetaDraw version 1.0.5 was utilized to review the PSMs of modified and unmodified tau peptides (samples of these peptides are included in Figures AIII.2 and AIII.3).

Tubulin polymerization assay

Tubulin polymerization in the presence of recombinant tau proteins was assessed using the Tubulin Polymerization Assay Kit (Cytoskeleton, #BK011P). Kit reagents were reconstituted and stored as indicated in the manual. The assay began by incubating the 96-well plate provided with the kit at 37 °C for 10 minutes (Synergy H1 Hybrid Multi-Mode Reader and Gen5 software v3.11, BioTek). Meanwhile, recombinant tau proteins were prepared as 10 μM stocks in general tubulin buffer (80 mM PIPES pH 6.9, 2 mM $MgCl_2$,

and 0.5 mM EGTA) and left at room temperature. Then, a tubulin master mix was prepared and kept on ice using the recipe for enhancer detection (kit manual): 355 µl of Buffer 1, 4.4 ul of 100 mM GTP, and 85 µ of tubulin 10 mg/ml. Once the 10-minute incubation of the 96-well plate was over, recombinant tau (10 µM stocks) were loaded (5 µl) onto the plate and warmed up to 37 °C for exactly 1 minute. Then, the tubulin master mix was loaded (50 µl) on each tau protein sample yielding a final tau concentration of 1 µM. Fluorescence signal was measured for 1 hour to monitor tubulin polymerization using the kinetic mode at excitation and emission wavelengths of 360 nm and 450 nm, respectively. Each tau protein sample was loaded in duplicate (technical replicates) with a sample size of 4 (independent biological replicates). Background levels of blank (general tubulin buffer only) were subtracted from the fluorescence readings before further analyzing the data. Nonlinear regression using “specific binding with Hill slope” was used to fit the tubulin polymerization data in GraphPad Prism v10.2.1 and calculate the steady state equilibrium (V_{max}) along with the time to reach half maximal polymerization (K_d). K_d could not be calculated for SUMO1- and SUMO2-modified hT40 and hT39 proteins because they failed to induce enough polymerization (fluorescence) for proper fitting using specific binding with Hill slope.

Microtubule-binding assay

Assays were performed in using Microtubule Binding Protein Spin-Down Assay Biochem Kit (Cytoskeleton, #BK029). Kit reagents were reconstituted as indicated in the manual. Tubulin aliquots (20 µl) were thawed, supplemented with cushion buffer (2 µl; 80 mM PIPES pH 7.0, 1 mM $MgCl_2$, 1 mM EGTA, and 60% sucrose), and incubated at 35 °C for exactly 40 minutes. Then, general tubulin buffer (200 µl; 80mM PIPES pH 7.0,

1 mM $MgCl_2$, and 1 mM EGTA) supplemented with paclitaxel at 20 μM was added to the polymerized tubulin. Microtubule-binding reactions were set up at room temperature including tubulin (20 μl), recombinant tau proteins (0.5 μM), and general tubulin buffer to a final volume of 50 μl. After 30 minutes of incubation at room temperature, binding reactions were then loaded on 100 μl of sucrose cushion buffer in 0.2 ml polycarbonate tubes (Thermo Scientific, #45233) followed by centrifugation at 100,000 RCF for 40 minutes. For all centrifugation steps, S100-AT3 Fixed Angle Rotor (Thermo Scientific, #45585) and Sorvall™ MTX 150 Micro-Ultracentrifuge (Thermo Scientific, #46960) were employed. Then, 30 μl of the supernatant were carefully removed (Sup) to avoid disturbing the microtubule pellet. Laemmli buffer was added to the supernatant immediately (6 μl of 6X Laemmli buffer). The rest of the supernatant was discarded, followed by washing the microtubule pellet with general tubulin buffer (100 μl) supplemented with 20 μM paclitaxel. The microtubule pellet was subjected to centrifugation at 100,000 RCF for an additional 20 minutes. The previous washing step was repeated one more time, followed by careful removal of the supernatant. The final pellet was resuspended in 60 μl of 1X Laemmli buffer. The assay was conducted 4 independent times.

For each biological replicate, Sup and Pellet (15 μl each) were subjected to SDS-PAGE. Unmodified, SUMO1-, and SUMO2-modified tau samples were loaded on two separate 4-20% Novex tris-glycine gels (Invitrogen, #WXP42020) that was run at 225 V for 40-45 minutes. After SDS-PAGE, the two gels were cut between the 250 and 37 kDa marker bands and added to the same transfer cassette to transfer onto one nitrocellulose membrane. This step allows for the quantification of all tau bands on the same blot to

minimize the variability in blotting procedure across samples. The rest of the blotting procedure was performed as described earlier. Primary antibodies used were the Tau5 antibody at 1:100,000 and the tubulin 5H1 antibody at 1:10,000 (Nicholas M. Kanaan at Michigan State University, RRID: AB_2832941) (Wang et al., 1993). Secondary antibodies used were goat anti-mouse IgG1 680 and goat anti-mouse IgM 800 (LI-COR Biosciences, #926-32280, RRID: AB_2814919) at 1:20,000 each. LI-COR Odyssey classic imager and Image Studio Lite Ver 5.2 were used to visualize labeled protein bands. Tau bands were quantified in all Sup and Pellet fractions followed by calculating the percentage of tau in Pellet relative to total tau:

$$\% \text{ Tau in Pellet} = \text{Tau in Pellet}/(\text{Tau in Pellet} + \text{Tau in Sup}) \times 100$$

In vitro recombinant tau aggregation reaction

Aggregation of different tau proteins was induced by arachidonic acid (ARA; Cayman Chemical, #90010) in 200 µl reactions as described previously (Gamblin, King, Kuret, et al., 2000; Tiernan et al., 2016). Briefly, 2 µM of tau was induced to aggregate *in vitro* by incubation in tau aggregation buffer (10 mM sodium HEPES, 0.1 mM EDTA, 200 mM NaCl, 5 mM DTT, pH 7.6) without (unaggregated; ethanol vehicle) or with (aggregated) 75 µM ARA. ARA stocks were prepared in 100% ethanol at 2 mM immediately prior to use. Finally, ARA was added as the final component in the reaction sample and then the samples were gently mixed by minimally shaking the tube/cuvette. Aggregation reactions were incubated at room temperature for 6 hours.

Right angle laser light scattering

As tau polymerizes into larger masses while being exposed to a laser beam, the intensity of scattered light increases as a function of time (Gamblin, King, Dawson, et al., 2000). Therefore, laser light scattering (LLS) helps determine the aggregation kinetics of tau (Gamblin, King, Dawson, et al., 2000; Tiernan et al., 2016). LLS was measured using class IIb laser with wavelength of 475 nm and maximum power of 20 mW (B & W INC., model #BWI-475-20-E) and digital camera (Thor Labs, model #DCC1240M). Images were acquired using uc480 Viewer version 4.2 with the pixel clock set at 11 MHz. Images were acquired for hT40 samples at a frame rate of 2 fps and exposure of 250 ms, while a frame rate of 1 fps and exposure time to 600 ms was used for hT39 samples. Polymerization reactions of tau were transferred into glass cuvettes with path length of 5 mm (Starna Cells, #3-G-5), and laser light scattering was measured at time zero, prior to addition of ARA to obtain baseline measurements. After addition of ARA and gently mixing the samples, images were serially acquired at 1, 2, 3, 4, 5, 10, 15, 20, 25, 30, 35, 40, 45, 50, 55, 60, 75, 90, 105, 120, 150, 180, 240, 300, 360 minutes. Each experiment was conducted 4 independent times. Image analysis was performed with Adobe Photoshop CS6 (Adobe Systems INC.) using the marquee tool. The region of interest used for densitometry measurements was set to 150 pixels X 15 pixels and adjusted to the center of the glass cuvette within the band of scattered light. Pixel intensity was recorded using the histogram feature. Background levels at the zero-time point were subtracted from all readings to obtain corrected signal. Corrected scattered light intensity (corrected intensity) measurements during the 6 hours were fitted using nonlinear Finke-Watzky (FW) function (Morris et al., 2008) according to the following equation:

$$[B]_t = [A]_0 - ((k_1/k_2+[A]_0)/(1+(k_1/k_2[A]_0 \exp(k_1+k_2[A]_0)t))$$

To compare aggregation kinetics of different proteins, the following parameters were calculated: k_1 representing the rate constant of nucleation; k_2 representing the rate constant of elongation; $[A]_0$ representing maximum scattering at steady state. k_1 and k_2 could not be calculated for SUMO1- and SUMO2-modified hT40 and hT39 proteins because they failed to scatter enough light for proper fitting using FW formula.

Thioflavin S fluorescence

At the end of the tau aggregation reaction with ARA (described above), β-sheet containing aggregates were quantified using a thioflavin S assay as described (Tiernan et al., 2016). Immediately before starting the assay, a 0.0175% thioflavin S (ThS) solution was prepared in water, filtered through a 0.22 μM membrane, and protected from light. Then, 150 μl of each tau sample was mixed with 6 μl of ThS solution and incubated for 5 minutes at room temperature. The samples (150 μl/well) were then loaded onto a black 96-well plate (Costar, #3915) and immediately read using the Promega Glomax multi-detection system at 490 nm excitation and 510-570 nm emission wavelengths. Background levels of ThS fluorescence for unaggregated tau samples were subtracted from that of their respective aggregated tau samples to calculate the fold-change in ThS signal for each recombinant tau protein.

Sample preparation for imaging with transmission electron microscopy

Transmission electron microscopy (TEM) allows for the visualization of aggregate density and size, providing insights that help explain the results observed with LLS (Tiernan et al., 2016). To this end, uranyl acetate (UA; Electron Microscopy Sciences, #22400) solution was freshly prepared by dissolving 20 mg of UA in 1ml of deionized

water (DIW) (2% UA solution) at room temperature. After UA completely dissolves into DIW, the solution was sterile filtered using 0.22 μM membrane (Fisher Scientific, #13-1001-06). To prepare the grids, each unaggregated and aggregated tau sample (10 μl) was first fixed with 2% glutaraldehyde (Electron Microscopy Sciences, #16100) at room temperature for 10 minutes. Then, each sample (5 μl) was absorbed onto formvar-coated copper grids (Electron Microscopy Sciences, #FCF300-CU) for 1 minute, followed by one rapid rinse in DI water and another rapid rinse in UA solution. Finally, the grids were incubated with UA solution for 1 minute at room temperature, then the solution was wicked away, and grids were left to dry for at least 1.5 hours before imaging. Grids were prepared from 4 independent replicates of unaggregated and aggregated tau grids and imaged using JEOL JEM-1400 Plus electron microscope at 80 kV. Electron micrographs were captured and saved through AMT XR81 digital camera and AMT software version 602.6.

Quantitative TEM

For each grid, three images were captured at 5000X magnification for quantitative TEM. Electron micrographs were then processed using ImageJ v1.54 using a method like that described by Tiernan et al. (Tiernan et al., 2016). First, the image scale was adjusted according to the scale bar attached to the TEM images. Then, images were smoothed 5 times to allow for the automatic thresholding to capture the visible tau aggregates. The percentage of area occupied by aggregates (% Area) was collected by the “Analyze Particles” command. For the “Analyze Particles” command, size was set at 0-infinity and circularity was set at 0-1.

Output of “Analyze Particles” command was further processed using GraphPad Prism v10.2.1 to obtain frequency distribution using 700 nm^2-wide and 50 nm^2-wide bins

for hT40 and hT39, respectively. The sum of particles in 3 images/replicate was calculated and counted as 1 independent replicate, with a total of 4 independent replicates. The following populations of hT40 were plotted according to criteria like those reported by Tiernan et al. (Tiernan et al., 2016): < 700 nm^2 for globular aggregates only; 700-2100 nm^2 for globular aggregates > 700 nm^2 along with short filaments; 2100-5000 nm^2 for short filaments only; > 5000 nm^2 for long filaments only. Aggregates of hT39 were globular in nature and split into sizes smaller and larger than 1600 nm^2.

Sandwich enzyme-linked immunosorbent assay (sELISA)

To detect pathological tau conformations using conformation-dependent antibodies (i.e. TOC1, TOMA1, TNT2, and Alz50), tau samples must be kept under native conditions (Castillo-Carranza, Sengupta, et al., 2014; Combs et al., 2016; Combs et al., 2017; Jicha et al., 1997; Ward et al., 2013). Therefore, sandwich ELISA assays were employed to measure pathological tau conformations in 4 independent replicates. All steps were performed at room temperature. The following capture antibodies were used in sandwich ELISA assays: TOC1 (Nicholas M. Kanaan at Michigan State University, RRID: AB_2832939), TOMA1 (Millipore, #MABN819), TNT2 (Nicholas M. Kanaan at Michigan State University, RRID: AB_2736931), and Alz50 (P. Davies Albert Einstein College of Medicine, New York, USA, RRID: AB_2313937) in addition to Tau13 (Nicholas M. Kanaan at Michigan State University, RRID: AB_2721193) to measure total tau (Carmel et al., 1996; Castillo-Carranza, Sengupta, et al., 2014; Combs et al., 2016; Combs & Kanaan, 2017; Garcia-Sierra et al., 2003; Hyman, Van Hoesen, et al., 1988; Jicha et al., 1997; Patterson et al., 2011; Ward et al., 2013). Capture antibodies were diluted in borate saline buffer (100 mM borate acid, 25 mM sodium borate, 75 mM NaCl,

and 0.25 mM thimerosal) at 2 ng/µl. Then, sandwich ELISA plates (96-well plates, Corning, #3590) were coated with the capture antibodies (50 µl/well) for 1 hour. Wells were then washed 2 times with ELISA wash buffer (200 µl/well; 100 mM borate acid, 25 mM sodium borate, 75 mM NaCl, 0.25 mM thimerosal, 0.4% (w/v) bovine serum albumin, and 0.05% (v/v) Tween-20), followed by blocking with 5% NFDM in ELISA wash buffer (200 µl/well) for 1 hour. Two washes with ELISA wash buffer were performed, followed by the addition of unaggregated and aggregated tau samples for 1.5 hours. Tau samples were prepared from unaggregated and aggregated hT40 reactions in TBS buffer at the following concentrations (50 µl/well): 2.5 nM for Tau13; 5 nM for TNT2; 20 nM for TOC1 and Alz50; 15 0nM for TOMA1. Tau samples were prepared from unaggregated and aggregated hT39 reactions in TBS buffer at the following concentrations (50 µl/well): 2.5 nM for Tau13; 20 nM for Alz50; 50 nM for TNT2; 150 nM for TOC1 and TOMA1. Then, wells were washed 4 times with ELISA wash buffer (200 µl/well). The detection antibody R1 (Nicholas M. Kanaan at Michigan State University, RRID: AB_2832929) (Berry et al., 2004) was diluted at 1:10,000 in 5% NFDM and added to the wells (50 µl/well) for 1.5 hours. Then, sandwich ELISA wells were washed 4 times with ELISA wash buffer. The secondary antibody used was Goat Anti-Rabbit IgG Antibody (H+L), Peroxidase (Vector Laboratories, #PI-1000-1, RRID: AB_2916034) at 1:5,000 in 5% NFDM for 1 hour (50 µl/well). After 4 final washes with ELISA wash buffer, the peroxidase reaction was developed using 3,3′,5,5′-Tetramethylbenzidine (TMB; 50 µl/well; Sigma, #T0440). The peroxidase reaction was stopped with 4% sulphuric acid, followed by reading the absorbance at 450 nm using SpectraMax Plus 384 microplate reader (Molecular Devices).

The absorbance values were further processed using GraphPad Prism v10.2.1 according to the following equation to calculate the percentage light absorbed (% Light Abs, %A):

$$\%A = 100 - (100 * 10^{-A})$$

Seeding assay in tau biosensor cells

HEK293 cells stably expressing the repeat domain of tau with the P301S mutation fused to CFP or YFP (Tau RD P301S Biosensor Cells; ATCC, #CRL-3275, RRID: CVCL_DA04) were grown in DMEM (Gibco) supplemented with 10% FBS, 1% Penicillin-Streptomycin (Gibco), and 1x GlutaMAX (Gibco), and maintained at 37 °C and 5% CO_2 (Holmes et al., 2014). A cell aliquot was thawed and passaged at least once before use in experiments. Cells were plated at 12,000 cells/well in Poly-D-Lysine coated 96-well plates (100 µl media/well; Corning, #354461). After 24 hours, Lipofectamine 2000 (Invitrogen, #11668027) was used to deliver the following treatment samples into cells: unaggregated hT40, aggregated hT40 aggregates, unaggregated SUMO1-modified hT40, aggregated SUMO1-modified hT40, unaggregated SUMO2-modified hT40, and aggregated SUMO2-modified hT40 (at a final concentration of 150 nM). In two separate tubes, Lipofectamine reagent or protein sample was diluted in OptiMEM (Gibco, #31985062) and incubated at room temperature for 20 minutes. The first tube contained 1 µl Lipofectamine 2000 in addition to 9 µl OptiMEM, and the other tube contained 7.5 µl unaggregated or aggregated tau + 2.5 µl OptiMEM. Next, the Lipofectamine was mixed with the tau protein (20 µl) and incubated for an additional 20 minutes at room temperature. The Lipofectamine/protein mixture was then added to the cells (20 µl). Two days following treatment, cells were fixed with pre-warmed 4% paraformaldehyde

(Electron Microscopy Sciences, #15714-S) in 1X cytoskeleton buffer (10 mM MES, 138 mM KCl, 3 mM $MgCl_2$, and 4 mM EGTA, pH 6.1) for 20 min at room temperature. Then, cells were washed 3 times with 1X TBS, 5 minutes each. The nuclear stain DAPI (1:10,000) was included in the first wash.

Cells were imaged using a Lionheart FX Automated Microscope (BioTek) using a 10x objective. Nine images per well were captured with GFP and DAPI filter cubes using the same acquisition settings. Images were processed and analyzed using Gen5 software v3.11 (BioTek). Seeded aggregates and nuclei were detected in the GFP and DAPI channels, respectively, using separate sets of size and pixel-intensity thresholds. For each well, the total number of aggregates was normalized to the total number of cells (DAPI+ objects) to obtain the number of seeds per cell (seeds/cell = number of GFP+ objects/number of DAPI+ objects).

Statistics

Statistical analysis was performed using GraphPad Prism v10.2.1. One-way analysis of variance (ANOVA) followed by Holm-Sidak post-hoc test was employed to analyze the following results: V_{max} of tubulin polymerization assay; % Area from quantitative TEM of hT40. Welch's ANOVA test (used in cases of unequal variance across groups) followed by Dunnett's T3 multiple comparisons test were used to analyze the following data: Max of LLS; % Area from quantitative TEM of hT39. Two-way ANOVA followed by the post-hoc Holm-Sidak with all possible comparisons were used to analyze the following results: % Tau in pellet of microtubule-binding assay; Fold change in ThS fluorescence; % Light Abs of sandwich ELISA assays; Seeds/cell of seeding assay in RD cells. Differences in outcomes were deemed statistically significant at $p \leq 0.05$.

Results

Co-transformation of bacterial cells with tau and SUMOylation machinery produces SUMO-modified tau

To ensure successful SUMOylation of recombinant tau proteins, we subjected the recombinant tau proteins to western blot for SUMO1, SUMO2 and tau. Unmodified hT40 (Figure 4.1A and B) and hT39 (Figure 4.2A and B) did not have signal with the SUMO1 and SUMO2 antibodies. SUMO1-modified hT40 (Figure 4.1A and B) and hT39 (Figure 4.2A and B) were labeled by the SUMO1 antibody but not by the SUMO2 antibody. On the other hand, SUMO2-modified hT40 (Figure 4.1A and B) and hT39 (Figure 4.2A and B) were labelled by the SUMO2 antibody but not by the SUMO1 antibody. Both the unmodified and modified tau proteins showed similar reactivity to the Tau5 antibody, a pan-tau antibody (Figure 4.1A and B for hT40 proteins; Figure 4.2A and B for hT39 proteins lower panel).

Commercially available SUMO antibodies do not provide information on the lysine residues modified. We employed MS to determine the lysine residues modified by SUMO in hT40 and hT39 proteins. MS demonstrated that SUMO1 and SUMO2 modifications share several of the lysine residues on both hT40 and hT39, including K67, K87, K150, K174, K225, K234, K240, K254, K259, K267, K274, K311, K353, K369, K370, K375, and K395 (Figure 4.1C and 2C). Of note, SUMOylation at K281 and K298 by SUMO1 and SUMO2 were detectable only in hT40 given that both sites are located within the second microtubule-binding repeat (Figure 4.1C).

SUMO modifications were detected by mass shifts and diagnostics ion in SUMOylated hT40 and hT39 samples. At least three diagnostic ions were required to

confirm a specific lysine residue was modified with SUMOylation. Examples of mass shifts and diagnostics ions observed with SUMO-modified hT40 and hT39 proteins are included in Figures AIII.2 and AIII.3, respectively.

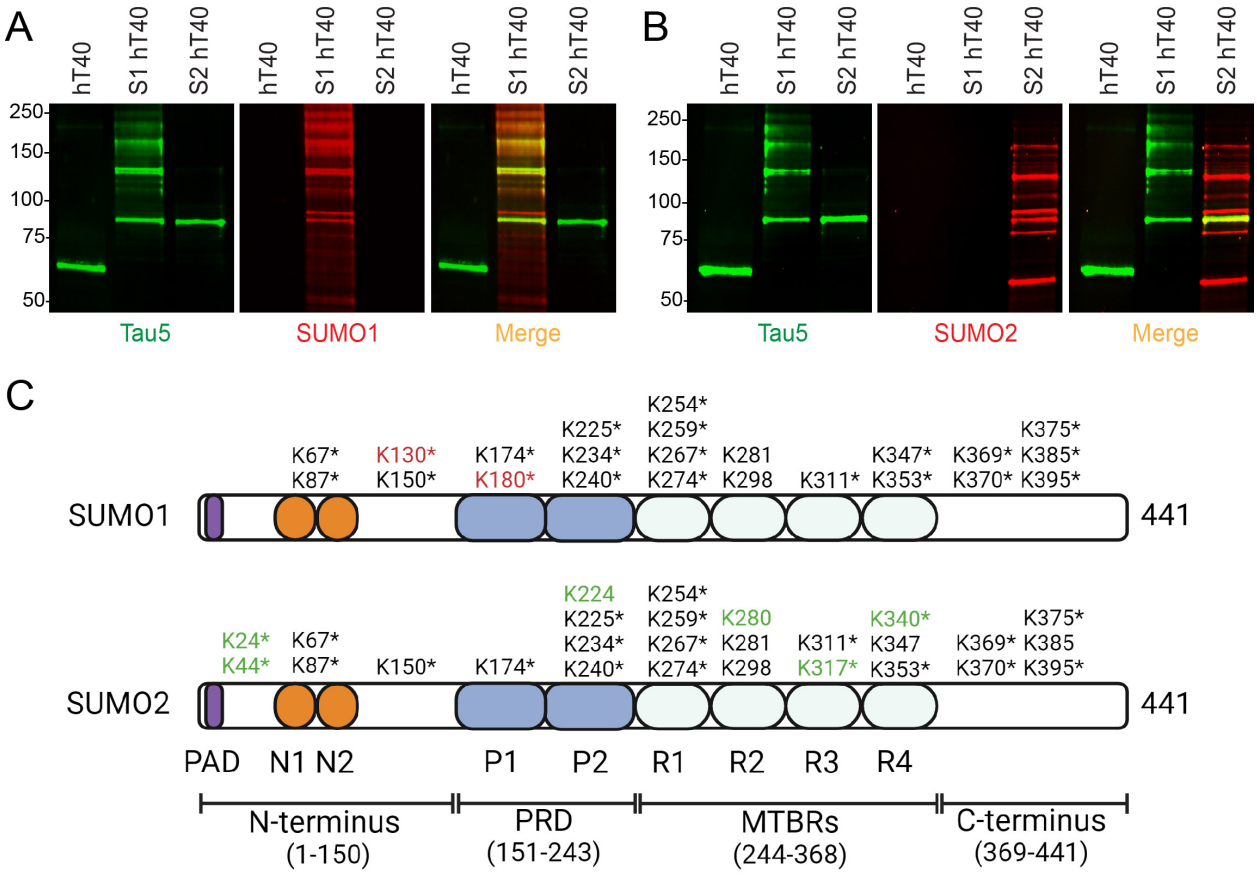

Figure 4.1. Identification of lysine residues on hT40 modified with SUMO1 and SUMO2.
A, western blot of hT40 proteins probed with the SUMO1 and Tau5 (total tau) antibodies. B, western blot of hT40 proteins probed with the SUMO2 and Tau5 (total tau) antibodies. C, lysine residues (K) modified with SUMO1 (upper panel) and SUMO2 (lower panel) on hT40 as detected by mass spectrometry. Residues are numbered according to the sequence of full-length tau (hT40, 2N4R, 441 amino acids). SUMOylation sites are concentrated within microtubule-binding repeats and the flanking regions. Modified K residues unique to SUMO1 are highlighted in red. Modified K residues unique to SUMO2 are highlighted in green. Asterisk * indicates that the modified K residues are shared with the hT39 isoform. Abbreviations: SUMOylation, modification with small-ubiquitin-like modifier protein; SUMO, small ubiquitin-like modifier; hT40, 2N4R tau isoform; PRD, proline rich domain; MTBRs, microtubule-binding repeats. Panel C created with BioRender.com.

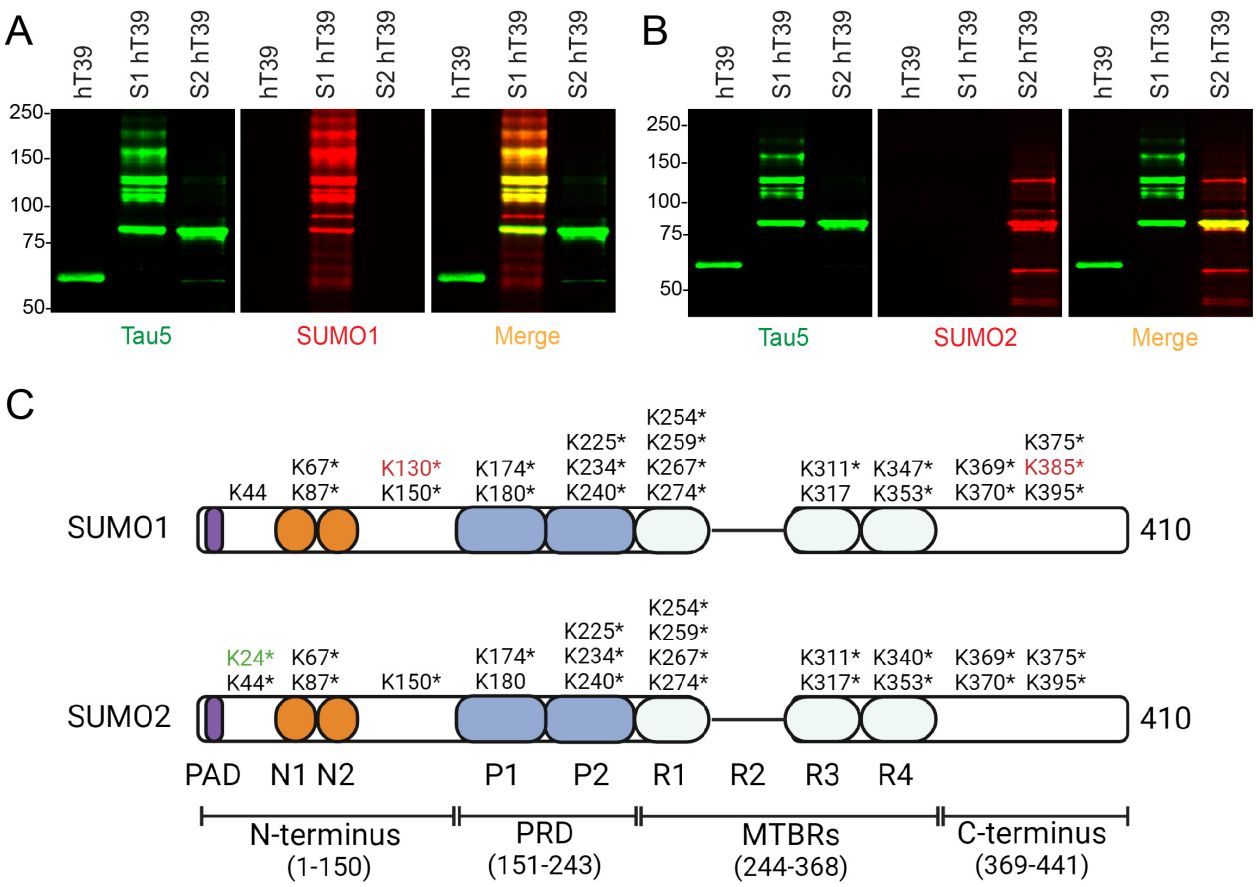

Figure 4.2. Identification of lysine residues on hT39 modified with SUMO1 and SUMO2.

A, western blot of hT39 proteins probed with the SUMO1 and Tau5 (total tau) antibodies. B, western blot of hT39 proteins probed with the SUMO2 and Tau5 (total tau) antibodies. C, lysine residues (K) modified with SUMO1 (upper panel) and SUMO2 (lower panel) on hT39 as detected by mass spectrometry. Residues are numbered according to the sequence of full-length tau (hT40, 2N4R, 441 amino acids). SUMOylation sites are concentrated within microtubule-binding repeats and the flanking regions. Modified K residues unique to SUMO1 are highlighted in red. Modified K residues unique to SUMO2 are highlighted in green. Asterisk * indicates that the modified K residues are shared with the hT40 isoform. Abbreviations: SUMOylation, modification with small-ubiquitin-like modifier protein; SUMO, small ubiquitin-like modifier; hT39, 2N3R tau isoform; PRD, proline rich domain; MTBRs, microtubule-binding repeats. Panel C created with BioRender.com.

SUMOylation of tau impedes microtubule polymerization in vitro

Tubulin polymerization assays were used to determine how SUMO modification affects tau's ability to modulate microtubule polymerization kinetics *in vitro* (Figure 4.3A and C). A statistically significant difference among the means of V_{max} for hT40 proteins was observed [one-way ANOVA: $F_{(2, 9)} = 54.75$, $p < 0.05$]. Modification of hT40 with SUMO1 ($t = 8.545$, $p < 0.05$) or SUMO2 ($t = 9.503$, $p < 0.05$) reduced the steady state polymerization relative to unmodified hT40 (Figure 4.3B, V_{max}). There was a statistically significant different among the means of V_{max} for hT39 proteins [$F_{(2, 9)} = 854.3$, $p < 0.05$]. SUMO1- ($t = 36.53$, $p < 0.05$) and SUMO2-modified hT39 ($t = 35.02$, $p < 0.05$) demonstrated lower steady state microtubule polymerization relative to unmodified hT39 (Figure 4.3D, V_{max}). K_d could not be calculated for SUMO1- and SUMO2-modified hT40 and hT39 proteins because they failed to induce enough polymerization (i.e. fluorescence signal) for proper fitting using specific binding with Hill slope.

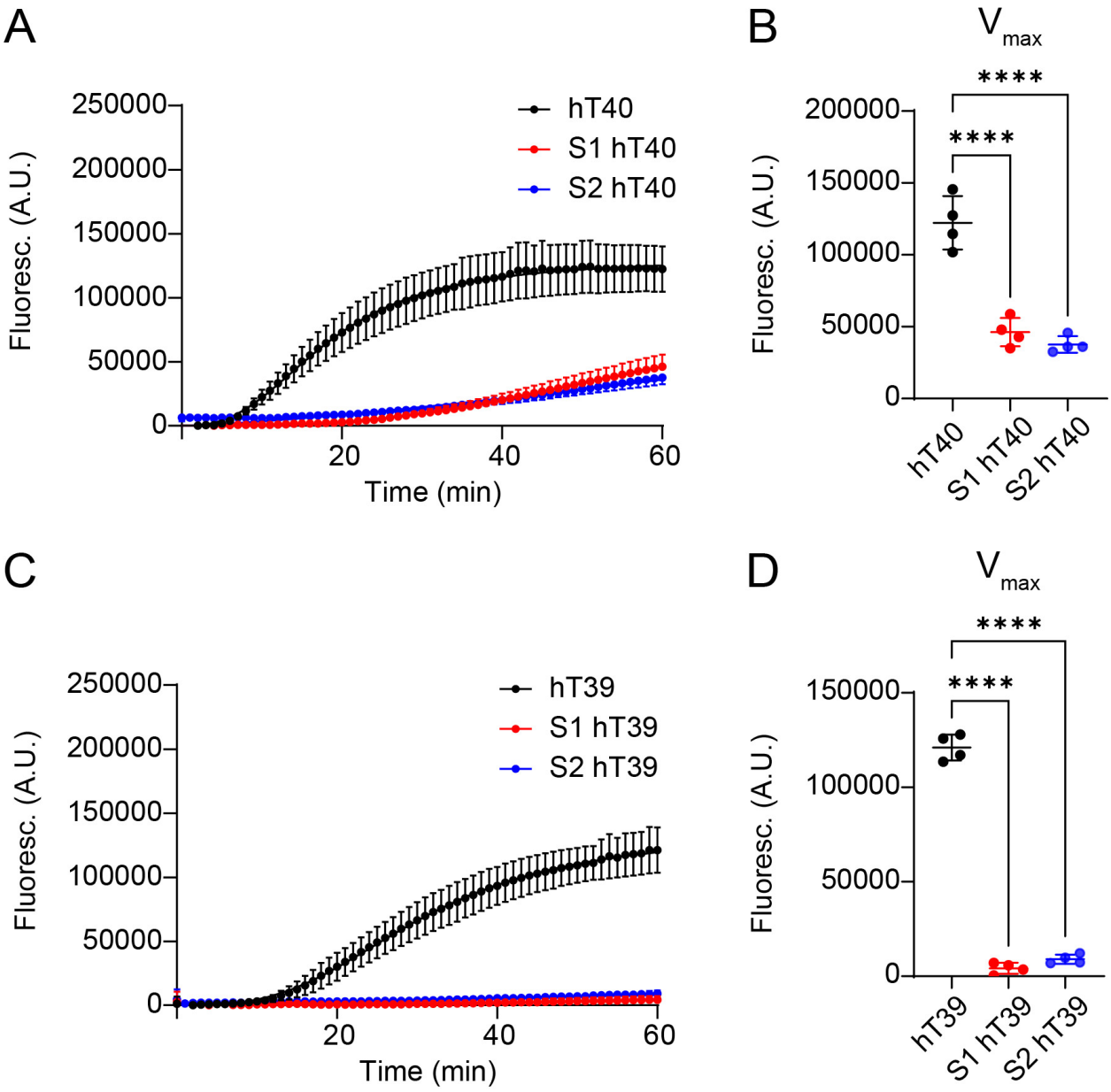

Figure 4.3. Modification of tau with SUMO1 or SUMO2 impedes tau-induced tubulin polymerization *in vitro*.
A, curve fit of fluorescence signal corresponding to microtubule polymerization in the presence of hT40 proteins over 60 minutes. B, V_{max} of microtubule polymerization for unmodified, SUMO1-, and SUMO2-modified hT40 proteins. C, curve fit of fluorescence signal corresponding to microtubule polymerization in the presence of hT39 proteins tau over 60 minutes. D, V_{max} of microtubule polymerization for unmodified, SUMO1-, and SUMO2-modified hT39 proteins. Abbreviations: SUMOylation, modification with small-ubiquitin-like modifier protein; SUMO, small ubiquitin-like modifier; hT40, 2N4R tau isoform; hT39, 2N3R tau isoform; V_{max}, steady state equilibrium. Data represented as mean +/- SD. * p≤0.05; ** p≤0.01; *** p≤0.001; **** p≤0.0001.

SUMOylation disrupts tau's binding to microtubules in vitro

Microtubule-binding assays were used to determine how SUMO modification affects tau's ability to bind pre-formed microtubules. Experiments were conducted using either the hT40 or hT39 tau isoforms independently (Figure 4.4A and B). Two-way ANOVA identified a significant interaction between the PTM status of hT40 proteins and the microtubule fraction (i.e. supernatant MT-unbound tau and pellet MT-bound tau) in the binding reaction [$F_{(2, 18)}$ = 64.22, $p < 0.05$]. Apart from SUMO2-modified hT40 (t = 0.9588, $p > 0.05$), there was a statistically significant increase in the percentage of hT40 protein in the pellet fraction upon adding them to pre-formed microtubules (Figure 4.4C; t = 15.87, $p < 0.05$ for hT40; t = 13.51, $p < 0.05$ for S1 hT40). A significant 22% reduction in the proportion of SUMO1-modified hT40 in the pelleted microtubule fraction relative to unmodified hT40 was detected (Figure 4.4C; t = 3.898, $p < 0.05$). The percentage of SUMO2-modified hT40 in the pelleted microtubule fraction was reduced by 89% relative to unmodified hT40 (Figure 4.4C; t = 16.83, $p < 0.05$). Relative to SUMO1-modified hT40, the proportion of SUMO2-modified hT40 was lower in the pelleted microtubule fraction by 86% (Figure 4.4C; t = 11.97, $p < 0.05$).

There was a significant interaction between PTM and the microtubule fraction in the binding reaction [$F_{(2, 18)}$ = 55.54, $p < 0.05$]. A statistically significant increase in the percentage of all hT39 proteins in the pellet fraction when pre-formed microtubules were present was observed (Figure 4.4D; t = 19.90, $p < 0.05$ for hT39; t = 6.294, $p < 0.05$ for S1 hT39; t = 7.837, $p < 0.05$ for S2 hT39). The proportion of SUMO1- and SUMO2-modified hT39 proteins were less abundant in the pelleted microtubule fraction when compared to unmodified hT39 by 70% and 63%, respectively (Figure 4.4D; t = 15.21, p <

0.05 for S1 hT39; $t = 13.54$, $p < 0.05$ for S2 hT39). The abundance of SUMO2-modified hT39 in the pelleted microtubule fraction was no different from SUMO1-modified hT39 (Figure 4.4D; $t = 1.668$, $p > 0.05$).

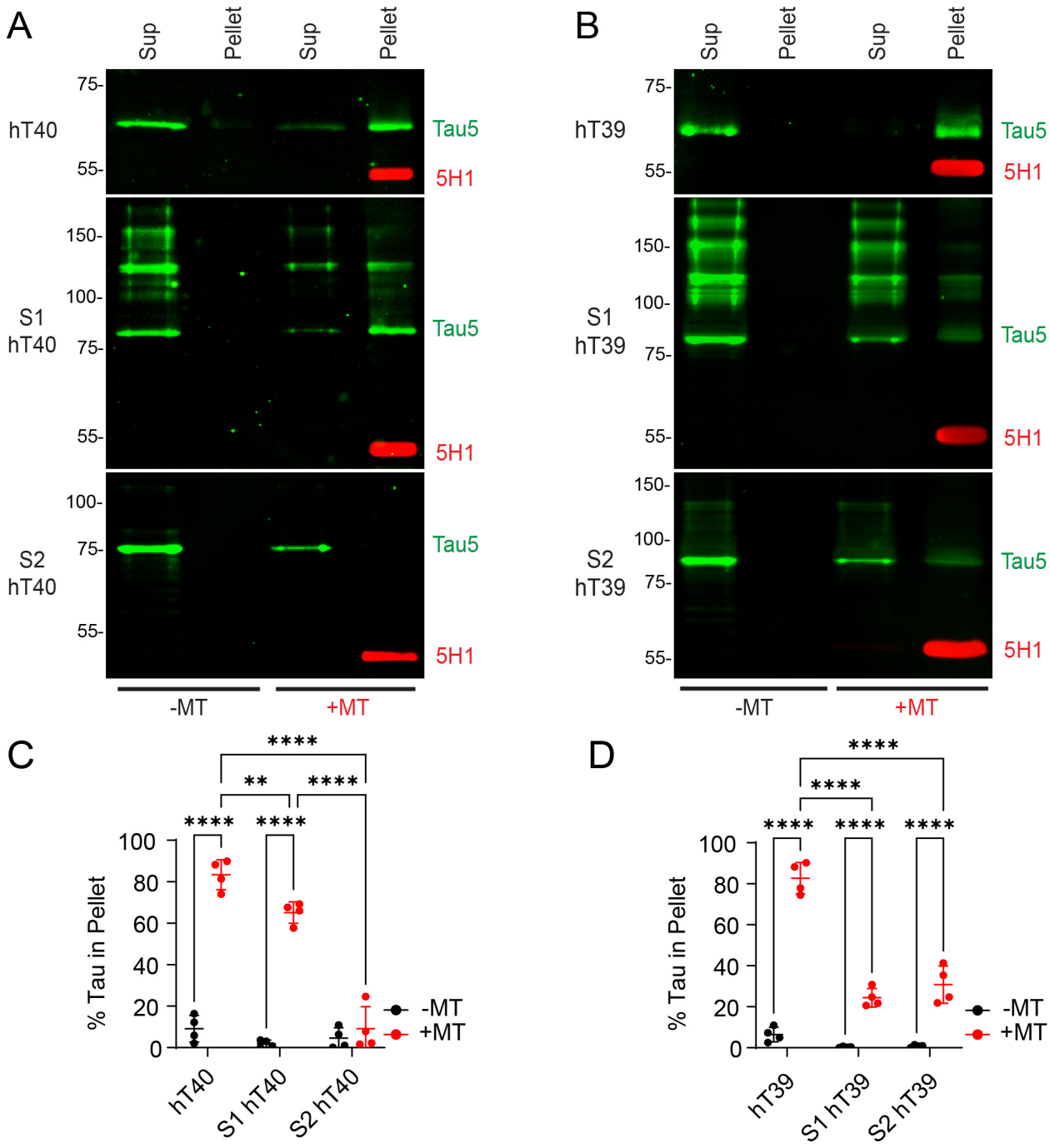

Figure 4.4. SUMOylation impedes binding of tau to microtubules *in vitro*.
A, representative western blot of microtubule-binding assay for unmodified, SUMO1-, and SUMO2-modified hT40 using Tau5 and 5H1 (tubulin) antibodies. B, representative western blot of microtubule-binding assay for unmodified, SUMO1-, and SUMO2-modified hT39 using Tau5 and 5H1 (tubulin) antibodies. C, quantification of the fraction of tau detected in the pellet of polymerized microtubules for unmodified, SUMO1-, and

Figure 4.4 (cont'd)
SUMO2-modified hT40. D, quantification of the fraction of tau detected in the pellet of polymerized microtubules for unmodified, SUMO1-, and SUMO2-modified hT39. Abbreviations: SUMOylation, modification with small-ubiquitin-like modifier protein; SUMO, small ubiquitin-like modifier; hT40, 2N4R tau isoform; hT39, 2N3R tau isoform; MTs, microtubules; Sup, supernatant. Data represented as mean ± SD. * p≤0.05; ** p≤0.01; *** p≤0.001; **** p≤0.0001.

SUMOylation of tau inhibits its aggregation in vitro

Right-angle LLS assays were used to determine the impact of SUMOylation on the kinetics of tau aggregation *in vitro* (Figure 4.5A and D). There was a significant difference across the maximum light scattering of hT40 proteins [Welch's ANOVA: $F_{(2, 4.492)} = 115.7$, $p < 0.05$]. We observed 82% and 97.5% reduction in the maximum light scattering with SUMO1- and SUMO2-modified hT40 compared to the unmodified hT40 (Figure 4.5B; $t = 12.10$, $p < 0.05$ for S1 hT40; $t = 15.76$, $p < 0.05$ for S2 hT40). Moreover, the maximum light scattering was 86.4% lower with SUMO2-modified hT40 when compared to SUMO1-modified hT40 (Figure 4.5B; $t = 4.939$, $p < 0.05$). k_1 and k_2 could not be calculated for SUMO1- and SUMO2-modified hT40 proteins because they failed to scatter enough light for proper fitting using FW formula.

A statistically significant difference was observed across the maximum light scattering of hT39 proteins [Welch's ANOVA: $F_{(2, 4.141)} = 137.1$, $p < 0.05$]. Both SUMO1 and SUMO2 modification of hT39 decreased the maximum light scattering by 95% and 92%, respectively, when compared to unmodified hT39 (Figure 4.5E; $t = 17.84$, $p < 0.05$ for S1 hT39; $t = 14.51$, $p < 0.05$ for S2 hT39). No significant difference in maximum light scattering was observed upon comparing SUMO1- to SUMO2-modified hT39 proteins (Figure 4.5E; $t = 0.7285$, $p > 0.05$). k_1 and k_2 could not be calculated for SUMO1- and

SUMO2-modified hT39 proteins because they failed to scatter enough light for proper fitting using FW formula.

SUMO modification of tau reduces its β-sheet containing aggregates in vitro

ThS assays were performed at the end of aggregation reactions to determine the extent of β-sheet containing aggregate formation *in vitro*. Two-way ANOVA revealed a statistically significant interaction between the PTM and aggregation status of proteins [$F_{(2, 17)}$ = 3754, $p < 0.05$ for hT40 proteins; $F_{(2, 18)}$ = 17.02, $p < 0.05$ for hT39 proteins]. Upon aggregating unmodified hT40 and hT39 proteins, there was a significant increase in the ThS signal compared to their respective unaggregated samples (Figure 4.5C and F; 450-fold increase, t = 108.1, $p < 0.05$ for unmodified hT40; 4.25-fold increase, t = 6.881, $p < 0.05$ for unmodified hT39).

Inducing the aggregation of SUMO2-modified hT40 increased the ThS signal relative to the unaggregated SUMO2-modified hT40 (Figure 4.5C; 6.5-fold increase, t = 6.120, $p < 0.05$). There was a significant reduction in the ThS signal upon inducing the aggregation of SUMO1-modified hT40 relative to the unaggregated SUMO1-modified hT40 (89% reduction, t = 6.120, $p < 0.05$). In addition, SUMO1-modified hT40 showed a higher ThS signal in the unaggregated state relative to unmodified and SUMO1-modified hT40 unaggregated samples (18.5-fold higher, t = 4.140, $p < 0.05$ for unmodified hT40; 3.6-fold higher, t = 2.940, $p < 0.05$ for SUMO2-modified hT40). The aggregated samples of unmodified hT40 showed a higher ThS signal compared to the aggregated SUMO1- and SUMO2-modified hT40 samples (227-fold higher, t = 107.8, $p < 0.05$ for SUMO1-modified hT40; 13.9-fold higher, t = 100.5, $p < 0.05$ for SUMO2-modified hT40). Moreover, the aggregated SUMO2-modified hT40 showed a higher ThS signal relative to the

aggregated samples of SUMO1-modified hT40 (16.4-fold higher, $t = 7.336$, $p < 0.05$). The aggregated samples of unmodified hT39 gave higher ThS signal compared to aggregated samples of SUMO1- and SUMO2-modified hT39 proteins (Figure 4.5F; 16.9-fold higher, $t = 8.466$, $p < 0.05$ for SUMO1-modified hT39; 19-fold higher, $t = 8.526$, $p < 0.05$ for SUMO2-modified hT39).

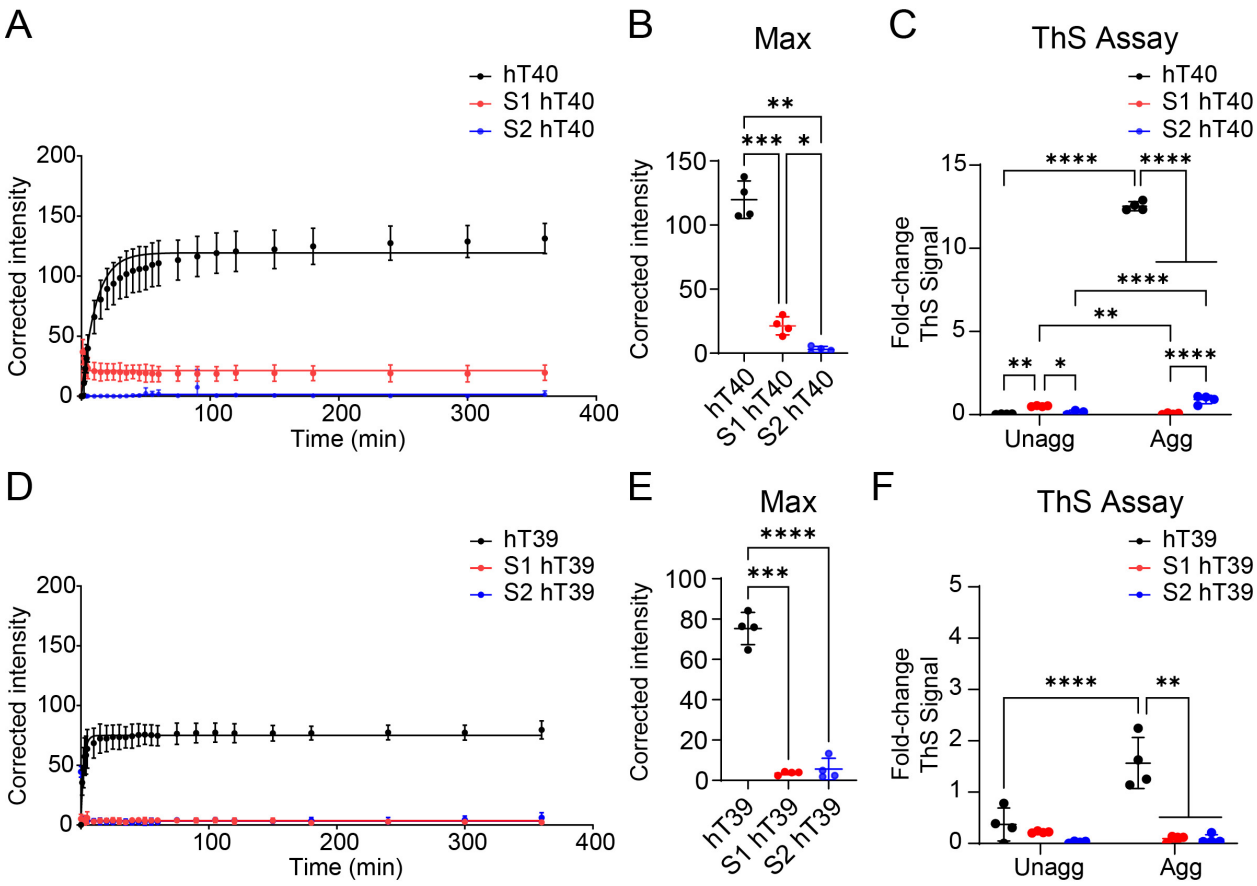

Figure 4.5. SUMOylation of tau reduces tau multimerization *in vitro*.
A, LLS of unmodified, SUMO1-, and SUMO2-modified hT40. B, max polymerization (V_{max}) for unmodified, SUMO1-, and SUMO2-modified hT40. C, thioflavin S assay for unaggregated and aggregated hT40 samples. D, LLS of unmodified, SUMO1-, and SUMO2-modified hT39. E, V_{max} for unmodified, SUMO1-, and SUMO2-modified hT39. F, thioflavin S assay for unaggregated and aggregated hT39 samples. Abbreviations: SUMOylation, modification with small-ubiquitin-like modifier protein; SUMO, small ubiquitin-like modifier; hT40, 2N4R tau isoform; hT39, 2N3R tau isoform; LLS, laser light scattering; max, maximum light scattering; ThS, thioflavin S. Data represented as mean ± SD. * p≤0.05; ** p≤0.01; *** p≤0.001; **** p≤0.0001.

SUMO modification decreases the formation of filamentous tau aggregates in vitro

Unaggregated and aggregated hT40 samples were visualized using TEM and the total mass (% Area) and size of aggregates was quantified (Figure 4.6A). One-way ANOVA demonstrated a statistically significant difference in the means of % area across the hT40 proteins [$F_{(2, 9)} = 25.71$, $p < 0.05$]. Aggregated SUMO1- and SUMO2-modified hT40 had lower % area when compared to unmodified hT40 (Figure 4.6D; $t = 6.301$, $p < 0.05$ for S1 hT40; $t = 6.115$, $p < 0.05$ for S2 hT40).

The number of globular aggregates < 700 nm^2 was higher with both SUMO1 and SUMO2 modifications of hT40 relative to unmodified hT40 (Figure 4.6C, upper panel). On the other hand, the number of short (2100-5000 nm^2) and long filamentous (> 5000 nm^2) aggregates was reduced with both SUMO modifications when compared to unmodified hT40 (Figure 4.6C, lower panel).

There was no significant difference in % area across the different hT39 proteins [Figure 4.6F; Welch's ANOVA: $F (2, 5.359) = 3.68$, $p > 0.05$]. SUMO1-modified hT39 demonstrated lower number of globular aggregates at all sizes when compared to unmodified hT39 (Figure 4.6E, upper and lower panels). The number of globular aggregates < 1600 nm^2 was similar between SUMO2-modified and unmodified hT39 (Figure 4.6E, upper panel). On the contrary, the number of globular aggregates > 1600 nm^2 was higher with SUMO2-modified hT39 relative to unmodified hT39 (Figure 4.6E, lower panel).

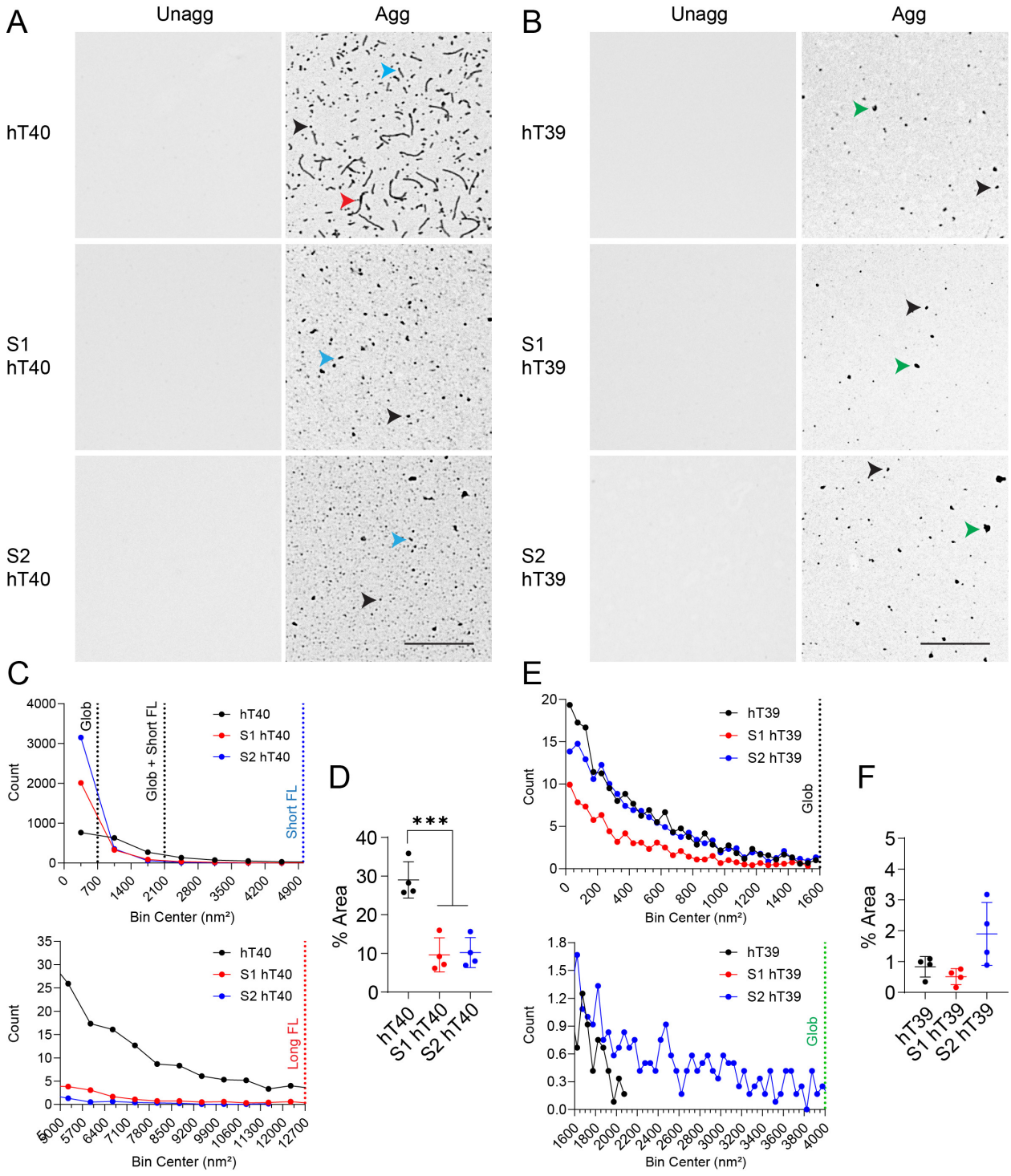

Figure 4.6. SUMOylation decreases the formation of filamentous tau aggregates *in vitro*.

A, electron micrograph of unaggregated and aggregated hT40 proteins. Scale bar: 800nm. Globular aggregates < 700 nm^2 highlighted with black arrowheads; short (2100-

Figure 4.6 (cont'd)
5000 nm^2) and long (> 5000 nm^2) filaments highlighted with blue and red arrowheads, respectively. B, electron micrograph of unaggregated and aggregated hT39 proteins. Scale bar: 800 nm. Globular aggregates < 1600 nm^2 highlighted with black arrowheads; globular aggregates > 1600 nm^2 highlighted with green arrowhead. C, size distribution of aggregates formed by unmodified, SUMO1-, and SUMO2-modified hT40 proteins. D, total mass of aggregates observed with unmodified, SUMO1-, and SUMO2-modified hT40 expressed as percentage of field area. E, size distribution of aggregates formed by unmodified, SUMO1-, and SUMO2-modified hT39 proteins. F, total mass of aggregates observed with unmodified, SUMO1-, and SUMO2-modified hT39 expressed as percentage of field area. Abbreviations: SUMOylation, modification with small-ubiquitin-like modifier protein; SUMO, small ubiquitin-like modifier; hT40, 2N4R tau isoform; hT39, 2N3R tau isoform; unagg, unaggregated; agg, aggregated; % Area, % of aggregates per field. Data represented as mean ± SD. * p≤0.05; ** p≤0.01; *** p≤0.001; **** p≤0.0001.

SUMO modification affects the formation of pathological tau conformations in vitro

For all unaggregated and aggregated hT40 and hT39 proteins, total tau levels were measured using Tau13 as capture antibody (Figure AIII.4). Sandwich ELISA results for all conformational tau antibodies were normalized to total tau levels to account for differences in Tau13 readings.

Several antibodies are available to detect oligomeric tau (Alhadidy & Kanaan, 2024; Castillo-Carranza, Gerson, et al., 2014; Patterson et al., 2011; Ward et al., 2013). Oligomeric tau species were quantified in unaggregated and aggregated tau samples using non-denaturing sandwich ELISAs with two different oligomeric tau antibodies (i.e. TOC1 and TOMA1). Sandwich ELISAs using TOC1 as capture antibody identified a statistically significant interaction between PTM and aggregation status (i.e. unaggregated or aggregated) of hT40 [$F_{(2, 18)} = 54.38$, $p < 0.05$] and hT39 proteins [$F_{(2, 18)} = 95.69$, $p < 0.05$]. Post-hoc analysis detected a significant increase in oligomeric tau with the aggregation of unmodified hT40 ($t = 13.89$, $p < 0.05$) and hT39 ($t = 17.40$, $p < 0.05$) relative to their respective unaggregated tau proteins (Figure 4.7A). In addition,

aggregated samples of SUMO1- and SUMO2-modified hT40 ($t = 12.64$, $p < 0.05$ for S1 hT40; $t = 11.19$, $p < 0.05$ for S2 hT40) and hT39 ($t = 17.75$, $p < 0.05$ for S1 hT39; $t = 16.81$, $p < 0.05$ for S2 hT39) gave little to no TOC1 signal, which was significantly lower relative to the aggregated samples of unmodified tau proteins (Figure 4.7A).

Next, we assessed the abundance of TOMA1-positive oligomeric tau species in the unmodified, SUMO1-modified, and SUMO2-modified tau samples. There was a statistically significant interaction between PTM and aggregation status of hT40 [two-way ANOVA: $F_{(2, 18)} = 55.34$, $p < 0.05$] and hT39 proteins [two-way ANOVA: $F_{(2, 18)} = 37.57$, $p < 0.05$]. Aggregation of unmodified, SUMO1-modified, and SUMO2-modified hT40 caused an increase in the TOMA1 signal when compared to their respective unaggregated samples (Figure 4.7B, left panel; $t = 16.65$, $p < 0.05$ for hT40; $t = 10.03$, $p < 0.05$ for S1 hT40; $t = 24.88$, $p < 0.05$ for S2 hT40). Aggregated SUMO1-modified hT40 showed lower TOMA1 signal relative to the aggregated samples of unmodified hT40 (Figure 4.7B, left panel; $t = 6.705$, $p < 0.05$). On the contrary, aggregated SUMO2-modified hT40 showed higher TOMA1 signal relative to the aggregated samples of unmodified hT40 ($t = 8.629$, $p < 0.05$) and SUMO1-modified hT40 ($t = 15.33$, $p < 0.05$) proteins (Figure 4.7B, left panel).

TOMA1 signal increased with aggregation of unmodified hT39 relative to the unaggregated hT39 tau samples (Figure 4.7B, right panel; $t = 10.70$, $p < 0.05$). No statistically significant differences were observed between the unaggregated and aggregated samples of SUMO1- and SUMO2-modified hT39 proteins (Figure 4.7B, right panel; $t = 0.08052$, $p > 0.05$ for S1 hT39; $t = 0.2639$, $p > 0.05$ for S2 hT39). Moreover, the TOMA1 signal in the aggregated SUMO1- and SUMO2-modified hT39 samples was lower

than the aggregated unmodified hT39 (Figure 4.7B, right panel; $t = 11.04$, $p < 0.05$ for S1 hT39; $t = 10.64$, $p < 0.05$ for S2 hT39).

Tau is known to adopt pathological conformations associated with modifications of monomeric tau and following multimerization (Alhadidy & Kanaan, 2024; Christensen et al., 2023; Hintermayer et al., 2020; Kanaan et al., 2011). Those conformations include exposure of the PAD of tau that spans amino acids 2-18 and whose abnormal exposure is linked to axonal transport dysfunction (Combs et al., 2021; Kanaan et al., 2011; LaPointe et al., 2009). Another misfolded conformation involves the N-terminus of tau coming into close proximity to the microtubule-binding region of tau, and it occurs early in disease before tau aggregation (Carmel et al., 1996; Hyman, Van Hoesen, et al., 1988; Jicha et al., 1997). The extent to which SUMO modification can influence the adoption of the two conformations was assessed using sandwich ELISA with two antibodies: TNT2 for PAD exposure and Alz50 for the misfolded conformation.

A statistically significant interaction was found between the PTM and aggregation status (i.e. unaggregated or aggregated) of hT40 [two-way ANOVA, $F_{(2, 18)} = 88.92$, $p < 0.05$] and hT39 [two-way ANOVA, $F_{(2, 18)} = 31.55$, $p < 0.05$] proteins. Regardless of the tau isoform, aggregated samples of unmodified tau showed higher TNT2 signal compared to the unaggregated samples (Figure 4.7C; $t = 17.27$, $p < 0.05$ for hT40; $t = 10.29$, $p < 0.05$ for hT39). No statistically significant differences were observed between the unaggregated and aggregated samples of SUMO1- and SUMO2-modified hT40 (Figure 4.7C, left panel; $t = 0.4983$, $p > 0.05$ for S1 hT40; $t = 1.426$, $p > 0.05$ for S2 hT40) and hT39 proteins (Figure 4.7C, right panel; $t = 0.4804$, $p > 0.05$ for S1 hT39; $t = 0.6452$, $p > 0.05$ for S2 hT39). The TNT2 signal in the aggregated SUMO1- and SUMO2-modified

hT40 samples was lower than the aggregated unmodified hT40 (Figure 4.7C, left panel; $t = 16.32$, $p < 0.05$ for S1 hT40; $t = 14.43$, $p < 0.05$ for S2 hT40). Similarly, the aggregated SUMO1- and SUMO2-modified hT39 samples had lower TNT2 signal than the aggregated unmodified hT39 (Figure 4.7C, right panel; $t = 11.23$, $p < 0.05$ for S1 hT39; $t = 11.45$, $p < 0.05$ for S2 hT39).

We detected a significant interaction between PTM and aggregation status of both hT40 [two-way ANOVA, $F_{(2, 18)} = 29.88$, $p < 0.05$] and hT39 [two-way ANOVA, $F_{(2, 18)} = 24.31$, $p < 0.05$] proteins with the Alz50 assay. Alz50-positive misfolded tau was higher in the aggregated samples of unmodified and SUMO2-modified hT40 samples relative to their respective unaggregated samples (Figure 4.7D, left panel; $t = 11.57$, $p < 0.05$ for hT40; $t = 3.484$, $p < 0.05$ for S2 hT40). However, there was no significant increase in the Alz50 signal between the unaggregated and aggregated samples of SUMO1-modified hT40 (Figure 4.7D, left panel; $t = 1.160$, $p > 0.05$). Alz50 signal was lower in the aggregated samples of SUMO1- and SUMO2-modified hT40 relative to the aggregated unmodified hT40 (Figure 4.7D, left panel; $t = 8.043$, $p < 0.05$ for S1 hT40; $t = 8.195$, $p < 0.05$ for S2 hT40).

The aggregated samples of unmodified and SUMO1-modified hT39, but not SUMO2-modified hT39, had higher Alz50 signal relative to their respective unaggregated samples (Figure 4.7D, right panel; $t = 10.52$, $p < 0.05$ for hT39; $t = 4.497$, $p < 0.05$ for S1 hT39; $t = 0.7464$, $p > 0.05$ for S2 hT39). Aggregated samples of SUMO2-modified hT39 showed lower Alz50 signal relative to the aggregated samples of unmodified ($t = 9.984$, $p < 0.05$) and SUMO1-modified hT39 ($t = 4.289$, $p < 0.05$) proteins (Figure 4.7D, right panel). Moreover, aggregated SUMO1-modified hT39 showed lower Alz50 signal relative

to the aggregated samples of unmodified hT39 (Figure 4.7D, right panel; $t = 5.969$, $p < 0.05$).

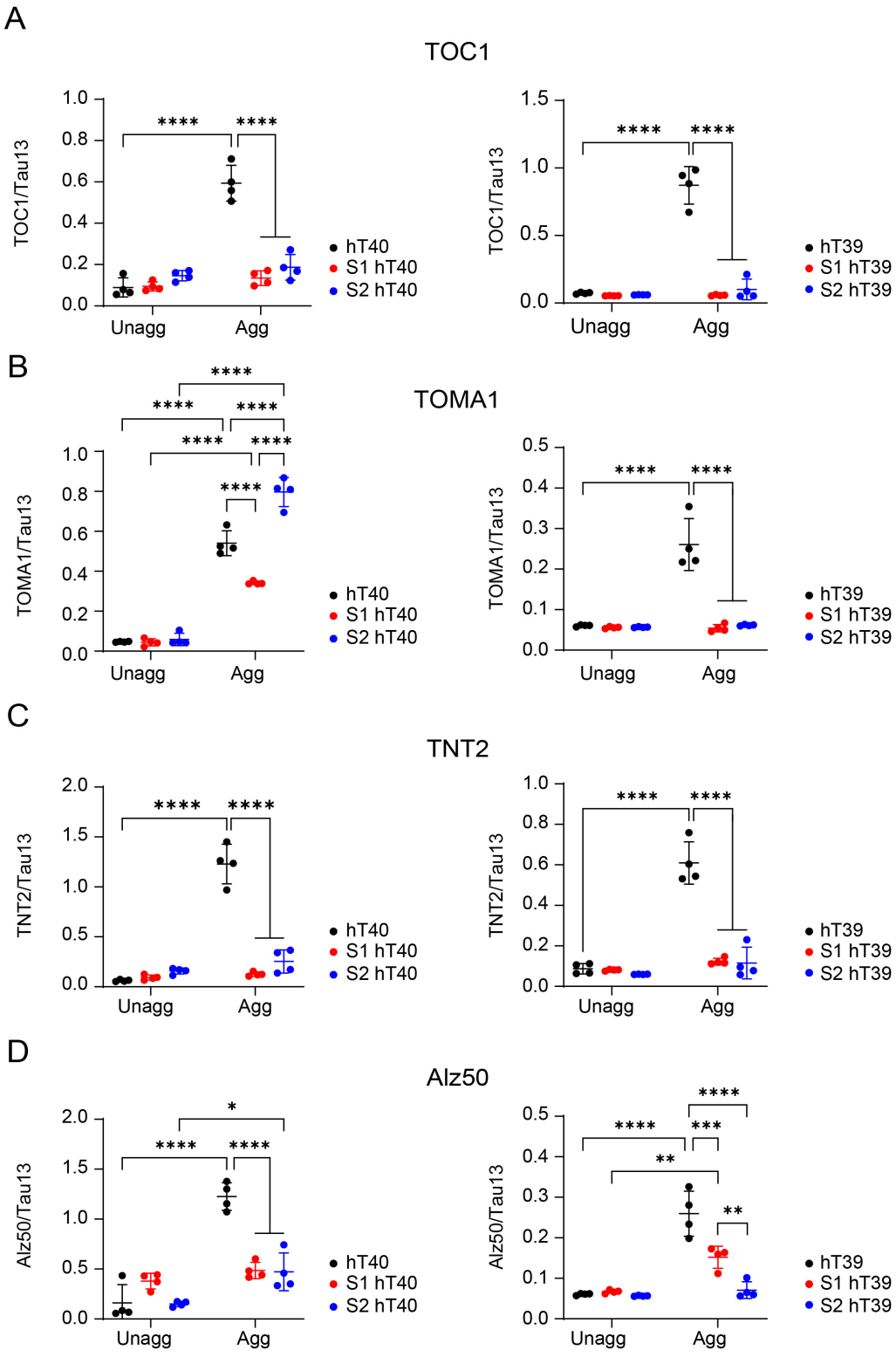

Figure 4.7. SUMOylation alters the formations of pathological tau conformations *in vitro*.

Figure 4.7 (cont'd)
A, sandwich ELISA assay measuring oligomeric tau in unaggregated and aggregated hT40 (left panel) and hT39 (right panel) proteins using TOC1 antibody for capture and R1 antibody for detection. B, sandwich ELISA assay measuring oligomeric tau in unaggregated and aggregated hT40 (left panel) and hT39 (right panel) proteins using TOMA1 antibody for capture and R1 antibody for detection. C, sandwich ELISA assay measuring PAD exposure in unaggregated and aggregated hT40 (left panel) and hT39 (right panel) proteins using TNT2 antibody for capture and R1 antibody for detection. D, sandwich ELISA assay measuring misfolded tau conformation in unaggregated and aggregated hT40 (left panel) and hT39 (right panel) proteins using Alz50 antibody for capture and R1 antibody for detection. Abbreviations: SUMOylation, modification with small-ubiquitin-like modifier protein; SUMO, small ubiquitin-like modifier; hT40, 2N4R tau isoform; hT39, 2N3R tau isoform; unagg, unaggregated; agg, aggregated; TOC1, tau oligomeric complex 1 antibody; TOMA1, oligomer-specific monoclonal antibody; TNT2, tau N-terminal 2 antibody to measure PAD exposure; Alz50, misfolded tau conformation antibody; R1, tau rabbit polyclonal antibody. Data represented as mean ± SD. * p≤0.05; ** p≤0.01; *** p≤0.001; **** p≤0.0001.

SUMOylation of tau reduces seeding in tau biosensor cells

Tau RD P301S biosensor cells were used to determine whether SUMO modification alters tau seeding competency. The seeding efficiencies of unaggregated and aggregated samples of unmodified, SUMO1-modified, and SUMO2-modified hT40 were tested (Figure 4.8A). We detected a significant interaction between PTM and aggregation status of hT40 proteins [$F_{(2, 18)} = 2147$, $p < 0.05$]. No seeding was observed with the unaggregated samples of unmodified, SUMO1-modified, and SUMO2-modified hT40 treated cells (Figure 4.8B). The aggregated samples of unmodified hT40 induced significantly more seeding in the cells relative to unaggregated hT40 ($t = 81.36$, $p < 0.05$). On the other hand, SUMO1- and SUMO2-modified hT40 aggregates failed to induce seeding in RD cells, showing seeding signal like their respective unaggregated hT40 samples (Figure 4.8B; $t = 0.22$, $p > 0.05$ for S1 hT40; $t = 2.023$, $p > 0.05$ for S2 hT40). Moreover, significantly less seeding was observed in the cells treated with SUMO1- and SUMO2-modified hT40 compared to the aggregates of unmodified hT40 (Figure 4.8B; t

= 81.69, p < 0.05 for S1 hT40; t = 77.89, p < 0.05 for S2 hT40). It is noteworthy that even though SUMO1- and SUMO2-modified hT40 aggregates show low levels of seeding, SUMO2-modified hT40 aggregates seeded significantly more (4-fold) when compared to SUMO1-modified hT40 aggregates (Figure 4.8B; t = 77.89, p < 0.05).

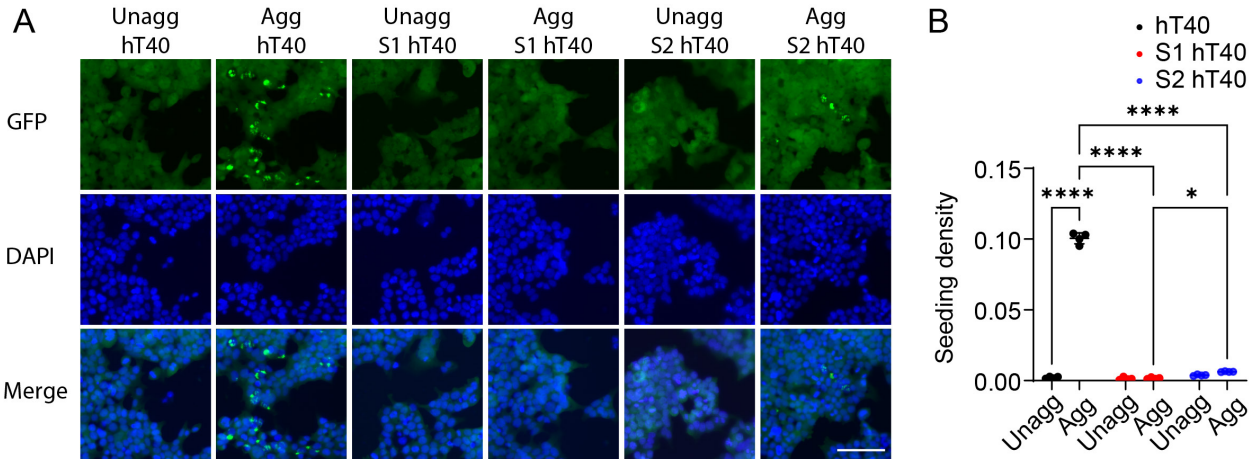

Figure 4.8. SUMOylation of tau reduces seeding in tau biosensor cells.
A, images of tau seeds in cells treated with unaggregated and aggregated hT40 proteins (green) along with DAPI staining (blue) as a surrogate for cell count. Scale bar: 200 µm. B, quantification of number of seeds per cell in cells treated with unaggregated and aggregated hT40 proteins. Abbreviations: SUMOylation, modification with small-ubiquitin-like modifier protein; SUMO, small ubiquitin-like modifier; hT40, 2N4R tau isoform; hT39, 2N3R tau isoform; Un, unaggregated; A, aggregated; GFP, green fluorescent protein channel (green); DAPI, 4',6-diamidino-2-phenylindole channel (blue). * p≤0.05; ** p≤0.01; *** p≤0.001; **** p≤0.0001.

Discussion

Several aspects of tau protein biology, including aggregation, conformational changes, microtubule binding, degradation, and clearance, are regulated by PTMs (Alhadidy & Kanaan, 2024; Alquezar et al., 2020). Tau is subject to SUMO modifications as reported in studies utilizing cell lines, animal models, and AD and PSP brains (Dorval & Fraser, 2006; Luo et al., 2014; Takahashi et al., 2008; Takamura et al., 2022). However, the impact of SUMOyation on tau pathobiology was not thoroughly investigated apart from

its relationship with other PTMs such as phosphorylation and ubiquitination (Dorval & Fraser, 2006; Luo et al., 2014).

In this work, we produced recombinant tau proteins modified with either SUMO1 or SUMO2 by co-transforming bacterial cells with tau and SUMOylation machinery. Our MS data shows that hT40 and hT39 isoforms are modified by SUMOylation on lysine residues located mainly (about 60% of residues) within the microtubule-binding repeats (MTBRs) region of tau (amino acids 244-368) (Alhadidy & Kanaan, 2024). SUMO1 and SUMO2 modification sites share the same lysine residues with a few exceptions. For example, K130 is a unique modification site by SUMO1 in both tau isoforms. On the other hand, K24, K280, and K340 are unique for SUMO2 modification.

A previously published report investigated two potential SUMO1 modification sites (based on the SUMO consensus motif ΨKXE) by site-directed mutagenesis: K340 and K385 (Dorval & Fraser, 2006). Mutating K340 to arginine significantly reduced modification of hT40 with SUMO1 but mutating K385 did not, suggesting that K340 is the main SUMO1 modification site (Dorval & Fraser, 2006; Luo et al., 2014). These findings seem at odds with our results using recombinant tau protein modified with SUMO1 (detected on K347 and K385). We detected no peptide special matches (PSMs) that spanned K340 in our SUMO1-modified hT40 and hT39 samples (K340 in hT40 corresponds to K309 in hT39). This may be driven by SUMO1 modification at K340 interfering with tau digestion using the Lys-C and Asp-N enzymes. It would be useful in future studies to try different combinations of enzymatic digestions to increase the number of PSMs spanning K340 of tau proteins.

Droval et al. ruled out K385 as a SUMOylation site of tau utilizing site-directed mutagenesis and enrichment of SUMO-modified proteins (His tag) followed by tau detection with western blot (Dorval & Fraser, 2006). Furthermore, they used the same approach to conclude that tau is not subject to modification with SUMO2/3 as much as SUMO1. On the other hand, MS (used in our study) is a highly sensitive technique whose lower limit of detection is at the femtomolar range (Ho et al., 2003). Therefore, it is not surprising that MS may detect SUMO1 modification at K385 or SUMO2 modification sites on tau. However, conducting absolute quantitative MS using isotope-labelled standards is critical to determine the relative level of tau modification with SUMO1 and SUMO2 at different sites (Kito & Ito, 2008). We also identified novel SUMO1 and SUMO2 modification sites in tau that do not match the SUMO consensus motif ΨKXE (i.e. sites other than K340 and K385) as reported in previous studies (Dorval & Fraser, 2006; Luo et al., 2014; Rodriguez et al., 2001; Sampson et al., 2001). In addition to the higher sensitivity of MS, recent studies consistently report that at least 40% of known SUMOylation sites do not conform to the ΨKXE motif (Chang et al., 2018; Zhao et al., 2014).

PTMs of tau are also known to impact tau's ability to modulate microtubule dynamics and binding (Alonso et al., 1994; Amniai et al., 2009; Black et al., 1996; Breuzard et al., 2013; Cleveland et al., 1977; Cohen et al., 2011; Haj-Yahya et al., 2020; Weingarten et al., 1975). Our results show that the binding of SUMOylated tau to polymerized microtubules was reduced with both SUMO modifications. Moreover, the extent of microtubule polymerization was significantly reduced by the introduction of SUMO1 or SUMO2 onto tau. One potential cause of impaired microtubule binding and

regulation may be the location of SUMO modification sites. According to the jaws model of tau-microtubule interaction, the microtubule-binding repeats of tau mediate the catalytic activity of tau as an inducer of microtubule polymerization (Mukrasch et al., 2007; Preuss et al., 1997). In addition, the jaws of tau flanking the microtubule-binding region [including the fifth microtubule binding repeat (R'; amino acids 369-399) along with amino acids 225-231 and 243-246 in the second PRD] are critical for tau to bind microtubules (El Mammeri et al., 2022; Mukrasch et al., 2007; Preuss et al., 1997). Given that the majority of SUMOylation sites are located within the microtubule-binding region of tau (60% of modification sites), it is possible that SUMOylation is sterically interfering with tau's ability to induce microtubule polymerization. Our MS data also show that SUMOylation of tau takes place within R' (e.g. K370, K375, and K395) along with the second PRD (e.g. K225, K234, and K240). Both regions are part of the tau jaws (Mukrasch et al., 2007; Preuss et al., 1997); thus, SUMOylation at these sites may explain the reduced ability of tau to bind microtubules.

The findings that SUMOylation inhibits tau's binding to microtubules is intriguing and raise questions that require further investigation. Phosphorylation of tau at certain sites (such as S262 and S214) is known to facilitate detachment of tau from microtubules (Man et al., 2023; Schneider et al., 1999). Furthermore, the group that first identified SUMOylation as a PTM of tau showed that detaching tau from microtubules (by depolymerizing microtubules with colchicine) increases the SUMOylation levels of tau (Dorval & Fraser, 2006). It is plausible that as tau phosphorylation increases and binding affinity for microtubules is reduced, SUMOylation of tau may occur and further reduce

microtubules binding. Thus, elucidating the role played by tau SUMOylation in regulating microtubules dynamics and cellular cytoskeleton warrants further investigation.

We found that hT40 aggregation is reduced upon SUMOylation (LLS, ThS, and TEM). Moreover, there is a shift in the aggregate morphology from filamentous into globular tau aggregates when tau is SUMOylated. In the case of hT39, the extent of aggregation is reduced upon SUMOylation (LLS) with no apparent change in the morphology of tau aggregates. These findings may seem contradictory to what one might expect based on the previous studies on tau SUMOylation (Luo et al., 2014; Takamura et al., 2022). In HEK293 cells, SUMOylation of tau was associated with reduced ubiquitination and increased accumulation of tau aggregates (Luo et al., 2014). It is possible that SUMOylation of tau is initiated early in disease and acts as a protective mechanism that is outcompeted by other pathophysiological processes (e.g. increased tau phosphorylation and inhibition of lysosomal and proteasomal degradation) culminating in tau aggregation. Future work should aim to test this hypothesis by studying the combinatorial effect of phosphorylation and SUMOylation on tau aggregation using recombinant tau proteins and *in vivo* models.

PTMs are intimately linked to the adoption of pathological tau conformations occurring in tauopathies, such as oligomerization (Alhadidy & Kanaan, 2024; Cox et al., 2016; Kanaan et al., 2016; Kanaan et al., 2020; Lasagna-Reeves et al., 2012; Patterson et al., 2011). Indeed, tau oligomers are linked to several disease mechanisms including mitochondrial and synaptic dysfunction (Lasagna-Reeves et al., 2011), reduced protein synthesis (Jiang et al., 2021), inhibited long-term potentiation (Hill et al., 2019), and memory impairment (Fa et al., 2016). In our experiments, we measured the abundance

of oligomeric tau species using TOC1 (Patterson et al., 2011; Ward et al., 2013) and TOMA1 antibodies (Castillo-Carranza, Gerson, et al., 2014; Montalbano et al., 2023).

Modifying hT39 with either SUMO1 or SUMO2 decreases the TOC1-positive and TOMA1-positive oligomeric tau species in aggregated samples. Similarly, modifying hT40 with either SUMO isoform decreases the TOC1-positive tau species upon aggregation. However, SUMOylation of hT40 decreased TOMA1-positive oligomers with SUMO1 and increased TOMA1-positive oligomers with SUMO2. This observation is of interest because it shows that SUMOylation can differentially modulate tau oligomers in a SUMO isoform-dependent fashion. Moreover, this finding is suggestive of a different conformation adopted by SUMO2-modified tau oligomers that is negative for TOC1 but positive for TOMA1. Characterization of unmodified, SUMO1-, and SUMO2-modified tau oligomers by methods such as atomic force microscopy will be necessary to further identify structural factors behind these differences.

PAD exposure is another pathological tau conformation that occurs early in AD and is linked to dysregulation of axonal transport (Kanaan et al., 2011). Ensuing hyperactivation of PP1-GSK3β pathway mediates the PAD exposure-induced dysregulation of axonal transport (Combs et al., 2021; LaPointe et al., 2009). In our experiments, we measured the extent of PAD exposure using the TNT2 antibody (Combs et al., 2016). We demonstrated that modifying hT40 and hT39 with either SUMO1 or SUMO2 decreases PAD exposure upon aggregating tau. These findings suggest SUMOylation of tau may be protective against this specific mechanism of PAD-induced transport impairment, but further studies are needed to confirm this potential effect.

The Diamond group and others demonstrated that tau seeding may play a role in propagating tau pathology between neurons in the brain and cell models (Holmes et al., 2014; Manca et al., 2023; Woerman et al., 2016). The seeding capability of tau is linked to conformational changes that either enhance or impede seeding (Dinkel et al., 2011; Falcon et al., 2015). In tau biosensor cells, we observed a reduced capability of both SUMO1- and SUMO2-modified hT40 aggregates to seed aggregation in cells. Nonetheless, SUMO2-modified hT40 showed slightly higher capability of seeding than SUMO1-modified hT40. This result suggests that the conformations of tau species formed by SUMOylation are not capable of robust tau seeding, which is consistent with reduced aggregation and reduced adoption of several pathogenic tau conformations. Unfortunately, a cell line that effectively assesses hT39 seeding was not available for testing, thus, the impacts of SUMOylation on 3R tau seeding remains unknown.

Tau assumes a misfolded conformation in disease conditions, which involves the N-terminus of tau folding over its microtubule-binding region (Jeganathan et al., 2008). This conformation precedes the formation of filamentous tau aggregates (Carmel et al., 1996) and is detected with the Alz50 and MC1 antibodies (Jicha et al., 1997; Wolozin et al., 1986). The Alz50 conformation is expected to increase in aggregated tau samples (Carmel et al., 1996); Indeed, this is what we observed for unmodified, SUMO2-modified hT40 and SUMO1-modified hT39. However, we found that SUMO1-modified hT40 and SUMO2-modified hT39 did not significantly differ from their respective unaggregated proteins. These data represent the third incidence where SUMO isoforms differentially affect the aggregation of hT40 and hT39. Taken together with the TOMA1 and seeding

results described above, these findings lend more support to the hypothesis that SUMO isoforms may differentially regulate the pathobiology of tau isoforms.

Collectively, it seems that SUMOylation decreases the formation of filamentous aggregates and pathological conformations of tau (with few exceptions). It is conceivable that the known pathological tau conformations of oligomerization, PAD exposure, misfolding, and seeding do not definitively represent all potential pathological conformations in tauopathies. For example, phosphorylation at sites within the AT8 epitope may inhibit axonal transport through a PAD-independent mechanism (Morris et al., 2020). In agreement, out results suggest that the know pathological conformations of tau are related yet show some degree of independence (e.g. SUMO2-hT40 aggregates are TOMA1-positive but TOC1-negative). It is possible that the globular aggregates formed by SUMOylated tau adopt a unique pathological conformation that has yet to be identified. Comparing the effects of the globular tau aggregates formed by the two SUMO isoforms on axonal transport may open a path to identify novel pathological tau conformation and/or signaling mechanism.

Tauopathies show that phosphorylated tau aggregates colocalize with SUMO1 but not SUMO2/3 staining in the brain (Luo et al., 2014; Takamura et al., 2022). Literature suggests two explanations for these phenomena: either global downregulation of protein modifications with SUMO2/3 in tauopathies and/or tau is inherently less susceptible to modification with SUMO2/3 (Dorval & Fraser, 2006; Lee et al., 2014). We detected SUMO2 modification on hT40 and hT39 mostly at the same sites as SUMO1 modification; therefore, it is unlikely that tau is inherently less susceptible to modification by SUMO2/3. In fact, *in vitro* and *in vivo* models of Aβ pathology show a downregulation of protein

modifications with SUMO2/3 but not consistently with SUMO1 (Lee et al., 2014; Soares et al., 2022). Given the differential regulation of pathological tau conformations by SUMO1 and SUMO2, it is plausible that the brain may induce a compensatory mechanism that differentially regulate protein modifications with SUMO1 and SUMO2/3. Further investigation of dysregulated SUMOylation in tauopathies and mouse models may provide valuable insights on the pathobiology of tau.

In summary, we report novel SUMOylation sites on the hT40 and hT39 isoforms of tau. SUMOylation of tau interferes with its ability to bind microtubules and induce their polymerization, potentially disrupting normal tau functioning. In addition, SUMOylation inhibits the tau aggregation, tau seeding, and reduces the pathological conformations of tau (except for TOMA1-positive oligomers with SUMO2-modified hT40). Notably, SUMO isoforms affect the pathobiology of tau in an isoform-dependent manner (e.g. TOMA1, Alz50, and seeding in hT40; Alz50 in hT39). Studying SUMOylation in animal models of tauopathies and human patients will continue to shed light on our understanding of the roles SUMOylation plays in tau biology and pathobiology.

CHAPTER 5: DISSERTATION DISCUSSION

Abstract

The goal of this dissertation was to identify the contribution of three understudied post-translational modification (PTMs), polyamination, O-linked-N-acetyl β-d-N-glucosaminylation (O-GlcNAcylation), and SUMOylation, to the pathobiology of tau protein. To answer this question, our approach included using recombinant tau proteins modified with each PTM (spermidine for polyamination; O-GlcNAc for O-GlcNAcylation; small ubiquitin-like modifier-1 (SUMO1) or SUMO2 proteins for SUMOylation) using either *in vitro* enzymatic reactions or bacterial co-transformation. Then, we determined the impact of each PTM on the ability of tau to bind and polymerize microtubules. The recombinant tau proteins also were utilized in a series of biochemical and biophysical assays to determine the impact of the three PTMs on pathological tau conformations, including tau aggregation, oligomerization, exposure of the phosphatase-activating domain, misfolding, and seeding. Our findings provide important insights by expanding the current knowledge of tau protein biology and pathobiology and opening avenues for further investigation.

Microtubule Binding and Polymerization

Microtubule binding and polymerization is dependent on two regions of tau: the microtubule-binding repeats (MTBRs) and the flanking jaws (collectively referred to as the microtubule binding core) (Butner & Kirschner, 1991; Devred et al., 2004; Gustke et al., 1994; Kadavath et al., 2018; Kadavath et al., 2015; Mukrasch et al., 2007; Preuss et al., 1997). MTBRs are linked to the catalytic capability of tau induce microtubule polymerization, while the tau jaws are crucial for targeting tau to microtubules (Mukrasch et al., 2007; Preuss et al., 1997). Furthermore, specific lysine (K) residues within or flanking the MTBR region of tau are linked to its ability to interfere with a hydrophobic pocket in between tubulin heterodimers (Barbier et al., 2019; Kadavath et al., 2015). Previous work clearly demonstrated the regulation of tau-induced microtubule polymerization and binding mediated by post-translational modifications (PTMs). Most PTMs taking place within the MTBR region or jaws of tau interfere with tau's ability to bind to or induce the assembly of microtubules (Ait-Bouziad et al., 2020; Biernat et al., 1993; Carlomagno et al., 2017; Cohen et al., 2011; Drewes et al., 1995; Flach et al., 2014; Funk et al., 2014; Xia et al., 2023; Yang et al., 2023).

In this work, SUMOylation sites detected on recombinant tau proteins are located mainly within the MTBR region and jaws of tau. Furthermore, SUMOylation of tau happens at or nearby K residues critical for tau's ability to interact with the tubulin heterodimer. It is no surprise that SUMOylation of tau by either small ubiquitin-like modifider-1 (SUMO1) or SUMO2 isoforms interferes with both the binding of tau to and polymerization of microtubules. It is also possible that SUMOylation within those two regions causes steric hinderance and/or decreases their positive charge considering that

SUMO1 and SUMO2 proteins are negatively charged at physiological pH (Melchior & Pichler, 2004). One way to test this hypothesis is to run SUMO-modified tau proteins on isoelectric focusing gels that separate proteins based on their isoelectric points in pH gradients (Pergande & Cologna, 2017).

Unlike SUMOylation, most O-linked-N-acetyl β-d-N-glucosaminylation (O-GlcNAcylation) serine/threonine (S/T) residues are located within the proline-rich domain (PRD) and C-terminus of tau with the MTBR region spared. Tubulin polymerization assays do not reveal an impact of O-GlcNAcylation on tau-induced microtubule polymerization. This observation agrees with sparing S/T residues within the MTBRs from modification by O-GlcNAc. Further investigation showed that O-GlcNAcylation of hT40 increases its binding to microtubules, while O-GlcNAcylation of hT39 decreases its binding. O-GlcNAcylation take place on the tau microtubule-binding “jaws” located within the second PRD (amino acids 199-243) and the fifth MTBR of tau (R’, amino acids 370-400), and this explains why binding to microtubules is altered. However, the direction of change in microtubule binding by the different isoforms of tau is intriguing and highlights another aspect of PTMs regulating the tau-microtubule interactions in an isoform-dependent fashion.

As explained in Chapter 3, sequestration of the R’ from water by dynamicity of the second PRD along with the first MTBR (R1, amino acids 244-274) is crucial for tau-microtubule interactions (El Mammeri et al., 2022). By comparing O-GlcNAcylation sites, hT39 is more modified by O-GlcNAc on R’ than hT40 while hT40 is more modified by O-GlcNAc on the second PRD than hT39. Differences in distribution of O-GlcNAc sites on the different tau isoforms may give O-GlcNAcylated hT40 higher ability to bind

microtubules. This effect is likely mediated by enhanced sequestration of the R' domain through limiting water access to the R' and increasing water access to the dynamic second PRD. Testing this hypothesis directly with O-GlcNAcylated hT40 and hT39 protein using nuclear magnetic resonance (NMR) may help to confirm the mechanism by which O-GlcNAcylation regulates tau's binding to microtubules (El Mammeri et al., 2022).

Polyamination showed a different profile of regulating the tau-microtubule interactions. Little to no difference in tau binding to microtubules was detected upon polyaminating tau with spermidine (SPD). Considering that no glutamine (Q) residues were modified by SPD polyamination within the tau jaws, the results of microtubule-binding assays appear consistent with this finding. On the other hand, microtubule polymerization was enhanced by SPD polyamination of the hT40 and hT39 isoforms. This finding is intriguing because MTBRs of tau are almost completely spared from SPD polyamination (except for Q307 in hT40). Polyamination of tau occurs predominantly within the N-terminus of tau, and only one site was detected at the C-terminus (Q424). It is well-known that the PRD and microtubule-binding core of tau carry a net positive charge, while the N-terminus carries a net negative charge (Brandt et al., 2020; Castro et al., 2019). Furthermore, the N-terminus of tau (amino acids 1-150) interacts with the PRD and MTBR regions regulating their binding to tubulin/microtubules (Gustke et al., 1994; McKibben & Rhoades, 2019). Given the highly positively charged nature of SPD, it is possible that a lower negative charge on the N-terminus of polyaminated tau increases accessibility for tubulin/microtubules to the PRD and MTBR regions (Bae et al., 2018).

Proposed Refinement of Jaws Model of Tau-Microtubule Interactions

The traditional jaws model of tau-microtubule interactions emphasizes the importance of two regions upstream and downstream of the MTBR region for targeting tau to microtubules: the second PRD and R' (Mukrasch et al., 2007). Deleting either of the two domains or reducing their positive charge (e.g. by phosphorylation at T231, S235, and S396) markedly reduces the binding of tau to microtubules (Gustke et al., 1994; Sengupta et al., 1998). Recent findings along with our studies on tau O-GlcNAcylation suggest a refined jaws model, where sequestration of the R' and dynamicity of the second PRD are potent modulators of tau binding to microtubules (El Mammeri et al., 2022; Kadavath et al., 2018; Kadavath et al., 2015). Even though some PTMs of tau at the second PRD (e.g. phosphorylation) can potentially increase its dynamicity by increasing polarity/hydrophilicity, they may also come with the expense of decreasing the positive charge on the PRD (Alquezar et al., 2020; Di Primio et al., 2017; Rani et al., 2020). On the other hand, modifications that increase polarity/hydrophilicity without reducing the positive charge of PRD (e.g. O-GlcNAcylation) can potentially increase binding of tau to microtubules (Ma & Hart, 2014; Vaidyanathan et al., 2014).

Proposed Two-Step Gating and Assembly Model of Tau-induced Microtubule Polymerization

It is conceivable that the interaction of tau with soluble tubulin and polymerized microtubules is similarly regulated (Amniai et al., 2009; Fung et al., 2020). In agreement, the MTBR and jaws of tau are potent regulators of the tau-induced microtubule polymerization (Fauquant et al., 2011; Goode et al., 1997; Savastano et al., 2021). As early as the 1990s, it was appreciated that the N-terminus of tau interferes with its ability

to induce polymerization of microtubules and this was later confirmed by other groups (Derisbourg et al., 2015; McKibben & Rhoades, 2019; Scott et al., 1992). Our findings show that accumulation of the positively charged SPD on the N-terminus of tau enhances the rate of microtubule assembly. Conversely, modifications of tau that increase the net negative charge on its N-terminus (e.g. the R5L mutation) interfere with its ability to polymerize and stabilize microtubules (Cario, Savastano, et al., 2022; Cario, Wickramasinghe, et al., 2022; Mutreja et al., 2019). The model proposed by the Rhoades group is compelling where the N-terminus of tau acts as a gating mechanism that controls the interaction of tubulin/microtubules with the microtubule-binding core of tau (Kadavath et al., 2015; McKibben & Rhoades, 2019). This places the N-terminal PTMs in a potentially crucial region of tau that impacts its microtubule-related biology and pathobiology.

Tau Polymerization into Filamentous Aggregates

Paired helical filaments (PHFs) and straight filaments (SFs) represent the building blocks of neurofibrillary tau tangles (NFTs); therefore, the formation of filamentous tau aggregates is a crucial event in the development of NFTs (Crowther & Wischik, 1985; Kidd, 1963; Wischik et al., 1985; Yagishita et al., 1981). The building blocks of filaments feature the same core of two tau protofilaments comprising amino acids 306-378 packed differently in PHFs and SFs (Fitzpatrick et al., 2017). A common pathway through which tau transforms into filamentous structures involves conformational transition from random coil or globally folded soluble monomer to insoluble β-sheet structure containing conformations (von Bergen et al., 2005). Two hexapeptide motifs (PHF* and PHF) are particularly important for this transition: 275-VQIINK-280 and 306-VQIVYK-311 located in

R2 (amino acids 275-305) and R3 (amino acids 306-336) of the MTBR region, respectively (von Bergen et al., 2001; von Bergen et al., 2000). Furthermore, *in vitro* studies provided evidence that 306-VQIVYK-311 is necessary for the aggregation of both 4R and 3R tau isoforms (Chen et al., 2019; Ganguly et al., 2015; Li & Lee, 2006).

In our studies (Chapter 4), SUMOylation of tau converges on the MTBR region of tau with both SUMO1 and SUMO2 isoforms. SUMO1 and SUMO2 modify K311 within 306-VQIVYK-311 motif of R3; SUMO2 modifies K280 within 275-VQIINK-280 motif of R2. Therefore, it is likely that SUMOylation inhibits the formation of filamentous tau aggregates by directly interfering with the two hexapeptide motifs necessary for β-sheet structures.

In addition to the MTBR region, the N-terminus of tau intramolecularly regulates its polymerization into filamentous structures (King et al., 2000). In fact, removal of the N-terminal domain from full-length tau protein inhibits tau polymerization into filamentous structures (Gamblin et al., 2003). On the other hand, some PTMs (e.g. the R5L mutation) located in the N-terminal region enhance tau polymerization (Gamblin et al., 2003). Furthermore, N-terminal fragments of tau inhibit its polymerization likely by intermolecularly stabilizing an interaction between the MTBRs and C-terminal domains of tau (Horowitz et al., 2006). Taken together, evidence points to a complex mechanism through which N-terminus regulate tau polymerization by intramolecular and intermolecular interactions.

As demonstrated in Chapter 2, SPD polyamination of tau inhibits its polymerization into filamentous aggregates. Given that SPD modifications have low/no abundance in the MTBR region, it is unlikely that alterations in the MTBRs mediate this inhibition. Instead,

at least 70% of the identified SPD-modified Q residues are located on the N-terminus of tau between residues Q6-Q124. It seems that decreasing (via removal of N-terminus or SPD polyamination) or increasing (via the R5L mutation) negative charge on the N-terminus inhibits or stimulates tau polymerization, respectively. Thus, it is plausible that SPD polyamination induces a conformational change that reduces the N-terminal domain enhancement of tau polymerization. In fact, we have evidence (i.e. sandwich ELISA assays in Chapter 2) that the N-terminus of polyaminated tau undergoes a conformational change that increases exposure of the phosphatase-activating domain (PAD) and the Alz50 misfolded conformation (Carmel et al., 1996; Combs et al., 2016).

A third regulatory mechanism of tau polymerization involves the C-terminus of tau (Abraha et al., 2000). Biophysical investigation of full-length tau using fluorescence resonance energy transfer (FRET) and deletion mutants indicated that the C-terminus of tau folds over the MTBR region near 314-DLSKVTS-320 motif in R3 (Abraha et al., 2000; Jeganathan et al., 2008). Unlike the N-terminus of tau, the C-terminus of tau intramolecularly inhibits its polymerization into filamentous aggregates (Abraha et al., 2000; Hornakova et al., 2022). Truncation (e.g. Δ392-441 linked to the MN423 epitope of tangle evolution) and phosphorylation (e.g. S396 and S404) of the C-terminus partially reverse this inhibition, promoting tau polymerization (Abraha et al., 2000; Cantrelle et al., 2021; Rankin et al., 2007). Furthermore, the C-terminal fragment spanning amino acids 422-441 (produced by caspase 3 cleavage in disease) intermolecularly inhibits the polymerization of tau into filaments aggregates (Berry et al., 2003).

In this work (Chapter 3), we demonstrated that O-GlcNAcylation inhibits the extent and/or rate of tau polymerization; these findings agree with previously published reports

by other groups (Cantrelle et al., 2021; Yuzwa et al., 2014). Of note, O-GlcNAcylation of tau induces a mild reduction in the number of filamentous tau aggregates. Previous work suggested that O-GlcNAcylation alters local conformations in the C-terminus of tau that decrease its polymerization and slightly interfere with filament assembly (Cantrelle et al., 2021). Given that O-GlcNAcylation occurs mainly in the C-terminus of tau, it is plausible that O-GlcNAc further stabilizes the polymerization inhibitory brakes exerted by the C-terminus of tau.

Propensity to Seed Tau Aggregation

Spreading of tau pathology from one brain region to another is a leading hypothesis in the field, and spreading is believed to follow a characteristic pattern that depends on the functional connectivity of neurons rather than their proximity (Ahmed et al., 2014; Braak & Braak, 1991; Franzmeier et al., 2020; Mezias et al., 2017; Schoonhoven et al., 2023). Neuronal activity induces release of tau into the extracellular space through synaptic and nonsynaptic mechanisms (Calafate et al., 2015; Fontaine et al., 2016; Pooler et al., 2013; Takeda et al., 2015; Yamada et al., 2014). Then, neighboring cells internalize the released tau through either fluid-phase endocytosis or receptor-mediated endocytosis (e.g. heparan sulfate proteoglycans and low-density lipoprotein receptor-related protein 1) (Clavaguera et al., 2009; Frost et al., 2009; Guo & Lee, 2011, 2013; Holmes et al., 2013; Rauch et al., 2020). The tau species that propagate from one cell to another remain elusive, but evidence supports the involvement of nearly all tau species ranging from monomeric to fibrillar forms (Takeda, 2019).

After entering neighboring cells, the transmitted tau acts as a template to seed tau aggregate formation (Clavaguera et al., 2009; de Calignon et al., 2012; Fu et al., 2016;

Liu et al., 2012). Studies in Alzheimer's disease (AD) and animal models of tauopathy suggest that seeding activity precedes and correlates with the development and progression of tau pathology (Frey et al., 2023; Holmes et al., 2014). Like the case with propagation, the tau species that seeds aggregation of endogenous tau in the recipient cell is still poorly defined; evidence suggests that fibrils, soluble oligomers, and even monomers seed aggregation under certain conditions (Jackson et al., 2016; Jiang et al., 2020; Mirbaha et al., 2018; Takeda et al., 2015; Wesseling et al., 2020). Of note, synthetic tau fibrils made from recombinant human tau are also seeding competent (Falcon et al., 2015; Iba et al., 2013; Wu et al., 2013). Further characterization indicated that the two hexapeptide motifs in R2 and R3 that regulate the transition of tau into β-sheet structures are also critical for its seeding capability (Annadurai et al., 2022; Falcon et al., 2015; Mirbaha et al., 2018). The two hexapeptides motifs alter the conformation adopted by tau aggregates, regulating its propensity to seed aggregation (Despres et al., 2019; Falcon et al., 2015; Sanders et al., 2014).

In this dissertation, we showed that all three PTMs (polyamination, O-GlcNAcylation, and SUMOylation) decrease the seeding capability of 4R tau aggregates. That was also accompanied by a reduction in the level of β-sheet content and filamentous structures in tau aggregates. The contribution of tau PTMs to the regulation of seeding activity is a growing area of investigation. Taken together, our results are strongly suggestive of a critical role played by PTMs in regulation tau conformations responsible for seeding activity.

Pathological Tau Conformations

Given that NFTs are not as toxic as once thought, earlier conformations and multimeric species of tau that are antecedent to fibrillar aggregation have drawn increasing attention (Cowan & Mudher, 2013). The formation of tau oligomers is considered an early event in the progressive accumulation of pathological tau in tauopathies (Lasagna-Reeves et al., 2012; Maeda et al., 2007; Maeda et al., 2006; Patterson et al., 2011). Oligomers are sufficient to cause synaptic, mitochondrial, and electrophysiological dysfunction as well as dysregulated axonal transport and bioenergetics (Cox et al., 2016; Kanaan et al., 2016; Lasagna-Reeves et al., 2012; Maeda et al., 2007; Maeda et al., 2006; Niewiadomska et al., 2021; Patterson et al., 2011). Furthermore, tau undergoes an additional change early in human disease that exerts pathogenicity through conformational exposure of the PAD (Combs et al., 2016; Combs & Kanaan, 2017; Kanaan et al., 2011). Excessive exposure of PAD in the extreme N-terminus of tau activates a signaling pathway that disrupts axonal transport (Kanaan et al., 2011; Morris & Brady, 2022; Mueller et al., 2021). A third early conformational change that is believed to set the stage for tau to aggregate is the misfolded tau conformation, where the N-terminus abnormally folds over the MTBR (Carmel et al., 1996; Jicha et al., 1997; Ksiezak-Reding et al., 1988). In human disease, these conformations are universal in different tauopathies such as AD, corticobasal degeneration (CBD), and Pick's disease (PiD) (Castillo-Carranza, Gerson, et al., 2014; Combs et al., 2016; Cox et al., 2016; Ferrer et al., 2014; Montalbano et al., 2023). Taken together, a picture emerges that the pathophysiology of tauopathies share common mechanisms of conformational changes

and toxicity that involve oligomerization, PAD exposure, and misfolding of tau early in disease (Alhadidy & Kanaan, 2024).

Our work lends further support to the hypothesis that common mechanisms of conformational tau changes take place in disease. For the most part, we found the direction of change (i.e. increase or decrease) in one pathological tau conformation generally parallels that of other conformations. For example, an increase in all pathological tau conformations was observed with SPD polyamination before and after aggregation. On the other hand, we noticed a reduction in most pathological tau conformations with SUMOylation upon aggregation. Even though the effects of O-GlcNAcylation are isoform-dependent, the direction of change in pathological tau conformations is similar for each isoform upon aggregation (i.e. all pathological tau conformations increase with O-GlcNAcylated hT39 and remain unaltered with O-GlcNAcylated hT40).

However, we encountered one prominent deviation upon SUMOylating hT40 proteins. A subgroup of tau oligomers (TOMA1-positive oligomers) is increased with SUMO2 modification, while another oligomeric tau subgroup (TOC1-positive oligomers) is decreased. Given that SUMO2 protein is relatively larger in size (11 kDa) when compared to chemical PTMs (e.g. phosphorylation), it is possible that the SUMO2 modification is interfering with the TOC1 epitope (amino acids 290-224) but not the TOMA1 epitope (15917643; 23979027). In fact, two SUMO2 modification sites are located on or close to the TOC1 epitope: K224 and K225. No information is currently available on TOMA1 epitope. However, it is critical to address this concern by denaturing SUMO1- and SUMO2-modified hT40 proteins to expose the continuous TOC1 epitope

(e.g. western blot or dot blot) (Cox et al., 2016). Assuming that no interference is observed with the TOC1 epitope, then our results would confirm the idea that multiple species of tau oligomers exist and show positive reactivity with different tau oligomer-specific antibodies. This finding would agree with a report by the Binder group that TOC1 antibody labels a subpopulation of tau oligomers (Patterson et al., 2011). Furthermore, such a finding is significant because it suggests that PTMs may provide a subtle degree of regulation at the levels of oligomer ensembles not well-appreciated previously (Lo et al., 2019).

On- and Off-Filament Pathways of Tau Polymerization

Under physiological conditions, tau lacks a stable three-dimensional structure and assumes an ensemble of conformations *in vitro,* such as the paperclip conformation (Abraha et al., 2000; Jeganathan et al., 2006). In disease conditions, tau undergoes conformational changes that instigate a cascade of self-assembly that may (on-pathway) or may not (off-pathway) lead to the eventual formation of filamentous aggregates (Dear et al., 2020; Gerson et al., 2016; Kjaergaard et al., 2018; Muschol & Hoyer, 2023).

The three PTMs examined in this dissertation show distinct profiles on the relationship between filamentous aggregates and pathological conformations of tau: reduction in filamentous aggregates along with an increase in pathological conformations and oligomers with polyamination, mild reduction in filamentous aggregates along with no change or an increase in pathological tau conformations and oligomers with O-GlcNAcylation, and reduction in filamentous aggregates, pathological conformations (mostly) and oligomers with SUMOylation.

Polyamination

As shown in Chapter 2, SPD polyaminated tau preparations have higher levels of pathological conformations in the unaggregated and aggregated states relative to unmodified tau preparations. The higher levels of pathological conformations in SPD polyaminated tau are hard to reconcile with the accompanying reduction (hT40) or no change (hT39) in aggregated mass compared to unmodified tau. One potential explanation is that SPD polyamination alters conformation of tau at the monomeric and/or low order multimer levels that are not big enough to capture by transmission electron microscopy (TEM) but can still be captured with sandwich ELISAs. Another explanation is the observation that the final SPD polyaminated tau preparations had residual multimers from the polyamination reaction proven hard to remove during purification (observed as stable multimers by western blots). Therefore, it is plausible that the residual multimers from the polyamination reaction are contributors to the higher levels of pathological tau conformations. It seems that the residual multimers do not favor elongation upon aggregation, and this explains the reduction in filamentous/β-sheet structures. In fact, the residual multimers in the SPD polyaminated tau preparations are reminiscent of the recombinant tau dimers used to develop the TOC1 antibody as they also did not favor elongation upon inducing aggregation (Patterson et al., 2011). Instead, the tau dimers used to develop the TOC1 antibody favored off-pathway oligomerization. Taken together, our findings with polyaminated tau are strongly suggestive of the emergence of off-pathway multimers positive for the measured pathological conformations and do not favor the formation of filamentous aggregates.

O-GlcNAcylation

O-GlcNAcylation was examined in Chapter 3, where O-GlcNAcylation demonstrates either no change (hT40) or an increase (hT39) in pathological tau conformations. Upon O-GlcNAcylating hT40, there is a mild reduction in filamentous aggregates relative to unmodified tau. This mild shift may not contribute significantly to a change in the formation of pathological tau conformations (except for a mild decrease in TOC1-positive oligomers). It remains unknown whether a higher level of O-GlcNAcylation would further decrease the levels of known pathological tau conformations. Furthermore, we did not observe a change in pathological tau conformations in the unaggregated samples of O-GlcNAcylated hT40. In agreement, Yuzwa et al. reported that O-GlcNAcylation of hT40 does not affect the global tau fold in monomeric state (paperclip structure) (Yuzwa et al., 2014).

On the other hand, O-GlcNAcylating hT39 induces a mild increase in the size of globular aggregates accompanied by elevated levels of the examined pathological tau conformations. An increase in size may reflect further addition of monomeric tau to the growing globular aggregates, which may entail a change in the conformation of tau monomers. Therefore, O-GlcNAcylation of hT39 may favor a conformational change at the monomeric or low order multimeric levels that can still be captured with sandwich ELISAs. Taken together, it seems likely that O-GlcNAcylation favors the formation of globular structures positive for the four pathological conformations examined here.

SUMOylation

In Chapter 4, we demonstrated that SUMOylation reduces the formation of pathological tau conformations in both hT40 (except TOMA1-positive oligomers with SUMO2) and hT39 upon aggregation relative to unmodified tau. In the case of hT40, reduction in pathological conformations is co-incident with reduced aggregated mass compared to unmodified tau. Furthermore, SUMOylation significantly reduces filamentous tau aggregates and markedly increases globular structures that do not appear to show reactivity for the four pathological tau conformation antibodies tested here (except for TOMA1-positive oligomers with SUMO2-modified hT40). In the case of hT39, there are no changes in the aggregated mass upon aggregation even though all pathological tau conformations appear to exist at lower levels compared to unmodified hT39. Therefore, SUMOylation does not necessarily decrease tau polymerization by locking it into monomeric unaggregated state, but instead shifts monomeric tau into globular aggregates that are not readily detected by the four pathological conformations investigated here.

Future Directions

Polyamination

Cellular polyamines represent a group of nonacetylated (putrescine, spermine, and SPD) and acetylated metabolites (acetylated putrescine, acetylated spermine, and acetylated SPD) (Bae et al., 2018). In this dissertation, we investigated the impact of SPD polyamination on the pathobiology of tau protein (Chapter 2). We chose SPD because it is the most elevated polyamine in AD serum and brain (Inoue et al., 2013; Morrison & Kish, 1995; Sternberg et al., 2022). Nonetheless, the other nonacetylated and acetylated

polyamines may display a distinct profile in terms of regulating the biology and pathobiology of tau (Sandusky-Beltran et al., 2019; Sato et al., 2003). It is worthwhile to investigate the impact of polyamines other than SPD on tau pathobiology and its functional consequences.

One interesting observation for SPD polyamination is the increase in pathological tau conformations even without inducing aggregation. As described earlier, the residual multimers in SPD polyaminated tau preparations may explain this finding. Nonetheless, it is also possible that the increase in pathological tau conformations is also a manifestation of SPD-modified tau monomers displaying altered conformations and/or small order multimers (not visible on TEM). In the literature, there are examples of other PTMs alter tau conformations in unaggregated state (e.g. phosphomimic at S199/S202/T205 increases PAD exposure) (Christensen et al., 2023; Jeganathan et al., 2008). In future experiments, we may try additional purification methods to remove residual multimers from the tau preparation, while also obtaining high protein yields (e.g. size exclusion or anion/cation exchange chromatography) (Takeda et al., 2015).

As tau tangle pathology progresses in disease, it may undergo enzymatic cleavage by caspases (e.g. caspase 3 and caspase 6). Caspase 6 cleaves tau at D13, whereas caspase 3 cleaves tau at D421 (Horowitz et al., 2004; Rissman et al., 2004). PTMs may regulate the ability of caspases to cleave tau (e.g. pseudophosphorylation at S422 inhibits cleavage by caspase 3) (Guillozet-Bongaarts et al., 2006). We detected SPD polyamination sites that are relatively close to both truncation sites: Q6 and Q24 (surrounding D13) and Q424 (near D421). It would be interesting to determine whether SPD modification sites of tau affect the cleaving activity of caspases.

Most evidence on the role that the transglutaminase (TG) enzyme plays in regulating tau pathology through polyamination is correlative. For example, the activity of TG increases in AD and progressive supranuclear palsy (PSP) cases (G. V. Johnson et al., 1997; Zemaitaitis et al., 2003). Furthermore, TG colocalizes with tau pathology in AD, and the cross-linking bonds formed by TG are detectable in tau pathology in AD, PSP, and mouse models (Halverson et al., 2005; Singer et al., 2002; Wilhelmus et al., 2009; Zemaitaitis et al., 2000). *In vitro* studies determined the tau residues involved in its cross-linking by TG and showed that tau is also directly modifiable by polyamines in the presence of TG (Miller & Johnson, 1995; Murthy et al., 1998). Nonetheless, the extent of direct tau modifications by polyamines (e.g. SPD) in tauopathies and when these events take place during the development and progression of tangle pathology is still unclear. Possibly, the limited biochemical and mass spectrometry (MS) methods to detect polyaminated proteins is one reason for the lack of further information (Yu et al., 2015). It is also critical to determine whether the detected SPD polyamination sites in our study match the sites polyaminated on pathological tau in tauopathies.

The role played by polyamines in regulating tau pathology is a growing area of interest. Several reports investigated the dysregulation of polyamine pathways in human brain and mouse models of tauopathy, suggesting a polyamine stress response (Mein et al., 2022; Sandusky-Beltran et al., 2019; Sandusky-Beltran et al., 2021). Most of these reports assessed the mutual regulation exerted by polyamine metabolism and tau pathology (aggregates) in mouse models of tauopathy, but did not study the effects of polyamination modifications to the tau protein (Alhadidy & Kanaan, 2024; Ivanov et al., 2020). In future studies, it would be helpful to determine the impact that polyamine

metabolism has on tau aggregation as well as the other pathological tau conformations (i.e. oligomerization, PAD exposure, misfolding, and seeding). Furthermore, testing the effects of polyaminated tau in functional assays linked to oligomeric and PAD-exposed tau such as axonal transport is a critical next step in understanding the consequences of polyamination on tau (Brady et al., 1982; Mueller et al., 2023).

Finally, polyamines may alter the cellular biology in ways other than directly modifying tau protein. For example, polyamines regulate mitophagy and bioenergetics, receptor biology (e.g. glutamate and nicotinic receptors), ion channel activity, and inflammation (Guerra et al., 2016). Therefore, it is crucial to investigate the biology of polyamines in mouse models with a comprehensive approach that considers other biological processes along with the pathobiology of tau.

O-GlcNAcylation

The evidence relating O-GlcNAcylation to tau pathology comes from AD and animal models of tauopathy (Gatta et al., 2016; Graham et al., 2014; Hastings et al., 2017; Liu et al., 2004; Liu et al., 2009; Wang et al., 2020; Yuzwa et al., 2008). In AD brains, levels of O-GlcNAc-modified proteins including the modified soluble tau are reduced where O-GlcNAcylation and phosphorylation of tau are inversely proportional to each other (Gatta et al., 2016; Graham et al., 2014; Hastings et al., 2017; Liu et al., 2004; Liu et al., 2009; Wang et al., 2020; Yuzwa et al., 2008). The role played by O-GlcNAcylation in regulating tau pathology in tauopathies other than AD is less clear. Part of this limitation comes from the challenge to detect O-GlcNAcylation with biochemical and MS methods (Ma & Hart, 2017). Advances in methods of detecting O-GlcNAcylation will provide insights on the contribution of O-GlcNAcylation to the pathophysiology of tauopathies.

Furthermore, it will help to determine whether the O-GlcNAc-modified sites on the recombinant tau protein (e.g. S400) reflect the sites modified *in situ* (Morris et al., 2015).

Cleavage of tau by the action of caspases plays a role in the development and progression of tangle pathology (Horowitz et al., 2004; Rissman et al., 2004). In the case of O-GlcNAcylation, one modification site is particularly relevant for cleavage by caspases: S422. Assessing the impact of O-GlcNAcylation at this site on cleavage by caspases will provide insights on the interplay between PTMs and tangle evolution. Phosphorylation and O-GlcNAcylation of tau are mutually exclusive on S422; thus, it is useful to assess the differential regulation of caspase cleavage and other aspects of tau pathobiology by comparing O-GlcNAcylated tau to phosphorylated tau.

Accumulating evidence suggests differential regulation of tau isoforms (4R vs 3R) by PTMs (Chakraborty et al., 2023; Combs et al., 2011; Liu et al., 2016; Voss & Gamblin, 2009). Our results show that O-GlcNAcylation of tau may increase or not affect the pathological conformations in 3R and 4R isoforms, respectively. Validation of this differential regulation in functional assays linked to oligomeric and PAD-exposed tau such as axonal transport is a critical next step (Brady et al., 1982; Mueller et al., 2023). In addition, testing therapeutic approaches targeting O-GlcNAcylation [e.g. O-GlcNAcase (OGA) inhibitors] in mouse models expressing 4R and 3R tau transgenes will provide further insights on the therapeutic potential of O-GlcNAcylation (Rockenstein et al., 2015). It is possible that enhancing O-GlcNAcylation of tau by OGA inhibitors is a useful therapeutic target for 4R (e.g. CBD) but neither for 3R (e.g. PiD) nor 4R/3R (e.g. AD) tauopathies (Gotz et al., 2019).

SUMOylation

SUMO1 but not SUMO2 colocalizes with phosphorylated tau aggregates in AD and PSP (Luo et al., 2014; Takamura et al., 2022). However, it is not clear whether SUMO modifications also take place on soluble tau. Like polyamination and O-GlcNAcylation, SUMOylation is challenging to detect with biochemical and MS methods despite some recent advances (Lumpkin et al., 2017; Osula et al., 2012). Addressing this limitation is important to determine whether SUMOylation of tau starts early or late in the development and progression of disease.

In Chapter 4, we showed that SUMOylation markedly inhibits the formation of filamentous tau aggregates. Our results stand at odds with the published studies showing that SUMO1 is associated with tau accumulation and aggregation (Dorval & Fraser, 2006; Luo et al., 2014). One critical difference in the studies of tau SUMOylation in this dissertation is that we used purified recombinant tau proteins separated from the cellular milieu. In fact, the cellular environment integrates biological factors that may reveal an outcome of SUMOylation different from that observed in our *in vitro* protein studies. For instance, the previously published reported an interplay between SUMOylation and other PTMs of tau (e.g. phosphorylation and ubiquitination) that may alter tau clearance, concentration, and aggregation (Dorval & Fraser, 2006; Luo et al., 2014). To better match the other factors encountered by SUMOylated tau in the cell, futures studies using recombinant tau protein may examine combinations of phosphorylated tau along with different SUMO isoforms. Nadel et al. recently used a similar approach to study the impact of ubiquitination on tau phosphorylated at AD relevant sites (Drepper et al., 2020; Nadel et al., 2023). It is also critical to determine which phosphorylated sites coincides with

SUMOylated tau in tauopathies by MS or other approaches to guide future studies (Dorval & Fraser, 2006; Luo et al., 2014).

In this dissertation, recombinant tau proteins modified with polyamination and O-GlcNAcylation represent a mixture of modified and unmodified proteins. In addition, the site-specific patterns of modifications within single tau proteins are undoubtedly a mixture and adds complexity to identifying site-specific effects. SUMOylated tau proteins likely contain little to no unmodified tau because of the dual tag purification method utilized. Even though this approach allowed us to effectively dissect the effects of SUMOylation, it does not recapitulate the cellular conditions of having presumably both SUMOylated and non-SUMOylated tau proteins, with and without other PTMs. For example, regulation of tau biology by the truncated N-terminal and C-terminal fragments may be altered in the presence of SUMOylated and non-SUMOylated tau proteins (Abraha et al., 2000; Gamblin et al., 2003; Guillozet-Bongaarts et al., 2005; Horowitz et al., 2006; Horowitz et al., 2004). These approaches were initial attempts at understanding the potential impact of specific modifications, but the future of such work will require additional refinement to identify site-specific effects and the interplay between multiple PTMs.

An intriguing finding with SUMOylated proteins is the globular structures formed by SUMO2-modified hT40 protein upon aggregation. These structures display a different profile of pathological conformations with reduced TOC1-positivity, PAD exposure, and misfolding but increased TOMA1-positivity. Several pathological conformations usually coexist in human tauopathies and recombinant tau proteins (Castillo-Carranza, Gerson, et al., 2014; Combs et al., 2016; Cox et al., 2016; Ferrer et al., 2014; Montalbano et al., 2023). Therefore, it is critical to assess the structure of the unique globular aggregates by

structural approaches such as atomic force microscopy and cryogenic electron microscopy. Furthermore, it is worthwhile to test the effect of SUMO2-modified hT40 globular aggregates on axonal transport despite a lack of detectable increases in PAD exposure (Brady et al., 1982; Mueller et al., 2023). A recent report suggested that a conformation other than PAD exposure may also impair axonal transport potentially through JNK-mediated mechanisms (Morris et al., 2020).

Concluding Remarks

Tau is subject to a broad range of PTMs, including phosphorylation, acetylation, methylation, ubiquitination, nitration (Alquezar et al., 2020). A significant body of literature demonstrates that PTMs have roles in regulating tau localization, protein interactions, degradation, and aggregation, but the precise impact of specific and combinatorial PTMs on the tau's physiology and pathophysiology requires continued investigation (Alhadidy & Kanaan, 2024; Alquezar et al., 2020; Park et al., 2018).

Phosphorylation and acetylation are the most extensively studied PTMs of tau; yet tau is subject to a larger pool of PTMs that have received substantively less attention, such as carbamylation, prolyl-isomerization, polyamination, O-GlcNAcylation, and SUMOylation among others (Alhadidy & Kanaan, 2024). Furthermore, our understating of how PTMs of tau specifically regulate its transition into pathological conformations is still being developed by the field. Filling these knowledge gaps requires further investigation of the understudied territory of tau PTMs to gain a comprehensive picture of tau regulation.

In this dissertation, I utilized a set of *in vitro* assays to determine the contribution of some understudied PTMs of tau in its transition into pathological conformations (i.e.

PAD exposure and misfolding), globular aggregates (i.e. oligomers) and filamentous aggregates (Figure 5.1) (Alhadidy & Kanaan, 2024). I encountered three profiles of tau regulation with each PTM: reduction in filamentous aggregates along with an increase in pathological conformations with polyamination, a mild reduction in filamentous aggregates along with no change or an increase in pathological tau conformations with O-GlcNAcylation, and a reduction in filamentous aggregates and pathological conformations (mostly) with SUMOylation.

PTMs of tau are usually studied in the context of their impact on tau aggregation into filamentous structures, including the most studied phosphorylation and acetylation (Alhadidy & Kanaan, 2024). Based on its impact on filamentous tau aggregates, one may mistakenly hypothesize that tau polyamination with SPD is protective in tauopathies, but there is an associated increase in pathogenic conformations linked to toxicity mechanisms. In addition, most efforts testing therapeutic approaches that target PTMs utilize mouse models that express 4R tau isoforms (Lewis et al., 2000; Santacruz et al., 2005; Yoshiyama et al., 2007). For example, studying O-GlcNAcylation of 4R but not 3R tau isoforms may lead to the false impression that this PTM is protective in tauopathies: however, different tau isoforms comprising the pathological tau inclusions in each disease changes the interpretation with this modification (Gotz et al., 2019). The findings in this dissertation strongly endorse a more comprehensive approach to study tau PTMs that includes the consideration of pathological conformations and aggregation of tau isoforms.

A recent wave of research efforts aims at advancing our knowledge of tau conformations and developing antibodies for their detection. While some novel antibodies detect conformation(s) common across tauopathies, other conformation-dependent

antibodies differentiate tau pathology of AD from other dementias (Gibbons et al., 2019; Paterno et al., 2023; Verelst et al., 2020; Zupancic et al., 2023). Furthermore, novel conformation-dependent antibodies detect tau seeds common across tauopathies, while others differentiate tau seeds of AD and PSP from CBD and PiD (Gibbons et al., 2020; Hitt et al., 2023). Further investigation of these novel conformations and potential mechanisms of toxicity will expand the tools available for researchers to fully characterize the impact of PTMs on tau pathobiology.

It is critical to use a multi-pronged approach to generate hypotheses about the role of PTMs in regulating tau pathobiology. For example, SUMO1-modified tau proteins in this work showed a reduction in tau aggregation into filamentous structures. One may conclude that SUMO1 does not favor tau aggregation and consequently is not detectable in tau inclusions. Nonetheless, data from cell lines show that modifying tau with SUMO1 reduces its ubiquitination and further clearance by the proteasome and increases tau aggregation (Dorval & Fraser, 2006; Luo et al., 2014). Furthermore, SUMO1 colocalizes with tau inclusions in AD and PSP (Luo et al., 2014; Takamura et al., 2022). By integrating the data together, alternative explanations can be hypothesized to reconcile this apparent discrepancy. For instance, SUMOylation of tau may be inhibitory to filamentous aggregate formation but the combination of SUMOylation and phosphorylation may yield a different outcome. In fact, such a hypothesis was recently reported with the combination of ubiquitination and phosphorylation (Drepper et al., 2020; Nadel et al., 2023). Furthermore, it is also plausible that SUMOylation is a compensatory mechanism initiated to prevent the aggregation of phosphorylated tau. Along with the reduction of tau ubiquitination and clearance upon its SUMOylation, other pathophysiological processes may outcompete

SUMOylation culminating into aggregation of SUMOylated tau (Drepper et al., 2020; Nadel et al., 2023). A third possibility is that the globular aggregates formed by SUMOylated tau become sequestered into neurofibrillary tangles as they mature. Therefore, it is critical to include data from multiple *in vitro*, *in vivo*, and *in situ* systems for better understanding of tau regulation by PTMs.

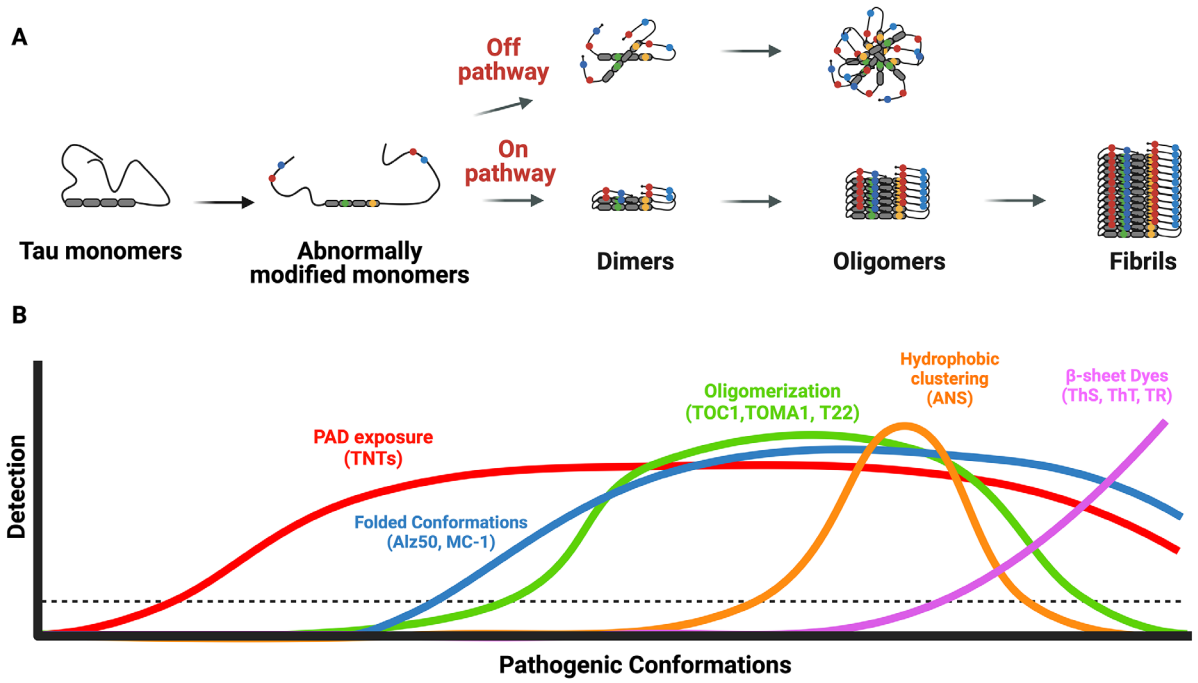

Figure 5.1. Summary of biochemical approaches to monitor transition of tau into various pathogenic conformations.
A, soluble tau monomers assume an ensemble of dynamic conformation(s), such as the paperclip structure, under physiological conditions. Abnormal modification with mutations, post-translational modifications, or other factors such as protein-protein interactions are thought to facilitate the adoption of abnormal conformations that facilitate the formation of multimeric species. Tau multimerization is dynamic and a complex ensemble of conformers are possible, some of which are oligomeric forms that are “off-pathway” for forming fibrils and others are” on-pathway” and will facilitate the formation of fibrillar structures. B, specific tools have utility in detecting various forms of tau during the cascade of changes from physiological monomers to abnormal conformations, oligomeric and fibrillar forms of tau. Early abnormal modifications and subsequent conformational changes are identified by some tau antibodies (e.g., exposure of the phosphatase-activating domain (PAD) by Tau N-Terminal (TNT) antibodies) in biochemical assays.

Figure 5.1 (cont'd)
Conformations of tau that precede its aggregation can be monitored by the Alz50 and MC-1 antibodies as well. Many of these early conformational changes are seen in oligomeric species, and additional antibody reagents are available that specifically bind tau oligomers [e.g., Tau Oligomeric Complex 1 (TOC1), Tau Oligomer Monoclonal Antibody (TOMA1), and T22]. As oligomeric species mature, they become identifiable through 8-Anilino-1-naphthalenesulfonic acid (ANS) assays because of the associated hydrophobic clustering. Finally, fibrillar forms of tau are rich in β-sheet structures and subsequently biochemical assays using fluorometric dyes [e.g., thioflavin S (ThS), thioflavin T (ThT) or thiazine red] that bind these structures identify the formation of filamentous tau aggregates. The seeding capacity of abnormal tau species from monomeric to fibrillar forms are identifiable using the RD biosensor cell assay (cells expressing mutant 4 microtubule-binding repeat domains of tau). Figure created with BioRender.com.

REFERENCES

2023 Alzheimer's disease facts and figures. (2023). *Alzheimers Dement*, *19*(4), 1598-1695. https://doi.org/10.1002/alz.13016

Abraha, A., Ghoshal, N., Gamblin, T. C., Cryns, V., Berry, R. W., Kuret, J., & Binder, L. I. (2000). C-terminal inhibition of tau assembly in vitro and in Alzheimer's disease. *J Cell Sci*, *113 Pt 21*, 3737-3745. https://doi.org/10.1242/jcs.113.21.3737

Acosta, D. M., Mancinelli, C., Bracken, C., & Eliezer, D. (2022). Post-translational modifications within tau paired helical filament nucleating motifs perturb microtubule interactions and oligomer formation. *J Biol Chem*, *298*(1), 101442. https://doi.org/10.1016/j.jbc.2021.101442

Acuna, M. L., Garcia-Morin, A., Orozco-Sepulveda, R., Ontiveros, C., Flores, A., Diaz, A. V., Gutierrez-Zubiate, I., Patil, A. R., Alvarado, L. A., Roy, S., Russell, W. K., & Rosas-Acosta, G. (2023). Alternative splicing of the SUMO1/2/3 transcripts affects cellular SUMOylation and produces functionally distinct SUMO protein isoforms. *Sci Rep*, *13*(1), 2309. https://doi.org/10.1038/s41598-023-29357-7

Adams, S. J., DeTure, M. A., McBride, M., Dickson, D. W., & Petrucelli, L. (2010). Three repeat isoforms of tau inhibit assembly of four repeat tau filaments. *PLoS One*, *5*(5), e10810. https://doi.org/10.1371/journal.pone.0010810

Ahmed, Z., Cooper, J., Murray, T. K., Garn, K., McNaughton, E., Clarke, H., Parhizkar, S., Ward, M. A., Cavallini, A., Jackson, S., Bose, S., Clavaguera, F., Tolnay, M., Lavenir, I., Goedert, M., Hutton, M. L., & O'Neill, M. J. (2014). A novel in vivo model of tau propagation with rapid and progressive neurofibrillary tangle pathology: the pattern of spread is determined by connectivity, not proximity. *Acta Neuropathol*, *127*(5), 667-683. https://doi.org/10.1007/s00401-014-1254-6

Ahmed, Z., Josephs, K. A., Gonzalez, J., DelleDonne, A., & Dickson, D. W. (2008). Clinical and neuropathologic features of progressive supranuclear palsy with severe pallido-nigro-luysial degeneration and axonal dystrophy. *Brain*, *131*(Pt 2), 460-472. https://doi.org/10.1093/brain/awm301

Ahn, K., Song, J. H., Kim, D. K., Park, M. H., Jo, S. A., & Koh, Y. H. (2009). Ubc9 gene polymorphisms and late-onset Alzheimer's disease in the Korean population: a genetic association study. *Neurosci Lett*, *465*(3), 272-275. https://doi.org/10.1016/j.neulet.2009.09.017

Ait-Bouziad, N., Chiki, A., Limorenko, G., Xiao, S., Eliezer, D., & Lashuel, H. A. (2020). Phosphorylation of the overlooked tyrosine 310 regulates the structure, aggregation, and microtubule- and lipid-binding properties of Tau. *J Biol Chem*, *295*(23), 7905-7922. https://doi.org/10.1074/jbc.RA119.012517

Ajit, D., Trzeciakiewicz, H., Tseng, J. H., Wander, C. M., Chen, Y., Ajit, A., King, D. P., & Cohen, T. J. (2019). A unique tau conformation generated by an acetylation-mimic substitution modulates P301S-dependent tau pathology and hyperphosphorylation. *J Biol Chem*, *294*(45), 16698-16711. https://doi.org/10.1074/jbc.RA119.009674

Alhadidy, M. M., & Kanaan, N. M. (2024). Biochemical approaches to assess the impact of post-translational modifications on pathogenic tau conformations using recombinant protein. *Biochem Soc Trans*, *52*(1), 301-318. https://doi.org/10.1042/BST20230596

Allsop, D. (2000). Introduction to Alzheimer's disease. *Methods Mol Med*, *32*, 1-21. https://doi.org/10.1385/1-59259-195-7:1

Alonso, A., Zaidi, T., Novak, M., Grundke-Iqbal, I., & Iqbal, K. (2001). Hyperphosphorylation induces self-assembly of tau into tangles of paired helical filaments/straight filaments. *Proc Natl Acad Sci U S A*, *98*(12), 6923-6928. https://doi.org/10.1073/pnas.121119298

Alonso, A. C., Zaidi, T., Grundke-Iqbal, I., & Iqbal, K. (1994). Role of abnormally phosphorylated tau in the breakdown of microtubules in Alzheimer disease. *Proc Natl Acad Sci U S A*, *91*(12), 5562-5566. https://doi.org/10.1073/pnas.91.12.5562

Alquezar, C., Arya, S., & Kao, A. W. (2020). Tau Post-translational Modifications: Dynamic Transformers of Tau Function, Degradation, and Aggregation. *Front Neurol*, *11*, 595532. https://doi.org/10.3389/fneur.2020.595532

Amniai, L., Barbier, P., Sillen, A., Wieruszeski, J. M., Peyrot, V., Lippens, G., & Landrieu, I. (2009). Alzheimer disease specific phosphoepitopes of Tau interfere with assembly of tubulin but not binding to microtubules. *FASEB J*, *23*(4), 1146-1152. https://doi.org/10.1096/fj.08-121590

Amorim, I. S., Challal, S., Cistarelli, L., Dorval, T., Abjean, L., Touzard, M., Arbez, N., Francois, A., Panayi, F., Jeggo, R., Cecon, E., Oishi, A., Dam, J., Jockers, R., & Machado, P. (2023). A seeding-based neuronal model of tau aggregation for use in drug discovery. *PLoS One*, *18*(4), e0283941. https://doi.org/10.1371/journal.pone.0283941

Andrade-Guerrero, J., Santiago-Balmaseda, A., Jeronimo-Aguilar, P., Vargas-Rodriguez, I., Cadena-Suarez, A. R., Sanchez-Garibay, C., Pozo-Molina, G., Mendez-Catala, C. F., Cardenas-Aguayo, M. D., Diaz-Cintra, S., Pacheco-Herrero, M., Luna-Munoz, J., & Soto-Rojas, L. O. (2023). Alzheimer's Disease: An Updated Overview of Its Genetics. *Int J Mol Sci*, *24*(4). https://doi.org/10.3390/ijms24043754

Annadurai, N., Malina, L., Malohlava, J., Hajduch, M., & Das, V. (2022). Tau R2 and R3 are essential regions for tau aggregation, seeding and propagation. *Biochimie*, *200*, 79-86. https://doi.org/10.1016/j.biochi.2022.05.013

Aquino-Gil, M., Pierce, A., Perez-Cervera, Y., Zenteno, E., & Lefebvre, T. (2017). OGT: a short overview of an enzyme standing out from usual glycosyltransferases. *Biochem Soc Trans*, *45*(2), 365-370. https://doi.org/10.1042/BST20160404

Arai, T., Guo, J. P., & McGeer, P. L. (2005). Proteolysis of non-phosphorylated and phosphorylated tau by thrombin. *J Biol Chem*, *280*(7), 5145-5153. https://doi.org/10.1074/jbc.M409234200

Arakhamia, T., Lee, C. E., Carlomagno, Y., Duong, D. M., Kundinger, S. R., Wang, K., Williams, D., DeTure, M., Dickson, D. W., Cook, C. N., Seyfried, N. T., Petrucelli, L., & Fitzpatrick, A. W. P. (2020). Posttranslational Modifications Mediate the Structural Diversity of Tauopathy Strains. *Cell*, *180*(4), 633-644 e612. https://doi.org/10.1016/j.cell.2020.01.027

Arendt, T., Stieler, J. T., & Holzer, M. (2016). Tau and tauopathies. *Brain Res Bull*, *126*(Pt 3), 238-292. https://doi.org/10.1016/j.brainresbull.2016.08.018

Arima, K. (2006). Ultrastructural characteristics of tau filaments in tauopathies: immuno-electron microscopic demonstration of tau filaments in tauopathies. *Neuropathology*, *26*(5), 475-483. https://doi.org/10.1111/j.1440-1789.2006.00669.x

Arima, K., Murayama, S., Oyanagi, S., Akashi, T., & Inose, T. (1992). Presenile dementia with progressive supranuclear palsy tangles and Pick bodies: an unusual degenerative disorder involving the cerebral cortex, cerebral nuclei, and brain stem nuclei. *Acta Neuropathol*, *84*(2), 128-134. https://doi.org/10.1007/BF00311384

Armstrong, M. J., Litvan, I., Lang, A. E., Bak, T. H., Bhatia, K. P., Borroni, B., Boxer, A. L., Dickson, D. W., Grossman, M., Hallett, M., Josephs, K. A., Kertesz, A., Lee, S. E., Miller, B. L., Reich, S. G., Riley, D. E., Tolosa, E., Troster, A. I., Vidailhet, M., & Weiner,

W. J. (2013). Criteria for the diagnosis of corticobasal degeneration. *Neurology*, *80*(5), 496-503. https://doi.org/10.1212/WNL.0b013e31827f0fd1

Arnold, C. S., Johnson, G. V., Cole, R. N., Dong, D. L., Lee, M., & Hart, G. W. (1996). The microtubule-associated protein tau is extensively modified with O-linked N-acetylglucosamine. *J Biol Chem*, *271*(46), 28741-28744. https://doi.org/10.1074/jbc.271.46.28741

Arriagada, P. V., Growdon, J. H., Hedley-Whyte, E. T., & Hyman, B. T. (1992). Neurofibrillary tangles but not senile plaques parallel duration and severity of Alzheimer's disease. *Neurology*, *42*(3 Pt 1), 631-639. https://doi.org/10.1212/wnl.42.3.631

Augustinack, J. C., Schneider, A., Mandelkow, E. M., & Hyman, B. T. (2002). Specific tau phosphorylation sites correlate with severity of neuronal cytopathology in Alzheimer's disease. *Acta Neuropathol*, *103*(1), 26-35. https://doi.org/10.1007/s004010100423

Azevedo, R., Jacquemin, C., Villain, N., Fenaille, F., Lamari, F., & Becher, F. (2022). Mass Spectrometry for Neurobiomarker Discovery: The Relevance of Post-Translational Modifications. *Cells*, *11*(8). https://doi.org/10.3390/cells11081279

Baas, P. W., & Qiang, L. (2019). Tau: It's Not What You Think. *Trends Cell Biol*, *29*(6), 452-461. https://doi.org/10.1016/j.tcb.2019.02.007

Bae, D. H., Lane, D. J. R., Jansson, P. J., & Richardson, D. R. (2018). The old and new biochemistry of polyamines. *Biochim Biophys Acta Gen Subj*, *1862*(9), 2053-2068. https://doi.org/10.1016/j.bbagen.2018.06.004

Balmik, A. A., Chidambaram, H., Dangi, A., Marelli, U. K., & Chinnathambi, S. (2020). HDAC6 ZnF UBP as the Modifier of Tau Structure and Function. *Biochemistry*, *59*(48), 4546-4562. https://doi.org/10.1021/acs.biochem.0c00585

Bancher, C., Brunner, C., Lassmann, H., Budka, H., Jellinger, K., Wiche, G., Seitelberger, F., Grundke-Iqbal, I., Iqbal, K., & Wisniewski, H. M. (1989). Accumulation of abnormally phosphorylated tau precedes the formation of neurofibrillary tangles in Alzheimer's disease. *Brain Res*, *477*(1-2), 90-99. https://doi.org/10.1016/0006-8993(89)91396-6

Bancher, C., Grundke-Iqbal, I., Iqbal, K., Fried, V. A., Smith, H. T., & Wisniewski, H. M. (1991). Abnormal phosphorylation of tau precedes ubiquitination in neurofibrillary

pathology of Alzheimer disease. *Brain Res*, *539*(1), 11-18. https://doi.org/10.1016/0006-8993(91)90681-k

Bancher, C., Lassmann, H., Budka, H., Grundke-Iqbal, I., Iqbal, K., Wiche, G., Seitelberger, F., & Wisniewski, H. M. (1987). Neurofibrillary tangles in Alzheimer's disease and progressive supranuclear palsy: antigenic similarities and differences. Microtubule-associated protein tau antigenicity is prominent in all types of tangles. *Acta Neuropathol*, *74*(1), 39-46. https://doi.org/10.1007/BF00688336

Barage, S. H., & Sonawane, K. D. (2015). Amyloid cascade hypothesis: Pathogenesis and therapeutic strategies in Alzheimer's disease. *Neuropeptides*, *52*, 1-18. https://doi.org/10.1016/j.npep.2015.06.008

Barbier, P., Zejneli, O., Martinho, M., Lasorsa, A., Belle, V., Smet-Nocca, C., Tsvetkov, P. O., Devred, F., & Landrieu, I. (2019). Role of Tau as a Microtubule-Associated Protein: Structural and Functional Aspects. *Front Aging Neurosci*, *11*, 204. https://doi.org/10.3389/fnagi.2019.00204

Barthelemy, N. R., Mallipeddi, N., Moiseyev, P., Sato, C., & Bateman, R. J. (2019). Tau Phosphorylation Rates Measured by Mass Spectrometry Differ in the Intracellular Brain vs. Extracellular Cerebrospinal Fluid Compartments and Are Differentially Affected by Alzheimer's Disease. *Front Aging Neurosci*, *11*, 121. https://doi.org/10.3389/fnagi.2019.00121

Barthelemy, N. R., Toth, B., Manser, P. T., Sanabria-Bohorquez, S., Teng, E., Keeley, M., Bateman, R. J., Weimer, R. M., & Wildsmith, K. R. (2022). Site-Specific Cerebrospinal Fluid Tau Hyperphosphorylation in Response to Alzheimer's Disease Brain Pathology: Not All Tau Phospho-Sites are Hyperphosphorylated. *J Alzheimers Dis*, *85*(1), 415-429. https://doi.org/10.3233/JAD-210677

Bartolome-Nebreda, J. M., Trabanco, A. A., Velter, A. I., & Buijnsters, P. (2021). O-GlcNAcase inhibitors as potential therapeutics for the treatment of Alzheimer's disease and related tauopathies: analysis of the patent literature. *Expert Opin Ther Pat*, *31*(12), 1117-1154. https://doi.org/10.1080/13543776.2021.1947242

Berry, R. W., Abraha, A., Lagalwar, S., LaPointe, N., Gamblin, T. C., Cryns, V. L., & Binder, L. I. (2003). Inhibition of tau polymerization by its carboxy-terminal caspase cleavage fragment. *Biochemistry*, *42*(27), 8325-8331. https://doi.org/10.1021/bi027348m

Berry, R. W., Sweet, A. P., Clark, F. A., Lagalwar, S., Lapin, B. R., Wang, T., Topgi, S., Guillozet-Bongaarts, A. L., Cochran, E. J., Bigio, E. H., & Binder, L. I. (2004). Tau epitope display in progressive supranuclear palsy and corticobasal degeneration. *J Neurocytol*, *33*(3), 287-295. https://doi.org/10.1023/B:NEUR.0000044190.96426.b9

Bichmann, M., Prat Oriol, N., Ercan-Herbst, E., Schondorf, D. C., Gomez Ramos, B., Schwarzler, V., Neu, M., Schluter, A., Wang, X., Jin, L., Hu, C., Tian, Y., Ried, J. S., Haberkant, P., Gasparini, L., & Ehrnhoefer, D. E. (2021). SETD7-mediated monomethylation is enriched on soluble Tau in Alzheimer's disease. *Mol Neurodegener*, *16*(1), 46. https://doi.org/10.1186/s13024-021-00468-x

Biernat, J., Gustke, N., Drewes, G., Mandelkow, E. M., & Mandelkow, E. (1993). Phosphorylation of Ser262 strongly reduces binding of tau to microtubules: distinction between PHF-like immunoreactivity and microtubule binding. *Neuron*, *11*(1), 153-163. https://doi.org/10.1016/0896-6273(93)90279-z

Bittar, A., Al-Lahham, R., Bhatt, N., Moore, K., Montalbano, M., Jerez, C., Fung, L., McAllen, S., Ellsworth, A., & Kayed, R. (2022). Passive Immunotherapy Targeting Tau Oligomeric Strains Reverses Tauopathy Phenotypes in Aged Human-Tau Mice in a Mouse Model-Specific Manner. *J Alzheimers Dis*, *90*(3), 1103-1122. https://doi.org/10.3233/JAD-220518

Black, M. M., Slaughter, T., Moshiach, S., Obrocka, M., & Fischer, I. (1996). Tau is enriched on dynamic microtubules in the distal region of growing axons. *J Neurosci*, *16*(11), 3601-3619. https://doi.org/10.1523/JNEUROSCI.16-11-03601.1996

Boeve, B. F., & Hutton, M. (2008). Refining frontotemporal dementia with parkinsonism linked to chromosome 17: introducing FTDP-17 (MAPT) and FTDP-17 (PGRN). *Arch Neurol*, *65*(4), 460-464. https://doi.org/10.1001/archneur.65.4.460

Boyko, S., & Surewicz, W. K. (2022). Tau liquid-liquid phase separation in neurodegenerative diseases. *Trends Cell Biol*, *32*(7), 611-623. https://doi.org/10.1016/j.tcb.2022.01.011

Braak, H., Alafuzoff, I., Arzberger, T., Kretzschmar, H., & Del Tredici, K. (2006). Staging of Alzheimer disease-associated neurofibrillary pathology using paraffin sections and immunocytochemistry. *Acta Neuropathol*, *112*(4), 389-404. https://doi.org/10.1007/s00401-006-0127-z

Braak, H., & Braak, E. (1991). Neuropathological stageing of Alzheimer-related changes. *Acta Neuropathol*, *82*(4), 239-259. https://doi.org/10.1007/BF00308809

Brady, D. R., & Mufson, E. J. (1991). Alz-50 immunoreactive neuropil differentiates hippocampal complex subfields in Alzheimer's disease. *J Comp Neurol*, *305*(3), 489-507. https://doi.org/10.1002/cne.903050311

Brady, S. T., Lasek, R. J., & Allen, R. D. (1982). Fast axonal transport in extruded axoplasm from squid giant axon. *Science*, *218*(4577), 1129-1131. https://doi.org/10.1126/science.6183745

Brandt, R., Trushina, N. I., & Bakota, L. (2020). Much More Than a Cytoskeletal Protein: Physiological and Pathological Functions of the Non-microtubule Binding Region of Tau. *Front Neurol*, *11*, 590059. https://doi.org/10.3389/fneur.2020.590059

Breuzard, G., Hubert, P., Nouar, R., De Bessa, T., Devred, F., Barbier, P., Sturgis, J. N., & Peyrot, V. (2013). Molecular mechanisms of Tau binding to microtubules and its role in microtubule dynamics in live cells. *J Cell Sci*, *126*(Pt 13), 2810-2819. https://doi.org/10.1242/jcs.120832

Brici, D., Gotz, J., & Nisbet, R. M. (2018). A Novel Antibody Targeting Tau Phosphorylated at Serine 235 Detects Neurofibrillary Tangles. *J Alzheimers Dis*, *61*(3), 899-905. https://doi.org/10.3233/JAD-170610

Brier, M. R., Gordon, B., Friedrichsen, K., McCarthy, J., Stern, A., Christensen, J., Owen, C., Aldea, P., Su, Y., Hassenstab, J., Cairns, N. J., Holtzman, D. M., Fagan, A. M., Morris, J. C., Benzinger, T. L., & Ances, B. M. (2016). Tau and Abeta imaging, CSF measures, and cognition in Alzheimer's disease. *Sci Transl Med*, *8*(338), 338ra366. https://doi.org/10.1126/scitranslmed.aaf2362

Budd Haeberlein, S., Aisen, P. S., Barkhof, F., Chalkias, S., Chen, T., Cohen, S., Dent, G., Hansson, O., Harrison, K., von Hehn, C., Iwatsubo, T., Mallinckrodt, C., Mummery, C. J., Muralidharan, K. K., Nestorov, I., Nisenbaum, L., Rajagovindan, R., Skordos, L., Tian, Y., . . . Sandrock, A. (2022). Two Randomized Phase 3 Studies of Aducanumab in Early Alzheimer's Disease. *J Prev Alzheimers Dis*, *9*(2), 197-210. https://doi.org/10.14283/jpad.2022.30

Bugiani, O., Murrell, J. R., Giaccone, G., Hasegawa, M., Ghigo, G., Tabaton, M., Morbin, M., Primavera, A., Carella, F., Solaro, C., Grisoli, M., Savoiardo, M., Spillantini, M. G.,

Tagliavini, F., Goedert, M., & Ghetti, B. (1999). Frontotemporal dementia and corticobasal degeneration in a family with a P301S mutation in tau. *J Neuropathol Exp Neurol*, *58*(6), 667-677. https://doi.org/10.1097/00005072-199906000-00011

Butner, K. A., & Kirschner, M. W. (1991). Tau protein binds to microtubules through a flexible array of distributed weak sites. *J Cell Biol*, *115*(3), 717-730. https://doi.org/10.1083/jcb.115.3.717

Caamano-Moreno, M., & Gargini, R. (2023). Tauopathies: The Role of Tau in Cellular Crosstalk and Synaptic Dysfunctions. *Neuroscience*, *518*, 38-53. https://doi.org/10.1016/j.neuroscience.2022.02.034

Caillet-Boudin, M. L., Buee, L., Sergeant, N., & Lefebvre, B. (2015). Regulation of human MAPT gene expression. *Mol Neurodegener*, *10*, 28. https://doi.org/10.1186/s13024-015-0025-8

Calafate, S., Buist, A., Miskiewicz, K., Vijayan, V., Daneels, G., de Strooper, B., de Wit, J., Verstreken, P., & Moechars, D. (2015). Synaptic Contacts Enhance Cell-to-Cell Tau Pathology Propagation. *Cell Rep*, *11*(8), 1176-1183. https://doi.org/10.1016/j.celrep.2015.04.043

Cantrelle, F. X., Loyens, A., Trivelli, X., Reimann, O., Despres, C., Gandhi, N. S., Hackenberger, C. P. R., Landrieu, I., & Smet-Nocca, C. (2021). Phosphorylation and O-GlcNAcylation of the PHF-1 Epitope of Tau Protein Induce Local Conformational Changes of the C-Terminus and Modulate Tau Self-Assembly Into Fibrillar Aggregates. *Front Mol Neurosci*, *14*, 661368. https://doi.org/10.3389/fnmol.2021.661368

Cao, L., Liang, Y., Liu, Y., Xu, Y., Wan, W., & Zhu, C. (2018). Pseudo-phosphorylation at AT8 epitopes regulates the tau truncation at aspartate 421. *Exp Cell Res*, *370*(1), 103-115. https://doi.org/10.1016/j.yexcr.2018.06.010

Cardozo, C., & Michaud, C. (2002). Proteasome-mediated degradation of tau proteins occurs independently of the chymotrypsin-like activity by a nonprocessive pathway. *Arch Biochem Biophys*, *408*(1), 103-110. https://doi.org/10.1016/s0003-9861(02)00493-9

Cario, A., Savastano, A., Wood, N. B., Liu, Z., Previs, M. J., Hendricks, A. G., Zweckstetter, M., & Berger, C. L. (2022). The pathogenic R5L mutation disrupts formation of Tau complexes on the microtubule by altering local N-terminal structure. *Proc Natl Acad Sci U S A*, *119*(7). https://doi.org/10.1073/pnas.2114215119

Cario, A., Wickramasinghe, S. P., Rhoades, E., & Berger, C. L. (2022). The N-terminal disease-associated R5L Tau mutation increases microtubule shrinkage rate due to disruption of microtubule-bound Tau patches. *J Biol Chem*, *298*(11), 102526. https://doi.org/10.1016/j.jbc.2022.102526

Carlomagno, Y., Chung, D. C., Yue, M., Castanedes-Casey, M., Madden, B. J., Dunmore, J., Tong, J., DeTure, M., Dickson, D. W., Petrucelli, L., & Cook, C. (2017). An acetylation-phosphorylation switch that regulates tau aggregation propensity and function. *J Biol Chem*, *292*(37), 15277-15286. https://doi.org/10.1074/jbc.M117.794602

Carmel, G., Mager, E. M., Binder, L. I., & Kuret, J. (1996). The structural basis of monoclonal antibody Alz50's selectivity for Alzheimer's disease pathology. *J Biol Chem*, *271*(51), 32789-32795. https://doi.org/10.1074/jbc.271.51.32789

Castillo-Carranza, D. L., Gerson, J. E., Sengupta, U., Guerrero-Munoz, M. J., Lasagna-Reeves, C. A., & Kayed, R. (2014). Specific targeting of tau oligomers in Htau mice prevents cognitive impairment and tau toxicity following injection with brain-derived tau oligomeric seeds. *J Alzheimers Dis*, *40 Suppl 1*, S97-S111. https://doi.org/10.3233/JAD-132477

Castillo-Carranza, D. L., Sengupta, U., Guerrero-Munoz, M. J., Lasagna-Reeves, C. A., Gerson, J. E., Singh, G., Estes, D. M., Barrett, A. D., Dineley, K. T., Jackson, G. R., & Kayed, R. (2014). Passive immunization with Tau oligomer monoclonal antibody reverses tauopathy phenotypes without affecting hyperphosphorylated neurofibrillary tangles. *J Neurosci*, *34*(12), 4260-4272. https://doi.org/10.1523/JNEUROSCI.3192-13.2014

Castro, T. G., Munteanu, F. D., & Cavaco-Paulo, A. (2019). Electrostatics of Tau Protein by Molecular Dynamics. *Biomolecules*, *9*(3). https://doi.org/10.3390/biom9030116

Celen, A. B., & Sahin, U. (2020). Sumoylation on its 25th anniversary: mechanisms, pathology, and emerging concepts. *FEBS J*, *287*(15), 3110-3140. https://doi.org/10.1111/febs.15319

Chakraborty, P., Riviere, G., Hebestreit, A., de Opakua, A. I., Vorberg, I. M., Andreas, L. B., & Zweckstetter, M. (2023). Acetylation discriminates disease-specific tau deposition. *Nat Commun*, *14*(1), 5919. https://doi.org/10.1038/s41467-023-41672-1

Chang, C. C., Tung, C. H., Chen, C. W., Tu, C. H., & Chu, Y. W. (2018). SUMOgo: Prediction of sumoylation sites on lysines by motif screening models and the effects of

various post-translational modifications. *Sci Rep*, *8*(1), 15512. https://doi.org/10.1038/s41598-018-33951-5

Chang, E., Honson, N. S., Bandyopadhyay, B., Funk, K. E., Jensen, J. R., Kim, S., Naphade, S., & Kuret, J. (2009). Modulation and detection of tau aggregation with small-molecule ligands. *Curr Alzheimer Res*, *6*(5), 409-414. https://doi.org/10.2174/156720509789207976

Chang, E., Kim, S., Schafer, K. N., & Kuret, J. (2011). Pseudophosphorylation of tau protein directly modulates its aggregation kinetics. *Biochim Biophys Acta*, *1814*(2), 388-395. https://doi.org/10.1016/j.bbapap.2010.10.005

Chatterjee, S., Cassel, R., Schneider-Anthony, A., Merienne, K., Cosquer, B., Tzeplaeff, L., Halder Sinha, S., Kumar, M., Chaturbedy, P., Eswaramoorthy, M., Le Gras, S., Keime, C., Bousiges, O., Dutar, P., Petsophonsakul, P., Rampon, C., Cassel, J. C., Buee, L., Blum, D., . . . Boutillier, A. L. (2018). Reinstating plasticity and memory in a tauopathy mouse model with an acetyltransferase activator. *EMBO Mol Med*, *10*(11). https://doi.org/10.15252/emmm.201708587

Chen, D., Bali, S., Singh, R., Wosztyl, A., Mullapudi, V., Vaquer-Alicea, J., Jayan, P., Melhem, S., Seelaar, H., van Swieten, J. C., Diamond, M. I., & Joachimiak, L. A. (2023). FTD-tau S320F mutation stabilizes local structure and allosterically promotes amyloid motif-dependent aggregation. *Nat Commun*, *14*(1), 1625. https://doi.org/10.1038/s41467-023-37274-6

Chen, D., Drombosky, K. W., Hou, Z., Sari, L., Kashmer, O. M., Ryder, B. D., Perez, V. A., Woodard, D. R., Lin, M. M., Diamond, M. I., & Joachimiak, L. A. (2019). Tau local structure shields an amyloid-forming motif and controls aggregation propensity. *Nat Commun*, *10*(1), 2493. https://doi.org/10.1038/s41467-019-10355-1

Chen, L. (2018). What triggers tauopathy in chronic traumatic encephalopathy? *Neural Regen Res*, *13*(6), 985-986. https://doi.org/10.4103/1673-5374.233439

Chen, S. Y., Ho, C. T., Liu, W. W., Lucanic, M., Shih, H. M., Huang, P. H., & Cheng, H. J. (2018). Regulation of axon repulsion by MAX-1 SUMOylation and AP-3. *Proc Natl Acad Sci U S A*, *115*(35), E8236-E8245. https://doi.org/10.1073/pnas.1804373115

Chen, X., Chen, M., Schafer, N. P., & Wolynes, P. G. (2020). Exploring the interplay between fibrillization and amorphous aggregation channels on the energy landscapes of

tau repeat isoforms. *Proc Natl Acad Sci U S A*, *117*(8), 4125-4130. https://doi.org/10.1073/pnas.1921702117

Cherry, J. D., Esnault, C. D., Baucom, Z. H., Tripodis, Y., Huber, B. R., Alvarez, V. E., Stein, T. D., Dickson, D. W., & McKee, A. C. (2021). Tau isoforms are differentially expressed across the hippocampus in chronic traumatic encephalopathy and Alzheimer's disease. *Acta Neuropathol Commun*, *9*(1), 86. https://doi.org/10.1186/s40478-021-01189-4

Chetelat, G., Villemagne, V. L., Bourgeat, P., Pike, K. E., Jones, G., Ames, D., Ellis, K. A., Szoeke, C., Martins, R. N., O'Keefe, G. J., Salvado, O., Masters, C. L., Rowe, C. C., Australian Imaging, B., & Lifestyle Research, G. (2010). Relationship between atrophy and beta-amyloid deposition in Alzheimer disease. *Ann Neurol*, *67*(3), 317-324. https://doi.org/10.1002/ana.21955

Christensen, K. R., Beach, T. G., Serrano, G. E., & Kanaan, N. M. (2019). Pathogenic tau modifications occur in axons before the somatodendritic compartment in mossy fiber and Schaffer collateral pathways. *Acta Neuropathol Commun*, *7*(1), 29. https://doi.org/10.1186/s40478-019-0675-9

Christensen, K. R., Combs, B., Richards, C., Grabinski, T., Alhadidy, M. M., & Kanaan, N. M. (2023). Phosphomimetics at Ser199/Ser202/Thr205 in Tau Impairs Axonal Transport in Rat Hippocampal Neurons. *Mol Neurobiol*, *60*(6), 3423-3438. https://doi.org/10.1007/s12035-023-03281-3

Ciechanover, A. (2015). The unravelling of the ubiquitin system. *Nat Rev Mol Cell Biol*, *16*(5), 322-324. https://doi.org/10.1038/nrm3982

Clavaguera, F., Bolmont, T., Crowther, R. A., Abramowski, D., Frank, S., Probst, A., Fraser, G., Stalder, A. K., Beibel, M., Staufenbiel, M., Jucker, M., Goedert, M., & Tolnay, M. (2009). Transmission and spreading of tauopathy in transgenic mouse brain. *Nat Cell Biol*, *11*(7), 909-913. https://doi.org/10.1038/ncb1901

Cleveland, D. W., Hwo, S. Y., & Kirschner, M. W. (1977). Purification of tau, a microtubule-associated protein that induces assembly of microtubules from purified tubulin. *J Mol Biol*, *116*(2), 207-225. https://doi.org/10.1016/0022-2836(77)90213-3

Cohen, T. J., Friedmann, D., Hwang, A. W., Marmorstein, R., & Lee, V. M. (2013). The microtubule-associated tau protein has intrinsic acetyltransferase activity. *Nat Struct Mol Biol*, *20*(6), 756-762. https://doi.org/10.1038/nsmb.2555

Cohen, T. J., Guo, J. L., Hurtado, D. E., Kwong, L. K., Mills, I. P., Trojanowski, J. Q., & Lee, V. M. (2011). The acetylation of tau inhibits its function and promotes pathological tau aggregation. *Nat Commun*, *2*, 252. https://doi.org/10.1038/ncomms1255

Colnaghi, L., Russo, L., Natale, C., Restelli, E., Cagnotto, A., Salmona, M., Chiesa, R., & Fioriti, L. (2019). Super Resolution Microscopy of SUMO Proteins in Neurons. *Front Cell Neurosci*, *13*, 486. https://doi.org/10.3389/fncel.2019.00486

Combs, B., Christensen, K. R., Richards, C., Kneynsberg, A., Mueller, R. L., Morris, S. L., Morfini, G. A., Brady, S. T., & Kanaan, N. M. (2021). Frontotemporal Lobar Dementia Mutant Tau Impairs Axonal Transport through a Protein Phosphatase 1gamma-Dependent Mechanism. *J Neurosci*, *41*(45), 9431-9451. https://doi.org/10.1523/JNEUROSCI.1914-20.2021

Combs, B., & Gamblin, T. C. (2012). FTDP-17 tau mutations induce distinct effects on aggregation and microtubule interactions. *Biochemistry*, *51*(43), 8597-8607. https://doi.org/10.1021/bi3010818

Combs, B., Hamel, C., & Kanaan, N. M. (2016). Pathological conformations involving the amino terminus of tau occur early in Alzheimer's disease and are differentially detected by monoclonal antibodies. *Neurobiol Dis*, *94*, 18-31. https://doi.org/10.1016/j.nbd.2016.05.016

Combs, B., & Kanaan, N. M. (2017). Exposure of the Amino Terminus of Tau Is a Pathological Event in Multiple Tauopathies. *Am J Pathol*, *187*(6), 1222-1229. https://doi.org/10.1016/j.ajpath.2017.01.019

Combs, B., Tiernan, C. T., Hamel, C., & Kanaan, N. M. (2017). Production of recombinant tau oligomers in vitro. *Methods Cell Biol*, *141*, 45-64. https://doi.org/10.1016/bs.mcb.2017.06.005

Combs, B., Voss, K., & Gamblin, T. C. (2011). Pseudohyperphosphorylation has differential effects on polymerization and function of tau isoforms. *Biochemistry*, *50*(44), 9446-9456. https://doi.org/10.1021/bi2010569

Congdon, E. E., Ji, C., Tetlow, A. M., Jiang, Y., & Sigurdsson, E. M. (2023). Tau-targeting therapies for Alzheimer disease: current status and future directions. *Nat Rev Neurol*, *19*(12), 715-736. https://doi.org/10.1038/s41582-023-00883-2

Congdon, E. E., & Sigurdsson, E. M. (2018). Tau-targeting therapies for Alzheimer disease. *Nat Rev Neurol*, *14*(7), 399-415. https://doi.org/10.1038/s41582-018-0013-z

Constantinidis, J., Richard, J., & Tissot, R. (1974). Pick's disease. Histological and clinical correlations. *Eur Neurol*, *11*(4), 208-217. https://doi.org/10.1159/000114320

Cook, C., Carlomagno, Y., Gendron, T. F., Dunmore, J., Scheffel, K., Stetler, C., Davis, M., Dickson, D., Jarpe, M., DeTure, M., & Petrucelli, L. (2014). Acetylation of the KXGS motifs in tau is a critical determinant in modulation of tau aggregation and clearance. *Hum Mol Genet*, *23*(1), 104-116. https://doi.org/10.1093/hmg/ddt402

Cook, C., Stankowski, J. N., Carlomagno, Y., Stetler, C., & Petrucelli, L. (2014). Acetylation: a new key to unlock tau's role in neurodegeneration. *Alzheimers Res Ther*, *6*(3), 29. https://doi.org/10.1186/alzrt259

Corneveaux, J. J., Myers, A. J., Allen, A. N., Pruzin, J. J., Ramirez, M., Engel, A., Nalls, M. A., Chen, K., Lee, W., Chewning, K., Villa, S. E., Meechoovet, H. B., Gerber, J. D., Frost, D., Benson, H. L., O'Reilly, S., Chibnik, L. B., Shulman, J. M., Singleton, A. B., . . . Huentelman, M. J. (2010). Association of CR1, CLU and PICALM with Alzheimer's disease in a cohort of clinically characterized and neuropathologically verified individuals. *Hum Mol Genet*, *19*(16), 3295-3301. https://doi.org/10.1093/hmg/ddq221

Corsellis, J. A., Bruton, C. J., & Freeman-Browne, D. (1973). The aftermath of boxing. *Psychol Med*, *3*(3), 270-303. https://doi.org/10.1017/s0033291700049588

Costantini, L. C., Barr, L. J., Vogel, J. L., & Henderson, S. T. (2008). Hypometabolism as a therapeutic target in Alzheimer's disease. *BMC Neurosci*, *9 Suppl 2*(Suppl 2), S16. https://doi.org/10.1186/1471-2202-9-S2-S16

Cowan, C. M., & Mudher, A. (2013). Are tau aggregates toxic or protective in tauopathies? *Front Neurol*, *4*, 114. https://doi.org/10.3389/fneur.2013.00114

Cox, K., Combs, B., Abdelmesih, B., Morfini, G., Brady, S. T., & Kanaan, N. M. (2016). Analysis of isoform-specific tau aggregates suggests a common toxic mechanism

involving similar pathological conformations and axonal transport inhibition. *Neurobiol Aging*, *47*, 113-126. https://doi.org/10.1016/j.neurobiolaging.2016.07.015

Cripps, D., Thomas, S. N., Jeng, Y., Yang, F., Davies, P., & Yang, A. J. (2006). Alzheimer disease-specific conformation of hyperphosphorylated paired helical filament-Tau is polyubiquitinated through Lys-48, Lys-11, and Lys-6 ubiquitin conjugation. *J Biol Chem*, *281*(16), 10825-10838. https://doi.org/10.1074/jbc.M512786200

Crowther, R. A. (1991). Straight and paired helical filaments in Alzheimer disease have a common structural unit. *Proc Natl Acad Sci U S A*, *88*(6), 2288-2292. https://doi.org/10.1073/pnas.88.6.2288

Crowther, R. A., & Goedert, M. (2000). Abnormal tau-containing filaments in neurodegenerative diseases. *J Struct Biol*, *130*(2-3), 271-279. https://doi.org/10.1006/jsbi.2000.4270

Crowther, R. A., & Wischik, C. M. (1985). Image reconstruction of the Alzheimer paired helical filament. *EMBO J*, *4*(13B), 3661-3665. https://doi.org/10.1002/j.1460-2075.1985.tb04132.x

D'Souza, I., Poorkaj, P., Hong, M., Nochlin, D., Lee, V. M., Bird, T. D., & Schellenberg, G. D. (1999). Missense and silent tau gene mutations cause frontotemporal dementia with parkinsonism-chromosome 17 type, by affecting multiple alternative RNA splicing regulatory elements. *Proc Natl Acad Sci U S A*, *96*(10), 5598-5603. https://doi.org/10.1073/pnas.96.10.5598

David, D. C., Layfield, R., Serpell, L., Narain, Y., Goedert, M., & Spillantini, M. G. (2002). Proteasomal degradation of tau protein. *J Neurochem*, *83*(1), 176-185. https://doi.org/10.1046/j.1471-4159.2002.01137.x

de Calignon, A., Polydoro, M., Suarez-Calvet, M., William, C., Adamowicz, D. H., Kopeikina, K. J., Pitstick, R., Sahara, N., Ashe, K. H., Carlson, G. A., Spires-Jones, T. L., & Hyman, B. T. (2012). Propagation of tau pathology in a model of early Alzheimer's disease. *Neuron*, *73*(4), 685-697. https://doi.org/10.1016/j.neuron.2011.11.033

de Leon, M. J., Convit, A., Wolf, O. T., Tarshish, C. Y., DeSanti, S., Rusinek, H., Tsui, W., Kandil, E., Scherer, A. J., Roche, A., Imossi, A., Thorn, E., Bobinski, M., Caraos, C., Lesbre, P., Schlyer, D., Poirier, J., Reisberg, B., & Fowler, J. (2001). Prediction of cognitive decline in normal elderly subjects with 2-[(18)F]fluoro-2-deoxy-D-

glucose/poitron-emission tomography (FDG/PET). *Proc Natl Acad Sci U S A*, *98*(19), 10966-10971. https://doi.org/10.1073/pnas.191044198

De Santi, S., de Leon, M. J., Rusinek, H., Convit, A., Tarshish, C. Y., Roche, A., Tsui, W. H., Kandil, E., Boppana, M., Daisley, K., Wang, G. J., Schlyer, D., & Fowler, J. (2001). Hippocampal formation glucose metabolism and volume losses in MCI and AD. *Neurobiol Aging*, *22*(4), 529-539. https://doi.org/10.1016/s0197-4580(01)00230-5

de Silva, R., Lashley, T., Strand, C., Shiarli, A. M., Shi, J., Tian, J., Bailey, K. L., Davies, P., Bigio, E. H., Arima, K., Iseki, E., Murayama, S., Kretzschmar, H., Neumann, M., Lippa, C., Halliday, G., MacKenzie, J., Ravid, R., Dickson, D., . . . Mann, D. M. (2006). An immunohistochemical study of cases of sporadic and inherited frontotemporal lobar degeneration using 3R- and 4R-specific tau monoclonal antibodies. *Acta Neuropathol*, *111*(4), 329-340. https://doi.org/10.1007/s00401-006-0048-x

De Vivo, G., Di Lorenzo, R., Ricotta, M., & Gentile, V. (2009). Role of the transglutaminase enzymes in the nervous system and their possible involvement in neurodegenerative diseases. *Curr Med Chem*, *16*(36), 4767-4773. https://doi.org/10.2174/092986709789909594

Dear, A. J., Meisl, G., Saric, A., Michaels, T. C. T., Kjaergaard, M., Linse, S., & Knowles, T. P. J. (2020). Identification of on- and off-pathway oligomers in amyloid fibril formation. *Chem Sci*, *11*(24), 6236-6247. https://doi.org/10.1039/c9sc06501f

Derisbourg, M., Leghay, C., Chiappetta, G., Fernandez-Gomez, F. J., Laurent, C., Demeyer, D., Carrier, S., Buee-Scherrer, V., Blum, D., Vinh, J., Sergeant, N., Verdier, Y., Buee, L., & Hamdane, M. (2015). Role of the Tau N-terminal region in microtubule stabilization revealed by new endogenous truncated forms. *Sci Rep*, *5*, 9659. https://doi.org/10.1038/srep09659

Despres, C., Di, J., Cantrelle, F. X., Li, Z., Huvent, I., Chambraud, B., Zhao, J., Chen, J., Chen, S., Lippens, G., Zhang, F., Linhardt, R., Wang, C., Klarner, F. G., Schrader, T., Landrieu, I., Bitan, G., & Smet-Nocca, C. (2019). Major Differences between the Self-Assembly and Seeding Behavior of Heparin-Induced and in Vitro Phosphorylated Tau and Their Modulation by Potential Inhibitors. *ACS Chem Biol*, *14*(6), 1363-1379. https://doi.org/10.1021/acschembio.9b00325

Desterro, J. M., Rodriguez, M. S., Kemp, G. D., & Hay, R. T. (1999). Identification of the enzyme required for activation of the small ubiquitin-like protein SUMO-1. *J Biol Chem*, *274*(15), 10618-10624. https://doi.org/10.1074/jbc.274.15.10618

DeVos, S. L., Corjuc, B. T., Oakley, D. H., Nobuhara, C. K., Bannon, R. N., Chase, A., Commins, C., Gonzalez, J. A., Dooley, P. M., Frosch, M. P., & Hyman, B. T. (2018). Synaptic Tau Seeding Precedes Tau Pathology in Human Alzheimer's Disease Brain. *Front Neurosci*, *12*, 267. https://doi.org/10.3389/fnins.2018.00267

Devred, F., Barbier, P., Douillard, S., Monasterio, O., Andreu, J. M., & Peyrot, V. (2004). Tau induces ring and microtubule formation from alphabeta-tubulin dimers under nonassembly conditions. *Biochemistry*, *43*(32), 10520-10531. https://doi.org/10.1021/bi0493160

Di Primio, C., Quercioli, V., Siano, G., Rovere, M., Kovacech, B., Novak, M., & Cattaneo, A. (2017). The Distance between N and C Termini of Tau and of FTDP-17 Mutants Is Modulated by Microtubule Interactions in Living Cells. *Front Mol Neurosci*, *10*, 210. https://doi.org/10.3389/fnmol.2017.00210

Dickey, C. A., Dunmore, J., Lu, B., Wang, J. W., Lee, W. C., Kamal, A., Burrows, F., Eckman, C., Hutton, M., & Petrucelli, L. (2006). HSP induction mediates selective clearance of tau phosphorylated at proline-directed Ser/Thr sites but not KXGS (MARK) sites. *FASEB J*, *20*(6), 753-755. https://doi.org/10.1096/fj.05-5343fje

Dickey, C. A., Kamal, A., Lundgren, K., Klosak, N., Bailey, R. M., Dunmore, J., Ash, P., Shoraka, S., Zlatkovic, J., Eckman, C. B., Patterson, C., Dickson, D. W., Nahman, N. S., Jr., Hutton, M., Burrows, F., & Petrucelli, L. (2007). The high-affinity HSP90-CHIP complex recognizes and selectively degrades phosphorylated tau client proteins. *J Clin Invest*, *117*(3), 648-658. https://doi.org/10.1172/JCI29715

Dickey, C. A., Yue, M., Lin, W. L., Dickson, D. W., Dunmore, J. H., Lee, W. C., Zehr, C., West, G., Cao, S., Clark, A. M., Caldwell, G. A., Caldwell, K. A., Eckman, C., Patterson, C., Hutton, M., & Petrucelli, L. (2006). Deletion of the ubiquitin ligase CHIP leads to the accumulation, but not the aggregation, of both endogenous phospho- and caspase-3-cleaved tau species. *J Neurosci*, *26*(26), 6985-6996. https://doi.org/10.1523/JNEUROSCI.0746-06.2006

Dickson, D. W., Bergeron, C., Chin, S. S., Duyckaerts, C., Horoupian, D., Ikeda, K., Jellinger, K., Lantos, P. L., Lippa, C. F., Mirra, S. S., Tabaton, M., Vonsattel, J. P., Wakabayashi, K., Litvan, I., & Office of Rare Diseases of the National Institutes of, H. (2002). Office of Rare Diseases neuropathologic criteria for corticobasal degeneration. *J Neuropathol Exp Neurol*, *61*(11), 935-946. https://doi.org/10.1093/jnen/61.11.935

Dickson, D. W., Kouri, N., Murray, M. E., & Josephs, K. A. (2011). Neuropathology of frontotemporal lobar degeneration-tau (FTLD-tau). *J Mol Neurosci*, *45*(3), 384-389. https://doi.org/10.1007/s12031-011-9589-0

Ding, H., Dolan, P. J., & Johnson, G. V. (2008). Histone deacetylase 6 interacts with the microtubule-associated protein tau. *J Neurochem*, *106*(5), 2119-2130. https://doi.org/10.1111/j.1471-4159.2008.05564.x

Dinkel, P. D., Siddiqua, A., Huynh, H., Shah, M., & Margittai, M. (2011). Variations in filament conformation dictate seeding barrier between three- and four-repeat tau. *Biochemistry*, *50*(20), 4330-4336. https://doi.org/10.1021/bi2004685

Donahue, C. P., Muratore, C., Wu, J. Y., Kosik, K. S., & Wolfe, M. S. (2006). Stabilization of the tau exon 10 stem loop alters pre-mRNA splicing. *J Biol Chem*, *281*(33), 23302-23306. https://doi.org/10.1074/jbc.C600143200

Dorval, V., & Fraser, P. E. (2006). Small ubiquitin-like modifier (SUMO) modification of natively unfolded proteins tau and alpha-synuclein. *J Biol Chem*, *281*(15), 9919-9924. https://doi.org/10.1074/jbc.M510127200

Dorval, V., & Fraser, P. E. (2007). SUMO on the road to neurodegeneration. *Biochim Biophys Acta*, *1773*(6), 694-706. https://doi.org/10.1016/j.bbamcr.2007.03.017

Drepper, F., Biernat, J., Kaniyappan, S., Meyer, H. E., Mandelkow, E. M., Warscheid, B., & Mandelkow, E. (2020). A combinatorial native MS and LC-MS/MS approach reveals high intrinsic phosphorylation of human Tau but minimal levels of other key modifications. *J Biol Chem*, *295*(52), 18213-18225. https://doi.org/10.1074/jbc.RA120.015882

Drewes, G., Trinczek, B., Illenberger, S., Biernat, J., Schmitt-Ulms, G., Meyer, H. E., Mandelkow, E. M., & Mandelkow, E. (1995). Microtubule-associated protein/microtubule affinity-regulating kinase (p110mark). A novel protein kinase that regulates tau-microtubule interactions and dynamic instability by phosphorylation at the Alzheimer-specific site serine 262. *J Biol Chem*, *270*(13), 7679-7688. https://doi.org/10.1074/jbc.270.13.7679

Dudek, S. M., & Johnson, G. V. (1993). Transglutaminase catalyzes the formation of sodium dodecyl sulfate-insoluble, Alz-50-reactive polymers of tau. *J Neurochem*, *61*(3), 1159-1162. https://doi.org/10.1111/j.1471-4159.1993.tb03636.x

Eckermann, K., Mocanu, M. M., Khlistunova, I., Biernat, J., Nissen, A., Hofmann, A., Schonig, K., Bujard, H., Haemisch, A., Mandelkow, E., Zhou, L., Rune, G., & Mandelkow, E. M. (2007). The beta-propensity of Tau determines aggregation and synaptic loss in inducible mouse models of tauopathy. *J Biol Chem*, *282*(43), 31755-31765. https://doi.org/10.1074/jbc.M705282200

Eichmann, C., Campioni, S., Kowal, J., Maslennikov, I., Gerez, J., Liu, X., Verasdonck, J., Nespovitaya, N., Choe, S., Meier, B. H., Picotti, P., Rizo, J., Stahlberg, H., & Riek, R. (2016). Preparation and Characterization of Stable alpha-Synuclein Lipoprotein Particles. *J Biol Chem*, *291*(16), 8516-8527. https://doi.org/10.1074/jbc.M115.707968

Eidenmuller, J., Fath, T., Hellwig, A., Reed, J., Sontag, E., & Brandt, R. (2000). Structural and functional implications of tau hyperphosphorylation: information from phosphorylation-mimicking mutated tau proteins. *Biochemistry*, *39*(43), 13166-13175. https://doi.org/10.1021/bi001290z

Eidenmuller, J., Fath, T., Maas, T., Pool, M., Sontag, E., & Brandt, R. (2001). Phosphorylation-mimicking glutamate clusters in the proline-rich region are sufficient to simulate the functional deficiencies of hyperphosphorylated tau protein. *Biochem J*, *357*(Pt 3), 759-767. https://doi.org/10.1042/0264-6021:3570759

El Mammeri, N., Dregni, A. J., Duan, P., Wang, H. K., & Hong, M. (2022). Microtubule-binding core of the tau protein. *Sci Adv*, *8*(29), eabo4459. https://doi.org/10.1126/sciadv.abo4459

Elbaum-Garfinkle, S., & Rhoades, E. (2012). Identification of an aggregation-prone structure of tau. *J Am Chem Soc*, *134*(40), 16607-16613. https://doi.org/10.1021/ja305206m

Ellmer, D., Brehs, M., Haj-Yahya, M., Lashuel, H. A., & Becker, C. F. W. (2019). Single Posttranslational Modifications in the Central Repeat Domains of Tau4 Impact its Aggregation and Tubulin Binding. *Angew Chem Int Ed Engl*, *58*(6), 1616-1620. https://doi.org/10.1002/anie.201805238

Ercan, E., Eid, S., Weber, C., Kowalski, A., Bichmann, M., Behrendt, A., Matthes, F., Krauss, S., Reinhardt, P., Fulle, S., & Ehrnhoefer, D. E. (2017). A validated antibody panel for the characterization of tau post-translational modifications. *Mol Neurodegener*, *12*(1), 87. https://doi.org/10.1186/s13024-017-0229-1

Ercan-Herbst, E., Ehrig, J., Schondorf, D. C., Behrendt, A., Klaus, B., Gomez Ramos, B., Prat Oriol, N., Weber, C., & Ehrnhoefer, D. E. (2019). A post-translational modification signature defines changes in soluble tau correlating with oligomerization in early stage Alzheimer's disease brain. *Acta Neuropathol Commun*, *7*(1), 192. https://doi.org/10.1186/s40478-019-0823-2

Fa, M., Puzzo, D., Piacentini, R., Staniszewski, A., Zhang, H., Baltrons, M. A., Li Puma, D. D., Chatterjee, I., Li, J., Saeed, F., Berman, H. L., Ripoli, C., Gulisano, W., Gonzalez, J., Tian, H., Costa, J. A., Lopez, P., Davidowitz, E., Yu, W. H., . . . Arancio, O. (2016). Extracellular Tau Oligomers Produce An Immediate Impairment of LTP and Memory. *Sci Rep*, *6*, 19393. https://doi.org/10.1038/srep19393

Falcon, B., Cavallini, A., Angers, R., Glover, S., Murray, T. K., Barnham, L., Jackson, S., O'Neill, M. J., Isaacs, A. M., Hutton, M. L., Szekeres, P. G., Goedert, M., & Bose, S. (2015). Conformation determines the seeding potencies of native and recombinant Tau aggregates. *J Biol Chem*, *290*(2), 1049-1065. https://doi.org/10.1074/jbc.M114.589309

Falcon, B., Zhang, W., Murzin, A. G., Murshudov, G., Garringer, H. J., Vidal, R., Crowther, R. A., Ghetti, B., Scheres, S. H. W., & Goedert, M. (2018). Structures of filaments from Pick's disease reveal a novel tau protein fold. *Nature*, *561*(7721), 137-140. https://doi.org/10.1038/s41586-018-0454-y

Fath, T., Eidenmuller, J., & Brandt, R. (2002). Tau-mediated cytotoxicity in a pseudohyperphosphorylation model of Alzheimer's disease. *J Neurosci*, *22*(22), 9733-9741. https://doi.org/10.1523/JNEUROSCI.22-22-09733.2002

Fauquant, C., Redeker, V., Landrieu, I., Wieruszeski, J. M., Verdegem, D., Laprevote, O., Lippens, G., Gigant, B., & Knossow, M. (2011). Systematic identification of tubulin-interacting fragments of the microtubule-associated protein Tau leads to a highly efficient promoter of microtubule assembly. *J Biol Chem*, *286*(38), 33358-33368. https://doi.org/10.1074/jbc.M111.223545

Feany, M. B., & Dickson, D. W. (1995). Widespread cytoskeletal pathology characterizes corticobasal degeneration. *Am J Pathol*, *146*(6), 1388-1396. https://www.ncbi.nlm.nih.gov/pubmed/7778678

https://www.ncbi.nlm.nih.gov/pmc/articles/PMC1870913/pdf/amjpathol00054-0108.pdf

Ferrer, I., Lopez-Gonzalez, I., Carmona, M., Arregui, L., Dalfo, E., Torrejon-Escribano, B., Diehl, R., & Kovacs, G. G. (2014). Glial and neuronal tau pathology in tauopathies:

characterization of disease-specific phenotypes and tau pathology progression. *J Neuropathol Exp Neurol*, *73*(1), 81-97. https://doi.org/10.1097/NEN.0000000000000030

Fischer, D., Mukrasch, M. D., Biernat, J., Bibow, S., Blackledge, M., Griesinger, C., Mandelkow, E., & Zweckstetter, M. (2009). Conformational changes specific for pseudophosphorylation at serine 262 selectively impair binding of tau to microtubules. *Biochemistry*, *48*(42), 10047-10055. https://doi.org/10.1021/bi901090m

Fischer, I. (2023). Big Tau: What We Know, and We Need to Know. *eNeuro*, *10*(5). https://doi.org/10.1523/ENEURO.0052-23.2023

Fischer, I., & Baas, P. W. (2020). Resurrecting the Mysteries of Big Tau. *Trends Neurosci*, *43*(7), 493-504. https://doi.org/10.1016/j.tins.2020.04.007

Fitzpatrick, A. W. P., Falcon, B., He, S., Murzin, A. G., Murshudov, G., Garringer, H. J., Crowther, R. A., Ghetti, B., Goedert, M., & Scheres, S. H. W. (2017). Cryo-EM structures of tau filaments from Alzheimer's disease. *Nature*, *547*(7662), 185-190. https://doi.org/10.1038/nature23002

Flach, K., Ramminger, E., Hilbrich, I., Arsalan-Werner, A., Albrecht, F., Herrmann, L., Goedert, M., Arendt, T., & Holzer, M. (2014). Axotrophin/MARCH7 acts as an E3 ubiquitin ligase and ubiquitinates tau protein in vitro impairing microtubule binding. *Biochim Biophys Acta*, *1842*(9), 1527-1538. https://doi.org/10.1016/j.bbadis.2014.05.029

Fontaine, S. N., Zheng, D., Sabbagh, J. J., Martin, M. D., Chaput, D., Darling, A., Trotter, J. H., Stothert, A. R., Nordhues, B. A., Lussier, A., Baker, J., Shelton, L., Kahn, M., Blair, L. J., Stevens, S. M., Jr., & Dickey, C. A. (2016). DnaJ/Hsc70 chaperone complexes control the extracellular release of neurodegenerative-associated proteins. *EMBO J*, *35*(14), 1537-1549. https://doi.org/10.15252/embj.201593489

Franzmeier, N., Neitzel, J., Rubinski, A., Smith, R., Strandberg, O., Ossenkoppele, R., Hansson, O., Ewers, M., & Alzheimer's Disease Neuroimaging, I. (2020). Functional brain architecture is associated with the rate of tau accumulation in Alzheimer's disease. *Nat Commun*, *11*(1), 347. https://doi.org/10.1038/s41467-019-14159-1

Frey, B., Holzinger, D., Taylor, K., Ehrnhoefer, D. E., Striebinger, A., Biesinger, S., Gasparini, L., O'Neill, M. J., Wegner, F., Barghorn, S., Hoglinger, G. U., & Heym, R. G. (2023). Tau seed amplification assay reveals relationship between seeding and

pathological forms of tau in Alzheimer's disease brain. *Acta Neuropathol Commun*, *11*(1), 181. https://doi.org/10.1186/s40478-023-01676-w

Frost, B., Jacks, R. L., & Diamond, M. I. (2009). Propagation of tau misfolding from the outside to the inside of a cell. *J Biol Chem*, *284*(19), 12845-12852. https://doi.org/10.1074/jbc.M808759200

Fu, H., Hussaini, S. A., Wegmann, S., Profaci, C., Daniels, J. D., Herman, M., Emrani, S., Figueroa, H. Y., Hyman, B. T., Davies, P., & Duff, K. E. (2016). 3D Visualization of the Temporal and Spatial Spread of Tau Pathology Reveals Extensive Sites of Tau Accumulation Associated with Neuronal Loss and Recognition Memory Deficit in Aged Tau Transgenic Mice. *PLoS One*, *11*(7), e0159463. https://doi.org/10.1371/journal.pone.0159463

Fujino, Y., Delucia, M. W., Davies, P., & Dickson, D. W. (2004). Ballooned neurones in the limbic lobe are associated with Alzheimer type pathology and lack diagnostic specificity. *Neuropathol Appl Neurobiol*, *30*(6), 676-682. https://doi.org/10.1111/j.1365-2990.2004.00593.x

Fung, H. Y. J., McKibben, K. M., Ramirez, J., Gupta, K., & Rhoades, E. (2020). Structural Characterization of Tau in Fuzzy Tau:Tubulin Complexes. *Structure*, *28*(3), 378-384 e374. https://doi.org/10.1016/j.str.2020.01.004

Funk, K. E., Thomas, S. N., Schafer, K. N., Cooper, G. L., Liao, Z., Clark, D. J., Yang, A. J., & Kuret, J. (2014). Lysine methylation is an endogenous post-translational modification of tau protein in human brain and a modulator of aggregation propensity. *Biochem J*, *462*(1), 77-88. https://doi.org/10.1042/BJ20140372

Furman, J. L., Vaquer-Alicea, J., White, C. L., 3rd, Cairns, N. J., Nelson, P. T., & Diamond, M. I. (2017). Widespread tau seeding activity at early Braak stages. *Acta Neuropathol*, *133*(1), 91-100. https://doi.org/10.1007/s00401-016-1644-z

Gallo, J. M., Noble, W., & Martin, T. R. (2007). RNA and protein-dependent mechanisms in tauopathies: consequences for therapeutic strategies. *Cell Mol Life Sci*, *64*(13), 1701-1714. https://doi.org/10.1007/s00018-007-6513-4

Gamblin, T. C., Berry, R. W., & Binder, L. I. (2003). Tau polymerization: role of the amino terminus. *Biochemistry*, *42*(7), 2252-2257. https://doi.org/10.1021/bi0272510

Gamblin, T. C., King, M. E., Dawson, H., Vitek, M. P., Kuret, J., Berry, R. W., & Binder, L. I. (2000). In vitro polymerization of tau protein monitored by laser light scattering: method and application to the study of FTDP-17 mutants. *Biochemistry*, *39*(20), 6136-6144. https://doi.org/10.1021/bi000201f

Gamblin, T. C., King, M. E., Kuret, J., Berry, R. W., & Binder, L. I. (2000). Oxidative regulation of fatty acid-induced tau polymerization. *Biochemistry*, *39*(46), 14203-14210. https://doi.org/10.1021/bi001876l

Ganguly, P., Do, T. D., Larini, L., LaPointe, N. E., Sercel, A. J., Shade, M. F., Feinstein, S. C., Bowers, M. T., & Shea, J. E. (2015). Tau assembly: the dominant role of PHF6 (VQIVYK) in microtubule binding region repeat R3. *J Phys Chem B*, *119*(13), 4582-4593. https://doi.org/10.1021/acs.jpcb.5b00175

Garcia-Sierra, F., Ghoshal, N., Quinn, B., Berry, R. W., & Binder, L. I. (2003). Conformational changes and truncation of tau protein during tangle evolution in Alzheimer's disease. *J Alzheimers Dis*, *5*(2), 65-77. https://doi.org/10.3233/jad-2003-5201

Garcia-Sierra, F., Hauw, J. J., Duyckaerts, C., Wischik, C. M., Luna-Munoz, J., & Mena, R. (2000). The extent of neurofibrillary pathology in perforant pathway neurons is the key determinant of dementia in the very old. *Acta Neuropathol*, *100*(1), 29-35. https://doi.org/10.1007/s004010051189

Garcia-Sierra, F., Jarero-Basulto, J. J., Kristofikova, Z., Majer, E., Binder, L. I., & Ripova, D. (2012). Ubiquitin is associated with early truncation of tau protein at aspartic acid(421) during the maturation of neurofibrillary tangles in Alzheimer's disease. *Brain Pathol*, *22*(2), 240-250. https://doi.org/10.1111/j.1750-3639.2011.00525.x

Gatta, E., Lefebvre, T., Gaetani, S., dos Santos, M., Marrocco, J., Mir, A. M., Cassano, T., Maccari, S., Nicoletti, F., & Mairesse, J. (2016). Evidence for an imbalance between tau O-GlcNAcylation and phosphorylation in the hippocampus of a mouse model of Alzheimer's disease. *Pharmacol Res*, *105*, 186-197. https://doi.org/10.1016/j.phrs.2016.01.006

Geddes, J. F., Vowles, G. H., Nicoll, J. A., & Revesz, T. (1999). Neuronal cytoskeletal changes are an early consequence of repetitive head injury. *Acta Neuropathol*, *98*(2), 171-178. https://doi.org/10.1007/s004010051066

Gerson, J. E., Mudher, A., & Kayed, R. (2016). Potential mechanisms and implications for the formation of tau oligomeric strains. *Crit Rev Biochem Mol Biol*, *51*(6), 482-496. https://doi.org/10.1080/10409238.2016.1226251

Ghetti, B., Murrell, J. R., Zolo, P., Spillantini, M. G., & Goedert, M. (2000). Progress in hereditary tauopathies: a mutation in the Tau gene (G389R) causes a Pick disease-like syndrome. *Ann N Y Acad Sci*, *920*, 52-62. https://doi.org/10.1111/j.1749-6632.2000.tb06905.x

Gibbons, G. S., Kim, S. J., Robinson, J. L., Changolkar, L., Irwin, D. J., Shaw, L. M., Lee, V. M., & Trojanowski, J. Q. (2019). Detection of Alzheimer's disease (AD) specific tau pathology with conformation-selective anti-tau monoclonal antibody in co-morbid frontotemporal lobar degeneration-tau (FTLD-tau). *Acta Neuropathol Commun*, *7*(1), 34. https://doi.org/10.1186/s40478-019-0687-5

Gibbons, G. S., Kim, S. J., Wu, Q., Riddle, D. M., Leight, S. N., Changolkar, L., Xu, H., Meymand, E. S., O'Reilly, M., Zhang, B., Brunden, K. R., Trojanowski, J. Q., & Lee, V. M. Y. (2020). Conformation-selective tau monoclonal antibodies inhibit tau pathology in primary neurons and a mouse model of Alzheimer's disease. *Mol Neurodegener*, *15*(1), 64. https://doi.org/10.1186/s13024-020-00404-5

Giraud, M. F., Desterro, J. M., & Naismith, J. H. (1998). Structure of ubiquitin-conjugating enzyme 9 displays significant differences with other ubiquitin-conjugating enzymes which may reflect its specificity for sumo rather than ubiquitin. *Acta Crystallogr D Biol Crystallogr*, *54*(Pt 5), 891-898. https://doi.org/10.1107/s0907444998002480

Glenner, G. G., & Wong, C. W. (1984). Alzheimer's disease: initial report of the purification and characterization of a novel cerebrovascular amyloid protein. *Biochem Biophys Res Commun*, *120*(3), 885-890. https://doi.org/10.1016/s0006-291x(84)80190-4

Goedert, M. (2009). Oskar Fischer and the study of dementia. *Brain*, *132*(Pt 4), 1102-1111. https://doi.org/10.1093/brain/awn256

Goedert, M., Crowther, R. A., Scheres, S. H. W., & Spillantini, M. G. (2024). Tau and neurodegeneration. *Cytoskeleton (Hoboken)*, *81*(1), 95-102. https://doi.org/10.1002/cm.21812

Goedert, M., Eisenberg, D. S., & Crowther, R. A. (2017). Propagation of Tau Aggregates and Neurodegeneration. *Annu Rev Neurosci*, *40*, 189-210. https://doi.org/10.1146/annurev-neuro-072116-031153

Goedert, M., Jakes, R., Crowther, R. A., Cohen, P., Vanmechelen, E., Vandermeeren, M., & Cras, P. (1994). Epitope mapping of monoclonal antibodies to the paired helical filaments of Alzheimer's disease: identification of phosphorylation sites in tau protein. *Biochem J*, *301 (Pt 3)*(Pt 3), 871-877. https://doi.org/10.1042/bj3010871

Goedert, M., Jakes, R., & Vanmechelen, E. (1995). Monoclonal antibody AT8 recognises tau protein phosphorylated at both serine 202 and threonine 205. *Neurosci Lett*, *189*(3), 167-169. https://doi.org/10.1016/0304-3940(95)11484-e

Goedert, M., & Spillantini, M. G. (2000). Tau mutations in frontotemporal dementia FTDP-17 and their relevance for Alzheimer's disease. *Biochim Biophys Acta*, *1502*(1), 110-121. https://doi.org/10.1016/s0925-4439(00)00037-5

Goedert, M., Wischik, C. M., Crowther, R. A., Walker, J. E., & Klug, A. (1988). Cloning and sequencing of the cDNA encoding a core protein of the paired helical filament of Alzheimer disease: identification as the microtubule-associated protein tau. *Proc Natl Acad Sci U S A*, *85*(11), 4051-4055. https://doi.org/10.1073/pnas.85.11.4051

Gomez-Isla, T., Hollister, R., West, H., Mui, S., Growdon, J. H., Petersen, R. C., Parisi, J. E., & Hyman, B. T. (1997). Neuronal loss correlates with but exceeds neurofibrillary tangles in Alzheimer's disease. *Ann Neurol*, *41*(1), 17-24. https://doi.org/10.1002/ana.410410106

Gomez-Isla, T., Price, J. L., McKeel, D. W., Jr., Morris, J. C., Growdon, J. H., & Hyman, B. T. (1996). Profound loss of layer II entorhinal cortex neurons occurs in very mild Alzheimer's disease. *J Neurosci*, *16*(14), 4491-4500. https://doi.org/10.1523/JNEUROSCI.16-14-04491.1996

Gong, C. X., Liu, F., & Iqbal, K. (2016). O-GlcNAcylation: A regulator of tau pathology and neurodegeneration. *Alzheimers Dement*, *12*(10), 1078-1089. https://doi.org/10.1016/j.jalz.2016.02.011

Gong, C. X., Singh, T. J., Grundke-Iqbal, I., & Iqbal, K. (1993). Phosphoprotein phosphatase activities in Alzheimer disease brain. *J Neurochem*, *61*(3), 921-927. https://doi.org/10.1111/j.1471-4159.1993.tb03603.x

Goode, B. L., Denis, P. E., Panda, D., Radeke, M. J., Miller, H. P., Wilson, L., & Feinstein, S. C. (1997). Functional interactions between the proline-rich and repeat regions of tau enhance microtubule binding and assembly. *Mol Biol Cell*, *8*(2), 353-365. https://doi.org/10.1091/mbc.8.2.353

Gorsky, M. K., Burnouf, S., Dols, J., Mandelkow, E., & Partridge, L. (2016). Acetylation mimic of lysine 280 exacerbates human Tau neurotoxicity in vivo. *Sci Rep*, *6*, 22685. https://doi.org/10.1038/srep22685

Gorsky, M. K., Burnouf, S., Sofola-Adesakin, O., Dols, J., Augustin, H., Weigelt, C. M., Gronke, S., & Partridge, L. (2017). Pseudo-acetylation of multiple sites on human Tau proteins alters Tau phosphorylation and microtubule binding, and ameliorates amyloid beta toxicity. *Sci Rep*, *7*(1), 9984. https://doi.org/10.1038/s41598-017-10225-0

Gotz, J., Halliday, G., & Nisbet, R. M. (2019). Molecular Pathogenesis of the Tauopathies. *Annu Rev Pathol*, *14*, 239-261. https://doi.org/10.1146/annurev-pathmechdis-012418-012936

Graff-Radford, N. R., Damasio, A. R., Hyman, B. T., Hart, M. N., Tranel, D., Damasio, H., Van Hoesen, G. W., & Rezai, K. (1990). Progressive aphasia in a patient with Pick's disease: a neuropsychological, radiologic, and anatomic study. *Neurology*, *40*(4), 620-626. https://doi.org/10.1212/wnl.40.4.620

Graham, D. L., Gray, A. J., Joyce, J. A., Yu, D., O'Moore, J., Carlson, G. A., Shearman, M. S., Dellovade, T. L., & Hering, H. (2014). Increased O-GlcNAcylation reduces pathological tau without affecting its normal phosphorylation in a mouse model of tauopathy. *Neuropharmacology*, *79*, 307-313. https://doi.org/10.1016/j.neuropharm.2013.11.025

Grober, E., Dickson, D., Sliwinski, M. J., Buschke, H., Katz, M., Crystal, H., & Lipton, R. B. (1999). Memory and mental status correlates of modified Braak staging. *Neurobiol Aging*, *20*(6), 573-579. https://doi.org/10.1016/s0197-4580(99)00063-9

Grothe, M., Heinsen, H., & Teipel, S. J. (2012). Atrophy of the cholinergic Basal forebrain over the adult age range and in early stages of Alzheimer's disease. *Biol Psychiatry*, *71*(9), 805-813. https://doi.org/10.1016/j.biopsych.2011.06.019

Grothe, M. J., Barthel, H., Sepulcre, J., Dyrba, M., Sabri, O., Teipel, S. J., & Alzheimer's Disease Neuroimaging, I. (2017). In vivo staging of regional amyloid deposition. *Neurology*, *89*(20), 2031-2038. https://doi.org/10.1212/WNL.0000000000004643

Grover, A., Houlden, H., Baker, M., Adamson, J., Lewis, J., Prihar, G., Pickering-Brown, S., Duff, K., & Hutton, M. (1999). 5' splice site mutations in tau associated with the inherited dementia FTDP-17 affect a stem-loop structure that regulates alternative splicing of exon 10. *J Biol Chem*, *274*(21), 15134-15143. https://doi.org/10.1074/jbc.274.21.15134

Grundke-Iqbal, I., Iqbal, K., Quinlan, M., Tung, Y. C., Zaidi, M. S., & Wisniewski, H. M. (1986). Microtubule-associated protein tau. A component of Alzheimer paired helical filaments. *J Biol Chem*, *261*(13), 6084-6089. https://www.ncbi.nlm.nih.gov/pubmed/3084478

Grundke-Iqbal, I., Iqbal, K., Tung, Y. C., Quinlan, M., Wisniewski, H. M., & Binder, L. I. (1986). Abnormal phosphorylation of the microtubule-associated protein tau (tau) in Alzheimer cytoskeletal pathology. *Proc Natl Acad Sci U S A*, *83*(13), 4913-4917. https://doi.org/10.1073/pnas.83.13.4913

Grune, T., Botzen, D., Engels, M., Voss, P., Kaiser, B., Jung, T., Grimm, S., Ermak, G., & Davies, K. J. (2010). Tau protein degradation is catalyzed by the ATP/ubiquitin-independent 20S proteasome under normal cell conditions. *Arch Biochem Biophys*, *500*(2), 181-188. https://doi.org/10.1016/j.abb.2010.05.008

Grupe, A., Abraham, R., Li, Y., Rowland, C., Hollingworth, P., Morgan, A., Jehu, L., Segurado, R., Stone, D., Schadt, E., Karnoub, M., Nowotny, P., Tacey, K., Catanese, J., Sninsky, J., Brayne, C., Rubinsztein, D., Gill, M., Lawlor, B., . . . Williams, J. (2007). Evidence for novel susceptibility genes for late-onset Alzheimer's disease from a genome-wide association study of putative functional variants. *Hum Mol Genet*, *16*(8), 865-873. https://doi.org/10.1093/hmg/ddm031

Guerra, G. P., Rubin, M. A., & Mello, C. F. (2016). Modulation of learning and memory by natural polyamines. *Pharmacol Res*, *112*, 99-118. https://doi.org/10.1016/j.phrs.2016.03.023

Guillozet, A. L., Weintraub, S., Mash, D. C., & Mesulam, M. M. (2003). Neurofibrillary tangles, amyloid, and memory in aging and mild cognitive impairment. *Arch Neurol*, *60*(5), 729-736. https://doi.org/10.1001/archneur.60.5.729

Guillozet-Bongaarts, A. L., Cahill, M. E., Cryns, V. L., Reynolds, M. R., Berry, R. W., & Binder, L. I. (2006). Pseudophosphorylation of tau at serine 422 inhibits caspase cleavage: in vitro evidence and implications for tangle formation in vivo. *J Neurochem*, *97*(4), 1005-1014. https://doi.org/10.1111/j.1471-4159.2006.03784.x

Guillozet-Bongaarts, A. L., Garcia-Sierra, F., Reynolds, M. R., Horowitz, P. M., Fu, Y., Wang, T., Cahill, M. E., Bigio, E. H., Berry, R. W., & Binder, L. I. (2005). Tau truncation during neurofibrillary tangle evolution in Alzheimer's disease. *Neurobiol Aging*, *26*(7), 1015-1022. https://doi.org/10.1016/j.neurobiolaging.2004.09.019

Guillozet-Bongaarts, A. L., Glajch, K. E., Libson, E. G., Cahill, M. E., Bigio, E., Berry, R. W., & Binder, L. I. (2007). Phosphorylation and cleavage of tau in non-AD tauopathies. *Acta Neuropathol*, *113*(5), 513-520. https://doi.org/10.1007/s00401-007-0209-6

Guo, J. L., & Lee, V. M. (2011). Seeding of normal Tau by pathological Tau conformers drives pathogenesis of Alzheimer-like tangles. *J Biol Chem*, *286*(17), 15317-15331. https://doi.org/10.1074/jbc.M110.209296

Guo, J. L., & Lee, V. M. (2013). Neurofibrillary tangle-like tau pathology induced by synthetic tau fibrils in primary neurons over-expressing mutant tau. *FEBS Lett*, *587*(6), 717-723. https://doi.org/10.1016/j.febslet.2013.01.051

Guo, T., Noble, W., & Hanger, D. P. (2017). Roles of tau protein in health and disease. *Acta Neuropathol*, *133*(5), 665-704. https://doi.org/10.1007/s00401-017-1707-9

Gustke, N., Trinczek, B., Biernat, J., Mandelkow, E. M., & Mandelkow, E. (1994). Domains of tau protein and interactions with microtubules. *Biochemistry*, *33*(32), 9511-9522. https://doi.org/10.1021/bi00198a017

Haase, C., Stieler, J. T., Arendt, T., & Holzer, M. (2004). Pseudophosphorylation of tau protein alters its ability for self-aggregation. *J Neurochem*, *88*(6), 1509-1520. https://doi.org/10.1046/j.1471-4159.2003.02287.x

Haj-Yahya, M., Gopinath, P., Rajasekhar, K., Mirbaha, H., Diamond, M. I., & Lashuel, H. A. (2020). Site-Specific Hyperphosphorylation Inhibits, Rather than Promotes, Tau Fibrillization, Seeding Capacity, and Its Microtubule Binding. *Angew Chem Int Ed Engl*, *59*(10), 4059-4067. https://doi.org/10.1002/anie.201913001

Haj-Yahya, M., & Lashuel, H. A. (2018). Protein Semisynthesis Provides Access to Tau Disease-Associated Post-translational Modifications (PTMs) and Paves the Way to Deciphering the Tau PTM Code in Health and Diseased States. *J Am Chem Soc*, *140*(21), 6611-6621. https://doi.org/10.1021/jacs.8b02668

Halverson, R. A., Lewis, J., Frausto, S., Hutton, M., & Muma, N. A. (2005). Tau protein is cross-linked by transglutaminase in P301L tau transgenic mice. *J Neurosci*, *25*(5), 1226-1233. https://doi.org/10.1523/JNEUROSCI.3263-04.2005

Hamdane, M., Sambo, A. V., Delobel, P., Begard, S., Violleau, A., Delacourte, A., Bertrand, P., Benavides, J., & Buee, L. (2003). Mitotic-like tau phosphorylation by p25-Cdk5 kinase complex. *J Biol Chem*, *278*(36), 34026-34034. https://doi.org/10.1074/jbc.M302872200

Hampel, H., Hardy, J., Blennow, K., Chen, C., Perry, G., Kim, S. H., Villemagne, V. L., Aisen, P., Vendruscolo, M., Iwatsubo, T., Masters, C. L., Cho, M., Lannfelt, L., Cummings, J. L., & Vergallo, A. (2021). The Amyloid-beta Pathway in Alzheimer's Disease. *Mol Psychiatry*, *26*(10), 5481-5503. https://doi.org/10.1038/s41380-021-01249-0

Hasegawa, M., Smith, M. J., & Goedert, M. (1998). Tau proteins with FTDP-17 mutations have a reduced ability to promote microtubule assembly. *FEBS Lett*, *437*(3), 207-210. https://doi.org/10.1016/s0014-5793(98)01217-4

Hastings, N. B., Wang, X., Song, L., Butts, B. D., Grotz, D., Hargreaves, R., Fred Hess, J., Hong, K. K., Huang, C. R., Hyde, L., Laverty, M., Lee, J., Levitan, D., Lu, S. X., Maguire, M., Mahadomrongkul, V., McEachern, E. J., Ouyang, X., Rosahl, T. W., . . . Zhang, L. (2017). Inhibition of O-GlcNAcase leads to elevation of O-GlcNAc tau and reduction of tauopathy and cerebrospinal fluid tau in rTg4510 mice. *Mol Neurodegener*, *12*(1), 39. https://doi.org/10.1186/s13024-017-0181-0

Hauw, J. J., Verny, M., Delaere, P., Cervera, P., He, Y., & Duyckaerts, C. (1990). Constant neurofibrillary changes in the neocortex in progressive supranuclear palsy. Basic differences with Alzheimer's disease and aging. *Neurosci Lett*, *119*(2), 182-186. https://doi.org/10.1016/0304-3940(90)90829-x

He, X., Man, V. H., Gao, J., & Wang, J. (2023). Investigation of the Structure of Full-Length Tau Proteins with Coarse-Grained and All-Atom Molecular Dynamics Simulations. *ACS Chem Neurosci*, *14*(2), 209-217. https://doi.org/10.1021/acschemneuro.2c00381

Heckman, K. L., & Pease, L. R. (2007). Gene splicing and mutagenesis by PCR-driven overlap extension. *Nat Protoc*, *2*(4), 924-932. https://doi.org/10.1038/nprot.2007.132

Heinonen, O., Soininen, H., Sorvari, H., Kosunen, O., Paljarvi, L., Koivisto, E., & Riekkinen, P. J., Sr. (1995). Loss of synaptophysin-like immunoreactivity in the hippocampal formation is an early phenomenon in Alzheimer's disease. *Neuroscience*, *64*(2), 375-384. https://doi.org/10.1016/0306-4522(94)00422-2

Hendriks, I. A., Lyon, D., Su, D., Skotte, N. H., Daniel, J. A., Jensen, L. J., & Nielsen, M. L. (2018). Site-specific characterization of endogenous SUMOylation across species and organs. *Nat Commun*, *9*(1), 2456. https://doi.org/10.1038/s41467-018-04957-4

Henley, J. M., Craig, T. J., & Wilkinson, K. A. (2014). Neuronal SUMOylation: mechanisms, physiology, and roles in neuronal dysfunction. *Physiol Rev*, *94*(4), 1249-1285. https://doi.org/10.1152/physrev.00008.2014

Herrup, K. (2015). The case for rejecting the amyloid cascade hypothesis. *Nat Neurosci*, *18*(6), 794-799. https://doi.org/10.1038/nn.4017

Hershko, A., Heller, H., Elias, S., & Ciechanover, A. (1983). Components of ubiquitin-protein ligase system. Resolution, affinity purification, and role in protein breakdown. *J Biol Chem*, *258*(13), 8206-8214. https://www.ncbi.nlm.nih.gov/pubmed/6305978

Hill, E., Karikari, T. K., Moffat, K. G., Richardson, M. J. E., & Wall, M. J. (2019). Introduction of Tau Oligomers into Cortical Neurons Alters Action Potential Dynamics and Disrupts Synaptic Transmission and Plasticity. *eNeuro*, *6*(5). https://doi.org/10.1523/ENEURO.0166-19.2019

Hintermayer, M. A., Volkening, K., Moszczynski, A. J., Donison, N., & Strong, M. J. (2020). Tau protein phosphorylation at Thr(175) initiates fibril formation via accessibility of the N-terminal phosphatase-activating domain. *J Neurochem*, *155*(3), 313-326. https://doi.org/10.1111/jnc.14942

Hippius, H., & Neundorfer, G. (2003). The discovery of Alzheimer's disease. *Dialogues Clin Neurosci*, *5*(1), 101-108. https://doi.org/10.31887/DCNS.2003.5.1/hhippius

Hitt, B. D., Gupta, A., Singh, R., Yang, T., Beaver, J. D., Shang, P., White, C. L., 3rd, Joachimiak, L. A., & Diamond, M. I. (2023). Anti-tau antibodies targeting a conformation-

dependent epitope selectively bind seeds. *J Biol Chem*, *299*(11), 105252. https://doi.org/10.1016/j.jbc.2023.105252

Ho, C. S., Lam, C. W., Chan, M. H., Cheung, R. C., Law, L. K., Lit, L. C., Ng, K. F., Suen, M. W., & Tai, H. L. (2003). Electrospray ionisation mass spectrometry: principles and clinical applications. *Clin Biochem Rev*, *24*(1), 3-12. https://www.ncbi.nlm.nih.gov/pubmed/18568044

https://www.ncbi.nlm.nih.gov/pmc/articles/PMC1853331/pdf/cbr24_1p003.pdf

Hochmair, J., Exner, C., Betzel, C., Mandelkow, E., & Wegmann, S. (2023). Light Microscopy and Dynamic Light Scattering to Study Liquid-Liquid Phase Separation of Tau Proteins In Vitro. *Methods Mol Biol*, *2551*, 225-243. https://doi.org/10.1007/978-1-0716-2597-2_15

Hoffmann, R., Lee, V. M., Leight, S., Varga, I., & Otvos, L., Jr. (1997). Unique Alzheimer's disease paired helical filament specific epitopes involve double phosphorylation at specific sites. *Biochemistry*, *36*(26), 8114-8124. https://doi.org/10.1021/bi970380+

Holehouse, A. S., & Kragelund, B. B. (2024). The molecular basis for cellular function of intrinsically disordered protein regions. *Nat Rev Mol Cell Biol*, *25*(3), 187-211. https://doi.org/10.1038/s41580-023-00673-0

Holmes, B. B., DeVos, S. L., Kfoury, N., Li, M., Jacks, R., Yanamandra, K., Ouidja, M. O., Brodsky, F. M., Marasa, J., Bagchi, D. P., Kotzbauer, P. T., Miller, T. M., Papy-Garcia, D., & Diamond, M. I. (2013). Heparan sulfate proteoglycans mediate internalization and propagation of specific proteopathic seeds. *Proc Natl Acad Sci U S A*, *110*(33), E3138-3147. https://doi.org/10.1073/pnas.1301440110

Holmes, B. B., Furman, J. L., Mahan, T. E., Yamasaki, T. R., Mirbaha, H., Eades, W. C., Belaygorod, L., Cairns, N. J., Holtzman, D. M., & Diamond, M. I. (2014). Proteopathic tau seeding predicts tauopathy in vivo. *Proc Natl Acad Sci U S A*, *111*(41), E4376-4385. https://doi.org/10.1073/pnas.1411649111

Hong, M., Zhukareva, V., Vogelsberg-Ragaglia, V., Wszolek, Z., Reed, L., Miller, B. I., Geschwind, D. H., Bird, T. D., McKeel, D., Goate, A., Morris, J. C., Wilhelmsen, K. C., Schellenberg, G. D., Trojanowski, J. Q., & Lee, V. M. (1998). Mutation-specific functional impairments in distinct tau isoforms of hereditary FTDP-17. *Science*, *282*(5395), 1914-1917. https://doi.org/10.1126/science.282.5395.1914

Hornakova, L., Sinsky, J., Janubova, M., Mederlyova, A., Paulenka Ivanovova, N., Piestansky, J., Kovac, A., Galba, J., Skrabana, R., & Cehlar, O. (2022). Interaction kinetics reveal distinct properties of conformational ensembles of three-repeat and four-repeat tau proteins. *FEBS Lett*, *596*(9), 1178-1189. https://doi.org/10.1002/1873-3468.14339

Horowitz, P. M., LaPointe, N., Guillozet-Bongaarts, A. L., Berry, R. W., & Binder, L. I. (2006). N-terminal fragments of tau inhibit full-length tau polymerization in vitro. *Biochemistry*, *45*(42), 12859-12866. https://doi.org/10.1021/bi061325g

Horowitz, P. M., Patterson, K. R., Guillozet-Bongaarts, A. L., Reynolds, M. R., Carroll, C. A., Weintraub, S. T., Bennett, D. A., Cryns, V. L., Berry, R. W., & Binder, L. I. (2004). Early N-terminal changes and caspase-6 cleavage of tau in Alzheimer's disease. *J Neurosci*, *24*(36), 7895-7902. https://doi.org/10.1523/JNEUROSCI.1988-04.2004

Hou, Z., Chen, D., Ryder, B. D., & Joachimiak, L. A. (2021). Biophysical properties of a tau seed. *Sci Rep*, *11*(1), 13602. https://doi.org/10.1038/s41598-021-93093-z

Hough, R., Pratt, G., & Rechsteiner, M. (1986). Ubiquitin-lysozyme conjugates. Identification and characterization of an ATP-dependent protease from rabbit reticulocyte lysates. *J Biol Chem*, *261*(5), 2400-2408. https://www.ncbi.nlm.nih.gov/pubmed/3003114

Huang, A., & Stultz, C. M. (2008). The effect of a DeltaK280 mutation on the unfolded state of a microtubule-binding repeat in Tau. *PLoS Comput Biol*, *4*(8), e1000155. https://doi.org/10.1371/journal.pcbi.1000155

Hunt, J. B., Jr., Nash, K. R., Placides, D., Moran, P., Selenica, M. L., Abuqalbeen, F., Ratnasamy, K., Slouha, N., Rodriguez-Ospina, S., Savlia, M., Ranaweera, Y., Reid, P., Dickey, C. A., Uricia, R., Yang, C. G., Sandusky, L. A., Gordon, M. N., Morgan, D., & Lee, D. C. (2015). Sustained Arginase 1 Expression Modulates Pathological Tau Deposits in a Mouse Model of Tauopathy. *J Neurosci*, *35*(44), 14842-14860. https://doi.org/10.1523/JNEUROSCI.3959-14.2015

Huseby, C. J., Hoffman, C. N., Cooper, G. L., Cocuron, J. C., Alonso, A. P., Thomas, S. N., Yang, A. J., & Kuret, J. (2019). Quantification of Tau Protein Lysine Methylation in Aging and Alzheimer's Disease. *J Alzheimers Dis*, *71*(3), 979-991. https://doi.org/10.3233/JAD-190604

Hutton, M., Lendon, C. L., Rizzu, P., Baker, M., Froelich, S., Houlden, H., Pickering-Brown, S., Chakraverty, S., Isaacs, A., Grover, A., Hackett, J., Adamson, J., Lincoln, S., Dickson, D., Davies, P., Petersen, R. C., Stevens, M., de Graaff, E., Wauters, E., . . . Heutink, P. (1998). Association of missense and 5'-splice-site mutations in tau with the inherited dementia FTDP-17. *Nature*, *393*(6686), 702-705. https://doi.org/10.1038/31508

Hyman, B. T., Kromer, L. J., & Van Hoesen, G. W. (1988). A direct demonstration of the perforant pathway terminal zone in Alzheimer's disease using the monoclonal antibody Alz-50. *Brain Res*, *450*(1-2), 392-397. https://doi.org/10.1016/0006-8993(88)91582-x

Hyman, B. T., Van Hoesen, G. W., Damasio, A. R., & Barnes, C. L. (1984). Alzheimer's disease: cell-specific pathology isolates the hippocampal formation. *Science*, *225*(4667), 1168-1170. https://doi.org/10.1126/science.6474172

Hyman, B. T., Van Hoesen, G. W., Kromer, L. J., & Damasio, A. R. (1986). Perforant pathway changes and the memory impairment of Alzheimer's disease. *Ann Neurol*, *20*(4), 472-481. https://doi.org/10.1002/ana.410200406

Hyman, B. T., Van Hoesen, G. W., Wolozin, B. L., Davies, P., Kromer, L. J., & Damasio, A. R. (1988). Alz-50 antibody recognizes Alzheimer-related neuronal changes. *Ann Neurol*, *23*(4), 371-379. https://doi.org/10.1002/ana.410230410

Iba, M., Guo, J. L., McBride, J. D., Zhang, B., Trojanowski, J. Q., & Lee, V. M. (2013). Synthetic tau fibrils mediate transmission of neurofibrillary tangles in a transgenic mouse model of Alzheimer's-like tauopathy. *J Neurosci*, *33*(3), 1024-1037. https://doi.org/10.1523/JNEUROSCI.2642-12.2013

Ibanez, V., Pietrini, P., Alexander, G. E., Furey, M. L., Teichberg, D., Rajapakse, J. C., Rapoport, S. I., Schapiro, M. B., & Horwitz, B. (1998). Regional glucose metabolic abnormalities are not the result of atrophy in Alzheimer's disease. *Neurology*, *50*(6), 1585-1593. https://doi.org/10.1212/wnl.50.6.1585

Igarashi, K., & Kashiwagi, K. (2019). The functional role of polyamines in eukaryotic cells. *Int J Biochem Cell Biol*, *107*, 104-115. https://doi.org/10.1016/j.biocel.2018.12.012

Ikegami, K., Kimura, T., Katsuragi, S., Ono, T., Yamamoto, H., Miyamoto, E., & Miyakawa, T. (1996). Immunohistochemical examination of phosphorylated tau in granulovacuolar degeneration granules. *Psychiatry Clin Neurosci*, *50*(3), 137-140. https://doi.org/10.1111/j.1440-1819.1996.tb01678.x

Inoue, K., Tsutsui, H., Akatsu, H., Hashizume, Y., Matsukawa, N., Yamamoto, T., & Toyo'oka, T. (2013). Metabolic profiling of Alzheimer's disease brains. *Sci Rep*, *3*, 2364. https://doi.org/10.1038/srep02364

Irwin, D. J. (2016). Tauopathies as clinicopathological entities. *Parkinsonism Relat Disord*, *22 Suppl 1*(0 1), S29-33. https://doi.org/10.1016/j.parkreldis.2015.09.020

Irwin, D. J., Cohen, T. J., Grossman, M., Arnold, S. E., McCarty-Wood, E., Van Deerlin, V. M., Lee, V. M., & Trojanowski, J. Q. (2013). Acetylated tau neuropathology in sporadic and hereditary tauopathies. *Am J Pathol*, *183*(2), 344-351. https://doi.org/10.1016/j.ajpath.2013.04.025

Irwin, D. J., Cohen, T. J., Grossman, M., Arnold, S. E., Xie, S. X., Lee, V. M., & Trojanowski, J. Q. (2012). Acetylated tau, a novel pathological signature in Alzheimer's disease and other tauopathies. *Brain*, *135*(Pt 3), 807-818. https://doi.org/10.1093/brain/aws013

Ivanov, S. M., Atanasova, M., Dimitrov, I., & Doytchinova, I. A. (2020). Cellular polyamines condense hyperphosphorylated Tau, triggering Alzheimer's disease. *Sci Rep*, *10*(1), 10098. https://doi.org/10.1038/s41598-020-67119-x

Iwatsubo, T., Hasegawa, M., Esaki, Y., & Ihara, Y. (1992). Lack of ubiquitin immunoreactivities at both ends of neuropil threads. Possible bidirectional growth of neuropil threads. *Am J Pathol*, *140*(2), 277-282. https://www.ncbi.nlm.nih.gov/pubmed/1310831

https://www.ncbi.nlm.nih.gov/pmc/articles/PMC1886416/pdf/amjpathol00086-0035.pdf

Jack, C. R., Jr., Bennett, D. A., Blennow, K., Carrillo, M. C., Dunn, B., Haeberlein, S. B., Holtzman, D. M., Jagust, W., Jessen, F., Karlawish, J., Liu, E., Molinuevo, J. L., Montine, T., Phelps, C., Rankin, K. P., Rowe, C. C., Scheltens, P., Siemers, E., Snyder, H. M., . . . Contributors. (2018). NIA-AA Research Framework: Toward a biological definition of Alzheimer's disease. *Alzheimers Dement*, *14*(4), 535-562. https://doi.org/10.1016/j.jalz.2018.02.018

Jack, C. R., Jr., Knopman, D. S., Jagust, W. J., Shaw, L. M., Aisen, P. S., Weiner, M. W., Petersen, R. C., & Trojanowski, J. Q. (2010). Hypothetical model of dynamic biomarkers of the Alzheimer's pathological cascade. *Lancet Neurol*, *9*(1), 119-128. https://doi.org/10.1016/S1474-4422(09)70299-6

Jackson, S. J., Kerridge, C., Cooper, J., Cavallini, A., Falcon, B., Cella, C. V., Landi, A., Szekeres, P. G., Murray, T. K., Ahmed, Z., Goedert, M., Hutton, M., O'Neill, M. J., & Bose, S. (2016). Short Fibrils Constitute the Major Species of Seed-Competent Tau in the Brains of Mice Transgenic for Human P301S Tau. *J Neurosci*, *36*(3), 762-772. https://doi.org/10.1523/JNEUROSCI.3542-15.2016

Jeganathan, S., Hascher, A., Chinnathambi, S., Biernat, J., Mandelkow, E. M., & Mandelkow, E. (2008). Proline-directed pseudo-phosphorylation at AT8 and PHF1 epitopes induces a compaction of the paperclip folding of Tau and generates a pathological (MC-1) conformation. *J Biol Chem*, *283*(46), 32066-32076. https://doi.org/10.1074/jbc.M805300200

Jeganathan, S., von Bergen, M., Brutlach, H., Steinhoff, H. J., & Mandelkow, E. (2006). Global hairpin folding of tau in solution. *Biochemistry*, *45*(7), 2283-2293. https://doi.org/10.1021/bi0521543

Jiang, L., Lin, W., Zhang, C., Ash, P. E. A., Verma, M., Kwan, J., van Vliet, E., Yang, Z., Cruz, A. L., Boudeau, S., Maziuk, B. F., Lei, S., Song, J., Alvarez, V. E., Hovde, S., Abisambra, J. F., Kuo, M. H., Kanaan, N., Murray, M. E., . . . Wolozin, B. (2021). Interaction of tau with HNRNPA2B1 and N(6)-methyladenosine RNA mediates the progression of tauopathy. *Mol Cell*, *81*(20), 4209-4227 e4212. https://doi.org/10.1016/j.molcel.2021.07.038

Jiang, L., Zhao, J., Cheng, J. X., & Wolozin, B. (2020). Tau Oligomers and Fibrils Exhibit Differential Patterns of Seeding and Association With RNA Binding Proteins. *Front Neurol*, *11*, 579434. https://doi.org/10.3389/fneur.2020.579434

Jicha, G. A., Bowser, R., Kazam, I. G., & Davies, P. (1997). Alz-50 and MC-1, a new monoclonal antibody raised to paired helical filaments, recognize conformational epitopes on recombinant tau. *J Neurosci Res*, *48*(2), 128-132. https://doi.org/10.1002/(sici)1097-4547(19970415)48:2<128::aid-jnr5>3.0.co;2-e

Johnson, E. S., & Blobel, G. (1997). Ubc9p is the conjugating enzyme for the ubiquitin-like protein Smt3p. *J Biol Chem*, *272*(43), 26799-26802. https://doi.org/10.1074/jbc.272.43.26799

Johnson, E. S., Schwienhorst, I., Dohmen, R. J., & Blobel, G. (1997). The ubiquitin-like protein Smt3p is activated for conjugation to other proteins by an Aos1p/Uba2p heterodimer. *EMBO J*, *16*(18), 5509-5519. https://doi.org/10.1093/emboj/16.18.5509

Johnson, G. V., Cox, T. M., Lockhart, J. P., Zinnerman, M. D., Miller, M. L., & Powers, R. E. (1997). Transglutaminase activity is increased in Alzheimer's disease brain. *Brain Res*, *751*(2), 323-329. https://doi.org/10.1016/s0006-8993(96)01431-x

Josephs, K. A. (2017). Current Understanding of Neurodegenerative Diseases Associated With the Protein Tau. *Mayo Clin Proc*, *92*(8), 1291-1303. https://doi.org/10.1016/j.mayocp.2017.04.016

Josephs, K. A., Boeve, B. F., Duffy, J. R., Smith, G. E., Knopman, D. S., Parisi, J. E., Petersen, R. C., & Dickson, D. W. (2005). Atypical progressive supranuclear palsy underlying progressive apraxia of speech and nonfluent aphasia. *Neurocase*, *11*(4), 283-296. https://doi.org/10.1080/13554790590963004

Josephs, K. A., Katsuse, O., Beccano-Kelly, D. A., Lin, W. L., Uitti, R. J., Fujino, Y., Boeve, B. F., Hutton, M. L., Baker, M. C., & Dickson, D. W. (2006). Atypical progressive supranuclear palsy with corticospinal tract degeneration. *J Neuropathol Exp Neurol*, *65*(4), 396-405. https://doi.org/10.1097/01.jnen.0000218446.38158.61

Josephs, K. A., Whitwell, J. L., Ahmed, Z., Shiung, M. M., Weigand, S. D., Knopman, D. S., Boeve, B. F., Parisi, J. E., Petersen, R. C., Dickson, D. W., & Jack, C. R., Jr. (2008). Beta-amyloid burden is not associated with rates of brain atrophy. *Ann Neurol*, *63*(2), 204-212. https://doi.org/10.1002/ana.21223

Julien, C., Tremblay, C., Emond, V., Lebbadi, M., Salem, N., Jr., Bennett, D. A., & Calon, F. (2009). Sirtuin 1 reduction parallels the accumulation of tau in Alzheimer disease. *J Neuropathol Exp Neurol*, *68*(1), 48-58. https://doi.org/10.1097/NEN.0b013e3181922348

Kadavath, H., Cabrales Fontela, Y., Jaremko, M., Jaremko, L., Overkamp, K., Biernat, J., Mandelkow, E., & Zweckstetter, M. (2018). The Binding Mode of a Tau Peptide with Tubulin. *Angew Chem Int Ed Engl*, *57*(12), 3246-3250. https://doi.org/10.1002/anie.201712089

Kadavath, H., Hofele, R. V., Biernat, J., Kumar, S., Tepper, K., Urlaub, H., Mandelkow, E., & Zweckstetter, M. (2015). Tau stabilizes microtubules by binding at the interface between tubulin heterodimers. *Proc Natl Acad Sci U S A*, *112*(24), 7501-7506. https://doi.org/10.1073/pnas.1504081112

Kamah, A., Huvent, I., Cantrelle, F. X., Qi, H., Lippens, G., Landrieu, I., & Smet-Nocca, C. (2014). Nuclear magnetic resonance analysis of the acetylation pattern of the neuronal Tau protein. *Biochemistry*, *53*(18), 3020-3032. https://doi.org/10.1021/bi500006v

Kametani, F., Yoshida, M., Matsubara, T., Murayama, S., Saito, Y., Kawakami, I., Onaya, M., Tanaka, H., Kakita, A., Robinson, A. C., Mann, D. M. A., & Hasegawa, M. (2020). Comparison of Common and Disease-Specific Post-translational Modifications of Pathological Tau Associated With a Wide Range of Tauopathies. *Front Neurosci*, *14*, 581936. https://doi.org/10.3389/fnins.2020.581936

Kanaan, N. M. (2024). Tau here, tau there, tau almost everywhere: Clarifying the distribution of tau in the adult CNS. *Cytoskeleton (Hoboken)*, *81*(1), 107-115. https://doi.org/10.1002/cm.21820

Kanaan, N. M., Cox, K., Alvarez, V. E., Stein, T. D., Poncil, S., & McKee, A. C. (2016). Characterization of Early Pathological Tau Conformations and Phosphorylation in Chronic Traumatic Encephalopathy. *J Neuropathol Exp Neurol*, *75*(1), 19-34. https://doi.org/10.1093/jnen/nlv001

Kanaan, N. M., & Grabinski, T. (2021). Neuronal and Glial Distribution of Tau Protein in the Adult Rat and Monkey. *Front Mol Neurosci*, *14*, 607303. https://doi.org/10.3389/fnmol.2021.607303

Kanaan, N. M., Hamel, C., Grabinski, T., & Combs, B. (2020). Liquid-liquid phase separation induces pathogenic tau conformations in vitro. *Nat Commun*, *11*(1), 2809. https://doi.org/10.1038/s41467-020-16580-3

Kanaan, N. M., Morfini, G., Pigino, G., LaPointe, N. E., Andreadis, A., Song, Y., Leitman, E., Binder, L. I., & Brady, S. T. (2012). Phosphorylation in the amino terminus of tau prevents inhibition of anterograde axonal transport. *Neurobiol Aging*, *33*(4), 826 e815-830. https://doi.org/10.1016/j.neurobiolaging.2011.06.006

Kanaan, N. M., Morfini, G. A., LaPointe, N. E., Pigino, G. F., Patterson, K. R., Song, Y., Andreadis, A., Fu, Y., Brady, S. T., & Binder, L. I. (2011). Pathogenic forms of tau inhibit kinesin-dependent axonal transport through a mechanism involving activation of axonal phosphotransferases. *J Neurosci*, *31*(27), 9858-9868. https://doi.org/10.1523/JNEUROSCI.0560-11.2011

Kang, S. G., Eskandari-Sedighi, G., Hromadkova, L., Safar, J. G., & Westaway, D. (2020). Cellular Biology of Tau Diversity and Pathogenic Conformers. *Front Neurol*, *11*, 590199. https://doi.org/10.3389/fneur.2020.590199

Karenberg, A. (2001). [Early history of Pick's disease]. *Fortschr Neurol Psychiatr*, *69*(11), 545-550. https://doi.org/10.1055/s-2001-18378 (Zur Fruhgeschichte der Pickschen Erkrankung.)

Karran, E., Mercken, M., & De Strooper, B. (2011). The amyloid cascade hypothesis for Alzheimer's disease: an appraisal for the development of therapeutics. *Nat Rev Drug Discov*, *10*(9), 698-712. https://doi.org/10.1038/nrd3505

Kaufman, S. K., Del Tredici, K., Thomas, T. L., Braak, H., & Diamond, M. I. (2018). Tau seeding activity begins in the transentorhinal/entorhinal regions and anticipates phospho-tau pathology in Alzheimer's disease and PART. *Acta Neuropathol*, *136*(1), 57-67. https://doi.org/10.1007/s00401-018-1855-6

Kaufman, S. K., Sanders, D. W., Thomas, T. L., Ruchinskas, A. J., Vaquer-Alicea, J., Sharma, A. M., Miller, T. M., & Diamond, M. I. (2016). Tau Prion Strains Dictate Patterns of Cell Pathology, Progression Rate, and Regional Vulnerability In Vivo. *Neuron*, *92*(4), 796-812. https://doi.org/10.1016/j.neuron.2016.09.055

Keck, S., Nitsch, R., Grune, T., & Ullrich, O. (2003). Proteasome inhibition by paired helical filament-tau in brains of patients with Alzheimer's disease. *J Neurochem*, *85*(1), 115-122. https://doi.org/10.1046/j.1471-4159.2003.01642.x

Keller, J. N., Hanni, K. B., & Markesbery, W. R. (2000). Impaired proteasome function in Alzheimer's disease. *J Neurochem*, *75*(1), 436-439. https://doi.org/10.1046/j.1471-4159.2000.0750436.x

Kepp, K. P., Robakis, N. K., Hoilund-Carlsen, P. F., Sensi, S. L., & Vissel, B. (2023). The amyloid cascade hypothesis: an updated critical review. *Brain*, *146*(10), 3969-3990. https://doi.org/10.1093/brain/awad159

Kidd, M. (1963). Paired helical filaments in electron microscopy of Alzheimer's disease. *Nature*, *197*, 192-193. https://doi.org/10.1038/197192b0

Kim, J. H., Lee, J., Choi, W. H., Park, S., Park, S. H., Lee, J. H., Lim, S. M., Mun, J. Y., Cho, H. S., Han, D., Suh, Y. H., & Lee, M. J. (2021). CHIP-mediated hyperubiquitylation

of tau promotes its self-assembly into the insoluble tau filaments. *Chem Sci*, *12*(15), 5599-5610. https://doi.org/10.1039/d1sc00586c

Kimura, T., Ono, T., Takamatsu, J., Yamamoto, H., Ikegami, K., Kondo, A., Hasegawa, M., Ihara, Y., Miyamoto, E., & Miyakawa, T. (1996). Sequential changes of tau-site-specific phosphorylation during development of paired helical filaments. *Dementia*, *7*(4), 177-181. https://doi.org/10.1159/000106875

King, M. E., Gamblin, T. C., Kuret, J., & Binder, L. I. (2000). Differential assembly of human tau isoforms in the presence of arachidonic acid. *J Neurochem*, *74*(4), 1749-1757. https://doi.org/10.1046/j.1471-4159.2000.0741749.x

King, M. E., Ghoshal, N., Wall, J. S., Binder, L. I., & Ksiezak-Reding, H. (2001). Structural analysis of Pick's disease-derived and in vitro-assembled tau filaments. *Am J Pathol*, *158*(4), 1481-1490. https://doi.org/10.1016/S0002-9440(10)64099-0

Kito, K., & Ito, T. (2008). Mass spectrometry-based approaches toward absolute quantitative proteomics. *Curr Genomics*, *9*(4), 263-274. https://doi.org/10.2174/138920208784533647

Kjaergaard, M., Dear, A. J., Kundel, F., Qamar, S., Meisl, G., Knowles, T. P. J., & Klenerman, D. (2018). Oligomer Diversity during the Aggregation of the Repeat Region of Tau. *ACS Chem Neurosci*, *9*(12), 3060-3071. https://doi.org/10.1021/acschemneuro.8b00250

Kneynsberg, A., Combs, B., Christensen, K., Morfini, G., & Kanaan, N. M. (2017). Axonal Degeneration in Tauopathies: Disease Relevance and Underlying Mechanisms. *Front Neurosci*, *11*, 572. https://doi.org/10.3389/fnins.2017.00572

Komiya, M., Ito, A., Endo, M., Hiruma, D., Hattori, M., Saitoh, H., Yoshida, M., & Ozawa, T. (2017). A genetic screen to discover SUMOylated proteins in living mammalian cells. *Sci Rep*, *7*(1), 17443. https://doi.org/10.1038/s41598-017-17450-7

Konno, T., Morii, T., Hirata, A., Sato, S., Oiki, S., & Ikura, K. (2005). Covalent blocking of fibril formation and aggregation of intracellular amyloidgenic proteins by transglutaminase-catalyzed intramolecular cross-linking. *Biochemistry*, *44*(6), 2072-2079. https://doi.org/10.1021/bi047722d

Kopke, E., Tung, Y. C., Shaikh, S., Alonso, A. C., Iqbal, K., & Grundke-Iqbal, I. (1993). Microtubule-associated protein tau. Abnormal phosphorylation of a non-paired helical filament pool in Alzheimer disease. *J Biol Chem*, *268*(32), 24374-24384. https://www.ncbi.nlm.nih.gov/pubmed/8226987

Kordower, J. H., Chu, Y., Stebbins, G. T., DeKosky, S. T., Cochran, E. J., Bennett, D., & Mufson, E. J. (2001). Loss and atrophy of layer II entorhinal cortex neurons in elderly people with mild cognitive impairment. *Ann Neurol*, *49*(2), 202-213. https://www.ncbi.nlm.nih.gov/pubmed/11220740

Kosik, K. S., Joachim, C. L., & Selkoe, D. J. (1986). Microtubule-associated protein tau (tau) is a major antigenic component of paired helical filaments in Alzheimer disease. *Proc Natl Acad Sci U S A*, *83*(11), 4044-4048. https://doi.org/10.1073/pnas.83.11.4044

Koss, D. J., Jones, G., Cranston, A., Gardner, H., Kanaan, N. M., & Platt, B. (2016). Soluble pre-fibrillar tau and beta-amyloid species emerge in early human Alzheimer's disease and track disease progression and cognitive decline. *Acta Neuropathol*, *132*(6), 875-895. https://doi.org/10.1007/s00401-016-1632-3

Kovacs, G. G. (2015). Invited review: Neuropathology of tauopathies: principles and practice. *Neuropathol Appl Neurobiol*, *41*(1), 3-23. https://doi.org/10.1111/nan.12208

Kovacs, G. G. (2016). Molecular Pathological Classification of Neurodegenerative Diseases: Turning towards Precision Medicine. *Int J Mol Sci*, *17*(2). https://doi.org/10.3390/ijms17020189

Ksiezak-Reding, H., Davies, P., & Yen, S. H. (1988). Alz 50, a monoclonal antibody to Alzheimer's disease antigen, cross-reacts with tau proteins from bovine and normal human brain. *J Biol Chem*, *263*(17), 7943-7947. https://www.ncbi.nlm.nih.gov/pubmed/3131333

Ksiezak-Reding, H., Morgan, K., & Dickson, D. W. (1994). Tau immunoreactivity and SDS solubility of two populations of paired helical filaments that differ in morphology. *Brain Res*, *649*(1-2), 185-196. https://doi.org/10.1016/0006-8993(94)91063-4

Ksiezak-Reding, H., Tracz, E., Yang, L. S., Dickson, D. W., Simon, M., & Wall, J. S. (1996). Ultrastructural instability of paired helical filaments from corticobasal degeneration as examined by scanning transmission electron microscopy. *Am J Pathol*, *149*(2), 639-651. https://www.ncbi.nlm.nih.gov/pubmed/8702002

https://www.ncbi.nlm.nih.gov/pmc/articles/PMC1865307/pdf/amjpathol00032-0287.pdf

Ksiezak-Reding, H., & Wall, J. S. (2005). Characterization of paired helical filaments by scanning transmission electron microscopy. *Microsc Res Tech*, *67*(3-4), 126-140. https://doi.org/10.1002/jemt.20188

Ksiezak-Reding, H., Yang, G., Simon, M., & Wall, J. S. (1998). Assembled tau filaments differ from native paired helical filaments as determined by scanning transmission electron microscopy (STEM). *Brain Res*, *814*(1-2), 86-98. https://doi.org/10.1016/s0006-8993(98)01052-x

Kuchibhotla, K. V., Wegmann, S., Kopeikina, K. J., Hawkes, J., Rudinskiy, N., Andermann, M. L., Spires-Jones, T. L., Bacskai, B. J., & Hyman, B. T. (2014). Neurofibrillary tangle-bearing neurons are functionally integrated in cortical circuits in vivo. *Proc Natl Acad Sci U S A*, *111*(1), 510-514. https://doi.org/10.1073/pnas.1318807111

Kumar, A., & Zhang, K. Y. (2015). Advances in the development of SUMO specific protease (SENP) inhibitors. *Comput Struct Biotechnol J*, *13*, 204-211. https://doi.org/10.1016/j.csbj.2015.03.001

Kyalu Ngoie Zola, N., Balty, C., Pyr Dit Ruys, S., Vanparys, A. A. T., Huyghe, N. D. G., Herinckx, G., Johanns, M., Boyer, E., Kienlen-Campard, P., Rider, M. H., Vertommen, D., & Hanseeuw, B. J. (2023). Specific post-translational modifications of soluble tau protein distinguishes Alzheimer's disease and primary tauopathies. *Nat Commun*, *14*(1), 3706. https://doi.org/10.1038/s41467-023-39328-1

La Joie, R., Visani, A. V., Baker, S. L., Brown, J. A., Bourakova, V., Cha, J., Chaudhary, K., Edwards, L., Iaccarino, L., Janabi, M., Lesman-Segev, O. H., Miller, Z. A., Perry, D. C., O'Neil, J. P., Pham, J., Rojas, J. C., Rosen, H. J., Seeley, W. W., Tsai, R. M., . . . Rabinovici, G. D. (2020). Prospective longitudinal atrophy in Alzheimer's disease correlates with the intensity and topography of baseline tau-PET. *Sci Transl Med*, *12*(524). https://doi.org/10.1126/scitranslmed.aau5732

Lace, G., Savva, G. M., Forster, G., de Silva, R., Brayne, C., Matthews, F. E., Barclay, J. J., Dakin, L., Ince, P. G., Wharton, S. B., & Mrc, C. (2009). Hippocampal tau pathology is related to neuroanatomical connections: an ageing population-based study. *Brain*, *132*(Pt 5), 1324-1334. https://doi.org/10.1093/brain/awp059

Lane-Donovan, C., & Boxer, A. L. (2024). Disentangling tau: One protein, many therapeutic approaches. *Neurotherapeutics*, *21*(2), e00321. https://doi.org/10.1016/j.neurot.2024.e00321

Lang, A. E., Bergeron, C., Pollanen, M. S., & Ashby, P. (1994). Parietal Pick's disease mimicking cortical-basal ganglionic degeneration. *Neurology*, *44*(8), 1436-1440. https://doi.org/10.1212/wnl.44.8.1436

Langerscheidt, F., Wied, T., Al Kabbani, M. A., van Eimeren, T., Wunderlich, G., & Zempel, H. (2024). Genetic forms of tauopathies: inherited causes and implications of Alzheimer's disease-like TAU pathology in primary and secondary tauopathies. *J Neurol*. https://doi.org/10.1007/s00415-024-12314-3

Langworth-Green, C., Patel, S., Jaunmuktane, Z., Jabbari, E., Morris, H., Thom, M., Lees, A., Hardy, J., Zandi, M., & Duff, K. (2023). Chronic effects of inflammation on tauopathies. *Lancet Neurol*, *22*(5), 430-442. https://doi.org/10.1016/S1474-4422(23)00038-8

LaPointe, N. E., Morfini, G., Pigino, G., Gaisina, I. N., Kozikowski, A. P., Binder, L. I., & Brady, S. T. (2009). The amino terminus of tau inhibits kinesin-dependent axonal transport: implications for filament toxicity. *J Neurosci Res*, *87*(2), 440-451. https://doi.org/10.1002/jnr.21850

Lasagna-Reeves, C. A., Castillo-Carranza, D. L., Sengupta, U., Clos, A. L., Jackson, G. R., & Kayed, R. (2011). Tau oligomers impair memory and induce synaptic and mitochondrial dysfunction in wild-type mice. *Mol Neurodegener*, *6*, 39. https://doi.org/10.1186/1750-1326-6-39

Lasagna-Reeves, C. A., Castillo-Carranza, D. L., Sengupta, U., Sarmiento, J., Troncoso, J., Jackson, G. R., & Kayed, R. (2012). Identification of oligomers at early stages of tau aggregation in Alzheimer's disease. *FASEB J*, *26*(5), 1946-1959. https://doi.org/10.1096/fj.11-199851

Leal, S. L., & Yassa, M. A. (2013). Perturbations of neural circuitry in aging, mild cognitive impairment, and Alzheimer's disease. *Ageing Res Rev*, *12*(3), 823-831. https://doi.org/10.1016/j.arr.2013.01.006

LeDoux, M. S. (2014). *Movement disorders: Genetics and models*. Elsevier.

Lee, L., Dale, E., Staniszewski, A., Zhang, H., Saeed, F., Sakurai, M., Fa, M., Orozco, I., Michelassi, F., Akpan, N., Lehrer, H., & Arancio, O. (2014). Regulation of synaptic plasticity and cognition by SUMO in normal physiology and Alzheimer's disease. *Sci Rep*, *4*, 7190. https://doi.org/10.1038/srep07190

Lee, L., Sakurai, M., Matsuzaki, S., Arancio, O., & Fraser, P. (2013). SUMO and Alzheimer's disease. *Neuromolecular Med*, *15*(4), 720-736. https://doi.org/10.1007/s12017-013-8257-7

Leger, J., Kempf, M., Lee, G., & Brandt, R. (1997). Conversion of serine to aspartate imitates phosphorylation-induced changes in the structure and function of microtubule-associated protein tau. *J Biol Chem*, *272*(13), 8441-8446. https://doi.org/10.1074/jbc.272.13.8441

Lewis, J., McGowan, E., Rockwood, J., Melrose, H., Nacharaju, P., Van Slegtenhorst, M., Gwinn-Hardy, K., Paul Murphy, M., Baker, M., Yu, X., Duff, K., Hardy, J., Corral, A., Lin, W. L., Yen, S. H., Dickson, D. W., Davies, P., & Hutton, M. (2000). Neurofibrillary tangles, amyotrophy and progressive motor disturbance in mice expressing mutant (P301L) tau protein. *Nat Genet*, *25*(4), 402-405. https://doi.org/10.1038/78078

Li, Q., Shortreed, M. R., Wenger, C. D., Frey, B. L., Schaffer, L. V., Scalf, M., & Smith, L. M. (2017). Global Post-Translational Modification Discovery. *J Proteome Res*, *16*(4), 1383-1390. https://doi.org/10.1021/acs.jproteome.6b00034

Li, W., & Lee, V. M. (2006). Characterization of two VQIXXK motifs for tau fibrillization in vitro. *Biochemistry*, *45*(51), 15692-15701. https://doi.org/10.1021/bi061422+

Limorenko, G., & Lashuel, H. A. (2022). Revisiting the grammar of Tau aggregation and pathology formation: how new insights from brain pathology are shaping how we study and target Tauopathies. *Chem Soc Rev*, *51*(2), 513-565. https://doi.org/10.1039/d1cs00127b

Lindstedt, P. R., Taylor, R. J., Bernardes, G. J. L., & Vendruscolo, M. (2021). Facile Installation of Post-translational Modifications on the Tau Protein via Chemical Mutagenesis. *ACS Chem Neurosci*, *12*(3), 557-561. https://doi.org/10.1021/acschemneuro.0c00761

Litvan, I., Grimes, D. A., & Lang, A. E. (2000). Phenotypes and prognosis: clinicopathologic studies of corticobasal degeneration. *Adv Neurol*, *82*, 183-196. https://www.ncbi.nlm.nih.gov/pubmed/10624482

Liu, F., Iqbal, K., Grundke-Iqbal, I., & Gong, C. X. (2002). Involvement of aberrant glycosylation in phosphorylation of tau by cdk5 and GSK-3beta. *FEBS Lett*, *530*(1-3), 209-214. https://doi.org/10.1016/s0014-5793(02)03487-7

Liu, F., Iqbal, K., Grundke-Iqbal, I., Hart, G. W., & Gong, C. X. (2004). O-GlcNAcylation regulates phosphorylation of tau: a mechanism involved in Alzheimer's disease. *Proc Natl Acad Sci U S A*, *101*(29), 10804-10809. https://doi.org/10.1073/pnas.0400348101

Liu, F., Shi, J., Tanimukai, H., Gu, J., Gu, J., Grundke-Iqbal, I., Iqbal, K., & Gong, C. X. (2009). Reduced O-GlcNAcylation links lower brain glucose metabolism and tau pathology in Alzheimer's disease. *Brain*, *132*(Pt 7), 1820-1832. https://doi.org/10.1093/brain/awp099

Liu, K., Liu, Y., Li, L., Qin, P., Iqbal, J., Deng, Y., & Qing, H. (2016). Glycation alter the process of Tau phosphorylation to change Tau isoforms aggregation property. *Biochim Biophys Acta*, *1862*(2), 192-201. https://doi.org/10.1016/j.bbadis.2015.12.002

Liu, L., Drouet, V., Wu, J. W., Witter, M. P., Small, S. A., Clelland, C., & Duff, K. (2012). Trans-synaptic spread of tau pathology in vivo. *PLoS One*, *7*(2), e31302. https://doi.org/10.1371/journal.pone.0031302

Liu, M., Sui, D., Dexheimer, T., Hovde, S., Deng, X., Wang, K. W., Lin, H. L., Chien, H. T., Kweon, H. K., Kuo, N. S., Ayoub, C. A., Jimenez-Harrison, D., Andrews, P. C., Kwok, R., Bochar, D. A., Kuret, J., Fortin, J., Tsay, Y. G., & Kuo, M. H. (2020). Hyperphosphorylation Renders Tau Prone to Aggregate and to Cause Cell Death. *Mol Neurobiol*, *57*(11), 4704-4719. https://doi.org/10.1007/s12035-020-02034-w

Lo Cascio, F., Garcia, S., Montalbano, M., Puangmalai, N., McAllen, S., Pace, A., Palumbo Piccionello, A., & Kayed, R. (2020). Modulating disease-relevant tau oligomeric strains by small molecules. *J Biol Chem*, *295*(44), 14807-14825. https://doi.org/10.1074/jbc.RA120.014630

Lo, C. H., Lim, C. K., Ding, Z., Wickramasinghe, S. P., Braun, A. R., Ashe, K. H., Rhoades, E., Thomas, D. D., & Sachs, J. N. (2019). Targeting the ensemble of heterogeneous tau

oligomers in cells: A novel small molecule screening platform for tauopathies. *Alzheimers Dement*, *15*(11), 1489-1502. https://doi.org/10.1016/j.jalz.2019.06.4954

Lopez Salon, M., Morelli, L., Castano, E. M., Soto, E. F., & Pasquini, J. M. (2000). Defective ubiquitination of cerebral proteins in Alzheimer's disease. *J Neurosci Res*, *62*(2), 302-310. https://doi.org/10.1002/1097-4547(20001015)62:2<302::AID-JNR15>3.0.CO;2-L

LoPresti, P., Szuchet, S., Papasozomenos, S. C., Zinkowski, R. P., & Binder, L. I. (1995). Functional implications for the microtubule-associated protein tau: localization in oligodendrocytes. *Proc Natl Acad Sci U S A*, *92*(22), 10369-10373. https://doi.org/10.1073/pnas.92.22.10369

Lovestam, S., Koh, F. A., van Knippenberg, B., Kotecha, A., Murzin, A. G., Goedert, M., & Scheres, S. H. W. (2022). Assembly of recombinant tau into filaments identical to those of Alzheimer's disease and chronic traumatic encephalopathy. *Elife*, *11*. https://doi.org/10.7554/eLife.76494

Lumpkin, R. J., Gu, H., Zhu, Y., Leonard, M., Ahmad, A. S., Clauser, K. R., Meyer, J. G., Bennett, E. J., & Komives, E. A. (2017). Site-specific identification and quantitation of endogenous SUMO modifications under native conditions. *Nat Commun*, *8*(1), 1171. https://doi.org/10.1038/s41467-017-01271-3

Luna-Munoz, J., Chavez-Macias, L., Garcia-Sierra, F., & Mena, R. (2007). Earliest stages of tau conformational changes are related to the appearance of a sequence of specific phospho-dependent tau epitopes in Alzheimer's disease. *J Alzheimers Dis*, *12*(4), 365-375. https://doi.org/10.3233/jad-2007-12410

Lund, E. T., McKenna, R., Evans, D. B., Sharma, S. K., & Mathews, W. R. (2001). Characterization of the in vitro phosphorylation of human tau by tau protein kinase II (cdk5/p20) using mass spectrometry. *J Neurochem*, *76*(4), 1221-1232. https://doi.org/10.1046/j.1471-4159.2001.00130.x

Luo, H. B., Xia, Y. Y., Shu, X. J., Liu, Z. C., Feng, Y., Liu, X. H., Yu, G., Yin, G., Xiong, Y. S., Zeng, K., Jiang, J., Ye, K., Wang, X. C., & Wang, J. Z. (2014). SUMOylation at K340 inhibits tau degradation through deregulating its phosphorylation and ubiquitination. *Proc Natl Acad Sci U S A*, *111*(46), 16586-16591. https://doi.org/10.1073/pnas.1417548111

Ma, J., & Hart, G. W. (2014). O-GlcNAc profiling: from proteins to proteomes. *Clin Proteomics*, *11*(1), 8. https://doi.org/10.1186/1559-0275-11-8

Ma, J., & Hart, G. W. (2017). Analysis of Protein O-GlcNAcylation by Mass Spectrometry. *Curr Protoc Protein Sci*, *87*, 24 10 21-24 10 16. https://doi.org/10.1002/cpps.24

Maeda, S., Sahara, N., Saito, Y., Murayama, M., Yoshiike, Y., Kim, H., Miyasaka, T., Murayama, S., Ikai, A., & Takashima, A. (2007). Granular tau oligomers as intermediates of tau filaments. *Biochemistry*, *46*(12), 3856-3861. https://doi.org/10.1021/bi061359o

Maeda, S., Sahara, N., Saito, Y., Murayama, S., Ikai, A., & Takashima, A. (2006). Increased levels of granular tau oligomers: an early sign of brain aging and Alzheimer's disease. *Neurosci Res*, *54*(3), 197-201. https://doi.org/10.1016/j.neures.2005.11.009

Maeda, S., Sato, Y., & Takashima, A. (2018). Frontotemporal dementia with Parkinsonism linked to chromosome-17 mutations enhance tau oligomer formation. *Neurobiol Aging*, *69*, 26-32. https://doi.org/10.1016/j.neurobiolaging.2018.04.014

Mahady, L. J., Perez, S. E., Malek-Ahmadi, M., & Mufson, E. J. (2023). Oligomeric, phosphorylated, and truncated tau and spliceosome pathology within the entorhinal-hippocampal connectome across stages of Alzheimer's disease. *J Comp Neurol*, *531*(18), 2080-2108. https://doi.org/10.1002/cne.25466

Mahajan, R., Delphin, C., Guan, T., Gerace, L., & Melchior, F. (1997). A small ubiquitin-related polypeptide involved in targeting RanGAP1 to nuclear pore complex protein RanBP2. *Cell*, *88*(1), 97-107. https://doi.org/10.1016/s0092-8674(00)81862-0

Mair, W., Muntel, J., Tepper, K., Tang, S., Biernat, J., Seeley, W. W., Kosik, K. S., Mandelkow, E., Steen, H., & Steen, J. A. (2016). FLEXITau: Quantifying Post-translational Modifications of Tau Protein in Vitro and in Human Disease. *Anal Chem*, *88*(7), 3704-3714. https://doi.org/10.1021/acs.analchem.5b04509

Malpetti, M., Joie, R., & Rabinovici, G. D. (2022). Tau Beats Amyloid in Predicting Brain Atrophy in Alzheimer Disease: Implications for Prognosis and Clinical Trials. *J Nucl Med*, *63*(6), 830-832. https://doi.org/10.2967/jnumed.121.263694

Man, V. H., He, X., Gao, J., & Wang, J. (2023). Phosphorylation of Tau R2 Repeat Destabilizes Its Binding to Microtubules: A Molecular Dynamics Simulation Study. *ACS Chem Neurosci*, *14*(3), 458-467. https://doi.org/10.1021/acschemneuro.2c00611

Manca, M., Standke, H. G., Browne, D. F., Huntley, M. L., Thomas, O. R., Orru, C. D., Hughson, A. G., Kim, Y., Zhang, J., Tatsuoka, C., Zhu, X., Hiniker, A., Coughlin, D. G., Galasko, D., & Kraus, A. (2023). Tau seeds occur before earliest Alzheimer's changes and are prevalent across neurodegenerative diseases. *Acta Neuropathol*, *146*(1), 31-50. https://doi.org/10.1007/s00401-023-02574-0

Mandel, N., & Agarwal, N. (2022). Role of SUMOylation in Neurodegenerative Diseases. *Cells*, *11*(21). https://doi.org/10.3390/cells11213395

Mao, M., Xia, Q., Zhan, G. F., Chu, Q. J., Li, X., & Lian, H. K. (2022). SENP6 induces microglial polarization and neuroinflammation through de-SUMOylation of Annexin-A1 after cerebral ischaemia-reperfusion injury. *Cell Biosci*, *12*(1), 113. https://doi.org/10.1186/s13578-022-00850-2

Martin, L., Latypova, X., Wilson, C. M., Magnaudeix, A., Perrin, M. L., Yardin, C., & Terro, F. (2013). Tau protein kinases: involvement in Alzheimer's disease. *Ageing Res Rev*, *12*(1), 289-309. https://doi.org/10.1016/j.arr.2012.06.003

Martinez, P., Patel, H., You, Y., Jury, N., Perkins, A., Lee-Gosselin, A., Taylor, X., You, Y., Viana Di Prisco, G., Huang, X., Dutta, S., Wijeratne, A. B., Redding-Ochoa, J., Shahid, S. S., Codocedo, J. F., Min, S., Landreth, G. E., Mosley, A. L., Wu, Y. C., . . . Lasagna-Reeves, C. A. (2022). Bassoon contributes to tau-seed propagation and neurotoxicity. *Nat Neurosci*, *25*(12), 1597-1607. https://doi.org/10.1038/s41593-022-01191-6

MARTLAND, H. S. (1928). PUNCH DRUNK. *Journal of the American Medical Association*, *91*(15), 1103-1107. https://doi.org/10.1001/jama.1928.02700150029009

Masters, C. L., Simms, G., Weinman, N. A., Multhaup, G., McDonald, B. L., & Beyreuther, K. (1985). Amyloid plaque core protein in Alzheimer disease and Down syndrome. *Proc Natl Acad Sci U S A*, *82*(12), 4245-4249. https://doi.org/10.1073/pnas.82.12.4245

Matsuo, E. S., Shin, R. W., Billingsley, M. L., Van deVoorde, A., O'Connor, M., Trojanowski, J. Q., & Lee, V. M. (1994). Biopsy-derived adult human brain tau is phosphorylated at many of the same sites as Alzheimer's disease paired helical filament tau. *Neuron*, *13*(4), 989-1002. https://doi.org/10.1016/0896-6273(94)90264-x

Matsuzaki, S., Lee, L., Knock, E., Srikumar, T., Sakurai, M., Hazrati, L. N., Katayama, T., Staniszewski, A., Raught, B., Arancio, O., & Fraser, P. E. (2015). SUMO1 Affects

Synaptic Function, Spine Density and Memory. *Sci Rep*, *5*, 10730. https://doi.org/10.1038/srep10730

Matunis, M. J., Coutavas, E., & Blobel, G. (1996). A novel ubiquitin-like modification modulates the partitioning of the Ran-GTPase-activating protein RanGAP1 between the cytosol and the nuclear pore complex. *J Cell Biol*, *135*(6 Pt 1), 1457-1470. https://doi.org/10.1083/jcb.135.6.1457

Mawal-Dewan, M., Henley, J., Van de Voorde, A., Trojanowski, J. Q., & Lee, V. M. (1994). The phosphorylation state of tau in the developing rat brain is regulated by phosphoprotein phosphatases. *J Biol Chem*, *269*(49), 30981-30987. https://www.ncbi.nlm.nih.gov/pubmed/7983034

McKee, A. C., Abdolmohammadi, B., & Stein, T. D. (2018). The neuropathology of chronic traumatic encephalopathy. *Handb Clin Neurol*, *158*, 297-307. https://doi.org/10.1016/B978-0-444-63954-7.00028-8

McKee, A. C., Stein, T. D., Huber, B. R., Crary, J. F., Bieniek, K., Dickson, D., Alvarez, V. E., Cherry, J. D., Farrell, K., Butler, M., Uretsky, M., Abdolmohammadi, B., Alosco, M. L., Tripodis, Y., Mez, J., & Daneshvar, D. H. (2023). Chronic traumatic encephalopathy (CTE): criteria for neuropathological diagnosis and relationship to repetitive head impacts. *Acta Neuropathol*, *145*(4), 371-394. https://doi.org/10.1007/s00401-023-02540-w

McKee, A. C., Stein, T. D., Kiernan, P. T., & Alvarez, V. E. (2015). The neuropathology of chronic traumatic encephalopathy. *Brain Pathol*, *25*(3), 350-364. https://doi.org/10.1111/bpa.12248

McKee, A. C., Stern, R. A., Nowinski, C. J., Stein, T. D., Alvarez, V. E., Daneshvar, D. H., Lee, H. S., Wojtowicz, S. M., Hall, G., Baugh, C. M., Riley, D. O., Kubilus, C. A., Cormier, K. A., Jacobs, M. A., Martin, B. R., Abraham, C. R., Ikezu, T., Reichard, R. R., Wolozin, B. L., . . . Cantu, R. C. (2013). The spectrum of disease in chronic traumatic encephalopathy. *Brain*, *136*(Pt 1), 43-64. https://doi.org/10.1093/brain/aws307

McKibben, K. M., & Rhoades, E. (2019). Independent tubulin binding and polymerization by the proline-rich region of Tau is regulated by Tau's N-terminal domain. *J Biol Chem*, *294*(50), 19381-19394. https://doi.org/10.1074/jbc.RA119.010172

McMillan, P. J., Benbow, S. J., Uhrich, R., Saxton, A., Baum, M., Strovas, T., Wheeler, J. M., Baker, J., Liachko, N. F., Keene, C. D., Latimer, C. S., & Kraemer, B. C. (2023). Tau-

RNA complexes inhibit microtubule polymerization and drive disease-relevant conformation change. *Brain*, *146*(8), 3206-3220. https://doi.org/10.1093/brain/awad032

Mein, H., Jing, Y., Ahmad, F., Zhang, H., & Liu, P. (2022). Altered Brain Arginine Metabolism and Polyamine System in a P301S Tauopathy Mouse Model: A Time-Course Study. *Int J Mol Sci*, *23*(11). https://doi.org/10.3390/ijms23116039

Melchior, F., & Pichler, A. (2004). SUMO Modification. In W. J. Lennarz & M. D. Lane (Eds.), *Encyclopedia of Biological Chemistry* (pp. 130-134). Elsevier. https://doi.org/https://doi.org/10.1016/B0-12-443710-9/00647-5

Meng, J. X., Zhang, Y., Saman, D., Haider, A. M., De, S., Sang, J. C., Brown, K., Jiang, K., Humphrey, J., Julian, L., Hidari, E., Lee, S. F., Balmus, G., Floto, R. A., Bryant, C. E., Benesch, J. L. P., Ye, Y., & Klenerman, D. (2022). Hyperphosphorylated tau self-assembles into amorphous aggregates eliciting TLR4-dependent responses. *Nat Commun*, *13*(1), 2692. https://doi.org/10.1038/s41467-022-30461-x

Mercken, M., Vandermeeren, M., Lubke, U., Six, J., Boons, J., Van de Voorde, A., Martin, J. J., & Gheuens, J. (1992). Monoclonal antibodies with selective specificity for Alzheimer Tau are directed against phosphatase-sensitive epitopes. *Acta Neuropathol*, *84*(3), 265-272. https://doi.org/10.1007/BF00227819

Mesulam, M., Shaw, P., Mash, D., & Weintraub, S. (2004). Cholinergic nucleus basalis tauopathy emerges early in the aging-MCI-AD continuum. *Ann Neurol*, *55*(6), 815-828. https://doi.org/10.1002/ana.20100

Meyer, M. R., Tschanz, J. T., Norton, M. C., Welsh-Bohmer, K. A., Steffens, D. C., Wyse, B. W., & Breitner, J. C. (1998). APOE genotype predicts when--not whether--one is predisposed to develop Alzheimer disease. *Nat Genet*, *19*(4), 321-322. https://doi.org/10.1038/1206

Mezias, C., LoCastro, E., Xia, C., & Raj, A. (2017). Connectivity, not region-intrinsic properties, predicts regional vulnerability to progressive tau pathology in mouse models of disease. *Acta Neuropathol Commun*, *5*(1), 61. https://doi.org/10.1186/s40478-017-0459-z

Miller, M. L., & Johnson, G. V. (1995). Transglutaminase cross-linking of the tau protein. *J Neurochem*, *65*(4), 1760-1770. https://doi.org/10.1046/j.1471-4159.1995.65041760.x

Miller, R. M., Millikin, R. J., Rolfs, Z., Shortreed, M. R., & Smith, L. M. (2023). Enhanced Proteomic Data Analysis with MetaMorpheus. *Methods Mol Biol*, *2426*, 35-66. https://doi.org/10.1007/978-1-0716-1967-4_3

Min, S. W., Chen, X., Tracy, T. E., Li, Y., Zhou, Y., Wang, C., Shirakawa, K., Minami, S. S., Defensor, E., Mok, S. A., Sohn, P. D., Schilling, B., Cong, X., Ellerby, L., Gibson, B. W., Johnson, J., Krogan, N., Shamloo, M., Gestwicki, J., . . . Gan, L. (2015). Critical role of acetylation in tau-mediated neurodegeneration and cognitive deficits. *Nat Med*, *21*(10), 1154-1162. https://doi.org/10.1038/nm.3951

Min, S. W., Cho, S. H., Zhou, Y., Schroeder, S., Haroutunian, V., Seeley, W. W., Huang, E. J., Shen, Y., Masliah, E., Mukherjee, C., Meyers, D., Cole, P. A., Ott, M., & Gan, L. (2010). Acetylation of tau inhibits its degradation and contributes to tauopathy. *Neuron*, *67*(6), 953-966. https://doi.org/10.1016/j.neuron.2010.08.044

Minoura, I., & Muto, E. (2006). Dielectric measurement of individual microtubules using the electroorientation method. *Biophys J*, *90*(10), 3739-3748. https://doi.org/10.1529/biophysj.105.071324

Mirbaha, H., Chen, D., Morazova, O. A., Ruff, K. M., Sharma, A. M., Liu, X., Goodarzi, M., Pappu, R. V., Colby, D. W., Mirzaei, H., Joachimiak, L. A., & Diamond, M. I. (2018). Inert and seed-competent tau monomers suggest structural origins of aggregation. *Elife*, *7*. https://doi.org/10.7554/eLife.36584

Mirbaha, H., Chen, D., Mullapudi, V., Terpack, S. J., White, C. L., 3rd, Joachimiak, L. A., & Diamond, M. I. (2022). Seed-competent tau monomer initiates pathology in a tauopathy mouse model. *J Biol Chem*, *298*(8), 102163. https://doi.org/10.1016/j.jbc.2022.102163

Mondragon-Rodriguez, S., Perry, G., Luna-Munoz, J., Acevedo-Aquino, M. C., & Williams, S. (2014). Phosphorylation of tau protein at sites Ser(396-404) is one of the earliest events in Alzheimer's disease and Down syndrome. *Neuropathol Appl Neurobiol*, *40*(2), 121-135. https://doi.org/10.1111/nan.12084

Montalbano, M., Majmundar, L., Sengupta, U., Fung, L., & Kayed, R. (2023). Pathological tau signatures and nuclear alterations in neurons, astrocytes and microglia in Alzheimer's disease, progressive supranuclear palsy, and dementia with Lewy bodies. *Brain Pathol*, *33*(1), e13112. https://doi.org/10.1111/bpa.13112

Mori, H., Kondo, J., & Ihara, Y. (1987). Ubiquitin is a component of paired helical filaments in Alzheimer's disease. *Science*, *235*(4796), 1641-1644. https://doi.org/10.1126/science.3029875

Mori, H., Nishimura, M., Namba, Y., & Oda, M. (1994). Corticobasal degeneration: a disease with widespread appearance of abnormal tau and neurofibrillary tangles, and its relation to progressive supranuclear palsy. *Acta Neuropathol*, *88*(2), 113-121. https://doi.org/10.1007/BF00294503

Morishima-Kawashima, M., Hasegawa, M., Takio, K., Suzuki, M., Titani, K., & Ihara, Y. (1993). Ubiquitin is conjugated with amino-terminally processed tau in paired helical filaments. *Neuron*, *10*(6), 1151-1160. https://doi.org/10.1016/0896-6273(93)90063-w

Morishima-Kawashima, M., Hasegawa, M., Takio, K., Suzuki, M., Yoshida, H., Titani, K., & Ihara, Y. (1995). Proline-directed and non-proline-directed phosphorylation of PHF-tau. *J Biol Chem*, *270*(2), 823-829. https://doi.org/10.1074/jbc.270.2.823

Morishima-Kawashima, M., Hasegawa, M., Takio, K., Suzuki, M., Yoshida, H., Watanabe, A., Titani, K., & Ihara, Y. (1995). Hyperphosphorylation of tau in PHF. *Neurobiol Aging*, *16*(3), 365-371; discussion 371-380. https://doi.org/10.1016/0197-4580(95)00027-c

Morris, A. M., Watzky, M. A., Agar, J. N., & Finke, R. G. (2008). Fitting neurological protein aggregation kinetic data via a 2-step, minimal/"Ockham's razor" model: the Finke-Watzky mechanism of nucleation followed by autocatalytic surface growth. *Biochemistry*, *47*(8), 2413-2427. https://doi.org/10.1021/bi701899y

Morris, M., Knudsen, G. M., Maeda, S., Trinidad, J. C., Ioanoviciu, A., Burlingame, A. L., & Mucke, L. (2015). Tau post-translational modifications in wild-type and human amyloid precursor protein transgenic mice. *Nat Neurosci*, *18*(8), 1183-1189. https://doi.org/10.1038/nn.4067

Morris, S. L., & Brady, S. T. (2022). Tau phosphorylation and PAD exposure in regulation of axonal growth. *Front Cell Dev Biol*, *10*, 1023418. https://doi.org/10.3389/fcell.2022.1023418

Morris, S. L., Tsai, M. Y., Aloe, S., Bechberger, K., Konig, S., Morfini, G., & Brady, S. T. (2020). Defined Tau Phosphospecies Differentially Inhibit Fast Axonal Transport Through Activation of Two Independent Signaling Pathways. *Front Mol Neurosci*, *13*, 610037. https://doi.org/10.3389/fnmol.2020.610037

Morrison, L. D., & Kish, S. J. (1995). Brain polyamine levels are altered in Alzheimer's disease. *Neurosci Lett*, *197*(1), 5-8. https://doi.org/10.1016/0304-3940(95)11881-v

Morsch, R., Simon, W., & Coleman, P. D. (1999). Neurons may live for decades with neurofibrillary tangles. *J Neuropathol Exp Neurol*, *58*(2), 188-197. https://doi.org/10.1097/00005072-199902000-00008

Moszczynski, A. J., Yang, W., Hammond, R., Ang, L. C., & Strong, M. J. (2017). Threonine(175), a novel pathological phosphorylation site on tau protein linked to multiple tauopathies. *Acta Neuropathol Commun*, *5*(1), 6. https://doi.org/10.1186/s40478-016-0406-4

Mroczko, B., Groblewska, M., & Litman-Zawadzka, A. (2019). The Role of Protein Misfolding and Tau Oligomers (TauOs) in Alzheimer's Disease (AD). *Int J Mol Sci*, *20*(19). https://doi.org/10.3390/ijms20194661

Mueller, R. L., Combs, B., Alhadidy, M. M., Brady, S. T., Morfini, G. A., & Kanaan, N. M. (2021). Tau: A Signaling Hub Protein. *Front Mol Neurosci*, *14*, 647054. https://doi.org/10.3389/fnmol.2021.647054

Mueller, R. L., Kanaan, N. M., & Combs, B. (2023). Using Live-Cell Imaging to Measure the Effects of Pathological Proteins on Axonal Transport in Primary Hippocampal Neurons. *J Vis Exp*(202). https://doi.org/10.3791/66156

Mufson, E. J., Ma, S. Y., Cochran, E. J., Bennett, D. A., Beckett, L. A., Jaffar, S., Saragovi, H. U., & Kordower, J. H. (2000). Loss of nucleus basalis neurons containing trkA immunoreactivity in individuals with mild cognitive impairment and early Alzheimer's disease. *J Comp Neurol*, *427*(1), 19-30. https://doi.org/10.1002/1096-9861(20001106)427:1<19::aid-cne2>3.0.co;2-a

Mufson, E. J., Ma, S. Y., Dills, J., Cochran, E. J., Leurgans, S., Wuu, J., Bennett, D. A., Jaffar, S., Gilmor, M. L., Levey, A. I., & Kordower, J. H. (2002). Loss of basal forebrain P75(NTR) immunoreactivity in subjects with mild cognitive impairment and Alzheimer's disease. *J Comp Neurol*, *443*(2), 136-153. https://doi.org/10.1002/cne.10122

Mufson, E. J., Perez, S. E., Nadeem, M., Mahady, L., Kanaan, N. M., Abrahamson, E. E., Ikonomovic, M. D., Crawford, F., Alvarez, V., Stein, T., & McKee, A. C. (2016). Progression of tau pathology within cholinergic nucleus basalis neurons in chronic

traumatic encephalopathy: A chronic effects of neurotrauma consortium study. *Brain Inj*, *30*(12), 1399-1413. https://doi.org/10.1080/02699052.2016.1219058

Mukherjee, S., Dubois, C., Perez, K., Varghese, S., Birchall, I. E., Leckey, M., Davydova, N., McLean, C., Nisbet, R. M., Roberts, B. R., Li, Q. X., Masters, C. L., & Streltsov, V. A. (2023). Quantitative proteomics of tau and Abeta in detergent fractions from Alzheimer's disease brains. *J Neurochem*, *164*(4), 529-552. https://doi.org/10.1111/jnc.15713

Mukrasch, M. D., von Bergen, M., Biernat, J., Fischer, D., Griesinger, C., Mandelkow, E., & Zweckstetter, M. (2007). The "jaws" of the tau-microtubule interaction. *J Biol Chem*, *282*(16), 12230-12239. https://doi.org/10.1074/jbc.M607159200

Muller, C., Bauer, N. M., Schafer, I., & White, R. (2013). Making myelin basic protein - from mRNA transport to localized translation. *Front Cell Neurosci*, *7*, 169. https://doi.org/10.3389/fncel.2013.00169

Munari, F., Barracchia, C. G., Parolini, F., Tira, R., Bubacco, L., Assfalg, M., & D'Onofrio, M. (2020). Semisynthetic Modification of Tau Protein with Di-Ubiquitin Chains for Aggregation Studies. *Int J Mol Sci*, *21*(12). https://doi.org/10.3390/ijms21124400

Murrell, J. R., Spillantini, M. G., Zolo, P., Guazzelli, M., Smith, M. J., Hasegawa, M., Redi, F., Crowther, R. A., Pietrini, P., Ghetti, B., & Goedert, M. (1999). Tau gene mutation G389R causes a tauopathy with abundant pick body-like inclusions and axonal deposits. *J Neuropathol Exp Neurol*, *58*(12), 1207-1226. https://doi.org/10.1097/00005072-199912000-00002

Murthy, S. N., Wilson, J. H., Lukas, T. J., Kuret, J., & Lorand, L. (1998). Cross-linking sites of the human tau protein, probed by reactions with human transglutaminase. *J Neurochem*, *71*(6), 2607-2614. https://doi.org/10.1046/j.1471-4159.1998.71062607.x

Muschol, M., & Hoyer, W. (2023). Amyloid oligomers as on-pathway precursors or off-pathway competitors of fibrils. *Front Mol Biosci*, *10*, 1120416. https://doi.org/10.3389/fmolb.2023.1120416

Mutreja, Y., Combs, B., & Gamblin, T. C. (2019). FTDP-17 Mutations Alter the Aggregation and Microtubule Stabilization Propensity of Tau in an Isoform-Specific Fashion. *Biochemistry*, *58*(6), 742-754. https://doi.org/10.1021/acs.biochem.8b01039

Myeku, N., Clelland, C. L., Emrani, S., Kukushkin, N. V., Yu, W. H., Goldberg, A. L., & Duff, K. E. (2016). Tau-driven 26S proteasome impairment and cognitive dysfunction can be prevented early in disease by activating cAMP-PKA signaling. *Nat Med*, *22*(1), 46-53. https://doi.org/10.1038/nm.4011

Nacharaju, P., Ko, L., & Yen, S. H. (1997). Characterization of in vitro glycation sites of tau. *J Neurochem*, *69*(4), 1709-1719. https://doi.org/10.1046/j.1471-4159.1997.69041709.x

Nadel, C. M., Thwin, A. C., Callahan, M., Lee, K., Connelly, E., Craik, C. S., Southworth, D. R., & Gestwicki, J. E. (2023). The E3 Ubiquitin Ligase, CHIP/STUB1, Inhibits Aggregation of Phosphorylated Proteoforms of Microtubule-associated Protein Tau (MAPT). *J Mol Biol*, *435*(11), 168026. https://doi.org/10.1016/j.jmb.2023.168026

Naslund, J., Haroutunian, V., Mohs, R., Davis, K. L., Davies, P., Greengard, P., & Buxbaum, J. D. (2000). Correlation between elevated levels of amyloid beta-peptide in the brain and cognitive decline. *JAMA*, *283*(12), 1571-1577. https://doi.org/10.1001/jama.283.12.1571

Necula, M., & Kuret, J. (2004). Pseudophosphorylation and glycation of tau protein enhance but do not trigger fibrillization in vitro. *J Biol Chem*, *279*(48), 49694-49703. https://doi.org/10.1074/jbc.M405527200

Nelson, P. T., Alafuzoff, I., Bigio, E. H., Bouras, C., Braak, H., Cairns, N. J., Castellani, R. J., Crain, B. J., Davies, P., Del Tredici, K., Duyckaerts, C., Frosch, M. P., Haroutunian, V., Hof, P. R., Hulette, C. M., Hyman, B. T., Iwatsubo, T., Jellinger, K. A., Jicha, G. A., . . . Beach, T. G. (2012). Correlation of Alzheimer disease neuropathologic changes with cognitive status: a review of the literature. *J Neuropathol Exp Neurol*, *71*(5), 362-381. https://doi.org/10.1097/NEN.0b013e31825018f7

Neumann, M., Schulz-Schaeffer, W., Crowther, R. A., Smith, M. J., Spillantini, M. G., Goedert, M., & Kretzschmar, H. A. (2001). Pick's disease associated with the novel Tau gene mutation K369I. *Ann Neurol*, *50*(4), 503-513. https://doi.org/10.1002/ana.1223

Niblock, M., & Gallo, J. M. (2012). Tau alternative splicing in familial and sporadic tauopathies. *Biochem Soc Trans*, *40*(4), 677-680. https://doi.org/10.1042/BST20120091

Niewiadomska, G., Niewiadomski, W., Steczkowska, M., & Gasiorowska, A. (2021). Tau Oligomers Neurotoxicity. *Life (Basel)*, *11*(1). https://doi.org/10.3390/life11010028

Noble, W., Hanger, D. P., Miller, C. C., & Lovestone, S. (2013). The importance of tau phosphorylation for neurodegenerative diseases. *Front Neurol*, *4*, 83. https://doi.org/10.3389/fneur.2013.00083

Olfati, N., Shoeibi, A., & Litvan, I. (2022). Clinical Spectrum of Tauopathies. *Front Neurol*, *13*, 944806. https://doi.org/10.3389/fneur.2022.944806

Omalu, B. (2014). Chronic traumatic encephalopathy. *Prog Neurol Surg*, *28*, 38-49. https://doi.org/10.1159/000358761

Omalu, B. I., DeKosky, S. T., Hamilton, R. L., Minster, R. L., Kamboh, M. I., Shakir, A. M., & Wecht, C. H. (2006). Chronic traumatic encephalopathy in a national football league player: part II. *Neurosurgery*, *59*(5), 1086-1092; discussion 1092-1083. https://doi.org/10.1227/01.NEU.0000245601.69451.27

Omalu, B. I., DeKosky, S. T., Minster, R. L., Kamboh, M. I., Hamilton, R. L., & Wecht, C. H. (2005). Chronic traumatic encephalopathy in a National Football League player. *Neurosurgery*, *57*(1), 128-134; discussion 128-134. https://doi.org/10.1227/01.neu.0000163407.92769.ed

Osula, O., Swatkoski, S., & Cotter, R. J. (2012). Identification of protein SUMOylation sites by mass spectrometry using combined microwave-assisted aspartic acid cleavage and tryptic digestion. *J Mass Spectrom*, *47*(5), 644-654. https://doi.org/10.1002/jms.2959

Otvos, L., Jr., Feiner, L., Lang, E., Szendrei, G. I., Goedert, M., & Lee, V. M. (1994). Monoclonal antibody PHF-1 recognizes tau protein phosphorylated at serine residues 396 and 404. *J Neurosci Res*, *39*(6), 669-673. https://doi.org/10.1002/jnr.490390607

Paneque, A., Fortus, H., Zheng, J., Werlen, G., & Jacinto, E. (2023). The Hexosamine Biosynthesis Pathway: Regulation and Function. *Genes (Basel)*, *14*(4). https://doi.org/10.3390/genes14040933

Pantel, J. (2017). [Alzheimer's disease from Auguste Deter to the present : Progress, disappointments and open questions]. *Z Gerontol Geriatr*, *50*(7), 576-587. https://doi.org/10.1007/s00391-017-1307-2 (Alzheimer-Demenz von Auguste Deter bis heute : Fortschritte, Enttauschungen und offene Fragen.)

Park, M. H., & Igarashi, K. (2013). Polyamines and their metabolites as diagnostic markers of human diseases. *Biomol Ther (Seoul)*, *21*(1), 1-9. https://doi.org/10.4062/biomolther.2012.097

Park, S., Lee, J. H., Jeon, J. H., & Lee, M. J. (2018). Degradation or aggregation: the ramifications of post-translational modifications on tau. *BMB Rep*, *51*(6), 265-273. https://doi.org/10.5483/bmbrep.2018.51.6.077

Park, S. A., Ahn, S. I., & Gallo, J. M. (2016). Tau mis-splicing in the pathogenesis of neurodegenerative disorders. *BMB Rep*, *49*(8), 405-413. https://doi.org/10.5483/bmbrep.2016.49.8.084

Paterno, G., Torrellas, J., Bell, B. M., Gorion, K. M., Quintin, S. S., Hery, G. P., Prokop, S., & Giasson, B. I. (2023). Novel Conformation-Dependent Tau Antibodies Are Modulated by Adjacent Phosphorylation Sites. *Int J Mol Sci*, *24*(18). https://doi.org/10.3390/ijms241813676

Patterson, K. R., Remmers, C., Fu, Y., Brooker, S., Kanaan, N. M., Vana, L., Ward, S., Reyes, J. F., Philibert, K., Glucksman, M. J., & Binder, L. I. (2011). Characterization of prefibrillar Tau oligomers in vitro and in Alzheimer disease. *J Biol Chem*, *286*(26), 23063-23076. https://doi.org/10.1074/jbc.M111.237974

Perez, M., Cuadros, R., Smith, M. A., Perry, G., & Avila, J. (2000). Phosphorylated, but not native, tau protein assembles following reaction with the lipid peroxidation product, 4-hydroxy-2-nonenal. *FEBS Lett*, *486*(3), 270-274. https://doi.org/10.1016/s0014-5793(00)02323-1

Pergande, M. R., & Cologna, S. M. (2017). Isoelectric Point Separations of Peptides and Proteins. *Proteomes*, *5*(1). https://doi.org/10.3390/proteomes5010004

Permanne, B., Sand, A., Ousson, S., Neny, M., Hantson, J., Schubert, R., Wiessner, C., Quattropani, A., & Beher, D. (2022). O-GlcNAcase Inhibitor ASN90 is a Multimodal Drug Candidate for Tau and alpha-Synuclein Proteinopathies. *ACS Chem Neurosci*, *13*(8), 1296-1314. https://doi.org/10.1021/acschemneuro.2c00057

Perry, G., Friedman, R., Shaw, G., & Chau, V. (1987). Ubiquitin is detected in neurofibrillary tangles and senile plaque neurites of Alzheimer disease brains. *Proc Natl Acad Sci U S A*, *84*(9), 3033-3036. https://doi.org/10.1073/pnas.84.9.3033

Pires, G., & Drummond, E. (2021). It takes more than tau to tangle: using proteomics to determine how phosphorylated tau mediates toxicity in neurodegenerative diseases. *Neural Regen Res*, *16*(11), 2211-2212. https://doi.org/10.4103/1673-5374.310680

Pires, M., & Rego, A. C. (2023). Apoe4 and Alzheimer's Disease Pathogenesis-Mitochondrial Deregulation and Targeted Therapeutic Strategies. *Int J Mol Sci*, *24*(1). https://doi.org/10.3390/ijms24010778

Pooler, A. M., Phillips, E. C., Lau, D. H., Noble, W., & Hanger, D. P. (2013). Physiological release of endogenous tau is stimulated by neuronal activity. *EMBO Rep*, *14*(4), 389-394. https://doi.org/10.1038/embor.2013.15

Poorkaj, P., Bird, T. D., Wijsman, E., Nemens, E., Garruto, R. M., Anderson, L., Andreadis, A., Wiederholt, W. C., Raskind, M., & Schellenberg, G. D. (1998). Tau is a candidate gene for chromosome 17 frontotemporal dementia. *Ann Neurol*, *43*(6), 815-825. https://doi.org/10.1002/ana.410430617

Porzig, R., Singer, D., & Hoffmann, R. (2007). Epitope mapping of mAbs AT8 and Tau5 directed against hyperphosphorylated regions of the human tau protein. *Biochem Biophys Res Commun*, *358*(2), 644-649. https://doi.org/10.1016/j.bbrc.2007.04.187

Preuss, U., Biernat, J., Mandelkow, E. M., & Mandelkow, E. (1997). The 'jaws' model of tau-microtubule interaction examined in CHO cells. *J Cell Sci*, *110 (Pt 6)*, 789-800. https://doi.org/10.1242/jcs.110.6.789

Price, J. L., Ko, A. I., Wade, M. J., Tsou, S. K., McKeel, D. W., & Morris, J. C. (2001). Neuron number in the entorhinal cortex and CA1 in preclinical Alzheimer disease. *Arch Neurol*, *58*(9), 1395-1402. https://doi.org/10.1001/archneur.58.9.1395

Prokopovich, D. V., Whittaker, J. W., Muthee, M. M., Ahmed, A., & Larini, L. (2017). Impact of Phosphorylation and Pseudophosphorylation on the Early Stages of Aggregation of the Microtubule-Associated Protein Tau. *J Phys Chem B*, *121*(9), 2095-2103. https://doi.org/10.1021/acs.jpcb.7b00194

Puangmalai, N., Sengupta, U., Bhatt, N., Gaikwad, S., Montalbano, M., Bhuyan, A., Garcia, S., McAllen, S., Sonawane, M., Jerez, C., Zhao, Y., & Kayed, R. (2022). Lysine 63-linked ubiquitination of tau oligomers contributes to the pathogenesis of Alzheimer's disease. *J Biol Chem*, *298*(4), 101766. https://doi.org/10.1016/j.jbc.2022.101766

Puzzo, D., Argyrousi, E. K., Staniszewski, A., Zhang, H., Calcagno, E., Zuccarello, E., Acquarone, E., Fa, M., Li Puma, D. D., Grassi, C., D'Adamio, L., Kanaan, N. M., Fraser, P. E., & Arancio, O. (2020). Tau is not necessary for amyloid-beta-induced synaptic and memory impairments. *J Clin Invest*, *130*(9), 4831-4844. https://doi.org/10.1172/JCI137040

Qiang, L., Sun, X., Austin, T. O., Muralidharan, H., Jean, D. C., Liu, M., Yu, W., & Baas, P. W. (2018). Tau Does Not Stabilize Axonal Microtubules but Rather Enables Them to Have Long Labile Domains. *Curr Biol*, *28*(13), 2181-2189 e2184. https://doi.org/10.1016/j.cub.2018.05.045

Rane, J. S., Kumari, A., & Panda, D. (2019). An acetylation mimicking mutation, K274Q, in tau imparts neurotoxicity by enhancing tau aggregation and inhibiting tubulin polymerization. *Biochem J*, *476*(10), 1401-1417. https://doi.org/10.1042/BCJ20190042

Rani, L., Mittal, J., & Mallajosyula, S. S. (2020). Effect of Phosphorylation and O-GlcNAcylation on Proline-Rich Domains of Tau. *J Phys Chem B*, *124*(10), 1909-1918. https://doi.org/10.1021/acs.jpcb.9b11720

Rankin, C. A., Sun, Q., & Gamblin, T. C. (2007). Tau phosphorylation by GSK-3beta promotes tangle-like filament morphology. *Mol Neurodegener*, *2*, 12. https://doi.org/10.1186/1750-1326-2-12

Rauch, J. N., Luna, G., Guzman, E., Audouard, M., Challis, C., Sibih, Y. E., Leshuk, C., Hernandez, I., Wegmann, S., Hyman, B. T., Gradinaru, V., Kampmann, M., & Kosik, K. S. (2020). LRP1 is a master regulator of tau uptake and spread. *Nature*, *580*(7803), 381-385. https://doi.org/10.1038/s41586-020-2156-5

Raut, S., Bhalerao, A., Powers, M., Gonzalez, M., Mancuso, S., & Cucullo, L. (2023). Hypometabolism, Alzheimer's Disease, and Possible Therapeutic Targets: An Overview. *Cells*, *12*(16). https://doi.org/10.3390/cells12162019

Rebeiz, J. J., Kolodny, E. H., & Richardson, E. P., Jr. (1967). Corticodentatonigral degeneration with neuronal achromasia: a progressive disorder of late adult life. *Trans Am Neurol Assoc*, *92*, 23-26. https://www.ncbi.nlm.nih.gov/pubmed/5634049

Rebeiz, J. J., Kolodny, E. H., & Richardson, E. P., Jr. (1968). Corticodentatonigral degeneration with neuronal achromasia. *Arch Neurol*, *18*(1), 20-33. https://doi.org/10.1001/archneur.1968.00470310034003

Rewcastle, N. B., & Ball, M. J. (1968). Electron microscopic structure of the "inclusion bodies" in Pick's disease. *Neurology*, *18*(12), 1205-1213. https://doi.org/10.1212/wnl.18.12.1205

Reynolds, C. H., Betts, J. C., Blackstock, W. P., Nebreda, A. R., & Anderton, B. H. (2000). Phosphorylation sites on tau identified by nanoelectrospray mass spectrometry: differences in vitro between the mitogen-activated protein kinases ERK2, c-Jun N-terminal kinase and P38, and glycogen synthase kinase-3beta. *J Neurochem*, *74*(4), 1587-1595. https://doi.org/10.1046/j.1471-4159.2000.0741587.x

Ricciarelli, R., & Fedele, E. (2017). The Amyloid Cascade Hypothesis in Alzheimer's Disease: It's Time to Change Our Mind. *Curr Neuropharmacol*, *15*(6), 926-935. https://doi.org/10.2174/1570159X15666170116143743

Rissman, R. A., Poon, W. W., Blurton-Jones, M., Oddo, S., Torp, R., Vitek, M. P., LaFerla, F. M., Rohn, T. T., & Cotman, C. W. (2004). Caspase-cleavage of tau is an early event in Alzheimer disease tangle pathology. *J Clin Invest*, *114*(1), 121-130. https://doi.org/10.1172/JCI20640

Rizzu, P., Van Swieten, J. C., Joosse, M., Hasegawa, M., Stevens, M., Tibben, A., Niermeijer, M. F., Hillebrand, M., Ravid, R., Oostra, B. A., Goedert, M., van Duijn, C. M., & Heutink, P. (1999). High prevalence of mutations in the microtubule-associated protein tau in a population study of frontotemporal dementia in the Netherlands. *Am J Hum Genet*, *64*(2), 414-421. https://doi.org/10.1086/302256

Rockenstein, E., Overk, C. R., Ubhi, K., Mante, M., Patrick, C., Adame, A., Bisquert, A., Trejo-Morales, M., Spencer, B., & Masliah, E. (2015). A novel triple repeat mutant tau transgenic model that mimics aspects of pick's disease and fronto-temporal tauopathies. *PLoS One*, *10*(3), e0121570. https://doi.org/10.1371/journal.pone.0121570

Rodriguez, M. S., Dargemont, C., & Hay, R. T. (2001). SUMO-1 conjugation in vivo requires both a consensus modification motif and nuclear targeting. *J Biol Chem*, *276*(16), 12654-12659. https://doi.org/10.1074/jbc.M009476200

Rojas Quijano, F. A., Morrow, D., Wise, B. M., Brancia, F. L., & Goux, W. J. (2006). Prediction of nucleating sequences from amyloidogenic propensities of tau-related peptides. *Biochemistry*, *45*(14), 4638-4652. https://doi.org/10.1021/bi052226q

Sampson, D. A., Wang, M., & Matunis, M. J. (2001). The small ubiquitin-like modifier-1 (SUMO-1) consensus sequence mediates Ubc9 binding and is essential for SUMO-1 modification. *J Biol Chem*, *276*(24), 21664-21669. https://doi.org/10.1074/jbc.M100006200

Samudra, N., Lane-Donovan, C., VandeVrede, L., & Boxer, A. L. (2023). Tau pathology in neurodegenerative disease: disease mechanisms and therapeutic avenues. *J Clin Invest*, *133*(12). https://doi.org/10.1172/JCI168553

Sanders, D. W., Kaufman, S. K., DeVos, S. L., Sharma, A. M., Mirbaha, H., Li, A., Barker, S. J., Foley, A. C., Thorpe, J. R., Serpell, L. C., Miller, T. M., Grinberg, L. T., Seeley, W. W., & Diamond, M. I. (2014). Distinct tau prion strains propagate in cells and mice and define different tauopathies. *Neuron*, *82*(6), 1271-1288. https://doi.org/10.1016/j.neuron.2014.04.047

Sandusky-Beltran, L. A., Kovalenko, A., Ma, C., Calahatian, J. I. T., Placides, D. S., Watler, M. D., Hunt, J. B., Darling, A. L., Baker, J. D., Blair, L. J., Martin, M. D., Fontaine, S. N., Dickey, C. A., Lussier, A. L., Weeber, E. J., Selenica, M. B., Nash, K. R., Gordon, M. N., Morgan, D., & Lee, D. C. (2019). Spermidine/spermine-N(1)-acetyltransferase ablation impacts tauopathy-induced polyamine stress response. *Alzheimers Res Ther*, *11*(1), 58. https://doi.org/10.1186/s13195-019-0507-y

Sandusky-Beltran, L. A., Kovalenko, A., Placides, D. S., Ratnasamy, K., Ma, C., Hunt, J. B., Jr., Liang, H., Calahatian, J. I. T., Michalski, C., Fahnestock, M., Blair, L. J., Darling, A. L., Baker, J. D., Fontaine, S. N., Dickey, C. A., Gamsby, J. J., Nash, K. R., Abner, E., Selenica, M. B., & Lee, D. C. (2021). Aberrant AZIN2 and polyamine metabolism precipitates tau neuropathology. *J Clin Invest*, *131*(4). https://doi.org/10.1172/JCI126299

Santa-Maria, I., Perez, M., Hernandez, F., Avila, J., & Moreno, F. J. (2006). Characteristics of the binding of thioflavin S to tau paired helical filaments. *J Alzheimers Dis*, *9*(3), 279-285. https://doi.org/10.3233/jad-2006-9307

Santacruz, K., Lewis, J., Spires, T., Paulson, J., Kotilinek, L., Ingelsson, M., Guimaraes, A., DeTure, M., Ramsden, M., McGowan, E., Forster, C., Yue, M., Orne, J., Janus, C., Mariash, A., Kuskowski, M., Hyman, B., Hutton, M., & Ashe, K. H. (2005). Tau suppression in a neurodegenerative mouse model improves memory function. *Science*, *309*(5733), 476-481. https://doi.org/10.1126/science.1113694

Sato, C., Barthelemy, N. R., Mawuenyega, K. G., Patterson, B. W., Gordon, B. A., Jockel-Balsarotti, J., Sullivan, M., Crisp, M. J., Kasten, T., Kirmess, K. M., Kanaan, N. M.,

Yarasheski, K. E., Baker-Nigh, A., Benzinger, T. L. S., Miller, T. M., Karch, C. M., & Bateman, R. J. (2018). Tau Kinetics in Neurons and the Human Central Nervous System. *Neuron*, *97*(6), 1284-1298 e1287. https://doi.org/10.1016/j.neuron.2018.02.015

Sato, N., Ohtake, Y., Kohno, H., Abe, S., & Ohkubo, Y. (2003). Inhibitory and promotive effects of polyamines on transglutaminase-induced protein polymerization. *Protein Pept Lett*, *10*(4), 396-403. https://doi.org/10.2174/0929866033478816

Savastano, A., Flores, D., Kadavath, H., Biernat, J., Mandelkow, E., & Zweckstetter, M. (2021). Disease-Associated Tau Phosphorylation Hinders Tubulin Assembly within Tau Condensates. *Angew Chem Int Ed Engl*, *60*(2), 726-730. https://doi.org/10.1002/anie.202011157

Scheff, S. W., & Price, D. A. (2006). Alzheimer's disease-related alterations in synaptic density: neocortex and hippocampus. *J Alzheimers Dis*, *9*(3 Suppl), 101-115. https://doi.org/10.3233/jad-2006-9s312

Scheff, S. W., Price, D. A., Schmitt, F. A., DeKosky, S. T., & Mufson, E. J. (2007). Synaptic alterations in CA1 in mild Alzheimer disease and mild cognitive impairment. *Neurology*, *68*(18), 1501-1508. https://doi.org/10.1212/01.wnl.0000260698.46517.8f

Scheff, S. W., Price, D. A., Schmitt, F. A., & Mufson, E. J. (2006). Hippocampal synaptic loss in early Alzheimer's disease and mild cognitive impairment. *Neurobiol Aging*, *27*(10), 1372-1384. https://doi.org/10.1016/j.neurobiolaging.2005.09.012

Scheres, S. H., Zhang, W., Falcon, B., & Goedert, M. (2020). Cryo-EM structures of tau filaments. *Curr Opin Struct Biol*, *64*, 17-25. https://doi.org/10.1016/j.sbi.2020.05.011

Schneider, A., Biernat, J., von Bergen, M., Mandelkow, E., & Mandelkow, E. M. (1999). Phosphorylation that detaches tau protein from microtubules (Ser262, Ser214) also protects it against aggregation into Alzheimer paired helical filaments. *Biochemistry*, *38*(12), 3549-3558. https://doi.org/10.1021/bi981874p

Schoch, K. M., DeVos, S. L., Miller, R. L., Chun, S. J., Norrbom, M., Wozniak, D. F., Dawson, H. N., Bennett, C. F., Rigo, F., & Miller, T. M. (2016). Increased 4R-Tau Induces Pathological Changes in a Human-Tau Mouse Model. *Neuron*, *90*(5), 941-947. https://doi.org/10.1016/j.neuron.2016.04.042

Schoonhoven, D. N., Coomans, E. M., Millan, A. P., van Nifterick, A. M., Visser, D., Ossenkoppele, R., Tuncel, H., van der Flier, W. M., Golla, S. S. V., Scheltens, P., Hillebrand, A., van Berckel, B. N. M., Stam, C. J., & Gouw, A. A. (2023). Tau protein spreads through functionally connected neurons in Alzheimer's disease: a combined MEG/PET study. *Brain*, *146*(10), 4040-4054. https://doi.org/10.1093/brain/awad189

Schopfer, L. M., Girardo, B., Lockridge, O., & Larson, M. A. (2024). Mass Spectrometry of Putrescine, Spermidine, and Spermine Covalently Attached to Francisella tularensis Universal Stress Protein and Bovine Albumin. *Biochem Res Int*, *2024*, 7120208. https://doi.org/10.1155/2024/7120208

Schorova, L., & Martin, S. (2016). Sumoylation in Synaptic Function and Dysfunction. *Front Synaptic Neurosci*, *8*, 9. https://doi.org/10.3389/fnsyn.2016.00009

Schueller, E., Paiva, I., Blanc, F., Wang, X. L., Cassel, J. C., Boutillier, A. L., & Bousiges, O. (2020). Dysregulation of histone acetylation pathways in hippocampus and frontal cortex of Alzheimer's disease patients. *Eur Neuropsychopharmacol*, *33*, 101-116. https://doi.org/10.1016/j.euroneuro.2020.01.015

Scott, C. W., Klika, A. B., Lo, M. M., Norris, T. E., & Caputo, C. B. (1992). Tau protein induces bundling of microtubules in vitro: comparison of different tau isoforms and a tau protein fragment. *J Neurosci Res*, *33*(1), 19-29. https://doi.org/10.1002/jnr.490330104

Seeler, J. S., & Dejean, A. (2003). Nuclear and unclear functions of SUMO. *Nat Rev Mol Cell Biol*, *4*(9), 690-699. https://doi.org/10.1038/nrm1200

Selkoe, D. J. (2000). Toward a comprehensive theory for Alzheimer's disease. Hypothesis: Alzheimer's disease is caused by the cerebral accumulation and cytotoxicity of amyloid beta-protein. *Ann N Y Acad Sci*, *924*, 17-25. https://doi.org/10.1111/j.1749-6632.2000.tb05554.x

Selkoe, D. J., & Hardy, J. (2016). The amyloid hypothesis of Alzheimer's disease at 25 years. *EMBO Mol Med*, *8*(6), 595-608. https://doi.org/10.15252/emmm.201606210

Sengupta, A., Kabat, J., Novak, M., Wu, Q., Grundke-Iqbal, I., & Iqbal, K. (1998). Phosphorylation of tau at both Thr 231 and Ser 262 is required for maximal inhibition of its binding to microtubules. *Arch Biochem Biophys*, *357*(2), 299-309. https://doi.org/10.1006/abbi.1998.0813

Shahpasand, K., Uemura, I., Saito, T., Asano, T., Hata, K., Shibata, K., Toyoshima, Y., Hasegawa, M., & Hisanaga, S. (2012). Regulation of mitochondrial transport and inter-microtubule spacing by tau phosphorylation at the sites hyperphosphorylated in Alzheimer's disease. *J Neurosci*, *32*(7), 2430-2441. https://doi.org/10.1523/JNEUROSCI.5927-11.2012

Shammas, S. L., Garcia, G. A., Kumar, S., Kjaergaard, M., Horrocks, M. H., Shivji, N., Mandelkow, E., Knowles, T. P., Mandelkow, E., & Klenerman, D. (2015). A mechanistic model of tau amyloid aggregation based on direct observation of oligomers. *Nat Commun*, *6*, 7025. https://doi.org/10.1038/ncomms8025

Sharma, A. M., Thomas, T. L., Woodard, D. R., Kashmer, O. M., & Diamond, M. I. (2018). Tau monomer encodes strains. *Elife*, *7*. https://doi.org/10.7554/eLife.37813

Shi, Y., Zhang, W., Yang, Y., Murzin, A. G., Falcon, B., Kotecha, A., van Beers, M., Tarutani, A., Kametani, F., Garringer, H. J., Vidal, R., Hallinan, G. I., Lashley, T., Saito, Y., Murayama, S., Yoshida, M., Tanaka, H., Kakita, A., Ikeuchi, T., . . . Scheres, S. H. W. (2021). Structure-based classification of tauopathies. *Nature*, *598*(7880), 359-363. https://doi.org/10.1038/s41586-021-03911-7

Silva, M. C., & Haggarty, S. J. (2020). Tauopathies: Deciphering Disease Mechanisms to Develop Effective Therapies. *Int J Mol Sci*, *21*(23). https://doi.org/10.3390/ijms21238948

Singer, S. M., Zainelli, G. M., Norlund, M. A., Lee, J. M., & Muma, N. A. (2002). Transglutaminase bonds in neurofibrillary tangles and paired helical filament tau early in Alzheimer's disease. *Neurochem Int*, *40*(1), 17-30. https://doi.org/10.1016/s0197-0186(01)00061-4

Smet-Nocca, C., Broncel, M., Wieruszeski, J. M., Tokarski, C., Hanoulle, X., Leroy, A., Landrieu, I., Rolando, C., Lippens, G., & Hackenberger, C. P. (2011). Identification of O-GlcNAc sites within peptides of the Tau protein and their impact on phosphorylation. *Mol Biosyst*, *7*(5), 1420-1429. https://doi.org/10.1039/c0mb00337a

Soares, E. S., de Souza, A. C. G., Zanella, C. A., Carmichael, R. E., Henley, J. M., Wilkinson, K. A., & Cimarosti, H. I. (2022). Effects of amyloid-beta on protein SUMOylation and levels of mitochondrial proteins in primary cortical neurons. *IBRO Neurosci Rep*, *12*, 142-148. https://doi.org/10.1016/j.ibneur.2022.01.003

Soliman, A. S., Umstead, A., Grabinski, T., Kanaan, N. M., Lee, A., Ryan, J., Lamp, J., & Vega, I. E. (2021). EFhd2 brain interactome reveals its association with different cellular and molecular processes. *J Neurochem*, *159*(6), 992-1007. https://doi.org/10.1111/jnc.15517

Solodkin, A., & Van Hoesen, G. W. (1996). Entorhinal cortex modules of the human brain. *J Comp Neurol*, *365*(4), 610-617. https://doi.org/10.1002/(SICI)1096-9861(19960219)365:4<610::AID-CNE8>3.0.CO;2-7

Song, Y., Kirkpatrick, L. L., Schilling, A. B., Helseth, D. L., Chabot, N., Keillor, J. W., Johnson, G. V., & Brady, S. T. (2013). Transglutaminase and polyamination of tubulin: posttranslational modification for stabilizing axonal microtubules. *Neuron*, *78*(1), 109-123. https://doi.org/10.1016/j.neuron.2013.01.036

Spillantini, M. G., Van Swieten, J. C., & Goedert, M. (2000). Tau gene mutations in frontotemporal dementia and parkinsonism linked to chromosome 17 (FTDP-17). *Neurogenetics*, *2*(4), 193-205. https://doi.org/10.1007/pl00022972

Spittaels, K., Van den Haute, C., Van Dorpe, J., Geerts, H., Mercken, M., Bruynseels, K., Lasrado, R., Vandezande, K., Laenen, I., Boon, T., Van Lint, J., Vandenheede, J., Moechars, D., Loos, R., & Van Leuven, F. (2000). Glycogen synthase kinase-3beta phosphorylates protein tau and rescues the axonopathy in the central nervous system of human four-repeat tau transgenic mice. *J Biol Chem*, *275*(52), 41340-41349. https://doi.org/10.1074/jbc.M006219200

Steele, J. C., Richardson, J. C., & Olszewski, J. (1964). Progressive Supranuclear Palsy. A Heterogeneous Degeneration Involving the Brain Stem, Basal Ganglia and Cerebellum with Vertical Gaze and Pseudobulbar Palsy, Nuchal Dystonia and Dementia. *Arch Neurol*, *10*, 333-359. https://doi.org/10.1001/archneur.1964.00460160003001

Stein, T. D., Montenigro, P. H., Alvarez, V. E., Xia, W., Crary, J. F., Tripodis, Y., Daneshvar, D. H., Mez, J., Solomon, T., Meng, G., Kubilus, C. A., Cormier, K. A., Meng, S., Babcock, K., Kiernan, P., Murphy, L., Nowinski, C. J., Martin, B., Dixon, D., . . . McKee, A. C. (2015). Beta-amyloid deposition in chronic traumatic encephalopathy. *Acta Neuropathol*, *130*(1), 21-34. https://doi.org/10.1007/s00401-015-1435-y

Steinhilb, M. L., Dias-Santagata, D., Mulkearns, E. E., Shulman, J. M., Biernat, J., Mandelkow, E. M., & Feany, M. B. (2007). S/P and T/P phosphorylation is critical for tau neurotoxicity in Drosophila. *J Neurosci Res*, *85*(6), 1271-1278. https://doi.org/10.1002/jnr.21232

Stern, R. A., Daneshvar, D. H., Baugh, C. M., Seichepine, D. R., Montenigro, P. H., Riley, D. O., Fritts, N. G., Stamm, J. M., Robbins, C. A., McHale, L., Simkin, I., Stein, T. D., Alvarez, V. E., Goldstein, L. E., Budson, A. E., Kowall, N. W., Nowinski, C. J., Cantu, R. C., & McKee, A. C. (2013). Clinical presentation of chronic traumatic encephalopathy. *Neurology*, *81*(13), 1122-1129. https://doi.org/10.1212/WNL.0b013e3182a55f7f

Sternberg, Z., Podolsky, R., Nir, A., Yu, J., Nir, R., Halvorsen, S. W., Quinn, J. F., Kaye, J., & Kolb, C. (2022). Elevated spermidine serum levels in mild cognitive impairment, a potential biomarker of progression to Alzheimer dementia, a pilot study. *J Clin Neurosci*, *100*, 169-174. https://doi.org/10.1016/j.jocn.2022.04.028

Stopschinski, B. E., Del Tredici, K., Estill-Terpack, S. J., Ghebremedhin, E., Yu, F. F., Braak, H., & Diamond, M. I. (2021). Anatomic survey of seeding in Alzheimer's disease brains reveals unexpected patterns. *Acta Neuropathol Commun*, *9*(1), 164. https://doi.org/10.1186/s40478-021-01255-x

Stoub, T. R., Detoledo-Morrell, L., & Dickerson, B. C. (2014). Parahippocampal white matter volume predicts Alzheimer's disease risk in cognitively normal old adults. *Neurobiol Aging*, *35*(8), 1855-1861. https://doi.org/10.1016/j.neurobiolaging.2014.01.153

Stoub, T. R., deToledo-Morrell, L., Stebbins, G. T., Leurgans, S., Bennett, D. A., & Shah, R. C. (2006). Hippocampal disconnection contributes to memory dysfunction in individuals at risk for Alzheimer's disease. *Proc Natl Acad Sci U S A*, *103*(26), 10041-10045. https://doi.org/10.1073/pnas.0603414103

Strang, K. H., Sorrentino, Z. A., Riffe, C. J., Gorion, K. M., Vijayaraghavan, N., Golde, T. E., & Giasson, B. I. (2019). Phosphorylation of serine 305 in tau inhibits aggregation. *Neurosci Lett*, *692*, 187-192. https://doi.org/10.1016/j.neulet.2018.11.011

Suarez-Calvet, M., Karikari, T. K., Ashton, N. J., Lantero Rodriguez, J., Mila-Aloma, M., Gispert, J. D., Salvado, G., Minguillon, C., Fauria, K., Shekari, M., Grau-Rivera, O., Arenaza-Urquijo, E. M., Sala-Vila, A., Sanchez-Benavides, G., Gonzalez-de-Echavarri, J. M., Kollmorgen, G., Stoops, E., Vanmechelen, E., Zetterberg, H., . . . Study, A. (2020). Novel tau biomarkers phosphorylated at T181, T217 or T231 rise in the initial stages of the preclinical Alzheimer's continuum when only subtle changes in Abeta pathology are detected. *EMBO Mol Med*, *12*(12), e12921. https://doi.org/10.15252/emmm.202012921

Sui, D., Liu, M., & Kuo, M. H. (2015). In vitro aggregation assays using hyperphosphorylated tau protein. *J Vis Exp*(95), e51537. https://doi.org/10.3791/51537

Sui, D., Xu, X., Ye, X., Liu, M., Mianecki, M., Rattanasinchai, C., Buehl, C., Deng, X., & Kuo, M. H. (2015). Protein interaction module-assisted function X (PIMAX) approach to producing challenging proteins including hyperphosphorylated tau and active CDK5/p25 kinase complex. *Mol Cell Proteomics*, *14*(1), 251-262. https://doi.org/10.1074/mcp.O114.044412

Suk, T. R., Nguyen, T. T., Fisk, Z. A., Mitkovski, M., Geertsma, H. M., Parmasad, J. A., Heer, M. M., Callaghan, S. M., Benseler, F., Brose, N., Tirard, M., & Rousseaux, M. W. C. (2023). Characterizing the differential distribution and targets of Sumo1 and Sumo2 in the mouse brain. *iScience*, *26*(4), 106350. https://doi.org/10.1016/j.isci.2023.106350

Sun, Q., & Gamblin, T. C. (2009). Pseudohyperphosphorylation causing AD-like changes in tau has significant effects on its polymerization. *Biochemistry*, *48*(25), 6002-6011. https://doi.org/10.1021/bi900602h

Sydow, A., Van der Jeugd, A., Zheng, F., Ahmed, T., Balschun, D., Petrova, O., Drexler, D., Zhou, L., Rune, G., Mandelkow, E., D'Hooge, R., Alzheimer, C., & Mandelkow, E. M. (2011). Tau-induced defects in synaptic plasticity, learning, and memory are reversible in transgenic mice after switching off the toxic Tau mutant. *J Neurosci*, *31*(7), 2511-2525. https://doi.org/10.1523/JNEUROSCI.5245-10.2011

Tagliavini, F., & Pilleri, G. (1983). Neuronal counts in basal nucleus of Meynert in Alzheimer disease and in simple senile dementia. *Lancet*, *1*(8322), 469-470. https://doi.org/10.1016/s0140-6736(83)91462-9

Takahashi, K., Ishida, M., Komano, H., & Takahashi, H. (2008). SUMO-1 immunoreactivity co-localizes with phospho-Tau in APP transgenic mice but not in mutant Tau transgenic mice. *Neurosci Lett*, *441*(1), 90-93. https://doi.org/10.1016/j.neulet.2008.06.012

Takamura, H., Nakayama, Y., Ito, H., Katayama, T., Fraser, P. E., & Matsuzaki, S. (2022). SUMO1 Modification of Tau in Progressive Supranuclear Palsy. *Mol Neurobiol*, *59*(7), 4419-4435. https://doi.org/10.1007/s12035-022-02734-5

Takeda, S. (2019). Tau Propagation as a Diagnostic and Therapeutic Target for Dementia: Potentials and Unanswered Questions. *Front Neurosci*, *13*, 1274. https://doi.org/10.3389/fnins.2019.01274

Takeda, S., Wegmann, S., Cho, H., DeVos, S. L., Commins, C., Roe, A. D., Nicholls, S. B., Carlson, G. A., Pitstick, R., Nobuhara, C. K., Costantino, I., Frosch, M. P., Muller, D. J., Irimia, D., & Hyman, B. T. (2015). Neuronal uptake and propagation of a rare phosphorylated high-molecular-weight tau derived from Alzheimer's disease brain. *Nat Commun*, *6*, 8490. https://doi.org/10.1038/ncomms9490

Tan, J. M., Wong, E. S., Kirkpatrick, D. S., Pletnikova, O., Ko, H. S., Tay, S. P., Ho, M. W., Troncoso, J., Gygi, S. P., Lee, M. K., Dawson, V. L., Dawson, T. M., & Lim, K. L. (2008). Lysine 63-linked ubiquitination promotes the formation and autophagic clearance of protein inclusions associated with neurodegenerative diseases. *Hum Mol Genet*, *17*(3), 431-439. https://doi.org/10.1093/hmg/ddm320

Taniguchi-Watanabe, S., Arai, T., Kametani, F., Nonaka, T., Masuda-Suzukake, M., Tarutani, A., Murayama, S., Saito, Y., Arima, K., Yoshida, M., Akiyama, H., Robinson, A., Mann, D. M. A., Iwatsubo, T., & Hasegawa, M. (2016). Biochemical classification of tauopathies by immunoblot, protein sequence and mass spectrometric analyses of sarkosyl-insoluble and trypsin-resistant tau. *Acta Neuropathol*, *131*(2), 267-280. https://doi.org/10.1007/s00401-015-1503-3

Tanner, J. A., & Rabinovici, G. D. (2021). Relationship Between Tau and Cognition in the Evolution of Alzheimer's Disease: New Insights from Tau PET. *J Nucl Med*, *62*(5), 612-613. https://doi.org/10.2967/jnumed.120.257824

Terry, R. D., Gonatas, N. K., & Weiss, M. (1964). Ultrastructural Studies in Alzheimer's Presenile Dementia. *Am J Pathol*, *44*(2), 269-297. https://www.ncbi.nlm.nih.gov/pubmed/14119171

Thal, D. R., Rub, U., Orantes, M., & Braak, H. (2002). Phases of A beta-deposition in the human brain and its relevance for the development of AD. *Neurology*, *58*(12), 1791-1800. https://doi.org/10.1212/wnl.58.12.1791

Thomas, S. N., Funk, K. E., Wan, Y., Liao, Z., Davies, P., Kuret, J., & Yang, A. J. (2012). Dual modification of Alzheimer's disease PHF-tau protein by lysine methylation and ubiquitylation: a mass spectrometry approach. *Acta Neuropathol*, *123*(1), 105-117. https://doi.org/10.1007/s00401-011-0893-0

Tiernan, C. T., Combs, B., Cox, K., Morfini, G., Brady, S. T., Counts, S. E., & Kanaan, N. M. (2016). Pseudophosphorylation of tau at S422 enhances SDS-stable dimer formation and impairs both anterograde and retrograde fast axonal transport. *Exp Neurol*, *283*(Pt A), 318-329. https://doi.org/10.1016/j.expneurol.2016.06.030

Tiernan, C. T., Ginsberg, S. D., He, B., Ward, S. M., Guillozet-Bongaarts, A. L., Kanaan, N. M., Mufson, E. J., & Counts, S. E. (2018). Pretangle pathology within cholinergic nucleus basalis neurons coincides with neurotrophic and neurotransmitter receptor gene dysregulation during the progression of Alzheimer's disease. *Neurobiol Dis*, *117*, 125-136. https://doi.org/10.1016/j.nbd.2018.05.021

Tiernan, C. T., Mufson, E. J., Kanaan, N. M., & Counts, S. E. (2018). Tau Oligomer Pathology in Nucleus Basalis Neurons During the Progression of Alzheimer Disease. *J Neuropathol Exp Neurol*, *77*(3), 246-259. https://doi.org/10.1093/jnen/nlx120

Tortosa, E., Santa-Maria, I., Moreno, F., Lim, F., Perez, M., & Avila, J. (2009). Binding of Hsp90 to tau promotes a conformational change and aggregation of tau protein. *J Alzheimers Dis*, *17*(2), 319-325. https://doi.org/10.3233/JAD-2009-1049

Tracy, T. E., Sohn, P. D., Minami, S. S., Wang, C., Min, S. W., Li, Y., Zhou, Y., Le, D., Lo, I., Ponnusamy, R., Cong, X., Schilling, B., Ellerby, L. M., Huganir, R. L., & Gan, L. (2016). Acetylated Tau Obstructs KIBRA-Mediated Signaling in Synaptic Plasticity and Promotes Tauopathy-Related Memory Loss. *Neuron*, *90*(2), 245-260. https://doi.org/10.1016/j.neuron.2016.03.005

Trzeciakiewicz, H., Ajit, D., Tseng, J. H., Chen, Y., Ajit, A., Tabassum, Z., Lobrovich, R., Peterson, C., Riddick, N. V., Itano, M. S., Tripathy, A., Moy, S. S., Lee, V. M. Y., Trojanowski, J. Q., Irwin, D. J., & Cohen, T. J. (2020). An HDAC6-dependent surveillance mechanism suppresses tau-mediated neurodegeneration and cognitive decline. *Nat Commun*, *11*(1), 5522. https://doi.org/10.1038/s41467-020-19317-4

Trzeciakiewicz, H., Tseng, J. H., Wander, C. M., Madden, V., Tripathy, A., Yuan, C. X., & Cohen, T. J. (2017). A Dual Pathogenic Mechanism Links Tau Acetylation to Sporadic Tauopathy. *Sci Rep*, *7*, 44102. https://doi.org/10.1038/srep44102

Tseng, J. H., Ajit, A., Tabassum, Z., Patel, N., Tian, X., Chen, Y., Prevatte, A. W., Ling, K., Rigo, F., Meeker, R. B., Herring, L. E., & Cohen, T. J. (2021). Tau seeds are subject to aberrant modifications resulting in distinct signatures. *Cell Rep*, *35*(4), 109037. https://doi.org/10.1016/j.celrep.2021.109037

Tseng, J. H., & Cohen, T. J. (2024). The emerging nontraditional roles for tau in the brain. *Cytoskeleton (Hoboken)*, *81*(1), 89-94. https://doi.org/10.1002/cm.21811

Tsuboi, Y., Josephs, K. A., Boeve, B. F., Litvan, I., Caselli, R. J., Caviness, J. N., Uitti, R. J., Bott, A. D., & Dickson, D. W. (2005). Increased tau burden in the cortices of progressive supranuclear palsy presenting with corticobasal syndrome. *Mov Disord*, *20*(8), 982-988. https://doi.org/10.1002/mds.20478

Uddin, M. S., Kabir, M. T., Rahman, M. S., Behl, T., Jeandet, P., Ashraf, G. M., Najda, A., Bin-Jumah, M. N., El-Seedi, H. R., & Abdel-Daim, M. M. (2020). Revisiting the Amyloid Cascade Hypothesis: From Anti-Abeta Therapeutics to Auspicious New Ways for Alzheimer's Disease. *Int J Mol Sci*, *21*(16). https://doi.org/10.3390/ijms21165858

Uversky, V. N., Oldfield, C. J., & Dunker, A. K. (2008). Intrinsically disordered proteins in human diseases: introducing the D2 concept. *Annu Rev Biophys*, *37*, 215-246. https://doi.org/10.1146/annurev.biophys.37.032807.125924

Vaidyanathan, K., Durning, S., & Wells, L. (2014). Functional O-GlcNAc modifications: implications in molecular regulation and pathophysiology. *Crit Rev Biochem Mol Biol*, *49*(2), 140-163. https://doi.org/10.3109/10409238.2014.884535

Van der Jeugd, A., Hochgrafe, K., Ahmed, T., Decker, J. M., Sydow, A., Hofmann, A., Wu, D., Messing, L., Balschun, D., D'Hooge, R., & Mandelkow, E. M. (2012). Cognitive defects are reversible in inducible mice expressing pro-aggregant full-length human Tau. *Acta Neuropathol*, *123*(6), 787-805. https://doi.org/10.1007/s00401-012-0987-3

van der Kant, R., Goldstein, L. S. B., & Ossenkoppele, R. (2020). Amyloid-beta-independent regulators of tau pathology in Alzheimer disease. *Nat Rev Neurosci*, *21*(1), 21-35. https://doi.org/10.1038/s41583-019-0240-3

van Dyck, C. H., Swanson, C. J., Aisen, P., Bateman, R. J., Chen, C., Gee, M., Kanekiyo, M., Li, D., Reyderman, L., Cohen, S., Froelich, L., Katayama, S., Sabbagh, M., Vellas, B., Watson, D., Dhadda, S., Irizarry, M., Kramer, L. D., & Iwatsubo, T. (2023). Lecanemab in Early Alzheimer's Disease. *N Engl J Med*, *388*(1), 9-21. https://doi.org/10.1056/NEJMoa2212948

van Niekerk, E. A., Willis, D. E., Chang, J. H., Reumann, K., Heise, T., & Twiss, J. L. (2007). Sumoylation in axons triggers retrograde transport of the RNA-binding protein La. *Proc Natl Acad Sci U S A*, *104*(31), 12913-12918. https://doi.org/10.1073/pnas.0611562104

Vana, L., Kanaan, N. M., Ugwu, I. C., Wuu, J., Mufson, E. J., & Binder, L. I. (2011). Progression of tau pathology in cholinergic Basal forebrain neurons in mild cognitive impairment and Alzheimer's disease. *Am J Pathol*, *179*(5), 2533-2550. https://doi.org/10.1016/j.ajpath.2011.07.044

Varani, L., Hasegawa, M., Spillantini, M. G., Smith, M. J., Murrell, J. R., Ghetti, B., Klug, A., Goedert, M., & Varani, G. (1999). Structure of tau exon 10 splicing regulatory element RNA and destabilization by mutations of frontotemporal dementia and parkinsonism linked to chromosome 17. *Proc Natl Acad Sci U S A*, *96*(14), 8229-8234. https://doi.org/10.1073/pnas.96.14.8229

Vega, I. E. (2016). EFhd2, a Protein Linked to Alzheimer's Disease and Other Neurological Disorders. *Front Neurosci*, *10*, 150. https://doi.org/10.3389/fnins.2016.00150

Vega, I. E., Traverso, E. E., Ferrer-Acosta, Y., Matos, E., Colon, M., Gonzalez, J., Dickson, D., Hutton, M., Lewis, J., & Yen, S. H. (2008). A novel calcium-binding protein is associated with tau proteins in tauopathy. *J Neurochem*, *106*(1), 96-106. https://doi.org/10.1111/j.1471-4159.2008.05339.x

Vega, I. E., Umstead, A., & Kanaan, N. M. (2019). EFhd2 Affects Tau Liquid-Liquid Phase Separation. *Front Neurosci*, *13*, 845. https://doi.org/10.3389/fnins.2019.00845

Vejandla, B., Savani, S., Appalaneni, R., Veeravalli, R. S., & Gude, S. S. (2024). Alzheimer's Disease: The Past, Present, and Future of a Globally Progressive Disease. *Cureus*, *16*(1), e51705. https://doi.org/10.7759/cureus.51705

Verelst, J., Geukens, N., Eddarkaoui, S., Vliegen, D., De Smidt, E., Rosseels, J., Franssens, V., Molenberghs, S., Francois, C., Stoops, E., Bjerke, M., Engelborghs, S., Laghmouchi, M., Carmans, S., Buee, L., Vanmechelen, E., Winderickx, J., & Thomas, D. (2020). A Novel Tau Antibody Detecting the First Amino-Terminal Insert Reveals Conformational Differences Among Tau Isoforms. *Front Mol Biosci*, *7*, 48. https://doi.org/10.3389/fmolb.2020.00048

von Bergen, M., Barghorn, S., Biernat, J., Mandelkow, E. M., & Mandelkow, E. (2005). Tau aggregation is driven by a transition from random coil to beta sheet structure. *Biochim Biophys Acta*, *1739*(2-3), 158-166. https://doi.org/10.1016/j.bbadis.2004.09.010

von Bergen, M., Barghorn, S., Li, L., Marx, A., Biernat, J., Mandelkow, E. M., & Mandelkow, E. (2001). Mutations of tau protein in frontotemporal dementia promote aggregation of paired helical filaments by enhancing local beta-structure. *J Biol Chem*, *276*(51), 48165-48174. https://doi.org/10.1074/jbc.M105196200

von Bergen, M., Barghorn, S., Muller, S. A., Pickhardt, M., Biernat, J., Mandelkow, E. M., Davies, P., Aebi, U., & Mandelkow, E. (2006). The core of tau-paired helical filaments studied by scanning transmission electron microscopy and limited proteolysis. *Biochemistry*, *45*(20), 6446-6457. https://doi.org/10.1021/bi052530j

von Bergen, M., Friedhoff, P., Biernat, J., Heberle, J., Mandelkow, E. M., & Mandelkow, E. (2000). Assembly of tau protein into Alzheimer paired helical filaments depends on a local sequence motif ((306)VQIVYK(311)) forming beta structure. *Proc Natl Acad Sci U S A*, *97*(10), 5129-5134. https://doi.org/10.1073/pnas.97.10.5129

Voss, K., & Gamblin, T. C. (2009). GSK-3beta phosphorylation of functionally distinct tau isoforms has differential, but mild effects. *Mol Neurodegener*, *4*, 18. https://doi.org/10.1186/1750-1326-4-18

Vossel, K. A., Xu, J. C., Fomenko, V., Miyamoto, T., Suberbielle, E., Knox, J. A., Ho, K., Kim, D. H., Yu, G. Q., & Mucke, L. (2015). Tau reduction prevents Abeta-induced axonal transport deficits by blocking activation of GSK3beta. *J Cell Biol*, *209*(3), 419-433. https://doi.org/10.1083/jcb.201407065

Wang, D. S., Dickson, D. W., & Malter, J. S. (2008). Tissue transglutaminase, protein cross-linking and Alzheimer's disease: review and views. *Int J Clin Exp Pathol*, *1*(1), 5-18. https://www.ncbi.nlm.nih.gov/pubmed/18784819

https://www.ncbi.nlm.nih.gov/pmc/articles/PMC2480529/pdf/ijcep0001-0005.pdf

Wang, H., Yang, T., Sun, J., Zhang, S., & Liu, S. (2021). SENP1 modulates microglia-mediated neuroinflammation toward intermittent hypoxia-induced cognitive decline through the de-SUMOylation of NEMO. *J Cell Mol Med*, *25*(14), 6841-6854. https://doi.org/10.1111/jcmm.16689

Wang, J., Wang, X., Liu, R., Wang, Q., Grundke-Iqbal, I., & Iqbal, K. (2002). In vitro analysis of tau phosphorylation sites and its biological activity. *Chin Med Sci J*, *17*(1), 13-16. https://www.ncbi.nlm.nih.gov/pubmed/12894878

Wang, J., Wei, Z., Wang, Q., Grundke-Iqbal, I., & Iqbal, K. (2000). [Association of microtubule promoting and binding activity of tau with its phosphorylation sites]. *Zhongguo Yi Xue Ke Xue Yuan Xue Bao*, *22*(2), 120-123. https://www.ncbi.nlm.nih.gov/pubmed/12903511

Wang, P., Joberty, G., Buist, A., Vanoosthuyse, A., Stancu, I. C., Vasconcelos, B., Pierrot, N., Faelth-Savitski, M., Kienlen-Campard, P., Octave, J. N., Bantscheff, M., Drewes, G., Moechars, D., & Dewachter, I. (2017). Tau interactome mapping based identification of Otub1 as Tau deubiquitinase involved in accumulation of pathological Tau forms in vitro and in vivo. *Acta Neuropathol*, *133*(5), 731-749. https://doi.org/10.1007/s00401-016-1663-9

Wang, X., Li, W., Marcus, J., Pearson, M., Song, L., Smith, K., Terracina, G., Lee, J., Hong, K. K., Lu, S. X., Hyde, L., Chen, S. C., Kinsley, D., Melchor, J. P., Rubins, D. J., Meng, X., Hostetler, E., Sur, C., Zhang, L., . . . Smith, S. M. (2020). MK-8719, a Novel and Selective O-GlcNAcase Inhibitor That Reduces the Formation of Pathological Tau and Ameliorates Neurodegeneration in a Mouse Model of Tauopathy. *J Pharmacol Exp Ther*, *374*(2), 252-263. https://doi.org/10.1124/jpet.120.266122

Wang, Y., Loomis, P. A., Zinkowski, R. P., & Binder, L. I. (1993). A novel tau transcript in cultured human neuroblastoma cells expressing nuclear tau. *J Cell Biol*, *121*(2), 257-267. https://doi.org/10.1083/jcb.121.2.257

Wang, Y., & Mandelkow, E. (2016). Tau in physiology and pathology. *Nat Rev Neurosci*, *17*(1), 5-21. https://doi.org/10.1038/nrn.2015.1

Ward, S. M., Himmelstein, D. S., Lancia, J. K., Fu, Y., Patterson, K. R., & Binder, L. I. (2013). TOC1: characterization of a selective oligomeric tau antibody. *J Alzheimers Dis*, *37*(3), 593-602. https://doi.org/10.3233/JAD-131235

Waxman, L., Fagan, J. M., & Goldberg, A. L. (1987). Demonstration of two distinct high molecular weight proteases in rabbit reticulocytes, one of which degrades ubiquitin conjugates. *J Biol Chem*, *262*(6), 2451-2457. https://www.ncbi.nlm.nih.gov/pubmed/3029081

Weaver, C. L., Espinoza, M., Kress, Y., & Davies, P. (2000). Conformational change as one of the earliest alterations of tau in Alzheimer's disease. *Neurobiol Aging*, *21*(5), 719-727. https://doi.org/10.1016/s0197-4580(00)00157-3

Weber, A. R., Schuermann, D., & Schar, P. (2014). Versatile recombinant SUMOylation system for the production of SUMO-modified protein. *PLoS One*, *9*(7), e102157. https://doi.org/10.1371/journal.pone.0102157

Weeraratna, A. T., Kalehua, A., Deleon, I., Bertak, D., Maher, G., Wade, M. S., Lustig, A., Becker, K. G., Wood, W., 3rd, Walker, D. G., Beach, T. G., & Taub, D. D. (2007). Alterations in immunological and neurological gene expression patterns in Alzheimer's disease tissues. *Exp Cell Res*, *313*(3), 450-461. https://doi.org/10.1016/j.yexcr.2006.10.028

Weickert, S., Wawrzyniuk, M., John, L. H., Rudiger, S. G. D., & Drescher, M. (2020). The mechanism of Hsp90-induced oligomerizaton of Tau. *Sci Adv*, *6*(11), eaax6999. https://doi.org/10.1126/sciadv.aax6999

Weingarten, M. D., Lockwood, A. H., Hwo, S. Y., & Kirschner, M. W. (1975). A protein factor essential for microtubule assembly. *Proc Natl Acad Sci U S A*, *72*(5), 1858-1862. https://doi.org/10.1073/pnas.72.5.1858

Wen, Y., Yang, Q., Jiao, B., Zhang, W., Lin, J., Zhu, Y., Xu, Q., Zhou, H., Weng, L., Liao, X., Zhou, Y., Wang, J., Guo, J., Yan, X., Jiang, H., Tang, B., & Shen, L. (2023). Clinical features of progressive supranuclear palsy. *Front Aging Neurosci*, *15*, 1229491. https://doi.org/10.3389/fnagi.2023.1229491

Wesseling, H., Mair, W., Kumar, M., Schlaffner, C. N., Tang, S., Beerepoot, P., Fatou, B., Guise, A. J., Cheng, L., Takeda, S., Muntel, J., Rotunno, M. S., Dujardin, S., Davies, P., Kosik, K. S., Miller, B. L., Berretta, S., Hedreen, J. C., Grinberg, L. T., . . . Steen, J. A. (2020). Tau PTM Profiles Identify Patient Heterogeneity and Stages of Alzheimer's Disease. *Cell*, *183*(6), 1699-1713 e1613. https://doi.org/10.1016/j.cell.2020.10.029

Whitwell, J. L., Josephs, K. A., Murray, M. E., Kantarci, K., Przybelski, S. A., Weigand, S. D., Vemuri, P., Senjem, M. L., Parisi, J. E., Knopman, D. S., Boeve, B. F., Petersen, R. C., Dickson, D. W., & Jack, C. R., Jr. (2008). MRI correlates of neurofibrillary tangle pathology at autopsy: a voxel-based morphometry study. *Neurology*, *71*(10), 743-749. https://doi.org/10.1212/01.wnl.0000324924.91351.7d

Wilcock, G. K., & Esiri, M. M. (1982). Plaques, tangles and dementia. A quantitative study. *J Neurol Sci*, *56*(2-3), 343-356. https://doi.org/10.1016/0022-510x(82)90155-1

Wilhelmus, M. M., Grunberg, S. C., Bol, J. G., van Dam, A. M., Hoozemans, J. J., Rozemuller, A. J., & Drukarch, B. (2009). Transglutaminases and transglutaminase-catalyzed cross-links colocalize with the pathological lesions in Alzheimer's disease brain. *Brain Pathol*, *19*(4), 612-622. https://doi.org/10.1111/j.1750-3639.2008.00197.x

Wilkinson, K. A., Nakamura, Y., & Henley, J. M. (2010). Targets and consequences of protein SUMOylation in neurons. *Brain Res Rev*, *64*(1), 195-212. https://doi.org/10.1016/j.brainresrev.2010.04.002

Williams, D. R. (2006). Tauopathies: classification and clinical update on neurodegenerative diseases associated with microtubule-associated protein tau. *Intern Med J*, *36*(10), 652-660. https://doi.org/10.1111/j.1445-5994.2006.01153.x

Williams, D. R., de Silva, R., Paviour, D. C., Pittman, A., Watt, H. C., Kilford, L., Holton, J. L., Revesz, T., & Lees, A. J. (2005). Characteristics of two distinct clinical phenotypes in pathologically proven progressive supranuclear palsy: Richardson's syndrome and PSP-parkinsonism. *Brain*, *128*(Pt 6), 1247-1258. https://doi.org/10.1093/brain/awh488

Williams, D. R., Holton, J. L., Strand, K., Revesz, T., & Lees, A. J. (2007). Pure akinesia with gait freezing: a third clinical phenotype of progressive supranuclear palsy. *Mov Disord*, *22*(15), 2235-2241. https://doi.org/10.1002/mds.21698

Winsor, C. P. (1932). The Gompertz Curve as a Growth Curve. *Proc Natl Acad Sci U S A*, *18*(1), 1-8. https://doi.org/10.1073/pnas.18.1.1

Wischik, C. M., Crowther, R. A., Stewart, M., & Roth, M. (1985). Subunit structure of paired helical filaments in Alzheimer's disease. *J Cell Biol*, *100*(6), 1905-1912. https://doi.org/10.1083/jcb.100.6.1905

Wischik, C. M., Novak, M., Edwards, P. C., Klug, A., Tichelaar, W., & Crowther, R. A. (1988). Structural characterization of the core of the paired helical filament of Alzheimer disease. *Proc Natl Acad Sci U S A*, *85*(13), 4884-4888. https://doi.org/10.1073/pnas.85.13.4884

Wisniewski, H. M., Merz, P. A., & Iqbal, K. (1984). Ultrastructure of paired helical filaments of Alzheimer's neurofibrillary tangle. *J Neuropathol Exp Neurol*, *43*(6), 643-656. https://doi.org/10.1097/00005072-198411000-00008

Witman, G. B., Cleveland, D. W., Weingarten, M. D., & Kirschner, M. W. (1976). Tubulin requires tau for growth onto microtubule initiating sites. *Proc Natl Acad Sci U S A*, *73*(11), 4070-4074. https://doi.org/10.1073/pnas.73.11.4070

Woerman, A. L., Aoyagi, A., Patel, S., Kazmi, S. A., Lobach, I., Grinberg, L. T., McKee, A. C., Seeley, W. W., Olson, S. H., & Prusiner, S. B. (2016). Tau prions from Alzheimer's disease and chronic traumatic encephalopathy patients propagate in cultured cells. *Proc Natl Acad Sci U S A*, *113*(50), E8187-E8196. https://doi.org/10.1073/pnas.1616344113

Wolozin, B. L., Pruchnicki, A., Dickson, D. W., & Davies, P. (1986). A neuronal antigen in the brains of Alzheimer patients. *Science*, *232*(4750), 648-650. https://doi.org/10.1126/science.3083509

Wood, J. G., Mirra, S. S., Pollock, N. J., & Binder, L. I. (1986). Neurofibrillary tangles of Alzheimer disease share antigenic determinants with the axonal microtubule-associated protein tau (tau). *Proc Natl Acad Sci U S A*, *83*(11), 4040-4043. https://doi.org/10.1073/pnas.83.11.4040

Wszolek, Z. K., Tsuboi, Y., Ghetti, B., Pickering-Brown, S., Baba, Y., & Cheshire, W. P. (2006). Frontotemporal dementia and parkinsonism linked to chromosome 17 (FTDP-17). *Orphanet J Rare Dis*, *1*, 30. https://doi.org/10.1186/1750-1172-1-30

Wu, J. W., Herman, M., Liu, L., Simoes, S., Acker, C. M., Figueroa, H., Steinberg, J. I., Margittai, M., Kayed, R., Zurzolo, C., Di Paolo, G., & Duff, K. E. (2013). Small misfolded Tau species are internalized via bulk endocytosis and anterogradely and retrogradely transported in neurons. *J Biol Chem*, *288*(3), 1856-1870. https://doi.org/10.1074/jbc.M112.394528

Xia, Y., Bell, B. M., & Giasson, B. I. (2021). Tau K321/K353 pseudoacetylation within KXGS motifs regulates tau-microtubule interactions and inhibits aggregation. *Sci Rep*, *11*(1), 17069. https://doi.org/10.1038/s41598-021-96627-7

Xia, Y., Bell, B. M., & Giasson, B. I. (2023). Tau Lysine Pseudomethylation Regulates Microtubule Binding and Enhances Prion-like Tau Aggregation. *Int J Mol Sci*, *24*(9). https://doi.org/10.3390/ijms24098286

Xia, Y., Prokop, S., & Giasson, B. I. (2021). "Don't Phos Over Tau": recent developments in clinical biomarkers and therapies targeting tau phosphorylation in Alzheimer's disease

and other tauopathies. *Mol Neurodegener*, *16*(1), 37. https://doi.org/10.1186/s13024-021-00460-5

Xia, Y., Prokop, S., Gorion, K. M., Kim, J. D., Sorrentino, Z. A., Bell, B. M., Manaois, A. N., Chakrabarty, P., Davies, P., & Giasson, B. I. (2020). Tau Ser208 phosphorylation promotes aggregation and reveals neuropathologic diversity in Alzheimer's disease and other tauopathies. *Acta Neuropathol Commun*, *8*(1), 88. https://doi.org/10.1186/s40478-020-00967-w

Xue, C., Lin, T. Y., Chang, D., & Guo, Z. (2017). Thioflavin T as an amyloid dye: fibril quantification, optimal concentration and effect on aggregation. *R Soc Open Sci*, *4*(1), 160696. https://doi.org/10.1098/rsos.160696

Yagishita, S., Itoh, Y., Nan, W., & Amano, N. (1981). Reappraisal of the fine structure of Alzheimer's neurofibrillary tangles. *Acta Neuropathol*, *54*(3), 239-246. https://doi.org/10.1007/BF00687747

Yamada, K., Holth, J. K., Liao, F., Stewart, F. R., Mahan, T. E., Jiang, H., Cirrito, J. R., Patel, T. K., Hochgrafe, K., Mandelkow, E. M., & Holtzman, D. M. (2014). Neuronal activity regulates extracellular tau in vivo. *J Exp Med*, *211*(3), 387-393. https://doi.org/10.1084/jem.20131685

Yamada, T., McGeer, P. L., & McGeer, E. G. (1992). Appearance of paired nucleated, Tau-positive glia in patients with progressive supranuclear palsy brain tissue. *Neurosci Lett*, *135*(1), 99-102. https://doi.org/10.1016/0304-3940(92)90145-w

Yan, Y., Wang, X., Chaput, D., Shin, M. K., Koh, Y., Gan, L., Pieper, A. A., Woo, J. A., & Kang, D. E. (2022). X-linked ubiquitin-specific peptidase 11 increases tauopathy vulnerability in women. *Cell*, *185*(21), 3913-3930 e3919. https://doi.org/10.1016/j.cell.2022.09.002

Yang, H. D., Kim, D. H., Lee, S. B., & Young, L. D. (2016). History of Alzheimer's Disease. *Dement Neurocogn Disord*, *15*(4), 115-121. https://doi.org/10.12779/dnd.2016.15.4.115

Yang, J., Shen, N., Shen, J., Yang, Y., & Li, H. L. (2023). Complicated Role of Post-translational Modification and Protease-Cleaved Fragments of Tau in Alzheimer's Disease and Other Tauopathies. *Mol Neurobiol*. https://doi.org/10.1007/s12035-023-03867-x

Yang, S., Wang, Y., Mann, M., Wang, Q., Tian, E., Zhang, L., Cipollo, J. F., Ten Hagen, K. G., & Tabak, L. A. (2021). Improved online LC-MS/MS identification of O-glycosites by EThcD fragmentation, chemoenzymatic reaction, and SPE enrichment. *Glycoconj J*, *38*(2), 145-156. https://doi.org/10.1007/s10719-020-09952-w

Yang, X., & Qian, K. (2017). Protein O-GlcNAcylation: emerging mechanisms and functions. *Nat Rev Mol Cell Biol*, *18*(7), 452-465. https://doi.org/10.1038/nrm.2017.22

Ye, H., Han, Y., Li, P., Su, Z., & Huang, Y. (2022). The Role of Post-Translational Modifications on the Structure and Function of Tau Protein. *J Mol Neurosci*, *72*(8), 1557-1571. https://doi.org/10.1007/s12031-022-02002-0

Yoshiyama, Y., Higuchi, M., Zhang, B., Huang, S. M., Iwata, N., Saido, T. C., Maeda, J., Suhara, T., Trojanowski, J. Q., & Lee, V. M. (2007). Synapse loss and microglial activation precede tangles in a P301S tauopathy mouse model. *Neuron*, *53*(3), 337-351. https://doi.org/10.1016/j.neuron.2007.01.010

Yu, C. H., Chou, C. C., Lee, Y. J., Khoo, K. H., & Chang, G. D. (2015). Uncovering protein polyamination by the spermine-specific antiserum and mass spectrometric analysis. *Amino Acids*, *47*(3), 469-481. https://doi.org/10.1007/s00726-014-1879-8

Yu, Y., Run, X., Liang, Z., Li, Y., Liu, F., Liu, Y., Iqbal, K., Grundke-Iqbal, I., & Gong, C. X. (2009). Developmental regulation of tau phosphorylation, tau kinases, and tau phosphatases. *J Neurochem*, *108*(6), 1480-1494. https://doi.org/10.1111/j.1471-4159.2009.05882.x

Yuzwa, S. A., Cheung, A. H., Okon, M., McIntosh, L. P., & Vocadlo, D. J. (2014). O-GlcNAc modification of tau directly inhibits its aggregation without perturbing the conformational properties of tau monomers. *J Mol Biol*, *426*(8), 1736-1752. https://doi.org/10.1016/j.jmb.2014.01.004

Yuzwa, S. A., Macauley, M. S., Heinonen, J. E., Shan, X., Dennis, R. J., He, Y., Whitworth, G. E., Stubbs, K. A., McEachern, E. J., Davies, G. J., & Vocadlo, D. J. (2008). A potent mechanism-inspired O-GlcNAcase inhibitor that blocks phosphorylation of tau in vivo. *Nat Chem Biol*, *4*(8), 483-490. https://doi.org/10.1038/nchembio.96

Yuzwa, S. A., Shan, X., Macauley, M. S., Clark, T., Skorobogatko, Y., Vosseller, K., & Vocadlo, D. J. (2012). Increasing O-GlcNAc slows neurodegeneration and stabilizes tau against aggregation. *Nat Chem Biol*, *8*(4), 393-399. https://doi.org/10.1038/nchembio.797

Yuzwa, S. A., Yadav, A. K., Skorobogatko, Y., Clark, T., Vosseller, K., & Vocadlo, D. J. (2011). Mapping O-GlcNAc modification sites on tau and generation of a site-specific O-GlcNAc tau antibody. *Amino Acids*, *40*(3), 857-868. https://doi.org/10.1007/s00726-010-0705-1

Zabik, N. L., Imhof, M. M., & Martic-Milne, S. (2017). Structural evaluations of tau protein conformation: methodologies and approaches. *Biochem Cell Biol*, *95*(3), 338-349. https://doi.org/10.1139/bcb-2016-0227

Zemaitaitis, M. O., Kim, S. Y., Halverson, R. A., Troncoso, J. C., Lee, J. M., & Muma, N. A. (2003). Transglutaminase activity, protein, and mRNA expression are increased in progressive supranuclear palsy. *J Neuropathol Exp Neurol*, *62*(2), 173-184. https://doi.org/10.1093/jnen/62.2.173

Zemaitaitis, M. O., Lee, J. M., Troncoso, J. C., & Muma, N. A. (2000). Transglutaminase-induced cross-linking of tau proteins in progressive supranuclear palsy. *J Neuropathol Exp Neurol*, *59*(11), 983-989. https://doi.org/10.1093/jnen/59.11.983

Zhang, J. Y., Liu, S. J., Li, H. L., & Wang, J. Z. (2005). Microtubule-associated protein tau is a substrate of ATP/Mg(2+)-dependent proteasome protease system. *J Neural Transm (Vienna)*, *112*(4), 547-555. https://doi.org/10.1007/s00702-004-0196-x

Zhang, W., Falcon, B., Murzin, A. G., Fan, J., Crowther, R. A., Goedert, M., & Scheres, S. H. (2019). Heparin-induced tau filaments are polymorphic and differ from those in Alzheimer's and Pick's diseases. *Elife*, *8*. https://doi.org/10.7554/eLife.43584

Zhang, W., Tarutani, A., Newell, K. L., Murzin, A. G., Matsubara, T., Falcon, B., Vidal, R., Garringer, H. J., Shi, Y., Ikeuchi, T., Murayama, S., Ghetti, B., Hasegawa, M., Goedert, M., & Scheres, S. H. W. (2020). Novel tau filament fold in corticobasal degeneration. *Nature*, *580*(7802), 283-287. https://doi.org/10.1038/s41586-020-2043-0

Zhang, Y., Wu, K. M., Yang, L., Dong, Q., & Yu, J. T. (2022). Tauopathies: new perspectives and challenges. *Mol Neurodegener*, *17*(1), 28. https://doi.org/10.1186/s13024-022-00533-z

Zhao, J., & Huai, J. (2023). Role of primary aging hallmarks in Alzheimer s disease. *Theranostics*, *13*(1), 197-230. https://doi.org/10.7150/thno.79535

Zhao, Q., Xie, Y., Zheng, Y., Jiang, S., Liu, W., Mu, W., Liu, Z., Zhao, Y., Xue, Y., & Ren, J. (2014). GPS-SUMO: a tool for the prediction of sumoylation sites and SUMO-interaction motifs. *Nucleic Acids Res*, *42*(Web Server issue), W325-330. https://doi.org/10.1093/nar/gku383

Zheng-Fischhofer, Q., Biernat, J., Mandelkow, E. M., Illenberger, S., Godemann, R., & Mandelkow, E. (1998). Sequential phosphorylation of Tau by glycogen synthase kinase-3beta and protein kinase A at Thr212 and Ser214 generates the Alzheimer-specific epitope of antibody AT100 and requires a paired-helical-filament-like conformation. *Eur J Biochem*, *252*(3), 542-552. https://doi.org/10.1046/j.1432-1327.1998.2520542.x

Zhu, H. L., Meng, S. R., Fan, J. B., Chen, J., & Liang, Y. (2011). Fibrillization of human tau is accelerated by exposure to lead via interaction with His-330 and His-362. *PLoS One*, *6*(9), e25020. https://doi.org/10.1371/journal.pone.0025020

Zhu, Y., Shan, X., Yuzwa, S. A., & Vocadlo, D. J. (2014). The emerging link between O-GlcNAc and Alzheimer disease. *J Biol Chem*, *289*(50), 34472-34481. https://doi.org/10.1074/jbc.R114.601351

Zhukareva, V., Mann, D., Pickering-Brown, S., Uryu, K., Shuck, T., Shah, K., Grossman, M., Miller, B. L., Hulette, C. M., Feinstein, S. C., Trojanowski, J. Q., & Lee, V. M. (2002). Sporadic Pick's disease: a tauopathy characterized by a spectrum of pathological tau isoforms in gray and white matter. *Ann Neurol*, *51*(6), 730-739. https://doi.org/10.1002/ana.10222

Zupancic, J. M., Smith, M. D., Trzeciakiewicz, H., Skinner, M. E., Ferris, S. P., Makowski, E. K., Lucas, M. J., McArthur, N., Kane, R. S., Paulson, H. L., & Tessier, P. M. (2023). Quantitative flow cytometric selection of tau conformational nanobodies specific for pathological aggregates. *Front Immunol*, *14*, 1164080. https://doi.org/10.3389/fimmu.2023.1164080

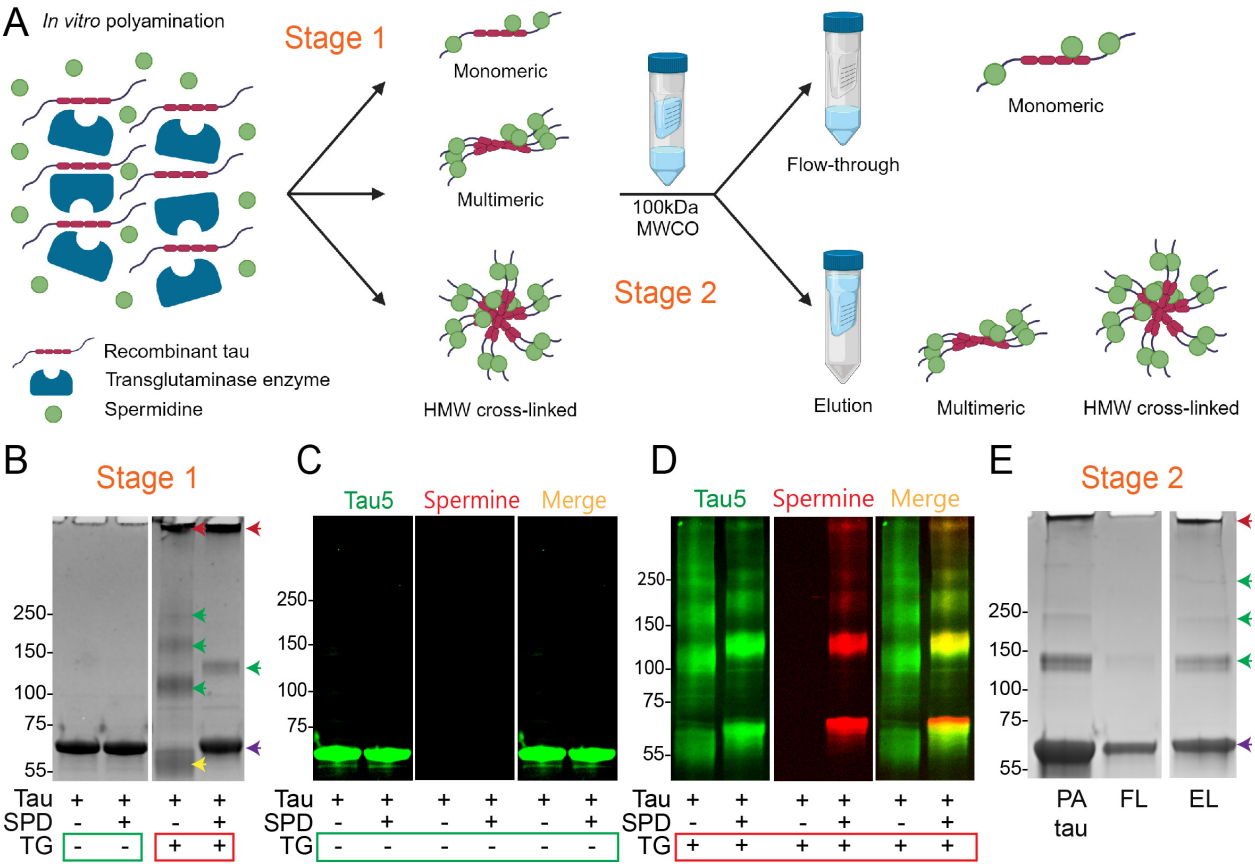

Figure AI.1. Production and purification strategy of SPD tau using hT40 as an example.

A, *in vitro* polyamination reaction with SPD is set up in the presence of the TG enzyme. The polyamination reaction (stage 1) produces a mixture of tau species that includes polyaminated monomeric, multimeric and HMW crosslinked tau. Passing the heterogenous mixture of polyaminated tau products through a membrane with 100 kDa MWCO (stage 2) separates the polyaminated monomeric (flow-through) from multimeric and crosslinked tau species (elution). B-D, mixing tau and SPD in the absence of TG does not produce SPD polyaminated/crosslinked tau (stage 1). A Coomassie stained gel (B) shows that in the absence of SPD TG gives rise to a mixture of crosslinked products that includes intraprotein crosslinked (yellow arrowhead), multimeric (green arrowheads) and HMW interprotein crosslinked (red arrowhead) tau species. Adding SPD to the reaction dramatically decreases the intraprotein crosslinked tau species, while producing SPD polyaminated monomeric tau (purple arrowhead). Immunoblot of samples (C) shows that SPD is not incorporated into tau proteins in the absence of TG enzyme. In contrast, the presence of TG alone (D) produces a mixed population of intraprotein and interprotein crosslinked tau species. When both TG and SPD are present polyaminated monomeric, multimeric and HMW crosslinked tau species are produced. E, the polyaminated tau (PA tau) was passed through a membrane with 100 kDa MWCO (stage 2). The flow-through

Figure AI.1 (cont'd)
(FL) contains mainly monomeric tau species (purple arrowhead), while only the elution (EL) contains the HMW interprotein crosslinked tau species. SPD polyaminated tau in the FL was used to conduct the experiments described in this work. The same strategy was used to purify a polyaminated version of the longest 3R tau isoform – hT39. Abbreviations: SPD, spermidine; TG, transglutaminase enzyme; hT40, 2N4R tau isoform; hT39, 2N3R tau isoform; PA tau, polyaminated tau; HMW, high molecular weight; MWCO, molecular weight cutoff. Panel A created with BioRender.com.

A

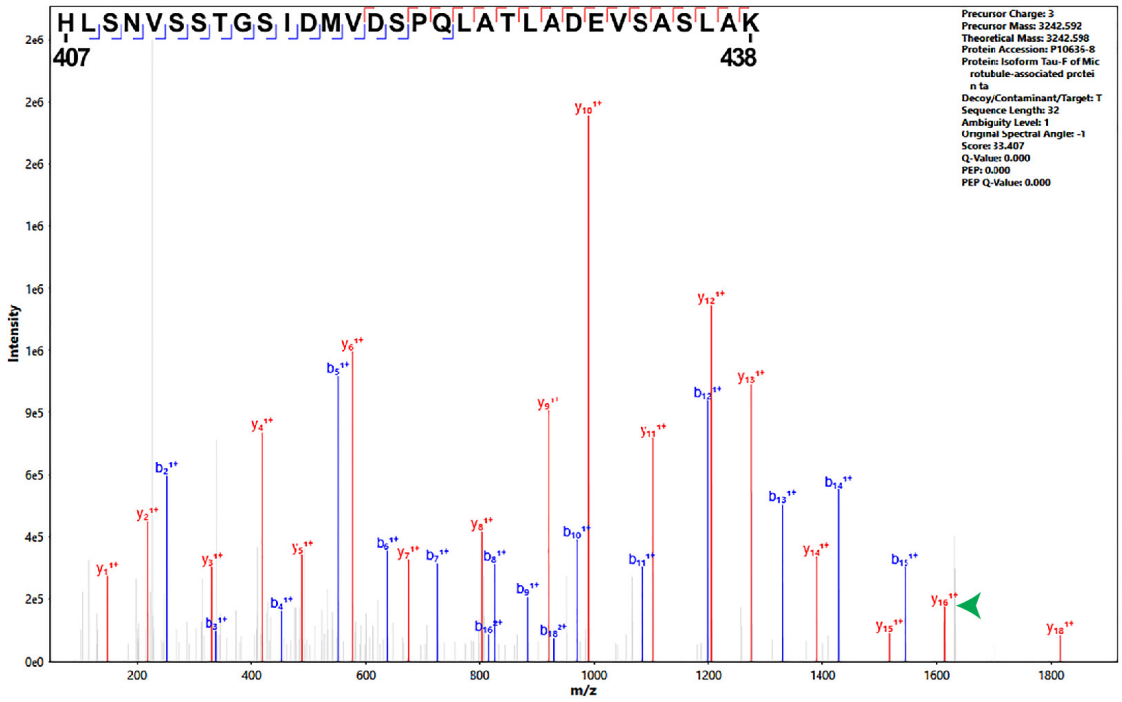

B

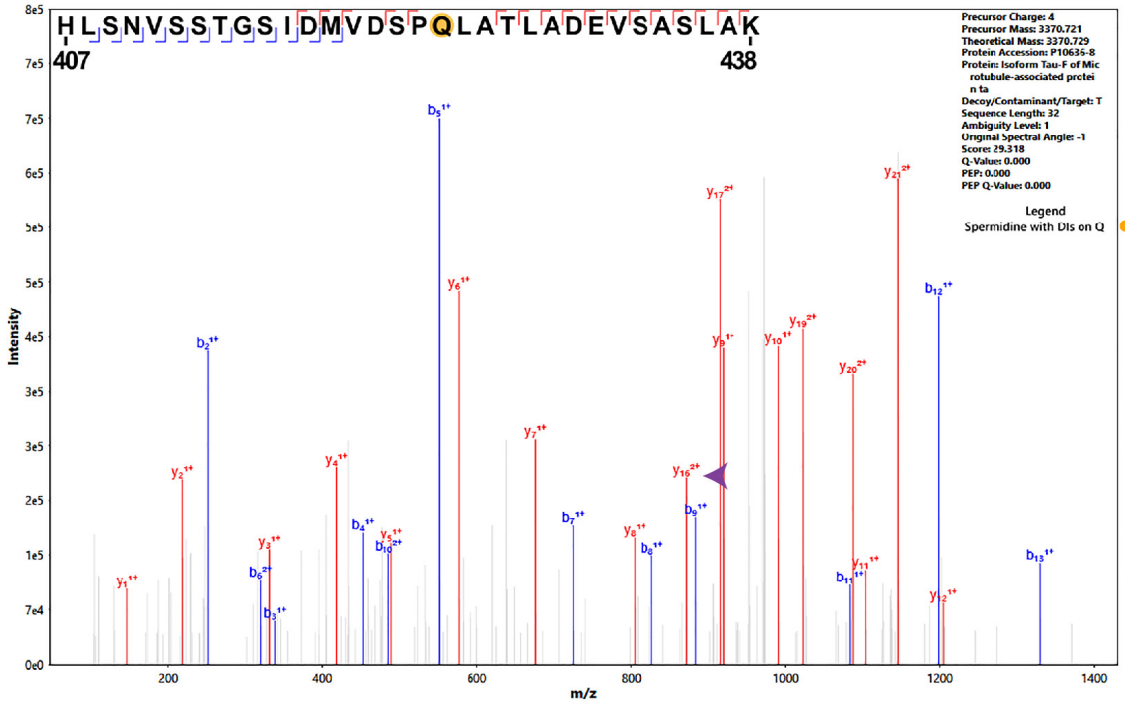

Figure AI.2. Sample mass spectra of tau peptides showing spermidine modification at Q424 of hT40.

Figure AI.2 (cont'd)
A, mass spectrum of peptide spanning amino acids 407-438 in unmodified hT40. All fragmented y-ions showed no change in mass corresponding to polyamination with SPD (e.g. y_{16}^{1+} m/z = 1613.88 equivalent to a mass of 1612.88 Da; green arrowhead). B, mass spectrum of peptide spanning amino acids 407-438 in SPD hT40. Fragmented y-ions from y_{16}-y_{20} carry a double positive charge with a mass shift corresponding to polyamination with SPD (e.g. y_{16}^{2+} m/z = 871.51 equivalent to a mass of 1741.02 Da; purple arrowhead). There was also a reduction in retention time of SPD-modified peptide relative to unmodified peptide 407-438. Abbreviations: SPD, spermidine; hT40, 2N4R tau isoform; m/z, mass-to-charge ratio.

A

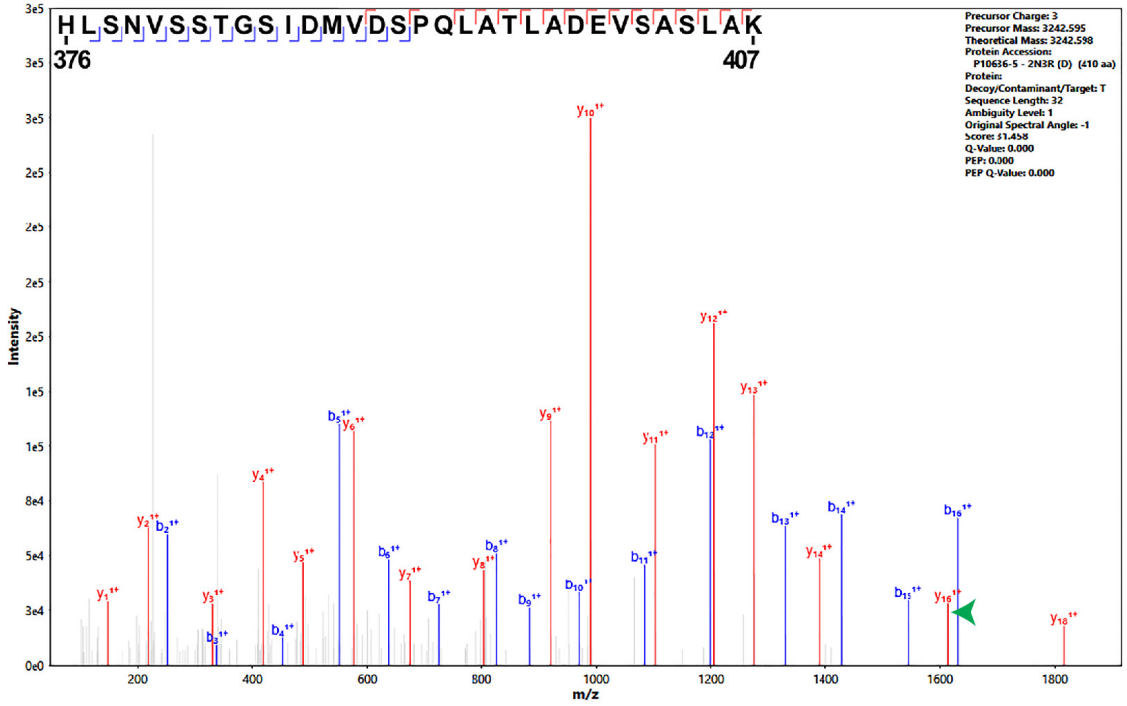

B

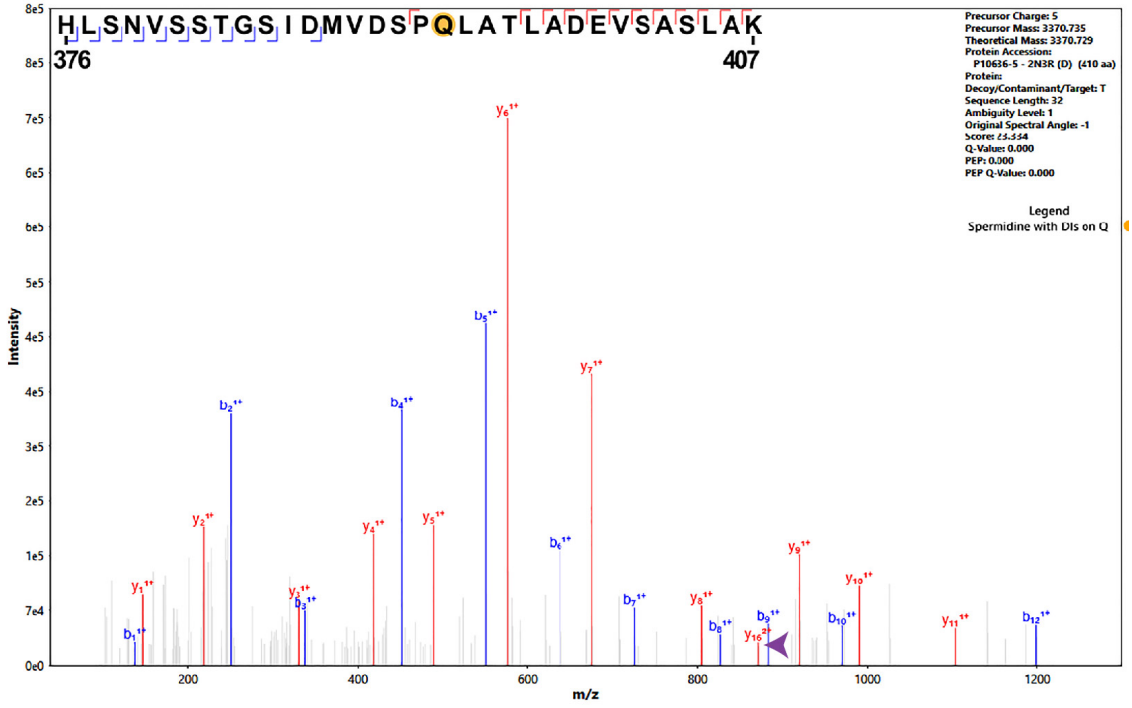

Figure AI.3. Sample mass spectra of tau peptides showing spermidine modification at Q424 of hT39.

Figure AI.3 (cont'd)
A, mass spectrum of peptide spanning amino acids 376-407 (corresponds to 407-438 of 2N4R tau isoform) in unmodified hT39. All fragmented y-ions showed no change in mass corresponding to polyamination with SPD (e.g. y161+ m/z = 1613.87 equivalent to a mass of 1612.87 Da; green arrowhead). B, mass spectrum of peptide spanning amino acids 376-407 in SPD hT39. Fragmented y162+ carries a double positive charge with a mass shift corresponding to polyamination with SPD (i.e. y162+ m/z = 871.51 equivalent to a mass of 1741.02 Da; purple arrowhead). There was also a reduction in retention time of SPD-modified peptide relative to unmodified peptide 376-407. Abbreviations: SPD, spermidine; hT39, 2N3R tau isoform; m/z, mass-to-charge ratio.

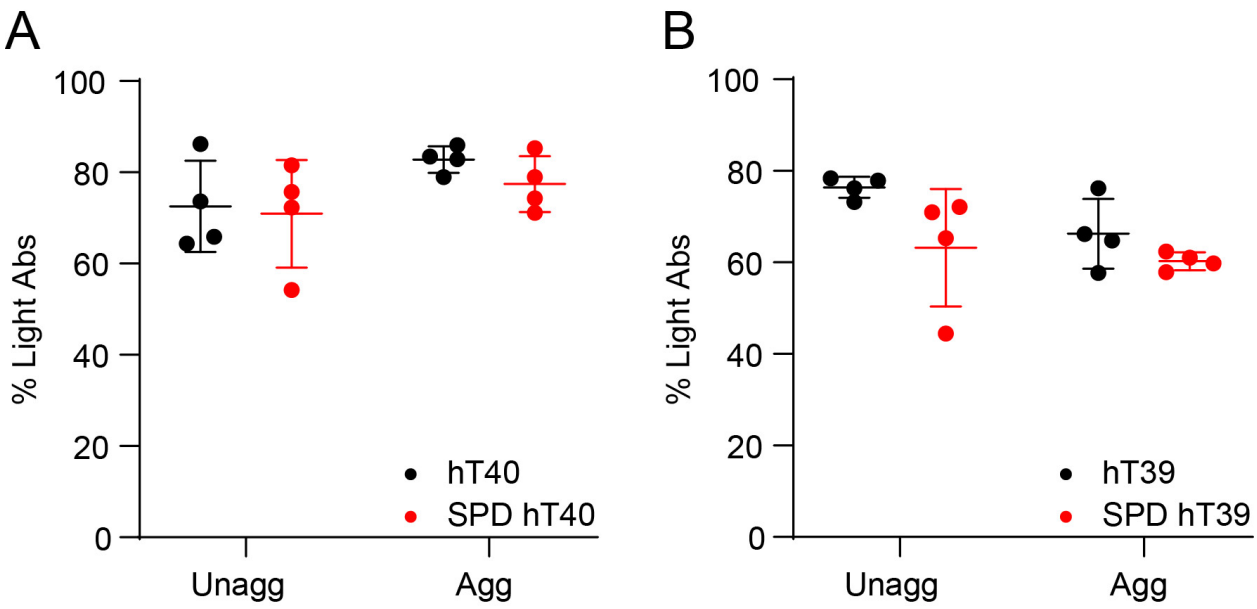

Figure AI.4. Sandwich ELISA assay to quantify total tau levels.
A, sandwich ELISA assay measuring total tau in unaggregated and aggregated hT40 proteins using Tau13 antibody for capture and R1 antibody for detection. B, sandwich ELISA assay measuring total tau in unaggregated and aggregated hT39 proteins using Tau13 antibody for capture and R1 antibody for detection. Abbreviations: SPD, spermidine; hT40, 2N4R tau isoform; hT39, 2N3R tau isoform; R1, tau rabbit polyclonal antibody. Data represented as mean ± SD.

A

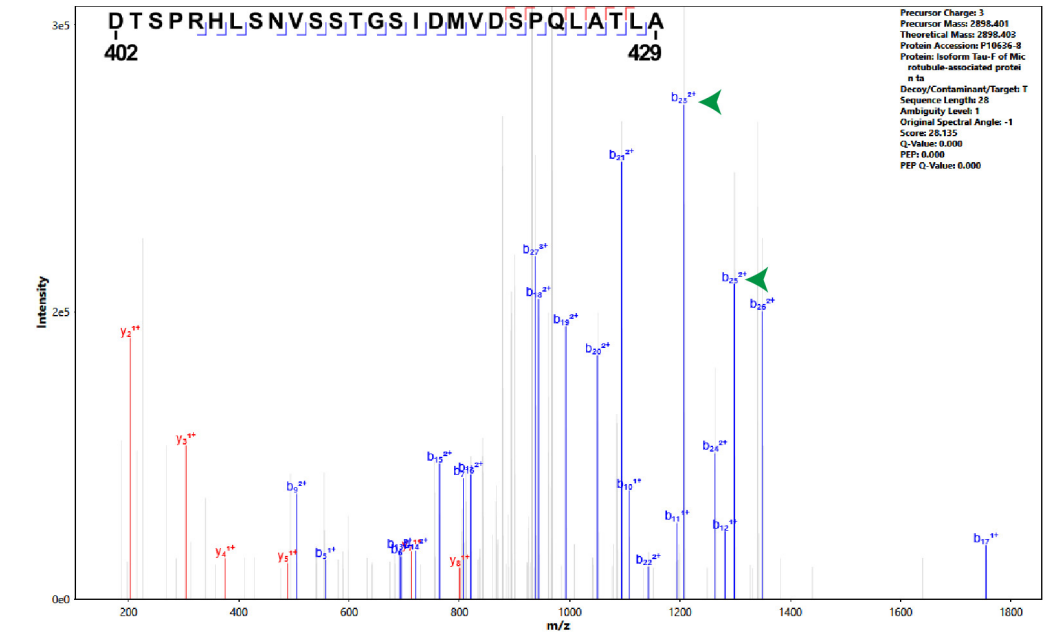

B

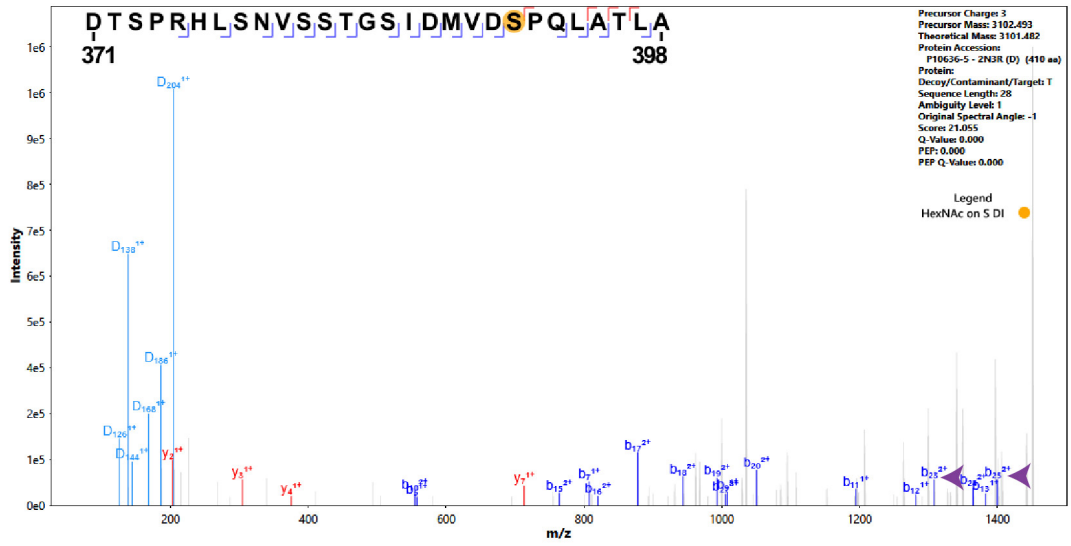

Figure AII.1. Sample mass spectra of tau peptides showing O-GlcNAc modification at S422 of hT40.

Figure AII.1 (cont'd)
A, mass spectrum of peptide spanning amino acids 402-429 in unmodified hT40. Fragmented y-ions showed no change in mass corresponding to O-GlcNAcylation (e.g. b_{23}^{2+} m/z = 1206.56 and b_{25}^{2+} m/z = 1298.62; green arrowheads). B, mass spectrum of peptide spanning amino acids 402-429 in O-GlcNAc-modified hT40. Fragmented b-ions show a mass shift corresponding to modification with O-GlcNAc (e.g. b_{23}^{2+} m/z = 1308.10 and b_{25}^{2+} m/z = 1400.16; purple arrowheads). In addition, all six diagnostic ions produced by O-GlcNAc fragmentation were observed with O-GlcNAc-modified hT40, but not unmodified hT40. Abbreviations: O-GlcNAc, O-linked-N-acetyl β-d-N-glucosamine; hT40, 2N4R tau isoform; m/z, mass-to-charge ratio; DI, diagnostic ion; D126+, diagnostic ion m/z 126Da; D138+, +, diagnostic ion m/z 138Da; D144+, diagnostic ion m/z 144Da; D168+, diagnostic ion m/z 168Da; D186+, diagnostic ion m/z 186Da D204+, diagnostic ion m/z 204Da.

A

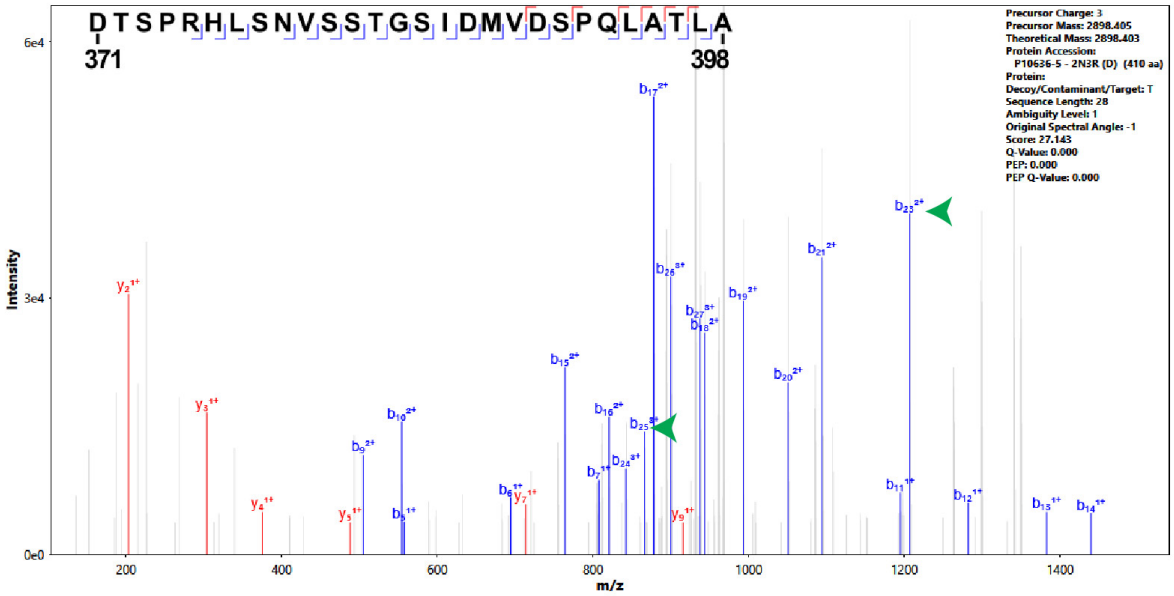

B

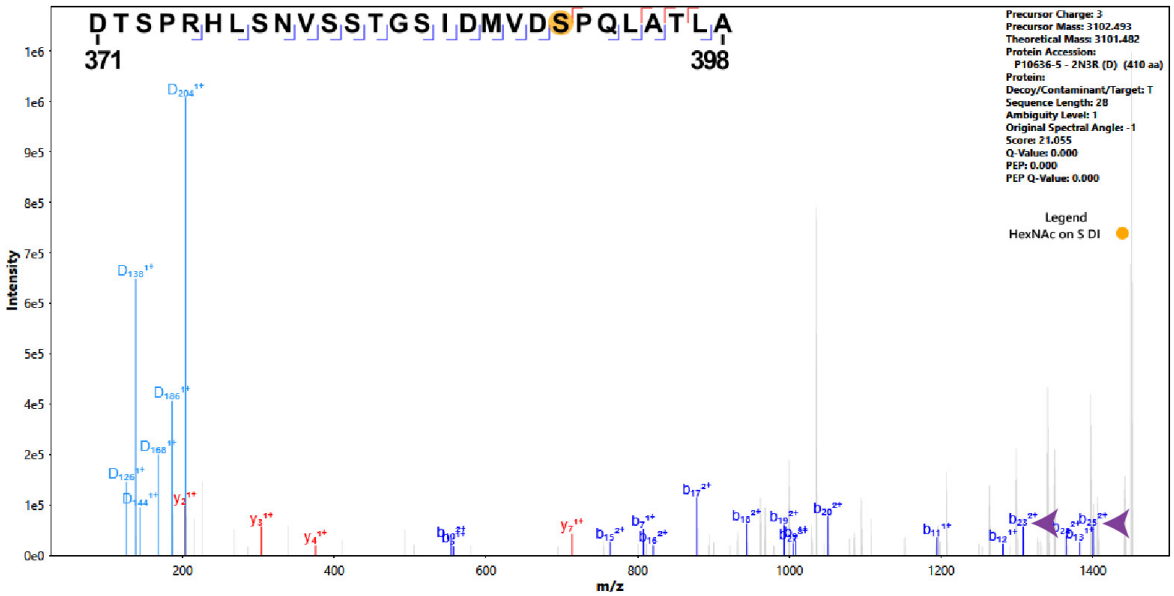

Figure AII.2. Sample mass spectra of tau peptides showing O-GlcNAc modification at S422 of hT39.

A, mass spectrum of peptide spanning amino acids 371-398 in unmodified hT39 (corresponding to 402-429 in hT40). Fragmented y-ions showed no change in mass corresponding to O-GlcNAcylation (e.g. b_{23}^{2+} m/z = 1206.56 and b_{25}^{3+} m/z = 866.08; green

Figure AII.2 (cont'd)
arrowheads). B, mass spectrum of peptide spanning amino acids 371-398 in O-GlcNAc-modified hT39. Fragmented b-ions show a mass shift corresponding to modification with O-GlcNAc (e.g. b232+ m/z = 1308.10 and b252+ m/z = 1400.16; purple arrowheads). In addition, all six diagnostic ions produced by O-GlcNAc fragmentation were observed with O-GlcNAc-modified hT39, but not unmodified hT39. Abbreviations: O-GlcNAc, O-linked-N-acetyl β-d-N-glucosamine; hT40, 2N4R tau isoform; hT39, 2N3R tau isoform; m/z, mass-to-charge ratio; DI, diagnostic ion; D126+, diagnostic ion m/z 126Da; D138+, +, diagnostic ion m/z 138Da; D144+, diagnostic ion m/z 144Da; D168+, diagnostic ion m/z 168Da; D186+, diagnostic ion m/z 186Da D204+, diagnostic ion m/z 204Da.

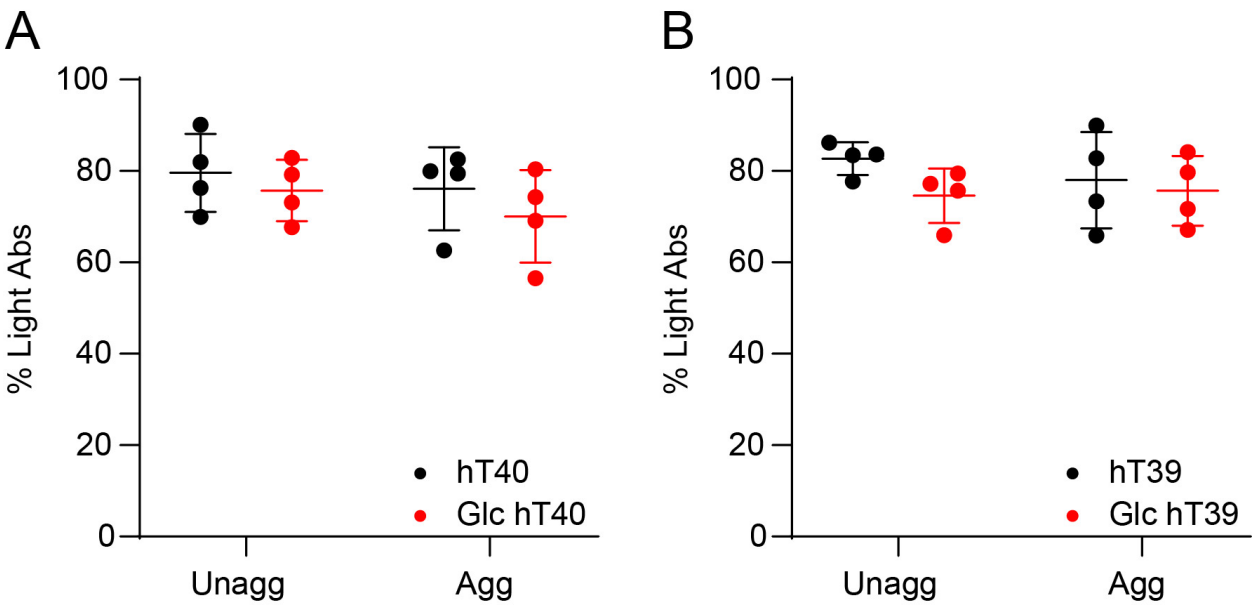

Figure AII.3. Sandwich ELISA assay to quantify total tau levels using the Tau13 antibody.
A, sandwich ELISA assay measuring total tau in unaggregated and aggregated hT40 proteins using Tau13 antibody for capture and R1 antibody for detection. B, sandwich ELISA assay measuring total tau in unaggregated and aggregated hT39 proteins using Tau13 antibody for capture and R1 antibody for detection. Abbreviations: O-GlcNAc, O-linked-N-acetyl β-d-N-glucosamine; hT40, 2N4R tau isoform; hT39, 2N3R tau isoform; R1, tau rabbit polyclonal antibody. Data represented as mean ± SD.

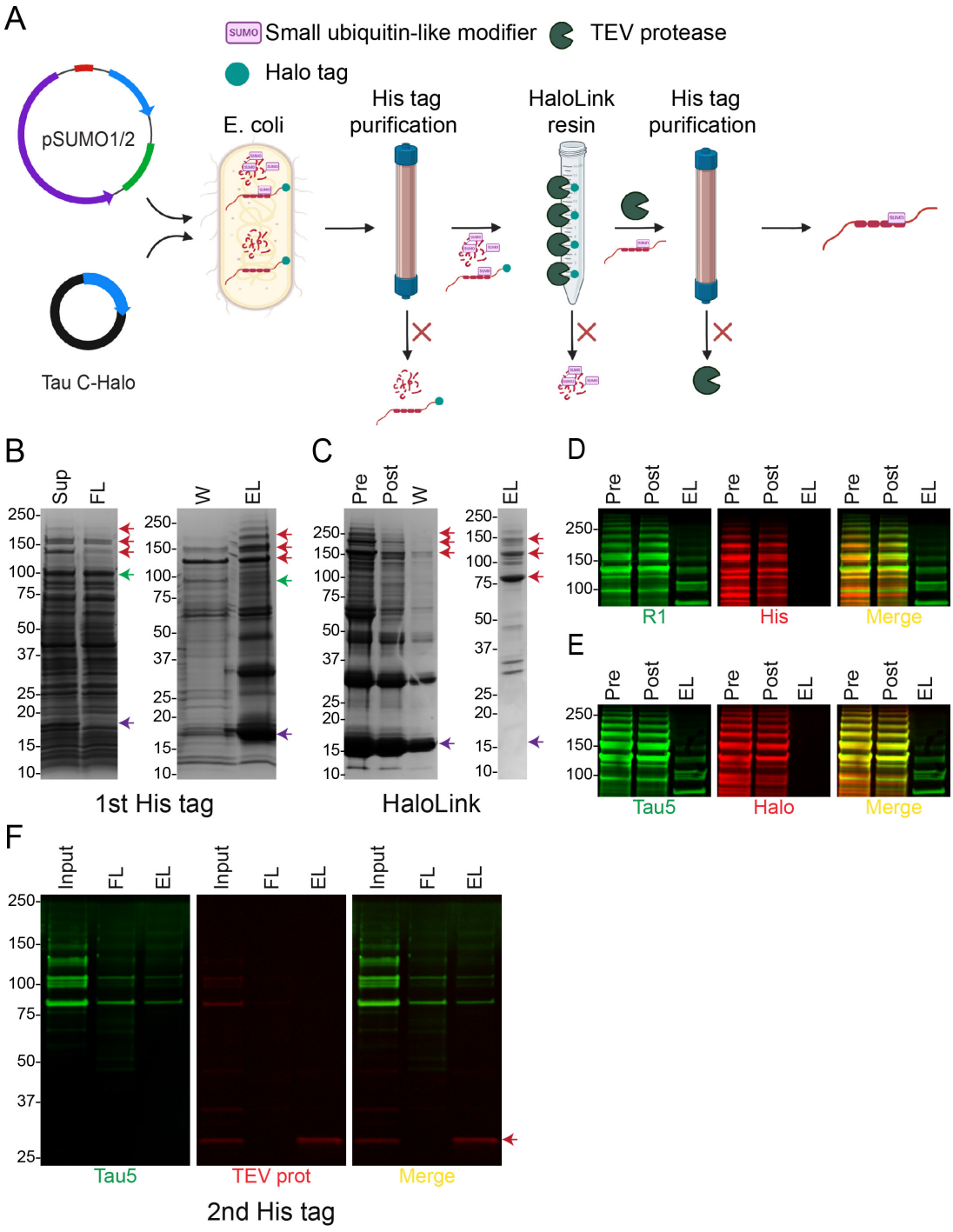

Figure AIII.1. Production and purification strategy of SUMO-modified tau using SUMO1-modified hT40 as an example.

Figure AIII.1 (cont'd)
A, bacterial cells were co-transformed with tau C-Halo and either pSUMO1 or pSUMO2 plasmids. We purified SUMOylated proteins using His tag-based purification of bacterial lysate (1st His tag). SUMOylated tau was captured from the other bacterial protein via HaloLink resin-based purification. Tau was eluted from the HaloLink resin using the TEV protease enzyme that serves 2 functions – cleaving tau off the HaloLink resin and cleaving His tag off the N-terminus of SUMO proteins. The TEV protease enzyme (with an N-terminal His tag) was removed from the final tau preparation via another round of His tag-based purification (2nd His tag). B, Coomassie stain of SDS-PAGE gel showing the supernatant (Sup), flow-through (FL), wash (W), and elution (EL) fractions of the first talon run. SUMOylated tau proteins were visible at molecular weight between 130-230 kDa, corresponding to Halo-tagged mono- or poly-/multi- SUMOylated tau products (red arrowheads). Band intensities of SUMOylated tau products were reduced in FL relative to Sup, suggesting they were successfully bound to the Talon column (his tag-based purification). Halo-tagged unmodified tau band was visible at around 100 kDa, and its intensity was not reduced in FL relative to Sup (green arrowhead). SUMO1 band was visible in Sup at about 18 kDa but not in FL; it was almost completely captured by the Talon column as revealed later in the elution fraction (purple arrowhead). C, Coomassie gel of the pre-binding, post-binding, W, and EL fractions of HaloLink purification. SUMOylated tau (red arrowheads) and SUMO1 bands (purple arrowhead) were markedly reduced in the post-binding samples relative to pre-binding. Upon eluting HaloLink resin-bound proteins with TEV protease enzyme, the primary bands were SUMOylated tau in the elution fraction at a reduced molecular weight between 90-210 kDa (red arrowheads). SUMO1 bands were almost completely absent in the elution fraction relative to the other lanes (purple arrowhead). D, western blot of the pre-binding, post-binding, and EL fractions of the HaloLink run probed with the tau R1 antibody (1:10,000) and His tag antibody (1:500; Millipore, #OB05-100UG, RRID: AB_564679). The His tag was detectable on SUMOylated tau bands in the pre- and post-binding samples but not in the elution sample, suggesting the successful cleavage of His tag off the N-terminus of SUMO1 protein. E, western blot of the pre-binding, post-binding, and EL fractions of the HaloLink run probed with the Tau5 antibody (1:100,000; Nicholas M. Kanaan at Michigan State University, RRID: AB_2721194) and HaloTag antibody (1:1,000; Promega, #G9281, RRID: AB_713650). The Halo tag was detectable on SUMOylated tau bands in the pre- and post-binding samples but not in the elution sample, suggesting the successful cleavage of the Halo tag from the C-terminus of SUMOylated tau protein. F, western blot of the input, FL, and EL fractions of the 2nd talon run probed with the Tau5 antibody and TEV protease antibody (1:1,000; Rockland, #200-401-B91S, RRID: AB_10894202). Input sample from the preceding HaloLink run had both tau and TEV protease enzyme. After passing the input sample through Talon column, tau comes out in the FL (because his tag was cleaved off) with no TEV protease. TEV protease comes out concentrated in the EL fraction along with any residual SUMOylated tau with His tag not cleaved off during elution from the HaloLink resin. SUMO1-modified hT40 in the FL was used to conduct the rest of experiments described in this work. Similar strategy was used to purify a SUMOylated version of the longest 3R tau isoform–hT39. Abbreviations: SUMOylation, modification with small-ubiquitin-like modifier protein; SUMO, small

Figure AIII.1 (cont'd)
ubiquitin-like modifier; hT40, 2N4R tau isoform; hT39, 2N3R tau isoform; TEV protease, tobacco etch virus protease; pre, pre-binding sample; post, post-binding sample; FL, flow-through; W, wash; EL, elution. Panel A created with BioRender.com.

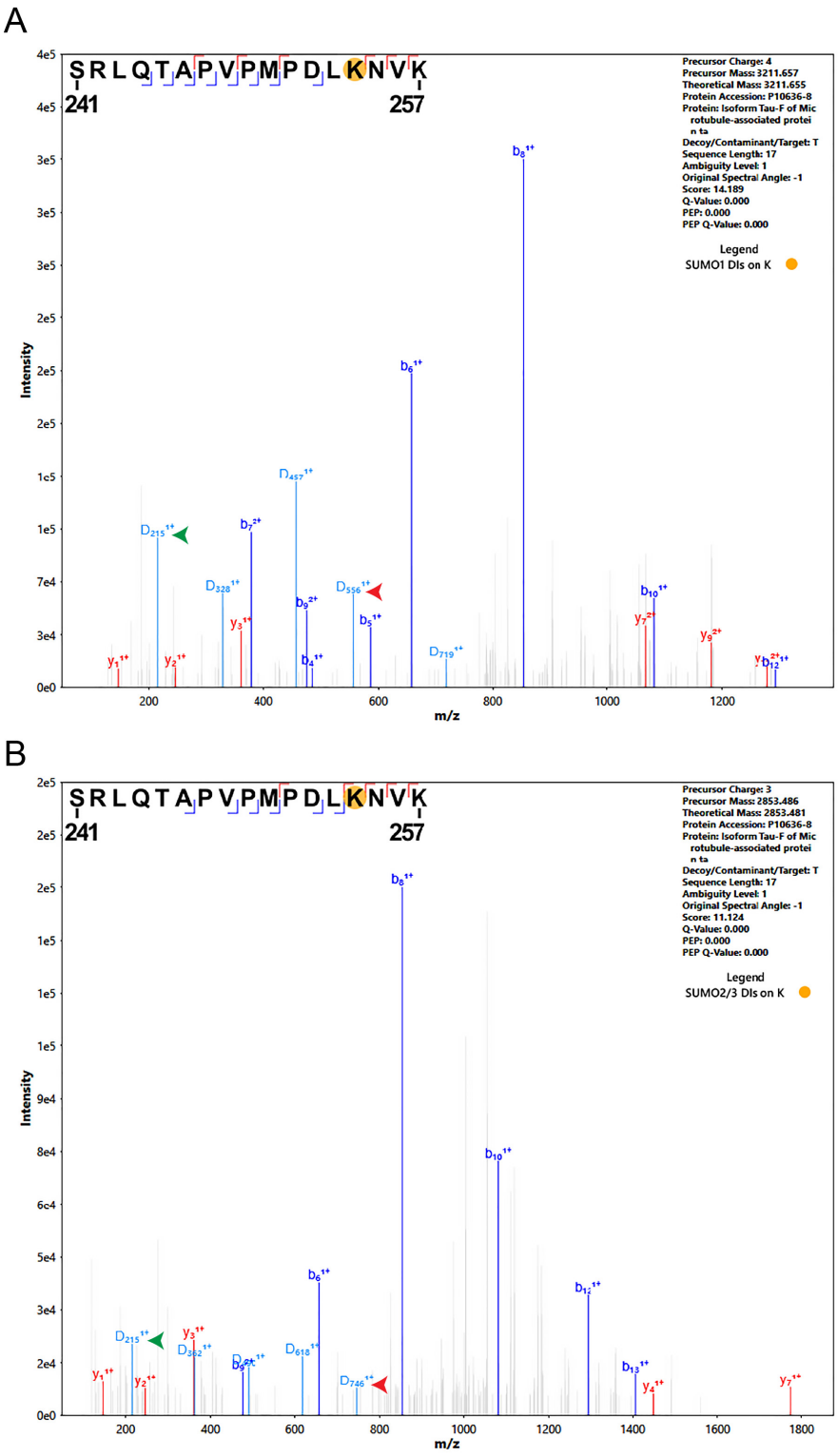

Figure AIII.2. Sample mass spectra of tau peptides showing SUMO modification at K254 of hT40.

Figure AIII.2 (cont'd)
A, mass spectrum of peptide spanning amino acids 241-257 in SUMO1-modified hT40. Fragmented y_7 shows mass shift corresponding to modification with SUMO1 (i.e. y_7^{2+} m/z = 1066.55 equivalent to a mass of 2131.1 Da). B, mass spectrum of peptide spanning amino acids 241-257 in SUMO2-modified hT40. Fragmented y_7 shows mass shift corresponding to modification with SUMO1 (i.e. y_7^{1+} m/z = 1773.91 equivalent to a mass of 1772.91 Da). Unmodified peptide spanning amino acids 241-257 shows a fragmented y_7^{2+} ion with a m/z of 407.24 D equivalent to mass of 812.48 Da (spectrum not shown). Some diagnostic ions are shared between SUMO1 and SUMO2 (e.g. D215+; green arrowhead). However, other diagnostic ions help distinguish between SUMO1 and SUMO2 modification (e.g. D556+ for SUMO1 and D746+ for SUMO2; red arrowheads) along with mass shifts. Abbreviations: SUMOylation, modification with small-ubiquitin-like modifier protein; hT40, 2N4R tau isoform; m/z, mass-to-charge ratio; DI, diagnostic ion.

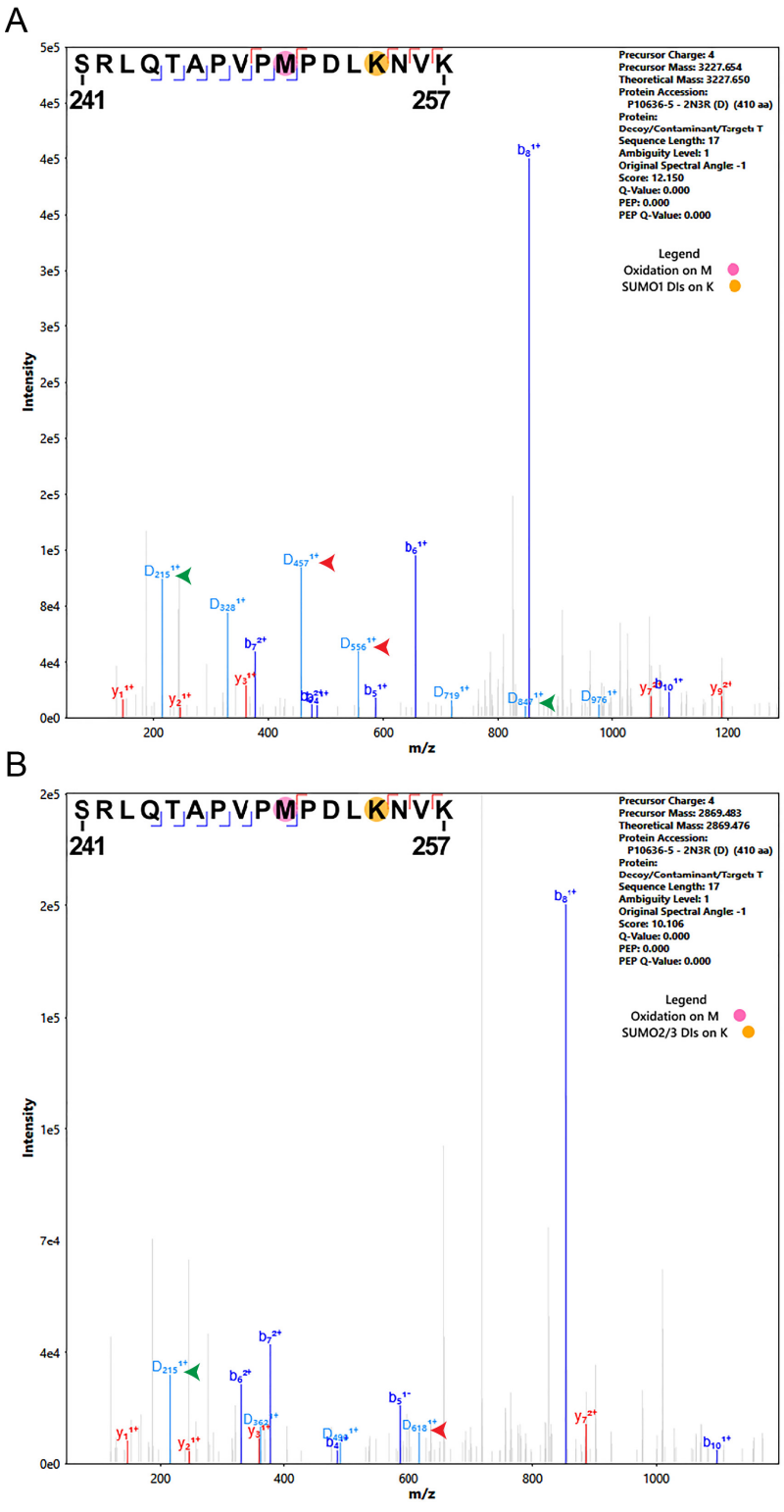

Figure AIII.3. Sample mass spectra of tau peptides showing SUMO modification at K254 of hT40.

Figure AIII.3 (cont'd)
A, mass spectrum of peptide spanning amino acids 241-257 in SUMO1-modified hT39. Fragmented y7 shows mass shift corresponding to modification with SUMO1 (i.e. y72+ m/z = 1066.54 equivalent to a mass of 2131.08 Da). B, mass spectrum of peptide spanning amino acids 241-257 in SUMO2-modified hT39. Fragmented y7 shows mass shift corresponding to modification with SUMO1 (i.e. y72+ m/z = 887.457 equivalent to a mass of 1772.91 Da). Unmodified peptide spanning amino acids 241-257 shows a fragmented y72+ ion with a m/z of 407.245 equivalent to mass of 812.49 Da (spectrum not shown). Some diagnostic ions are shared between SUMO1 and SUMO2 (e.g. D215+ and D847+; green arrowhead). However, other diagnostic ions help distinguish between SUMO1 and SUMO2 modification (e.g. D457+ along with D556+ for SUMO1 and D618+ for SUMO2; red arrowheads) along with mass shifts. Abbreviations: SUMOylation, modification with small-ubiquitin-like modifier protein; hT39, 2N3R tau isoform; m/z, mass-to-charge ratio; DI, diagnostic ion.

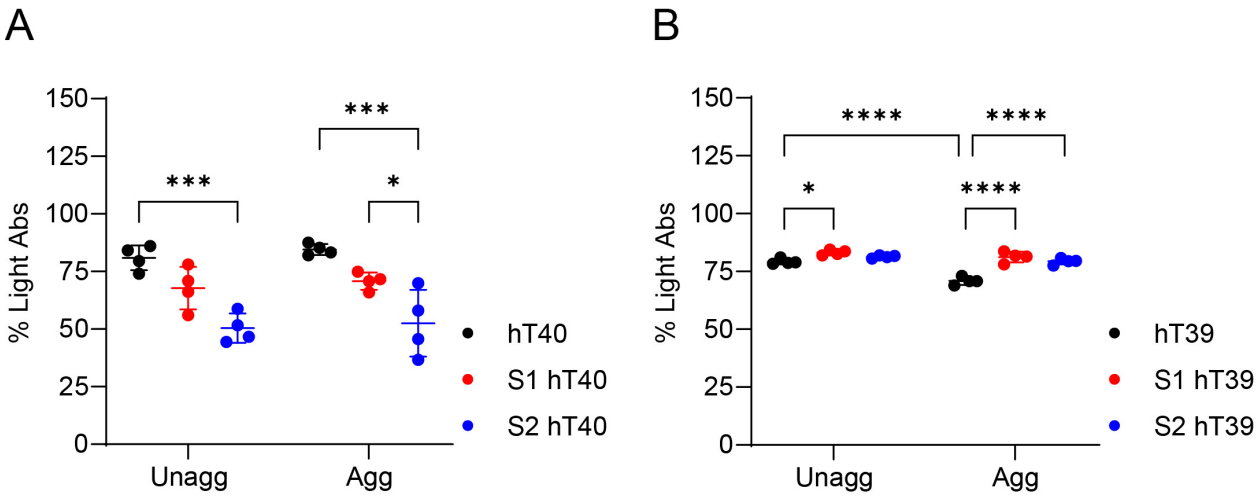

Figure AIII.4. Sandwich ELISA assay to quantify total tau levels using the Tau13 antibody.
A, sandwich ELISA assay measuring total tau in unaggregated and aggregated hT40 proteins using Tau13 antibody for capture and R1 antibody for detection. B, sandwich ELISA assay measuring total tau in unaggregated and aggregated hT39 proteins using Tau13 antibody for capture and R1 antibody for detection. Abbreviations: SUMOylation, modification with small-ubiquitin-like modifier protein; hT40, 2N4R tau isoform; hT39, 2N3R tau isoform; R1, tau rabbit polyclonal antibody. Data represented as mean ± SD. * p≤0.05; ** p≤0.01; *** p≤0.001; **** p≤0.0001.